FINITE ELEMENT ANALYSIS OF LAYER NON-UNIFORMITY IN POLYMER COEXTRUSION FLOWS

By

AGUSTIN TORRES RIQUELME, Mech. Eng.

A Thesis

Submitted to the School of Graduate Studies

in Partial Fulfillment of the Requirements

for the Degree

Doctor of Philosophy

McMaster University

May 1995

FINITE ELEMENT ANALYSIS OF LAYER NON-UNIFORMITY IN POLYMER COEXTRUSION FLOWS

...pero no cambia mi amor,
por más lejos que me encuentre,
ni el recuerdo, ni el dolor
de mi pueblo y de mi gente.
Y lo que cambió ayer,
tendrá que cambiar mañana,
así como cambio yo
en estas tierras lejanas...

Julio Numhauser.

DOCTOR OF PHILOSOPHY
(Chemical Engineering)

McMASTER UNIVERSITY
Hamilton, Ontario

TITLE:	Finite Element Analysis of Layer Non-Uniformity in Polymer Coextrusion Flows
AUTHOR:	Agustín Torres Riquelme, Mech. Eng. (Universidad del Zulia, Venezuela)
SUPERVISORS:	Drs. A. N. Hrymak and J. Vlachopoulos (Chemical Engineering)
NUMBER OF PAGES:	xxiii, 222

ABSTRACT

Coextrusion is an important polymer processing technology that consists of combining layers of different materials in their molten state to form a uniform structure. The final product has the combined properties of the individual components at a cost that is a fraction of lamination. Two basic problems have been defined in polymer coextrusion: the temporal instability of the polymer/polymer interface, and the problem of maintaining a uniform layer and thickness distribution across the die in steady state operation. This work is concerned with the latter problem class. Layer non-uniformity is a distortion of the internal interface that can be seen as a migration or displacement of the more viscous fluid by the less viscous one.

A three-dimensional finite element code was developed to study fundamental issues in the layer non-uniformity problem. One area of study is the contact line region (where the fluid/fluid interface meets the wall). Use of the classical no-slip condition leads to a mathematical singularity. In the past, this was circumvented by extrapolation methods. In this work, a localized slip model allowed a detailed study of the interface behavior near the wall. Also, a rigid (or "stick") contact line was used to explain certain experimentally observed interface shapes.

Based on experimental evidence, two distinct interface deformation mechanisms are proposed: Type I shows a displacement of the more viscous fluid by the less viscous

one, with a slippage of the contact line. In Type II, there is an intrusion of the less viscous fluid into the more viscous fluid. Type I and II deformations can be captured using the 3-D thermal model formulation described in this work, but the shape depends on the interplay between the material and die parameters. The value of the slip coefficient at the contact line is important and may be a fundamental characteristic of the particular polymer melt / polymer melt / die material system.

A detailed study of the effect of thermal and geometrical parameters on the final interface shape was conducted. It was found that the thermal dependence of viscosity plays the most important role in determining the final interface shape as compared against other material parameters. The effect of this parameter is more pronounced near the die walls, where the viscous dissipation is higher. The code shows excellent agreement with experimental data for polycarbonate/polycarbonate extrusion systems.

An alternative analysis for the three-dimensional flow of viscoelastic flow in ducts was presented as an attempt to explain experimentally observed complicated interface shapes that cannot be captured by a Generalized Newtonian Fluid model. A modified Phan-Thien Tanner model and a second-order model are used in conjunction with a space-marching finite element code based on the Parabolized Navier-Stokes equations to study the secondary flows in channels.

DEDICATORIA

Resulta para mí muy difícil -proviniendo de un país donde la gratuidad y universalidad de la educación superior existen sólo como bellas frases de la Constitución y se han convertido más en lujo que en derecho de los ciudadanos; de un país donde la superación académica, más que necesidad, se convierte en vocación- poder agradecer con propiedad a quienes hicieron que este sueño de juventud se transformase en realidad. Este trabajo, los resultados obtenidos y las satisfacciones que me han producido, quisiera ofrecérselo a cuatro personas:

La primera de ellas, sin lugar a dudas, es mi esposa Carmen. Ella ha sabido entender mis anhelos, compartir mis triunfos, suavizar mis fracasos; su ser ha motivado mi lucha diaria y, sobre todo, le ha dado sentido a mi trabajo y a mi vida. También ha soportado estoicamente innumerables sacrificios durante estos años y me ha demostrado la profundidad del verdadero amor como amiga, esposa y compañera. Nuestra pequeña hija Irene es prueba viviente de ese gran amor.

A mi padre le agradezco haberme enseñado con su ejemplo diario, la responsabilidad, la honestidad, la integridad y el amor por la ciencia. Sus silentes aplausos resuenan en lo más profundo de mi alma día a día. A mi madre le debo el tesón, el coraje y todo su apoyo durante estos años. El ejemplo que ambos brindaron fue mi mejor guía; creo nunca podré pagarles con propiedad todo el sacrificio que hicieron para que pudiese llegar hasta aquí.

Finalmente, pero no por ello menos, hay una persona a quien le debo el haber venido a Canadá y desarrollado esta relación de amor y odio con los elementos finitos. Zeferino ha sido durante todos estos años un gran consejero y el mejor maestro que haya podido tener. Las conversaciones a la espera del computador fueron fuente de numerosas enseñanzas, desde filosofía hasta fútbol; junto a él aprendí la profesión de ingeniero e investigador. Sin duda alguna, Zeferino encarna en su acción y en su palabra la definición de *amigo* en su más fina y amplia acepción.

A ustedes cuatro, pues, les dejo con gran agrado, esta pequeña muestra de mi aprecio.

DEDICATED TO

It is extremely difficult for me -since I came from a country where gratuity and universality in post-secondary education are only beautiful words in the Constitution and they have become more a luxury than a citizen's right; a country where academic achievement, has become more a vocation than a necessity- to say thanks properly to those who made this youth's dream possible. I wish to dedicate this work, all its results and the satisfactions that they have provided me, to four persons:

First of all, without hesitation, is to my wife Carmen. She has understood all my desires, shared all my accomplishments and smoothed my losses: Her soul has motivated my daily fight and above all, she has given motivation to my work and sense to my life. She has also quietly done many sacrifices along all these years, and has shown to me true love as a friend, wife and companion. Our little daughter Irene is living proof of such a great love.

I wish to thank my father for teaching me, through his daily actions, responsibility, honesty, integrity, and love for science. His silent applause are being heard aloud in the deepest part of my soul day after day. My mother transmitted strength and courage to me, and confidence in me was present during all these years. My parents' behavior was my best guidance: I do not think I could ever pay them back properly for all the sacrifices they have made.

Last, but not least, there is a person to whom I am deeply indebted for this adventure in Canada, and for developing this relationship of love and hate with the finite element method. Zeferino has been through all these years an excellent counsellor and the best teacher I could ever had. All those conversations while waiting for the computer were a source of numerous lessons, from philosophy to soccer. Thanks to him I learned how to be an engineer and a researcher. Without any doubt, Zeferino embodies the word *friend* in his widest and finest acceptation.

To all you four I offer this small sample of my gratitude, with all my heart.

ACKNOWLEDGEMENTS

I want to express my deepest gratitude to my supervisors, Dr. A.N. Hrymak and Dr. J. Vlachopoulos. Not only they provided me with an outstanding atmosphere for performing research, but also their encouragement, guidance and advice was of great help during the course of this project.

The financial support of the Department of Chemical Engineering and the School of Graduate Studies of McMaster University, of Investigación y Desarrollo, C.A. (Venezuela), of Ontario Centre for Materials Research and of Shell Canada Company is gratefully acknowledged.

Special thanks to Joseph Dooley and Henk Pool, from the Dow Chemical Company, for making available experimental evidence to support this work, and for all the interesting and enlightening discussions.

To my wife Carmen and my daughter Irene, for providing love and companionship and for enlightening so many days of hard work away from home.

To all the people in Cappa-D and Compuplast, Inc., in particular to Elizabeth Takács, Céline Bellehumeur, Jiri Svabik, and Norberto Silvi for all the help provided and patience in listening to my speculations.

To all the people in the Chemical Engineering Department, for welcoming me and my work and for providing a friendly environment where work becomes a real pleasure. In particular, I want to thank Barb and Sara, for all their help.

Last, but not least, to the wonderful Latin American contingent I had the opportunity to meet. In particular, I want to thanks Marco, Cecilia, Crista, Eduardo, Beto, Daniel, Lulú, Miguel, the Gidi family, the Pérez family, the Irazuzta family and my fellow Venezuelans, David, the Bravo-Osorio, the Bravo-Reyes, the Aray, the Casas and the Rincón families, for showing that we, Latin Americans, belong to the same country, and for making us feel home away from home.

TABLE OF CONTENTS

LIST OF FIGURES.

LIST OF TABLES

LIST OF SYMBOLS

A: Material function for Mitsoulis' model; Tensor dependent function.

a: Material function for parabolic equation.

B: Dimensionless slip coefficient.

B: Tensor used in MPTT model.

b: Thermal dependence coefficient of viscosity; Material function for parabolic equation.

Br: Brinkmann Number.

c: Material function for parabolic equation; Concentration.

Ca: Capillary number.

C_p: Specific heat.

C_t: Right Cauchy-Green Tensor.

D: Diffusivity.

D_h: Hydraulic diameter.

D: Tensor used in MPTT model.

H: Mean Interface curvature.

I_j: j^{th} invariant of a tensor.

J: Jacobian of the isoparametric transformation for the volume integral.

J^*: Jacobian of the isoparametric transformation for the surface integral.

k: Thermal conductivity.

L: Characteristic Length.

L/D: Length to Diameter Ratio.

m: Deformation-history dependence of the stress tensor.

N: Shape function.

N_1: First normal stress difference.

N_2: Second normal stress difference.

N_p: Shape function for pressure.

n: Normal vector to the interface.

P: Pressure.

P^a: Axial pressure.

Pe: Peclét number.

Pr: Prandtl number.

q': Heat source.

Q: Volumetric flowrate.

R: Residual Vector.

R': Simplified momentum matrix used in segregated algorithms.

Re: Reynolds number.

R_x: Residual Vector of the x-momentum equation.

R_y: Residual Vector of the y-momentum equation.

R_z: Residual Vector of the z-momentum equation.

R_c: Residual Vector of the continuity equation.

R_k: Residual Vector of the kinematic boundary equation.

R_T: Residual Vector of the energy equation.

S: Deformation dependent tensor; source term in general parabolic equation.

T: Temperature.

T_1: Tensor used in CEF model.

T_2: Tensor used in CEF model.

T_e: Entrance temperature.

T_w: Wall temperature.

T_c: Centre-line temperature.

t: Tangent vector to the interface.

U: Characteristic Velocity.

u: Velocity vector.

u: x-component of the velocity vector.

v: y-component of the velocity vector.

V_s: Slip velocity.

w: z-component of the velocity vector.

Wi: Weissenberg number.

Wi_c: Weissenberg number using characteristic values.

Wi_w: Weissenberg number using wall shear-rate.

X: Vector of unknowns.

x: Coordinate vector (x,y,z).

Greek characters.

α: Coefficient for slip equation; Viscoelastic material parameter; Relaxation factor.

α_p: Relaxation factor for pressure.

α_v: Relaxation factor for velocity.

β: Slip coefficient.

Γ: Interfacial tension.

δ: Kronecker delta.

ε: Viscoelastic material parameter; Tolerance level.

ζ: Weighting factor for $\delta/\delta t$.; parent coordinate.

ζ_0: Reference value for ζ.

η: Viscosity function; parent coordinate.

η_0: Zero-shear viscosity.

η_v: Viscosity of the viscous component of the extra-stress tensor.

η_e: Viscosity of the elastic component of the extra-stress tensor.

θ: Critical shear rate.

θ_c: Contact angle.

$\dot{\gamma}$: Shear-rate tensor.

γ: Second Invariant of the shear-rate tensor.

λ: Characteristic retardation time, Relaxation factor for Carreau model.

λ_1: Constant for shear-rate dependence of viscosity in CEF model.

λ_2: Constant for shear-rate dependence of viscosity in CEF model.

μ: Viscosity coefficient.

ξ: Parent coordinate.

ρ: Density.

Σ: Sum.

τ: Extra-stress tensor.

σ_1: Constant for shear-rate dependence of viscosity in CEF model.

σ_2: Constant for shear-rate dependence of viscosity in CEF model.

ϕ: Integral models functions; primary variable.

ψ_1: First Normal Stress Coefficient.

ψ_2: Second Normal Stress Coefficient.

ω: Vortcity tensor.

Ω: Domain.

Mathematical Symbols.

∇: Gradient of a tensor.

∇^2: Divergence of a tensor.

$\partial/\partial t$: Partial derivative.

D/Dt: Substantial derivative.

$\Delta/\Delta t$: Contravariant Derivative of the strain-rate tensor.

$\delta/\delta t$: Keunings' objective derivative.

e: Exponential.

tr: Trace of a tensor.

•: Dot product.

: : Double-dot product of a tensor.

×: Cross-product.

Superscripts.

b: Power-law index in slip model.

E: Experimental value.

(e): Elemental approximation.

i: Iteration number.

n: Power-law index.

T: Transpose.

(1): Lower-convected derivative.

': Dimensional value; Corrective values.

Subscripts.

c: Characteristic value.

fs: Free-surface values.

i: Nodal value.

ij: Tensor component.

n: Newtonian component.

o: Reference value.

s, sl: Slip value.

v: Viscoelastic component.

w: Wall value.

x: $\partial / \partial x$.

y: $\partial / \partial y$.

z: $\partial / \partial z$.

xx: $\partial^2 / \partial x^2$.

yy: $\partial^2 / \partial y^2$.

zz: $\partial^2 / \partial z^2$.

1: Fluid 1.

(1): Upper-convected derivative.

2: Fluid 2.

∞: Infinity or ambient value.

CHAPTER 1

INTRODUCTION

1.1 Coextrusion process.

Coextrusion is rapidly becoming one of the most important technologies in the polymer processing industry for production of multilayered films and sheets with tailored properties. In this process, two or more polymer melts are brought together in a die to form a layered structure. The final product will have the added benefits of the individual components at a cost which is usually lower than laminating processes or other structures (Figure 1.1). It is assumed that little or no dispersion occurs between adjacent polymer melts, and the fluids are separated by well defined internal interfaces.

There are two basic methods to produce multilayer polymers. One is using a multimanifold die and the other is by means of a single manifold die using a feedblock system at the die inlet (Han and Shetty, 1976). The multimanifold (Figure 1.2a) die has the advantage that polymers with widely different rheological properties can be used. However, producing more than three layers becomes expensive due to increased mechanical complexity. The feedblock method (Figure 1.2b) can be used to extrude products having many layers but the viscosity ratio of the melts cannot be large because of material distribution problems and non-uniformity problems. Karagiannis (1989a) has presented an excellent review of the basic techniques and approaches used in coextrusion die design.

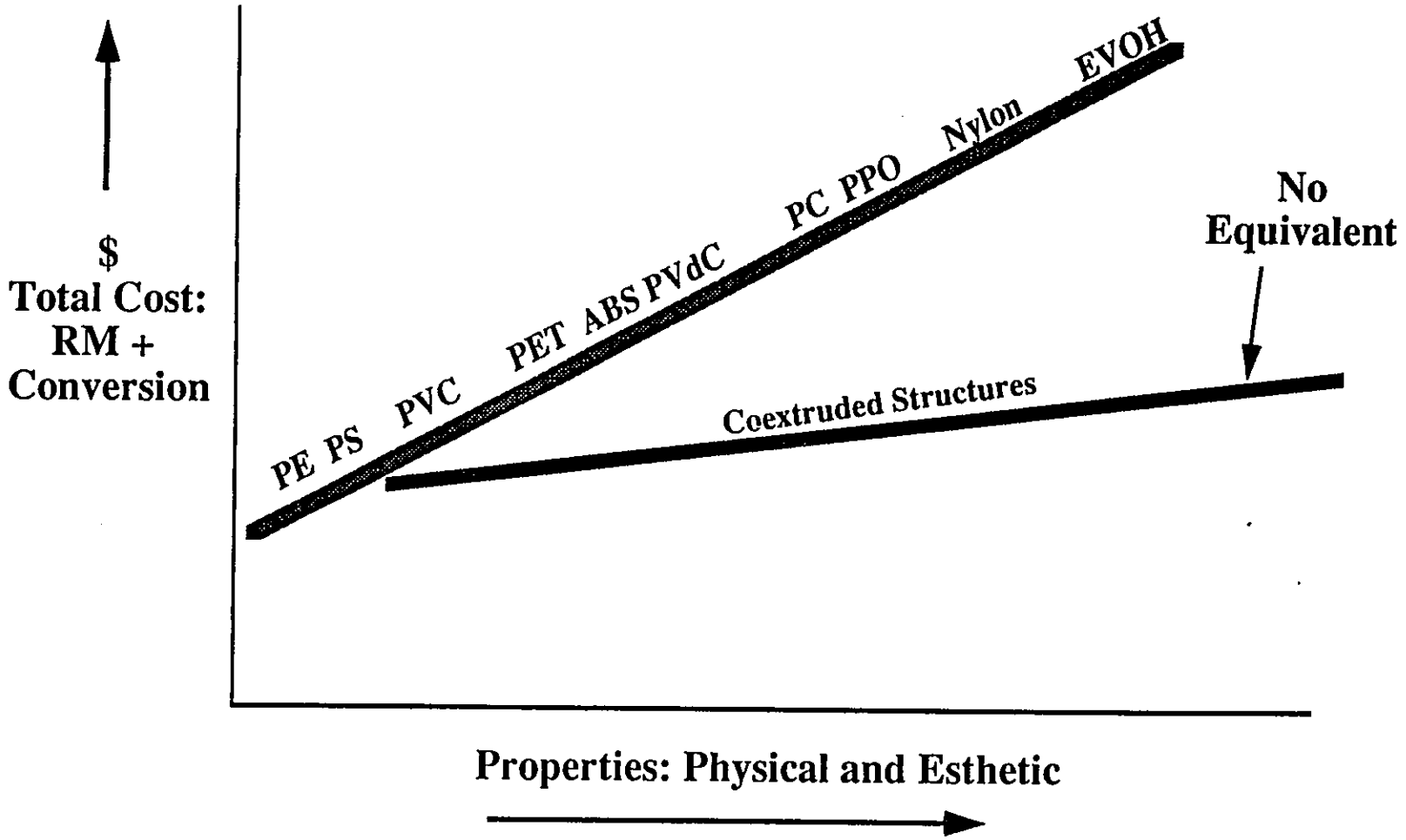

Figure 1.1. Goal of coextrusion (taken from Finch, 1991).

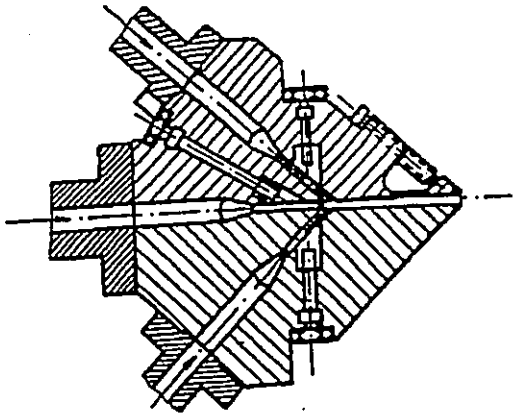

(a)

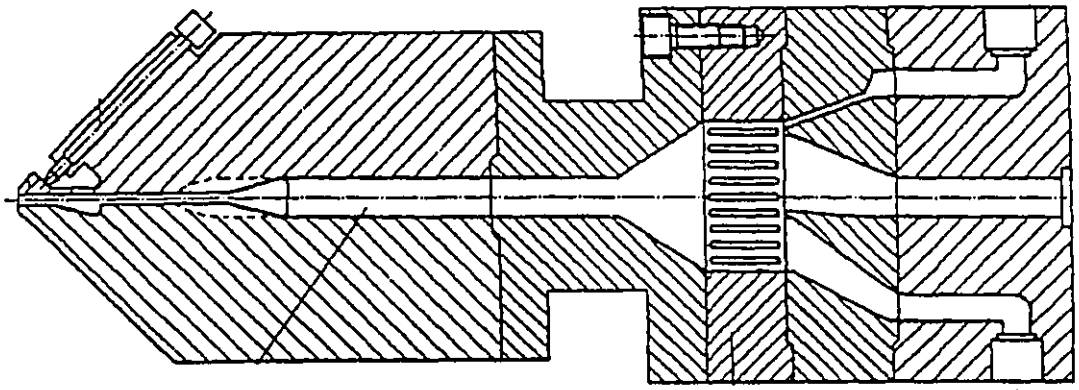

(b)

Figure 1.2. Coextrusion dies used. (a)Multimanifold. (b) Feedblock.

The flow arrangement in coextrusion can be summarized into two basic types: side-by-side and sheath-core coextrusion. In the former, a flat interface is formed between two or more polymers and each phase wets the die walls for its respective domain (Fig. 1.3a). In the latter, concentric layers of polymer form a sheath-core profile, i.e., only one polymer wets the die walls (Fig. 1.3b). Examples of side-by-side coextrusion are multilayer sheets and film. Sheath-core coextrusion is used, for example, to produce fibers with flame-retardant and/or antistatic properties. Annular coextrusion is found in applications such as wire coating but it can be considered as a particular type of sheath-core or concentric coextrusion (Fig. 1.3c). The main focus of this work is side-by-side coextrusion commonly found in flat film and sheet applications.

Two basic problem classes have been defined in polymer coextrusion: the temporal stability of the internal polymer/polymer interface in the flow direction and the problem of maintaining spatially uniform layer structure and thickness within the die in steady state operation. This work deals with the latter problem class. Layer non-uniformity can be described as a gross distortion of the internal interface as it flows through the die due to migration of the low viscosity fluid to high shear regions, as shown by previous experimental and numerical investigations (Everage, 1973, Southern and Ballman, 1973, Karagiannis et al., 1990, Torres et al., 1993). It is of critical importance in side-by-side coextrusion process to minimize the amount of interfacial distortion in order to obtain a product of uniform quality and structure across its width. In practice, this is achieved by an expensive trial-and-error procedure that involves controlling numerous inter-related factors, such as temperature profiles, pressure drops, flowrate ratios, die geometry, etc.

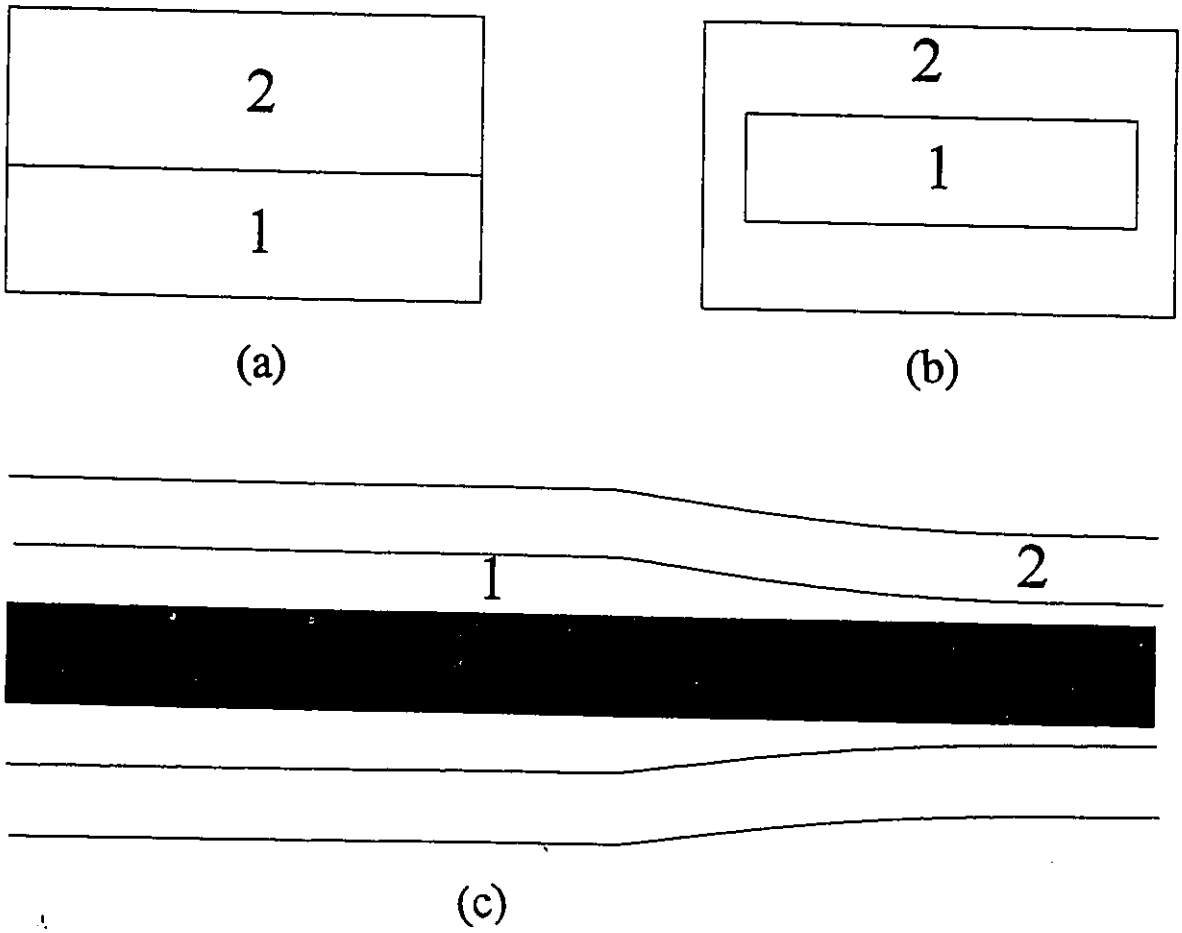

Figure 1.3. Flow arrangements in coextrusion. (a) Side-by-side. (b)Sheath-core. (c) Annular.

Numerical simulations have been used by both academic and industrial researchers to understand the effect of each of these factors and to predict layer distribution for a given die and operating conditions.

To fully understand the development of internal interfaces in coextrusion flows, a three dimensional analysis is necessary. The interfaces deform both along the axial direction as well as across the die width in a full three-dimensional fashion. A number of complications arise when a full three-dimensional simulation of the coextrusion process is attempted. There are a large number of variables to solve due to the mesh required to solve, with usually over 20,000 variables for simple problems. Multiple nonlinearities are present due to coupling between the energy and momentum conservation equations, as well as shear-thinning and thermal effects on apparent viscosity. The presence of internal interfaces means that the interface locations must be calculated with the other state variables. The size of the problem and the combined nonlinearities make the solution of the problem difficult and convergence slow. The presence of the fluid/fluid/wall contact line region creates a mathematical singularity if the no-slip boundary condition is applied. Thermal and elastic effects also affect the final interface shape (Takács et al., 1994; Torres et al., 1995; Dooley and Hughes, 1995).

In this work, a three dimensional finite element analysis for the analysis of non-Newtonian, thermally dependent bicomponent flows is presented. Also, a space-marching technique for the analysis of viscoelastic duct flow is proposed. The purpose is to gain more insight in the complex mechanisms that govern the interface development in coextrusion flow by developing mathematical and numerical tools for the prediction of

polymer coextrusion flows.

The objectives of this thesis are: 1) to propose suitable localized slip and stick models for relieving the mathematical singularity at the contact line and which capture experimentally observed interface shapes near the die wall; 2) to perform a detailed analysis of the thermal and geometrical effects in coextrusion flows; 3) to propose a numerical algorithm for the simulation of three-dimensional viscoelastic duct flow.

1.2 Thesis outline.

Chapter 2: The governing equations for purely viscous and viscoelastic flows are presented here, along with the intrinsic problems associated with its modelling (imposition of boundary conditions, hyperbolicity, free surfaces, etc.). A critical literature review on the topic of modelling polymer coextrusion flows is presented.

Chapter 3: The finite element techniques applied to the solution of Navier-Stokes and Parabolized Navier-Stokes equations are presented, along with a summary of the numerical problems encountered during the course of the research.

Chapter 4: This chapter includes the finite element analysis of the contact line behavior in coextrusion flows. Several slip models, including stick (no velocity at the wall) and extrapolation methods are studied. Interface shape deformation mechanisms depend on flow conditions and adhesion of the interface to the die walls. Comparison of the contact line boundary conditions with experimental evidence is provided.

Chapter 5: The effects of the various parameters, such as thermal dependence of viscosity, Pe and Br numbers are analyzed. The energy equation is added to an existing

three-dimensional finite element code for bicomponent flows. Convergence problems are present when the full set of momentum / energy / constitutive equations are solved together. The code is tested against experiments for low elasticity systems with good agreement.

Chapter 6: Given the complexity of a full three-dimensional analysis of viscoelastic flows, a simplified approach is presented here, based on the Parabolized Navier-Stokes equations. The three-dimensional domain is solved by sequentially analyzing two-dimensional cross-sections of the duct and marching in the main flow direction, thus reducing the size of the computational problem from three-dimensional to a sequence of two-dimensional simulations which captures secondary flows.

Chapter 7: This chapter summarizes the results obtained and proposes some suggestions for future work in the area.

CHAPTER 2

LITERATURE REVIEW AND MATHEMATICAL FORMULATION

2.1 Literature review.

In this section, a review of previous work in theoretical, experimental and numerical analysis of coextrusion is presented.

2.1.1 Experimental research in coextrusion.

From the fluid mechanics point of view, coextrusion is basically a two-phase-flow (liquid/liquid) problem. West (1911) calculated the interface propagation in a capillary tube for Newtonian fluids. Russell and Charles (1959), Bentwich (1964), and Yu and Sparrow (1967) made the first analytical calculations to study the interface location in sheath-core configurations, in oil / water systems. Yih (1967) was the first to note that the viscosity stratification plays a key role in the interface by studying the stability phenomena for plane Couette and Poiseuille stratified flow. Southern and Ballman (1973) made experiments using two commercial polystyrenes exhibiting viscosity crossover with shear rate (Figure 4.7). They found that the low viscosity fluid always encapsulates the more viscous fluid, in agreement with previous observations for oil/water flows done by Russell and Charles (1959). By doing experiments at the viscosity-crossover shear rate, an almost flat interface was obtained (Figure 2.1). They observed that elastic differences

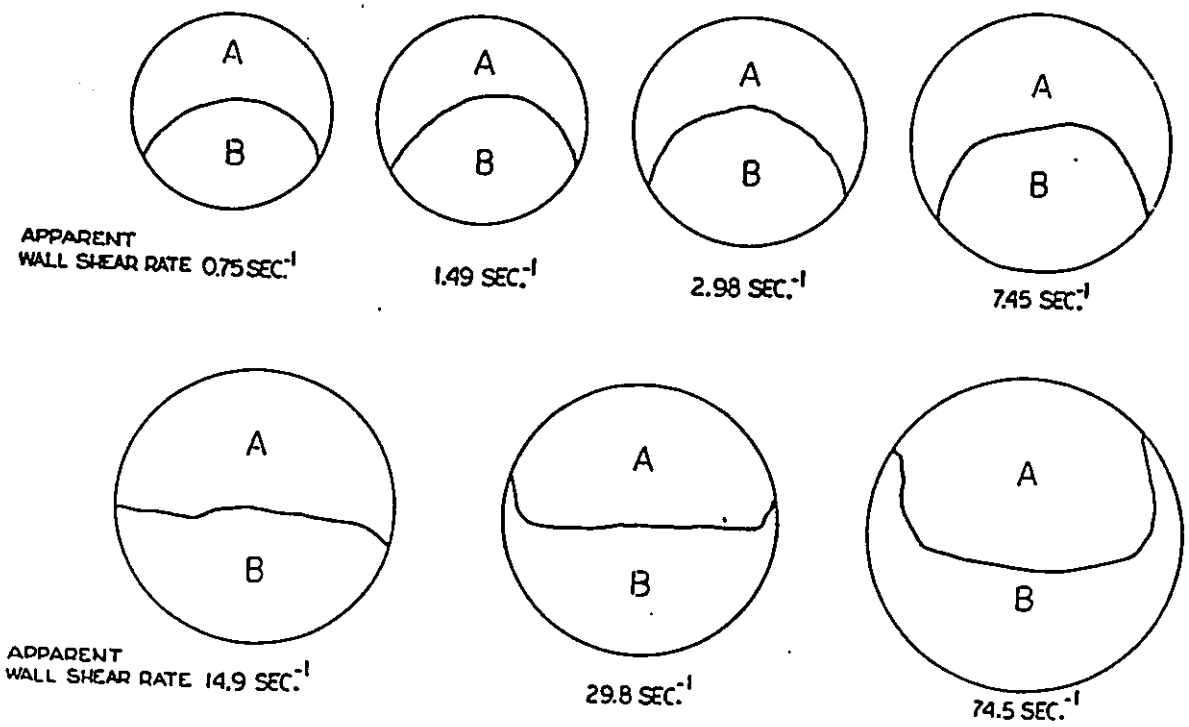

Figure 2.1. Interface shapes obtained by Southern and Ballman (1973).

in well matched viscosities produced have little effect on the interface shape for round dies. MacLean (1973) used the principle of minimum viscous dissipation in stratified flow between infinite parallel plates to show that the encapsulation of the more viscous fluid by the less viscous fluid is energetically preferred. Everage (1973) and Williams (1975) used this principle to prove the same for tube flow. Everage (1975) also studied the interface motion in the entrance region of infinite parallel plates, using nylon-6/nylon-6 systems. The results indicated that the interface motion takes place at two distinct rates: a rapid interface deformation (L/D≈2) attributed to a pressure rearrangement and the other is a very slowly irreversible curvature, where the lower viscosity fluid migrates towards the wall until total encapsulation occurs (Figure 2.2). Complete encapsulation requires a very large L/D to be achieved (120 L/D for the nylon/nylon system used by Everage). Lee and White (1974) also concluded, by experimental and theoretical analysis, that the low viscosity fluid encapsulates the high viscosity fluid irrespective of the elasticity characteristics of the two melts. Sornberger et al. (1986a,b) used finite difference analysis in two-dimensional simulations of two molten polymers in a die and concluded that thermal effects have a very small influence in the interface development in the gap/length direction of non-Newtonian fluids. Note that for immiscible materials the definition of interface is clear, but in the case of miscible materials, there is no interface as such, but rather a zone between material layer. The analysis for immiscible materials can be extended to miscible materials if the diffusion across the interface is small compared with other forces. For polymer melts at low Re number, this is the case.

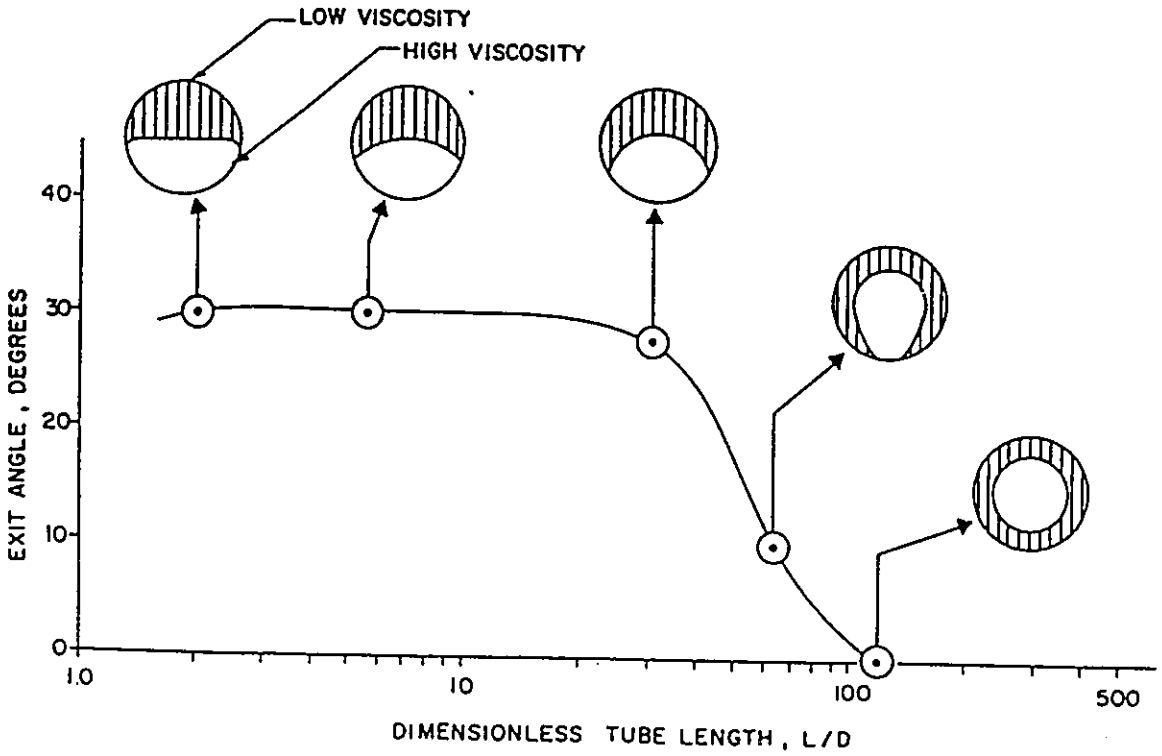

Figure 2.2. Interface deformation mechanisms as proposed by Everage (1975).

2.1.2 Stability analysis in coextrusion flows.

More recently, studies of the temporal interface deformation were performed using stability analysis and matched asymptotic expansions. Several researchers conducted studies for many configurations and situations in stratified and sheath-core multicomponent flows. All of the analyses were limited to one-dimensional (Hagen-Poiseuille) or two-dimensional flows, which is one of the biggest drawbacks of such methods. The advantage of linear stability analysis is the possibility of drawing neutral (or stable) curves, thus estimating which operating conditions are stable and which are not. Khomami (1990a) also found that the interface deformation is dominated by shear-thinning effects in addition to the viscosity effect observed for Newtonian fluids. Shear thinning effects can affect significantly the interfacial stability regime. Those regimes are different depending on the power-law model used (Khomami, 1990a). Khomami (1990b) also found that the dimensionless development length required for the interface to reach its final position is an increasing function of viscosity ratio and Reynolds number. Khomami (1990b) also found that normal stresses generated in a converging channel affect the interfacial stability of multiphase flows. Joseph et al. (1984) concluded that the sheath-core configuration with the more viscous fluid in the core is stable only when this fluid occupies most of the tube. However, the authors noted that the critical eigenvalue becomes imaginary for zero Reynolds number. Khan and Han (1976) also suggested, by means of stability analysis, that the elasticity does not play a key role in the interface deformation. Khan and Han (1977) split the three-dimensional interfacial instability on two two-dimensional problems, finding that the instabilities associated with the flow

direction are governed by the viscosity mismatch, while the instabilities in the cross-flow directions can be associated with the different elastic properties of the polymers. Su and Khomami (1992a,b) modified the interfacial boundary condition proposed by Khan and Han to take in consideration normal forces due to viscoelasticity and showed that elastic effects alone can induce instabilities, as opposed to the previous observations by Khan and Han (1977).

2.1.3 Numerical modeling in coextrusion.

Numerical methods have been employed extensively to model coextrusion flows. Lubrication Approximation Theory (LAT), Finite Difference, Finite Element and Boundary Element Methods have been used thus far. LAT is the simplest method but does not provide detailed flow information within the die. Basu (1981) used this method to study the non-isothermal superimposed flow of two polymers in wire coating coextrusion. Mitsoulis (1988) extended it to multilayer non-Newtonian coextrusion and created a code that can be easily used as a first approach in the coextrusion die design. Anturkar et al. (1990a,b,c) used the LAT to perform stability analysis of multilayer coextrusion flows.

Uhland (1977) used two-dimensional finite differences to study the interface deformation for power-law fluids, finding that the interface deformation in the gap/length direction is dependent on viscosity ratios, flowrate ratios and power-law indices. Chin and coworkers (1984) also used two-dimensional finite differences for studying the interface development inside the die. Interfaces were calculated by balancing the flow

rates and the interfacial position to satisfy continuity requirements. A coextrusion calculation, using the Finite Element Method (FEM), was done by Mitsoulis (1986) in modeling coextruded extrudate swelling. He simulated the flow of two immiscible fluids extruded concentrically from a capillary and an annular die. Since then, many researchers have used FEM in their calculations. Among them, Binding et al. (1987) predicts the vortex growth for flow in a T geometry and Luo and Mitsoulis (1990) used integral constitutive equations (K-BKZ model) for coextrudate swelling predictions.

One of the major difficulties in FEM, Finite Difference and Boundary Element Method calculations is the interface determination. This is a non-linear problem since the final shape of the internal free surface is not known a priori. Three basic approaches have been followed: the pathline method, the spine method and the use of streamlined finite elements.

In the pathline method, the free surface is determined by assuming that it lies on a streamline and that no flow can cross a streamline. This method has been successfully used in both swelling and interface calculation for viscous and viscoelastic fluid flow (see, for example, Nickell et al., 1974; Allan, 1977; Coleman, 1980; Crochet et al., 1984; Mitsoulis, 1984, 1986). At each iteration, a velocity field is obtained, then a new interface position is calculated based on that velocity field (the interface locations are modified to satisfy the requirement of no normal flows to the interface), a new mesh is created and used to obtain an updated velocity field. This procedure is repeated (Picard's method) until convergence is obtained. The convergence rate for this method is, in most cases, linear.

Kistler (1984) extended Ruschak's method (1980) for calculating interfaces and proposed the 'spine method' to discretize domains having free surfaces. In the spine method, the kinematic boundary condition at the interface (no flow normal to the free surface) and the dynamic boundary condition (continuity of stresses at the interface) are solved simultaneously with the Navier-Stokes equations, allowing the calculation of the velocity and pressure fields together with the interface locations in a coupled set of equations. For a detailed explanation of this method, see Kistler (1984) for the two-dimensional spine method and Karagiannis (1989a,b) for its extension to three dimensions. The major drawbacks of the spine approach are the addition of more unknowns (the interface positions) to a particular problem, the possibility of divergence if the interface undergoes a gross distortion, and the problem is made highly non-linear. Despite these limitations, the spine method has become a popular method because a Newton-Raphson algorithm can be developed for calculating velocities, pressures and interface locations simultaneously. Theoretically, such an algorithm will exhibit a quadratic rate of convergence and the number of iterations required to achieve the solution is reduced. In practice, the quadratic rate of convergence is achieved only near the final solution.

Recently, Papanastasiou et al. (1985) introduced the concept of 'streamlined finite elements'. This type of element allowed the determination of the interface without the introduction of additional degrees of freedom to the problem by assuming the interface is a stream-surface, making the simulation of multilayer flows tractable. However, streamlined finite elements are limited to problems with flows that are nearly one-

dimensional. The streamlined finite element method is similar to a pathline method imbedded within the set of equations.

Boundary elements have been used by Tran-Cong and Phan-Thien (1988a, 1988b, 1988c) and Bush and Phan-Thien (1985) in 3-D single component extrudate swell calculations. An excellent review of the available numerical techniques for free and moving boundaries was done by Wang and Lee (1989).

Karagiannis (1989a,b, 1990) developed a fully three-dimensional finite element code for studying isothermal bicomponent coextrusion flows. The external interface was parameterized using pathline methods, the internal interfaces using spines, and the location of the contact line was calculated using the extrapolation method of Dheur and Crochet (1987). Karagiannis (1990) simulated an experimental investigation of the interface deformation during side-by-side stratified flow inside a square die. The experiment was performed at the Dow Chemical (Nederland) B.V. facility at Terneusen, Netherlands. Despite qualitative agreement between experimental observations and numerical calculations, there is a quantitative disagreement due to: lack of information about the correct boundary conditions at the outlet and contact lines, the use of simplified constitutive equations and improper treatment of the contact line. As Karagiannis has pointed out "...more work is needed in understanding the importance of the boundary conditions at the die inflow and outflow planes and at the fluid/fluid/solid contact line in the absence of surface tension." (1989a). Torres et al. (1993, 1995) introduced the energy equation and a localized slip boundary condition for the contact line, respectively. Excellent agreement was found when comparison was made with low elasticity fluids, but

there is still a substantial disagreement in the case of more elastic fluids. Recent experiments (Dooley and Hughes, 1995) suggest that elasticity plays an important role in the final interface shape through secondary flows. The question of the appropriate outflow boundary condition remains an open question. If secondary flows are as important in determining the interface locations as recent experimentation suggests, the question of choosing the correct outlet boundary condition becomes even more important.

2.1.4 Contact lines.

An important part of this research is concerned with the problem of the contact line determination. Even though the contact line plays a role in many interesting physical situations (rivulet and coating flows, dry patch formation, die swell, bubble formation, spreading liquids, etc.) its flow mechanisms are complex and not completely understood.

A contact line can be defined as the intersection of two immiscible fluids and a solid. From a macroscopic point of view, the contact line is, in fact, a mathematical line (Figure 2.3). Two basic types of contact lines can be imagined: static and dynamic, the latter when one fluid is displacing another. The contact line is sometimes called the wetting line. At a molecular level the three phases (the two fluids and the solid) meet within a zone of very small but finite dimensions in which the structure and properties associated with one solid/fluid interface give way to those of the other (Blake, 1988; Davis, 1983). Similarly, the contact angle is defined as the angle between planes tangent to the fluid/fluid interface and the solid surface (Dussan, 1979; Blake, 1988; among many others). Once again, two types of contact angles can be defined: dynamic and static,

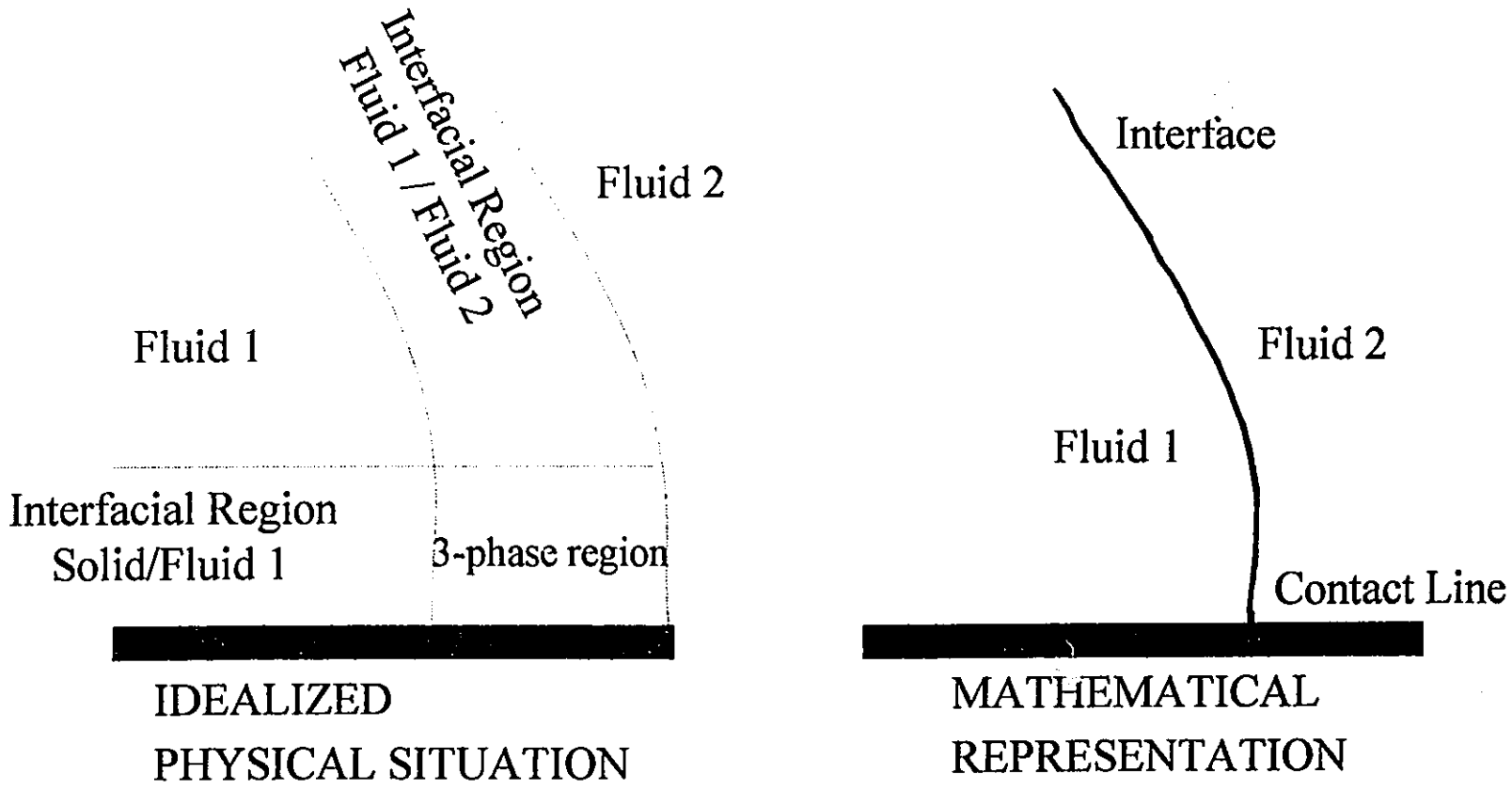

Figure 2.3. Description of a contact line.

depending on whether there is displacement of one fluid by the other. Of interest here is the moving contact line, since it is known that there is an effective displacement (leading to possible encapsulation) of the more viscous fluid by the less viscous within the die flow. Despite its occurrence in many situations, the dynamics of the fluid in the neighborhood of the contact line is poorly understood. Application of the Navier-Stokes equations together with the usual no-slip condition near the three phase-flow region produces a multivalued velocity and an unrealistic infinite force (or an unbounded wall shear stress) resisting the motion. This anomaly was first reported by Moffat (1964). Huh and Scriven (1971) were among the first to suggest that the no-slip condition may not be valid at the contact line. Later, Dussan and Davis (1974) showed that the force singularity is a direct consequence of the application of the no-slip boundary condition. Hocking (1976, 1977) and Li et al. (1990) proposed that a cause for the breakdown of the no-slip boundary condition can be attributed to irregularities of the wall surface. Hasson et al. (1970a, 1970b) proved that the wall surface and the fluid adherence (wettability) plays a significant role in the interface shape.

Several models have been proposed to alleviate the singularity at the contact line for high Ca number problems. One model is to assume a 'rolling' type of motion, in which the fluids roll over the wall, thus allowing a localized no-slip boundary condition. Yarnold (1938) and Schwartz et al. (1964) mentioned that this kind of motion exists for mercury moving through a capillary and a drop moving on an inclined plane. Mavridis (1988) used this type of behavior to explain the "fountain flow" phenomena in mold filling applications. Dussan and Davis (1974) analyzed this rolling motion from a more rigorous

mathematical point of view. This seems to be reasonable in the case of vanishing viscosity ratios (air/liquid/solid systems, for example) but no attempt of an analytical explanation has been made to justify its use in finite viscosity ratio systems. In high viscosity polymer flows, the ratio of the interfacial forces to viscous forces is very small and the contribution of interfacial tension to the final interface shape is negligible (Karagiannis et al., 1990; Torres et al, 1995).

Another solution allows the contact line to slip. Since its introduction, slip has became the most popular solution to the problem of contact lines for low viscosity systems (Huh and Scriven, 1971; Dussan, 1976a, 1976b, 1979; Hocking, 1976, 1977, 1981, 1982; Huh and Mason, 1977; Lowndes, 1980; Davis, 1983; Tilton, 1988; Blake, 1988; Wesson and Papanastasiou, 1988). Despite its popularity, the physical basis for slip and, moreover, the appropriate form of the slip boundary condition remains unknown (Blake, 1988). Most of the work has been carried on low viscosity, fluid/air systems. Joanny and Andelmann (1987), however, suggested that "... this idea [slip], although successful from a mathematical point of view, is not well justified from a physical point of view, except in the case of polymeric liquids of high molecular weight. There, the presence of entanglements causes a *plug flow*; hence entangled polymeric liquids behave as solids and therefore have a finite slip velocity on the solid surface...". Similar ideas have been proposed by de Gennes (1979) who states that polymer melts have very special spreading laws and certain flow regimes could be understood based on the idea that polymers flowing near a smooth surface tend to have an anomalous slippage. This idea is supported by the experimental work of Galt and Maxwell (1964).

As mentioned before, much work has been done finding an appropriate form for the slip boundary condition. The model most commonly used in fluid/air systems or single-fluid systems is the Navier (or linear) slip model (Huh and Scriven, 1971; Huh and Mason, 1977; Bruns, 1980; Silliman and Scriven, 1980; Wesson and Papanastasiou, 1988). Wesson and Papanastasiou found that the introduction of the slip boundary condition makes the problem of viscoelastic extrudate swell independent of mesh even though the slip condition does not help in reaching a solution for a high We number. Chafforeaux et al. (1979) and Ramamurthy (1986) proposed that certain polymers obey a power-law slip model of the form $V_s = \beta \tau^n + \alpha$, where τ is the wall shear stress and V_s the wall slip velocity, and *n* is the power-law index. Other researchers (Kozicki et al, 1970; Cohen and Metzner, 1985) found a similar relation for capillary flow of polymeric solutions. In all the cases studied, the power-law index n for slip of a polymer on a wall was found to be greater than 1 (Chafforeaux et al., 1979; Ramamurthy, 1986; Cohen and Metzner, 1985; Hatzikiriakos and Dealy, 1991). Hatzikiriakos et al. (1991, 1992 a,b,c, 1993a,b) have studied the slip boundary condition for polymer melts. Based on molecular-level analysis of how polymer and wall interact with each other, he has proposed several complex models for predicting slip velocities as a function of wall shear stress, temperature, interfacial tension and molecular characteristics of the polymers involved. These models involve an exponential dependence of slip velocity on temperature, polymer microstructure and wall shear stress.

Another theory with regards to polymer melts is that slip occurs only when a critical wall shear stress level is reached, i.e., the boundary condition is a yield-stress slip

boundary condition (Durbin, 1988). It is believed that a certain force is needed to dislodge the fluid from the wall (Ramamurthy, 1986).

The slip boundary condition applies only in a microscopic region of molecular magnitude (few Å at the most) near the contact line (Huh and Mason, 1977; Silliman and Scriven, 1980; Pomeau and Pumir, 1984; Tu, 1987) while the rest of the fluid wetting the die walls obeys the common no-slip boundary condition. Durbin (1988) and others have proposed several slip models including a smooth transition from the slip region to the no-slip region by making the β coefficient length-dependent. However, the extent and form of this slip length for general application is not clear.

Other authors suggest that the flow mechanism that probably governs the three-phase motion in the absence of surface tension is the condition of angle of contact, i.e., the proper boundary condition is to impose a fixed contact angle. For vanishing-viscosity-ratio systems (like air/water/solid), some authors (Dussan and Davis, 1974; Benney and Timson, 1980; Pismen and Nir, 1982; Ngan and Dussan, 1984) suggest that the hydrodynamic contact angle should be near 180°, i.e., the liquid advances in a "caterpillar-tread" rolling motion thus retaining the no-slip boundary condition.

It is important to note that most of the above deductions were done for low viscosity fluids and, in most cases, for air/water/solid systems. Few attempts have been done so far to study high viscosity flow systems and none has dealt with contact lines for highly viscous polymer flows. For polymeric fluids, most of the modeling work has been done through finite element calculations. However, there has not been a suitable contact line boundary condition proposed and alternative methods have been employed. Dheur

and Crochet (1987) used fixed contact angle and extrapolation methods for calculating the location of the contact point in two-dimensional simulations. The extrapolation method consists of locating the contact point by extrapolation of the interface shape which is calculated up to one node before the wall. Both methods produced basically the same results. Karagiannis (1989a) used the linear and polynomial extrapolation methods for his three-dimensional calculations and found that a linear extrapolation was sufficient.

It is obvious that a study of the possible boundary conditions for the contact line in high viscous fluid/fluid system is needed. This is the subject of Chapter 4.

2.1.5 Viscoelastic constitutive equations for polymer melts.

It is widely recognized that viscoelastic effects are important in polymer processing applications. A viscoelastic effect is defined as a flow phenomenon that can not be described on the basis of linear or non-linear purely viscous behavior, i.e., it has an elastic component. The classical Navier-Stokes equations are no longer valid since they are unable to describe certain fluid features, such as shear-rate dependence on viscosity, presence of normal stresses in shear flows, high resistance to elongational flows and others (Bird et. al, 1987). The major challenge is to formulate suitable constitutive equations capable of predicting all the experimentally observed non-Newtonian phenomena. All constitutive equations proposed so far, which are useful for polymer melt flows, are extremely complicated to handle, even for simple flows. The characteristic dimensionless number in viscoelastic flows is the Weissenberg number, Wi, which is the ratio of elastic forces to viscous forces and it is defined (for one-mode constitutive

equations) as $\lambda\dot{\gamma}_c$, where λ is a characteristic retardation time and $\dot{\gamma}_c$ is a characteristic velocity gradient (wall shear rate, $\dot{\gamma}_w$, or average velocity gradient, U/L, where U and L are average velocity and length, respectively). Mitsoulis (1984) reported typical values of Wi in the order of 10 for extrusion flows.

One of the most important problems to be addressed in viscoelastic flow modeling is the correct imposition of flow boundary conditions. Since viscoelastic fluids are "memory" fluids, i.e., present behavior is somehow dependent on its past stress history, this pre-history of the fluid motion must be specified. Also, the usual no-slip boundary condition at solid boundaries is not always appropriate in polymer processing of viscoelastic flows (Keunings, 1989, Ramamurthy, 1986). Outflow boundary conditions are also a major question in viscoelastic flow simulations if a secondary flow is present.

Viscoelastic constitutive equations can be classified into three major groups: empirical equations, differential models and single-integral models. Each of them may or may not contain a Newtonian component. The feature which makes viscoelastic constitutive equations of the differential or integral type difficult to handle is that the relation between stresses and velocity gradients is usually non-linear. In the models for which this relation is explicit, as in the empirical models, the constitutive equation fails to predict many of the relevant features of viscoelastic flows, or its validity is limited to low elastic levels.

For purposes of analysis, the extra-stress tensor τ can be decomposed into the sum of Newtonian and viscoelastic components, τ_n and τ_v, respectively. Depending on the definition of τ_v, a given model will be differential or integral. However, any differential

or integral model is implicit in terms of the viscoelastic extra-stress tensor. Empirical equations, being explicit in the viscoelastic extra-stress tensor, were among the first used in mathematical and computational modeling. Among the simple models, probably the most well known is the second order model, given by:

$$\tau_v = -\frac{1}{2}\psi_1 \frac{\Delta\dot{\gamma}}{\Delta t} + (\frac{1}{2}\psi_1 + \psi_2)(\dot{\gamma}\cdot\dot{\gamma})$$
$$\frac{\Delta\dot{\gamma}}{\Delta t} = u\cdot\nabla\dot{\gamma} + \frac{1}{2}[(\omega\cdot\dot{\gamma}) - (\dot{\gamma}\cdot\omega)] \qquad (2\text{-}1)$$

where ψ_1 and ψ_2 are constant material properties, u is the velocity vector, $\dot{\gamma}$ is the strain-rate tensor, ω is the vorticity tensor, and $\Delta\dot{\gamma} / \Delta t$ is the contravariant derivative of the strain rate tensor as defined by Oldroyd (1950). Equation (2-1) does not show the "viscous" component of the stress, $\eta\dot{\gamma}$. When material properties are functions of the shear rate, the second order model transforms into the CEF (Criminale-Ericksen-Filbey) equation (Bird et al., 1987). The above equation is explicit in terms of the extra-stress tensor components, and it can be substituted into the governing equation to yield a differential equation in terms of u and P. Note that these empirical constitutive equations should be used only for low elasticity problems (Vlachopoulos, 1990). Mitsoulis (1984) introduced a very simplified equation to model the swelling phenomena in two-dimensional flows. He considered the viscoelastic component of the extra-stress tensor to be:

---

1 Unless otherwise indicated in this section, τ without a subscript will indicate the viscoelastic tensor component of the extra-stress tensor from this point onwards.

$$\begin{aligned} \tau_{11} &= A\,\dot{\gamma}_{12}^{b} \\ \tau_{ij} &= 0 \quad ; \quad i \neq 1 \,; j \neq 1 \end{aligned} \tag{2-2}$$

where A and b are material functions. These models are only valid in slightly elastic unidirectional and slow flow situations. These explicit models would be useful in the first stages of an analysis. For the second-order model, the Giesekus-Tanner theorem states that any creeping, Newtonian velocity field is also a solution for the second-order incompressible fluid (Bird et al., 1987). The pressure field can be obtained from Newtonian solutions for plane flow by invoking the Giesekus-Tanner-Pipkin theorem (Mitsoulis, 1984). Another big advantage of second-order fluids is that the first and second normal stress differences are easily imposed and manipulated (Bird et al., 1987).

Differential and integral models may contain a purely viscous component (usually Newtonian) of the extra-stress tensor. Viscoelastic models without a purely viscous component may exhibit hyperbolic phenomena. Differential models can be written as (Keunings, 1989):

$$A(\tau)\cdot\tau + \lambda \frac{\delta\tau}{\delta t} = \mu_{v}\,\dot{\gamma} \tag{2-3}$$

where λ is a relaxation time, μ is a viscosity coefficient and A is a model-dependent tensor function. $\delta\tau/\delta t$ is defined by Keunings as "an objective derivative", i.e., a linear combination of lower- and upper-convected derivatives. Thus:

$$\frac{\delta\tau}{\delta t} = \zeta\tau^{(1)} + (1+\zeta)\tau_{(1)}$$
$$\tau^{(1)} = \frac{D\tau}{Dt} + \tau\cdot\nabla u^T + \nabla u\cdot\tau \qquad (2\text{-}4)$$
$$\tau_{(1)} = \frac{D\tau}{Dt} - \tau\cdot\nabla u - \nabla u^T\cdot\tau$$

where $\tau^{(1)}$ and $\tau_{(1)}$ are the lower-convected and upper-convected derivative of the extra-stress tensor, respectively, and ζ is a weighing factor. Equation (2.4) is implicit in terms of the extra-stress tensor, and represents a non-linear relation between stresses and velocity gradients. In principle, this general equation is capable of describing memory effects. Unfortunately, when classical Galerkin methods are used to discretize the momentum and constitutive equations, a number of numerical complications arise (Rajagopalan et al., 1990). Depending on the choice of the tensor-dependent function, $A(\tau)$, different models can be obtained. For Maxwell, Phan-Thien and Tanner (1977) and Giesekus (1982) models, $A(\tau)$ is defined as:

$$A=\delta$$
$$A = \exp\left[\frac{\epsilon\lambda}{\eta_v} tr(\tau)\right] \qquad (2\text{-}5)$$
$$A = \delta + \frac{\alpha\lambda}{\eta_v}\tau \qquad (\zeta=0)$$

respectively. ε and α are material properties. In principle, upper-convected (ζ=0), corotational (ζ=0.5) and lower-convected (ζ=1) models can be obtained, but this has been done only for Maxwell models. Based on rheometric data, ζ should be between 0 and 0.1 (Keunings, 1989). The upper-convected Maxwell model becomes the Oldroyd-B model with the introduction of a Newtonian viscosity. Multiple relaxation modes can be achieved by expanding the general equation to be a finite sum of partial stresses, each one having material properties associated with a particular relaxation mode.

A single-integral model calculates the viscoelastic extra-stress using a time integral of the deformation history. These models are more complicated than differential models and their use in numerical modeling is quite recent. All integral models are of the form:

$$\tau(t) = \int_{-\infty}^{t} m(t-t')\, S_t(t')\, dt'$$
$$S_t(t') = \phi_1(I_1,I_2)\left(C_t^{-1}(t') - \delta\right) + \phi_2(I_1,I_2)\left(C_t(t') - \delta\right) \qquad (2\text{-}6)$$

In the above expression, S_t is a deformation-dependent tensor, expressed as a function of the right Cauchy-Green tensor C_t and its inverse, known as the Finger tensor (Vlachopoulos, 1990). The functions Φ_1 and Φ_2 are dependent on the trace of the right Cauchy-Green tensor and the trace of the Finger tensor. The factor $m(t-t')$ is a function that reflects the deformation-history dependence of the stress field, usually expressed as a finite series of exponential functions. By specifying the functions Φ_1 and Φ_2 several models can be obtained. The most popular models are those of Lodge (1964), Doi and Edwards (1978a,b,c,d) and the K-BKZ model of Bernstein et al., (1963) and Kaye (1962).

Apart from their intrinsic complexity, integral models are difficult to implement in an Eulerian fluid flow description, because accurate particle path tracking is not easy.

Introduction of differential or integral models in a mathematical description within a given flow situation is a rather involved process. Even the introduction of one of the simplest models, such as a Maxwell fluid, leads to formidable expressions for the momentum equation. This can be seen by substituting the constitutive equation into the momentum equation. Moreover, the resulting system of equations have stresses, velocities and pressures as primitive variables due to the implicit nature of the constitutive equation. This leads to another complication: the imposition of inflow and outflow boundary conditions for the extra-stress tensor. So far, there is no adequate theory that provides appropriate information on how to implement these boundary conditions in general. It is important to note that for integral models used in conjunction with synthetic boundaries, some knowledge of the stress history outside the synthetic boundary is required in order to calculate the integral in Eq. (2-6). With differential models, the stress pre-history outside the inlet boundary is not required (Keunings, 1989).

Two main approaches have been developed for the solution of the viscoelastic fluid flow problem with implicit constitutive equations. In the *decoupled* approach, a guessed velocity field is used to calculate a stress field, which, in turn is used to get a new velocity field, until convergence is achieved. On the other hand, the *coupled* approach treats the stress field as another primary variable together with velocity and pressure field. Usually a Newton-Raphson scheme is used to obtain a quadratic rate of convergence as opposed to the decoupled method, which has intrinsically linear

convergence. The disadvantage of the coupled method is the large number of unknowns and the imposition of suitable boundary conditions for the stress field. Crochet (1989) and Keunings (1989) provide a detailed analysis of both approaches.

Crochet (1989) divided the current research in viscoelastic fluid flows into two separate, but not opposed trends. One group of researchers is trying to overcome the problem known as the High Weissenberg Number Problem (HWNP), which is a general description for failure to reach numerical convergence in a variety of problems for Wi>1. This group of researchers puts great emphasis on understanding the mathematical and numerical nature of the divergence by using relatively simple models and flow situations. By introducing subelements and streamline upwinding, higher Weissenberg number simulations can be achieved. As an alternative, Marchal and Crochet (1987) subdivide the basic nine-node Lagrangian element into subsets of linear elements for stresses, with the use of streamline upwinding techniques. Probably, the most comprehensive work in this field was done by Hughes and Brooks (1982), who introduced the streamline upwind Petrov-Galerkin method (artificial diffusivity along streamlines with no crossflow diffusion) to successfully deal with highly advective problems. This method was effectively used in viscoelastic fluid flow calculations by Marchal and Crochet (1987) and Debbaut et al. (1988) who found no limit in the Weissenberg number for Oldroyd-B, Phan Thien-Tanner and Giesekus-Leonov fluids in contractions.

The other trend followed in viscoelastic fluid flow simulations is to find suitable numerical methods for more realistic constitutive equations. One of the most important problems in modeling viscoelastic fluid flow is tracking the fluid particle path in order

to calculate the viscoelastic extra-stress tensor. This would imply the calculation of streamlines for every point in which such a calculation is needed. In order to avoid this difficulty, Papanastasiou et al. (1985) developed the concept of streamlined finite elements for flows without recirculation. The computational domain can be divided in series of stream surfaces which, in turn, can be subdivided into finite elements. By using this technique, the calculation of τ_v is only performed at a limited number of streamlines. Even though this method allows the use of more realistic integral models in simulations, such as K-BKZ (Dupont and Crochet, 1988; Luo and Mitsoulis, 1989,1990) and Doi-Edwards (Dupont et al., 1985) models, their performance is not better than the models developed for differential models. An extensive review of the publications in this area can be found in Crochet (1989) and Keunings (1989).

Most of the work done so far has been limited to two-dimensional, isothermal, steady-state flows. Attempts to include thermal effects and three-dimensional features increase the size of the system by adding the energy balance (and/or the third component in the momentum equation). Also, the thermal dependance of the viscoelastic parameters is not well understood yet.

2.2 Mathematical formulation.

The governing equations, in dimensionless form, for the steady-state flow of two viscous fluids inside a die, under the assumptions of incompressibility, creeping flow, and no body forces, are:

$$\nabla \cdot \tau_j - \nabla P_j = 0 \tag{2-7}$$

$$Pe(u_j \cdot \nabla T_j) = \nabla^2 T_j + Br(\tau_j : \nabla u_j) \tag{2-8}$$

$$\nabla \cdot u_j = 0 \tag{2-9}$$

where τ is the extra-stress tensor, P is the pressure, u is the velocity vector u= (u,v,w) and T is the temperature. Indices j=1 and j=2 refer to the lower and upper melt layers, respectively (Figure 2.4). Note that the eq. (2-7), (2-8) and (2-9) applies to any number of fluids. In this work, however, only bicomponent flows are studied. A Generalized Newtonian constitutive equation is used to model the stress-strain relation for polymers[2]:

$$\tau_{ij} = \eta_j \left(\frac{\partial u_i}{\partial x_j} + \frac{\partial u_j}{\partial x_i} \right) \tag{2-10}$$

where x is the coordinate vector, x=(x,y,z). The viscosity function is defined as:

---

2 More realistic constitutive equations for capturing viscoelastic phenomena are discussed in Chapter 6.

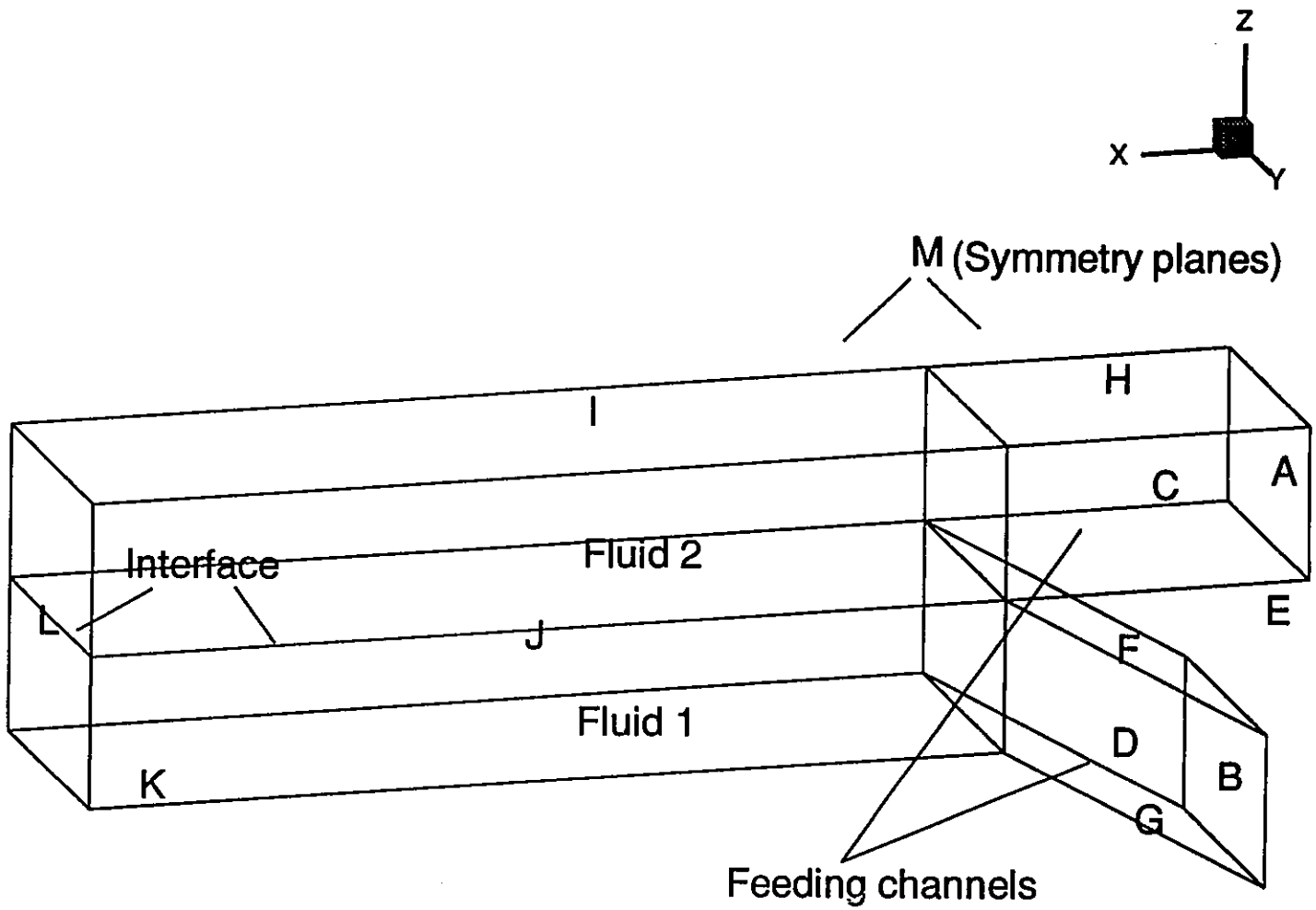

Figure 2.4. Schematic of a coextrusion die.

where,

$$I_2 = \dot{\gamma}_{ij}\dot{\gamma}_{ji}$$

$$\dot{\gamma}_{ij} = \frac{\partial u_j}{\partial x_i} + \frac{\partial u_i}{\partial x_j} \tag{2-12}$$

In (2-11), η_{0j} , λ_{cj}, b_j and n_j are material parameters. Note that the viscosity is temperature and shear-rate dependent. The dimensionless groups and variables used in equations (2-7) to (2-12) are:

$$Pe_j = \frac{\rho_j' C_{pj}' UL}{k_j'} \qquad Br_j = \frac{\eta_{01}' U^2}{k_j'(T_w - T_\infty)}$$

$$x_i = \frac{x_i'}{L} \qquad u = \frac{u'}{U}$$

$$P = \frac{P'L}{\eta_{01}U} \qquad \tau = \frac{\tau' L}{\eta_{01}U} \tag{2-13}$$

$$T = \frac{T' - T_0}{T_0 - T_\infty} \qquad \eta_j = \frac{\eta_j'}{\eta_{0j}}$$

$$b_j = b_j'(T_0 - T_\infty)$$

where Pe_j is the Peclet number for fluid j, Br_j is the Brinkmann number for fluid j, L is a characteristic length (in this case the die height), U is the total average velocity (total flowrate over total cross-sectional area for both fluids), η_{0j} is the zero-shear viscosity at the reference temperature of fluid j (assumed to be $T_0 = 250°C$ throughout this thesis), C_{pj} is the specific heat of fluid j, k_j is the thermal conductivity of fluid j, ρ_j is the density of fluid j, T_w and T_∞ are the wall and ambient temperatures, respectively, and a prime (') denotes a dimensional variable.

Boundary conditions are required to complete the problem formulation. A schematic of a typical feedblock die for two fluids is shown in Figure 2.4. At the die inlet area (surfaces A and B), either a fully developed or a flat profile for both velocities and temperatures are imposed. For the fully developed flow conditions, the momentum and energy conservation equations at the inlet plane reduce to Poisson-type equations, which are solved for the surfaces A and B to obtain the fully developed inlet velocity and temperature profiles, respectively:

$$\eta_j\left(\frac{\partial^2 u_j}{\partial y^2}+\frac{\partial^2 u_j}{\partial z^2}\right)=\frac{\partial P_j}{\partial x}$$
$$\frac{\partial^2 T_j}{\partial y^2}+\frac{\partial^2 T_j}{\partial z^2}=-Br_j\left[\left(\frac{\partial u_j}{\partial y}\right)^2+\left(\frac{\partial u_j}{\partial z}\right)^2\right] \qquad (2\text{-}14)$$

where u is the velocity in the main flow direction, which can be x for fluid 2 or the normal to surface B for fluid 1. At the die walls (surfaces C,D,E,F,G,H,K,I) the

temperature is fixed and the no-slip boundary condition is applied to the bulk fluid phase. Surface J contains the contact line, which is the intersection of the interface separating the two fluids and the die wall. Imposition of the no-slip boundary condition at the contact line leads to a well-known mathematical singularity (for example, Dussan, 1976 and Davis, 1983), often expressed as multivalued velocities or infinite shear stresses. The no-slip or stick model and several forms of localized slip models, were used by Torres et al., (1993) to capture more complicated interface shapes and to consider wall effects in polymer coextrusion. The appropriate contact line boundary condition is the subject of chapter 4. At the die exit, surface L, zero traction and zero cross flows ($v = w = 0$) are imposed.

At the interface away from the die wall, in the absence of normal forces due to viscoelasticity, the dynamic and kinematic boundary conditions are, respectively:

-Equilibrium of forces:

$$\begin{aligned} n\cdot\sigma_1 &= n\cdot\sigma_2 + \frac{2Hn}{Ca_j} \\ t_I\cdot\sigma_1 &= t_I\cdot\sigma_2 \\ t_{II}\cdot\sigma_1 &= t_{II}\cdot\sigma_2 \\ \sigma_j &= -P_j I + \tau_j \end{aligned} \qquad (2\text{-}15)$$

- Continuity of tangential velocities and vanishing velocity normal to the interface:

$$\begin{aligned} \boldsymbol{t}_I \cdot \boldsymbol{u}_1 &= \boldsymbol{t}_I \cdot \boldsymbol{u}_2 \\ \boldsymbol{t}_{II} \cdot \boldsymbol{u}_1 &= \boldsymbol{t}_{II} \cdot \boldsymbol{u}_2 \\ \boldsymbol{n} \cdot \boldsymbol{u} &= 0 \end{aligned} \qquad (2\text{-}16)$$

where σ is the total stress tensor for fluid j, $\boldsymbol{n}$ is the outward normal vector to the interface, and $\boldsymbol{t}_I$ and $\boldsymbol{t}_{II}$ are the tangential vectors at the interface (chosen to be aligned with the two principal directions that define the interface in the parent element), $H = -\nabla \boldsymbol{n}/2$ is the mean curvature of the interface, $Ca_j = \eta_{01} U/\Gamma_j$ is the capillary number and Γ_j is the interfacial tension for fluid j. For polymer melts, the effects of interfacial tension are outweighed by the viscous forces (Karagiannis, 1989a, Torres et al., 1995). Even though two given polymers may be miscible, little or no diffusion across the interface occurs in polymer coextrusion flows since the flow is mainly unidirectional with viscous forces much stronger than interfacial forces (see Chapter 5).

CHAPTER 3

BICOMPONENT FINITE ELEMENT MODEL

3.1 Introduction.

In this chapter, the Galerkin/Finite Element Method (G-FEM) is applied to the set of governing equations and boundary conditions (2-7),(2-8),(2-9),(2-10),(2-15),(2-16) that govern the flow of molten polymers inside a die. The G-FEM reduces the set of partial differential equations to a set of algebraic equations representing the discretized problem. Numerical considerations regarding the application of G-FEM to the bicomponent flow of polymer melts are also presented.

3.2 Galerkin method.

The finite element method has been used as a numerical method for structural analysis since the mid '50s. Several texts provide the necessary mathematical background of the method applied to fluid mechanics problems (Taylor and Hughes, 1981; Crochet et al., 1984; Dhatt and Touzot, 1984; Reddy, 1984; Burnett, 1987). The following paragraphs present the basics of the finite element method as applied to free surface problems in polymer melt flows.

The finite element method divides the flow domain into a number of finite elements, generally of tetrahedral or brick shapes, and the primitive variables (in this case, three velocity components, pressure, interface location, temperature, viscoelastic stress

components) are approximated within every finite element with low-order polynomials. Two types of elements were used in this project: the 27-node triquadratic brick element (Figure 3.1) and the 8-node trilinear brick element (Figure 3.2), both members of the Lagrangian family of elements. Within an element, nodal coordinates, velocity, pressure, temperature and viscoelastic stresses can be interpolated by:

$$
\begin{aligned}
u_i^{(e)} &= \sum_i^{ne} N_i(\xi,\eta,\zeta)\, u_i \\
x_i^{(e)} &= \sum_i^{ne} N_i(\xi,\eta,\zeta)\, x_i \\
P^{(e)} &= \sum_i^{ne} N_{P_i}(\xi,\eta,\zeta)\, P_i \\
T^{(e)} &= \sum_i^{ne} N_i(\xi,\eta,\zeta)\, T_i \\
\tau^{(e)} &= \sum_i^{ne} N_i(\xi,\eta,\zeta)\, \tau_i
\end{aligned}
\qquad (3\text{-}1)
$$

respectively, where u is the nodal vector of velocities (u,v,w), P is the nodal pressure, T is the nodal temperature, and τ is the nodal viscoelastic stress tensor. The superscript $^{(e)}$ indicates a local (element) approximation, while subscript $_{(i)}$ refer to node locations, *ne* being the number of nodes in an element. In order to get an accurate finite element solution, it is well known that pressure should be interpolated with basis functions that are one order lower that those for velocity (Taylor and Hood, 1973). Linear interpolating functions are used for pressure when quadratic interpolating functions are used for velocity components and temperature (in the case of the 27-node triquadratic brick

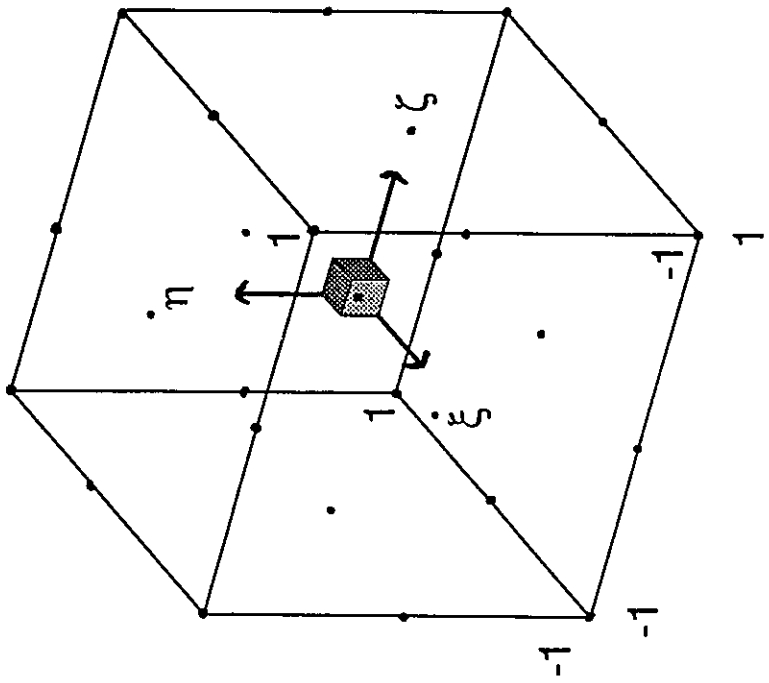

Figure 3.1. 27-node triquadratic element.

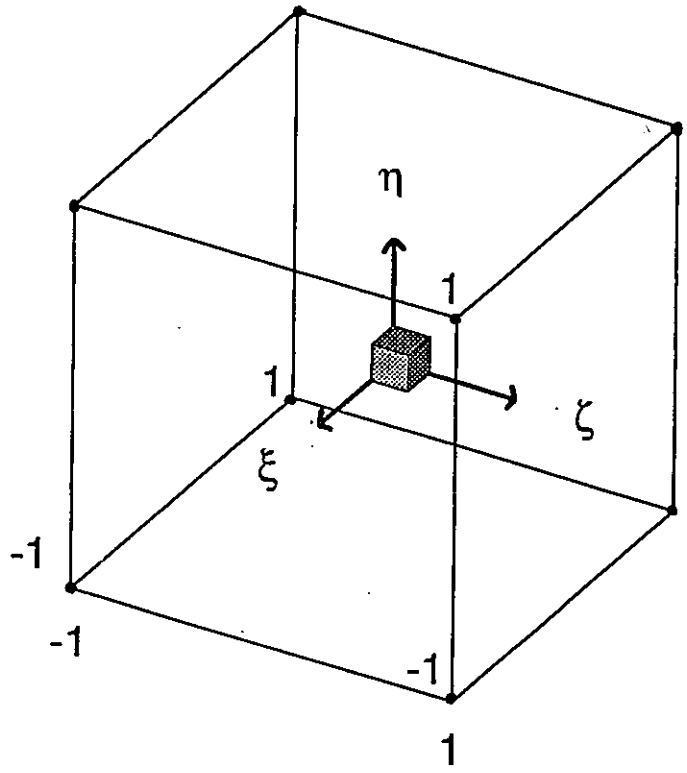

Figure 3.2. 8-node trilinear element.

element) For the 8-node trilinear brick element linear basis functions are used for velocities and temperature, the pressure is assumed to be constant within an element.

Coextrusion flows within the die are characterized by the presence of internal fluid/fluid interfaces. The first free surface calculations using the G-FEM were performed by Nickell et al. (1974) for air/fluid interfaces in extrudate swell. In this thesis, the spine method (Karagiannis, 1989a) is used to parameterize the free surface (interface). The free surface is calculated isoparametrically by assuming $\eta=1$ (the surface in the parent element that coincides with the interface). Therefore, the interface is located as:

$$x^{(e)} = \sum_{i}^{nfs} N_i(\xi,\eta=1,\zeta)x_i \tag{3-2}$$

where *nfs* is the number of nodes that define a free surface in an element. The finite element approximations for the field variables and geometry are inserted in the governing equations and boundary conditions. The finite element polynomial approximations do not satisfy the governing equations exactly and there remains a residual error for each discretized equation. These residuals are weighted with basis functions and integrated over the solution domain. In the standard Galerkin method the basis functions are chosen to be the same as the interpolating functions. The momentum and energy equations are weighted with the velocity and temperature interpolating functions while the continuity equation is weighted with the pressure interpolating functions (Reddy, 1984; Burnett, 1987). Application of this procedure gives the weak form of the governing equations:

$$\int_{\Omega} \{\nabla\cdot\sigma_k\} N^i d\Omega = 0 \tag{3-3}$$

$$\int_{\Omega} \{ \nabla \cdot u_k \} N_p^i d\Omega = 0 \tag{3-4}$$

$$\int_{\Omega} \{ Pe\ (u_k \cdot \nabla T_k) - \nabla^2 T_k - Br(\tau_k : \nabla u_k) \} N^i d\Omega = 0 \tag{3-5}$$

After transformation from global to local coordinates (Dhatt and Touzot, 1984) and the application of the divergence theorem to (3-3) to (3-5) within an element:

$$R_x^i = \int_{-1}^{1}\int_{-1}^{1}\int_{-1}^{1} \left[(-P+2\eta u_x) N_x^i + \eta(u_y+v_x) N_y^i + \eta(u_z+w_x) N_z^i \right] |J| d\xi d\eta d\zeta \tag{3-6}$$

$$R_y^i = \int_{-1}^{1}\int_{-1}^{1}\int_{-1}^{1} \left[\eta(u_y+v_x) N_x^i + \eta(-P+2\mu v_y) N_y^i + \eta(v_z+w_y) N_z^i \right] |J| d\xi d\eta d\zeta \tag{3-7}$$

$$R_z^i = \int_{-1}^{1}\int_{-1}^{1}\int_{-1}^{1} \left[\eta(u_z+w_x) N_x^i + \eta(v_z+w_y) N_y^i + \eta(-P+2\mu w_z) N_z^i \right] |J| d\xi d\eta d\zeta \tag{3-8}$$

$$R_T^i = \int_{-1}^{1}\int_{-1}^{1}\int_{-1}^{1}\left[N^i(uT_x+vT_y+wT_z)+N_x^iT_x+N_y^iT_y+N_z^iT_z-N^iBr\dot{\gamma}^2\right]|J|d\xi d\eta d\zeta \quad (3\text{-}9)$$

$$R_c^i = \int_{-1}^{1}\int_{-1}^{1}\int_{-1}^{1}\left[u_x+v_y+w_z\right]N_p^i|J|d\xi d\eta d\zeta \quad (3\text{-}10)$$

where N_x, N_y, N_z are the derivatives of the shape function with respect to x,y,z, respectively. The weighted residual of the kinematic boundary condition is:

$$R_k^i = \int_{-1}^{1}\int_{-1}^{1}\{n\cdot u\}N^i|J^*|d\xi d\zeta, \qquad \eta=1 \quad (3\text{-}11)$$

In the above equations, $|J|$ and $|J^*|$ are the Jacobian for the isoparametric transformation for the volume and surface integral, respectively:

$$\begin{aligned} |J| &= x_\xi y_\eta z_\zeta + x_\zeta y_\xi z_\eta + x_\xi y_\eta z_\zeta + x_\eta y_\zeta z_\xi + x_\zeta y_\eta z_\xi + x_\xi y_\zeta z_\eta + x_\eta y_\xi z_\zeta \\ |J^*| &= \left(n_1^2+n_2^2+n_3^2\right)^{\frac{1}{2}} \end{aligned} \quad (3\text{-}12)$$

where subscripts ξ,η,ζ indicate differentation with respect to local coordinates and n_1 , n_2 and n_3 are the components of the outward normal vector to the free surface, and subscripts indicate derivatives with respect to the subscript dimension.

The above procedure reduces the set of differential equations (2-7), (2-8), (2-9), (2-15), (2-16) in the flow domain to a set of algebraic equations within the finite elements. Coupling the equations for all the elements leads to a system of equations of the form:

$$\boldsymbol{R}(\boldsymbol{X}) = \mathbf{0} \tag{3-13}$$

where $\boldsymbol{R}$ is the vector of residuals and $\boldsymbol{X}$ is the vector of unknowns, defined as:

$$\boldsymbol{R}^T = \left[R_x{}^T, R_y{}^T, R_z{}^T, R_c{}^T, R_k{}^T, R_T{}^T\right] \tag{3-14}$$

$$\boldsymbol{X} = \left[U^T, P^T, h^T, T^T\right] \tag{3-15}$$

A Newton-Raphson procedure is used to solve the system of non-linear equations stated in (3-13). The Newton-Raphson method, together with the spine approach, solves the velocity, temperature and pressure fields and the interface locations simultaneously. A detailed explanation of the Newton-Raphson procedure applied to finite element calculations can be found in Dhatt and Touzot (1984, p. 297 ss). The calculation of the Jacobian entries ($\partial R/\partial X$) were done analytically and checked by a central difference scheme (Mavridis, 1988).

In equation (2-15) it was stated that one of the interfacial boundary conditions is the continuity of forces across the interface. However, this does not imply that the

pressure nor the normal stress components are continuous across the interface (Mavridis, 1988; Dheur and Crochet, 1987). The normal stress boundary condition at the interface, in the absence of interfacial tension and normal forces due to viscoelasticity, is defined as: (Mavridis et al., 1987)

$$(P_2 - P_1) = 2(\eta_1 - \eta_2)\frac{\partial u_t}{\partial t} \tag{3-16}$$

u_t is the tangential velocity at the interface and t is a tangential vector to the interface. This means that a pressure discontinuity will occur whenever the two fluids have different viscosities. It is also known that non-negligible interfacial tension effects can cause this discontinuity (Mavridis et al., 1987; Dheur and Crochet, 1987). One technique to tackle this problem is the use of two pressure variables per node at the interface (Mavridis, 1988) and the other approach is to use a penalty function formulation with discontinuous pressure across interfacial boundaries (Dheur and Crochet, 1987). Dheur and Crochet (1987) for two-dimensional calculations and Karagiannis (1989a) for the three-dimensional model concluded that both approaches produced the same result. The two pressure variable technique (also known as u-v-w-P_1-P_2-h formulation) was chosen for this work.

In this approach, two pressure variables are assigned to each node along the interface and the pressure is approximated using (3-1) and the continuity residual equation (3-10) is written separately for each fluid. In fluid 1, contributions to the continuity

residual are taken into account with respect to P_1, while P_2 is set to zero. In fluid 2, contributions are taken only with respect to P_2, while P_1 is set to zero.

The set of equations (3-13) is non-linear due to the shear-thinning feature of the polymers, the coupling between the energy and momentum equations and the presence of fluid/fluid interfaces. As mentioned above, a Newton-Raphson procedure is employed to solve the non-linear system of equations. Two termination criteria for the desired set of parameters and boundary conditions can be defined in a Newton-Raphson procedure:

$$\max_i |X^{n+1} - X^n| \leq \epsilon_1 = 10^{-3}$$
$$\max_i |R_i| \leq \epsilon_2 = 10^{-3} \qquad (3\text{-}17)$$

Both criteria must be satisfied for every problem in order to achieve convergence. The solution is also checked by calculating the difference between the inlet and outlet flowrates which, for all cases reported in this work, is less than 1%. Symmetry conditions were used (surface M in Figure. 2.4) to reduce the size of the solved problem. All calculations were done with IBM RS6000 370 AIX workstations (c. 26 DP LINPACK MFLOPS), a Silicon Graphics IRIS-4D/35 workstation (c. 4.5 MFLOPS) or a Multiflow 4.3 BSD Trace/Unix machine (c. 20 MFLOPS) using a Fortran 90 compiler.

3.3 Numerical considerations.

Numerical integration and solution of the system of equations.

The numerical integration performed in the code (eq. 3-6 to 3-11) uses the Gauss method (Zienkiewicz, 1987) with three quadrature points, except for the slip boundary condition, where four weight points were used.

A modified version of the frontal solver routine of Taylor and Hood (1973) is used to solve equation (3-12). The solver was developed in such a way that allows a core solution (no disk access needed) or a disk-storage routine, depending on the size of the problem and the computer RAM capacity.

Interface update scheme.

In this work, the interface is described using the spine technique of Kistler and Scriven (1984), and its extension to three-dimensional flows of Karagiannis (1989a). The big advantage of the spine technique over the traditional pathline method (Nickell et al., 1974) is that it allows a simultaneous calculation of interface locations together with the field variables of interest.

In the spine method, the interface is parameterized on three-dimensional lines that are defined by two fixed end points (at the bottom and top die walls). Nodal positions are then assigned along this line. The interface is located in a midside point, and its relative location with respect to the two fixed end points that define the spine is denoted by h (Figure 3.3):

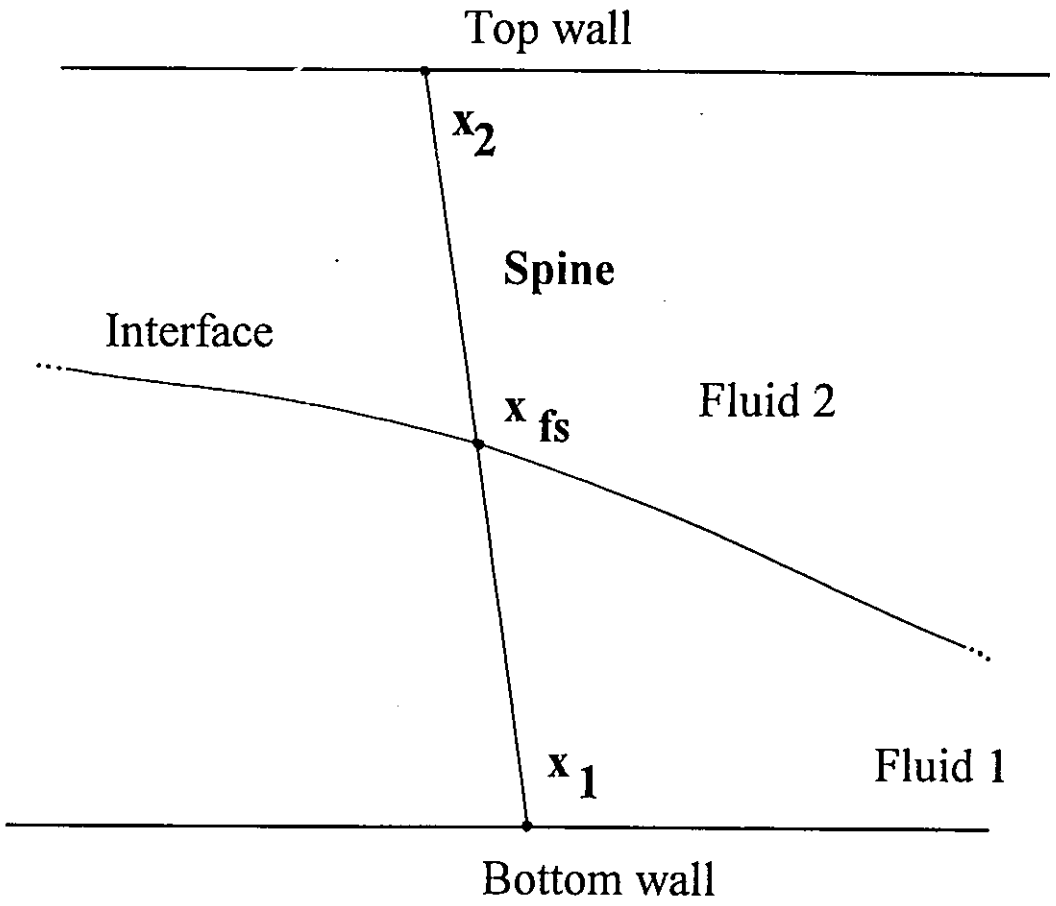

Figure 3.3. Spine definition.

$$x = x_1 + w(z)(x_2 - x_1)$$

$$h = \frac{x_{fs} - x_1}{x_2 - x_1} \tag{3-18}$$

where w(z) is the relative location of point x and x_{fs} is the free surface location. At the element level, the internal free surface (interface) is described in the classical finite element representation:

$$x_{fs} = \sum_{i=1}^{nfs} x_{fs}{}^{i}\, \phi^{i}(\xi, \eta=1, \zeta) \tag{3-19}$$

where *nfs* indicates the number of nodes on the interface. Every elemental interface is therefore defined uniquely by the spines that passes through the interfacial nodes (Figure 3.4). At the end of every iteration, the element locations are modified according to the newly calculated interface location. For highly non-linear problems, a relaxation factor for the interface update may be introduced:

$$x_{fs}^{i+1} = \alpha x_{fs}^{*} + (1-\alpha) x_{fs}^{i} \tag{3-20}$$

where x_{fs}* is the calculated interface, α is a relaxation factor ($0 \le \alpha \le 1$), and the superscript ^{i} indicates the iteration counter.

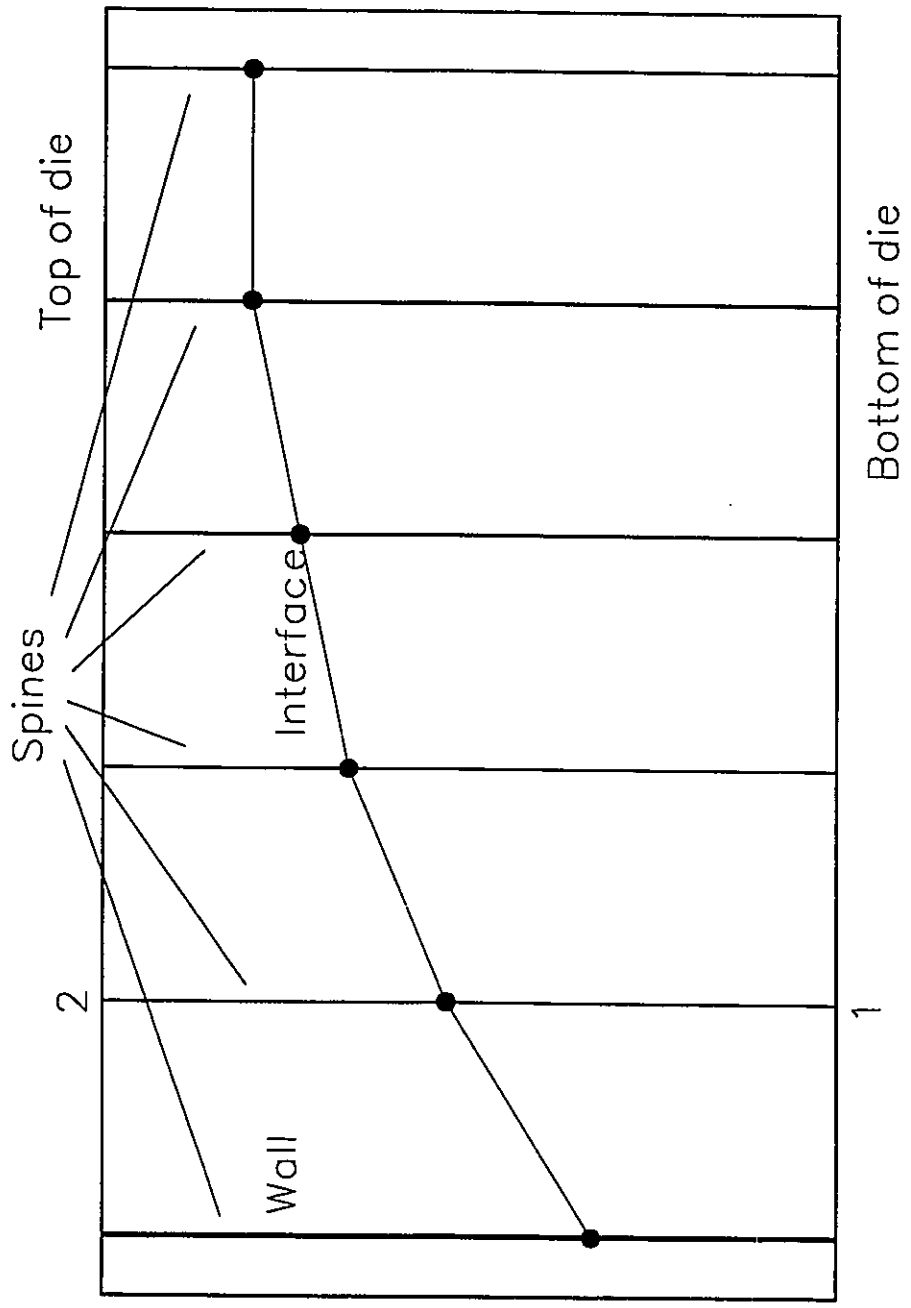

Figure 3.4. Spines used as a definition for elemental free surfaces.

Convergence and zero-th order method.

After applying the G-FEM to the governing equations, a non-linear system of equations results, which is solved using a Newton-Raphson method. Newton-Raphson and related solution strategies are known for a quadratic rate of convergence, but the convergence radius is problem dependent. If the initial estimate of the field variables is far away from the final solution, straightforward application of a Newton method may result in divergence. The problem at hand is highly nonlinear due to: the presence of free surfaces (internal interfaces), nonlinearity (in terms of temperature and velocity) of the local slip boundary condition, thermal and shear-rate dependence of viscosity, and the coupling between the velocity field and temperature field through the viscous dissipation term. These nonlinearities can cause failure of the Newton method to converge. A zero-order continuation method is used to improve the convergence. Parameters such as *Pe*, *Br*, *b*, *n* (power-law index), λ (Carreau parameter), and some critical boundary conditions, such as wall and inlet temperatures are increased from values at which convergence is attained to desired values in defined increments (usually 3-4 steps are used; fixed increments used till the final value is reached). The system of equations is solved for a relaxed termination criteria ($\varepsilon_1 = \varepsilon_2 = 10^{-2}$) and this solution is used as an initial estimate for the next set of parameters. When the final set of parameters and boundary conditions are reached, strict termination criteria are employed. This method has proven to be extremely robust, but it is computationally expensive.

Upwinding.

It is well known that the finite element modeling of moderate to high convective problems is prone to numerical instabilities and spurious oscillations in the solution. The most comprehensive work on the numerical problems in convection flows is the work of Hughes and Brooks (1982). Hughes and Brooks (1982) proposed a modification to the G-FEM, that is known as the "Streamline-Upwind Petrov-Galerkin" finite elements, or SUPG. SUPG-FEM allows the modeling of highly advective fluids by modifying the shape functions (or the Gauss weights for the numerical integrations) by a term that is a function of the cross-flow velocity magnitude in the element centre. However, the numerical difficulties associated with high *Pe* or high *Re* number calculations (spurious oscillations in temperature and velocity fields, lack of convergence) were not found in the simulations presented here. A possible explanation is that the flow is mainly unidirectional (the u component of velocity is much larger as compared to v,w components) with the possible exception of the meeting point of the two flow channels. However, at this location, the grid is very refined and the local *Pe* number is small. The very good agreement between numerical and experimental results and the facts that all equation residuals were below 10^{-3} when convergence is achieved also indicates that no significant numerical problems were encountered (Chapter 5).

CHAPTER 4

BOUNDARY CONDITIONS FOR CONTACT LINES

4.1 Introduction.

As mentioned in Chapter 2, imposition of the contact line boundary condition is not an easy task. The physics of the three-phase (fluid / fluid / wall) region is not completely understood from a molecular point of view. Introduction of the common no-slip boundary condition leads to a multivalued velocity at the contact line and to an infinite shear stress, both of which are unrealistic. The no-slip boundary condition was universally adopted after a series of mathematical proposals from Stokes (1851) being confirmed based on the experimental evidence provided by Whetman (1890) and others, in the absence of contact lines. Thus, the question of the appropriate contact line boundary condition remained open. In this thesis, the idea of slip as a local continuum approximation is introduced to overcome the singularity at the contact line.

4.2 Extrapolation method.

Dheur and Crochet (1987) proposed the extrapolation method to calculate the contact line position in finite element simulations to avoid the lack of convergence when the no-slip boundary condition is used. This method simply calculates the contact point location by linearly extrapolating the shape of the interface near the wall to the contact

point using the calculated coordinates for the interface (see Figure 4.1). Karagiannis et al. (1989a) extended the linear extrapolation method to three-dimensional calculations. He also used higher-order polynomials for extrapolating the contact line, and noticed that higher-order extrapolations produced similar results as linear extrapolation. Extrapolation is the simplest method to calculate the location of the contact line and avoids the consideration of the correct boundary condition at the contact line. Extrapolation methods do not consider wall effects and, computationally, the use of the extrapolation method in finite element calculations with a Newton-Raphson solving scheme presents the drawback of reducing the convergence rate from quadratic to superlinear at best.

4.3 The linear (Navier) slip condition.

As early as 1827, Navier proposed a one-dimensional slip boundary condition of the form (Silliman and Scriven, 1980):

$$-(1/\beta)\,\boldsymbol{t}\cdot(u-u_s) = \boldsymbol{n}\boldsymbol{t}:\sigma \qquad (4\text{-}1)$$

In the above expression, $\boldsymbol{t}$ is the unit tangent to the surface, $\boldsymbol{n}$ is the unit normal to the surface, u is the slip velocity and u_s is the wall velocity, σ is the wall stress tensor and β is the slip coefficient, which can be made length-dependent or viscosity-dependent. Silliman and Scriven (1980) introduced a negative sign to express that the momentum transfer across the velocity discontinuity occurs from the faster-moving to the slower-moving fluid.

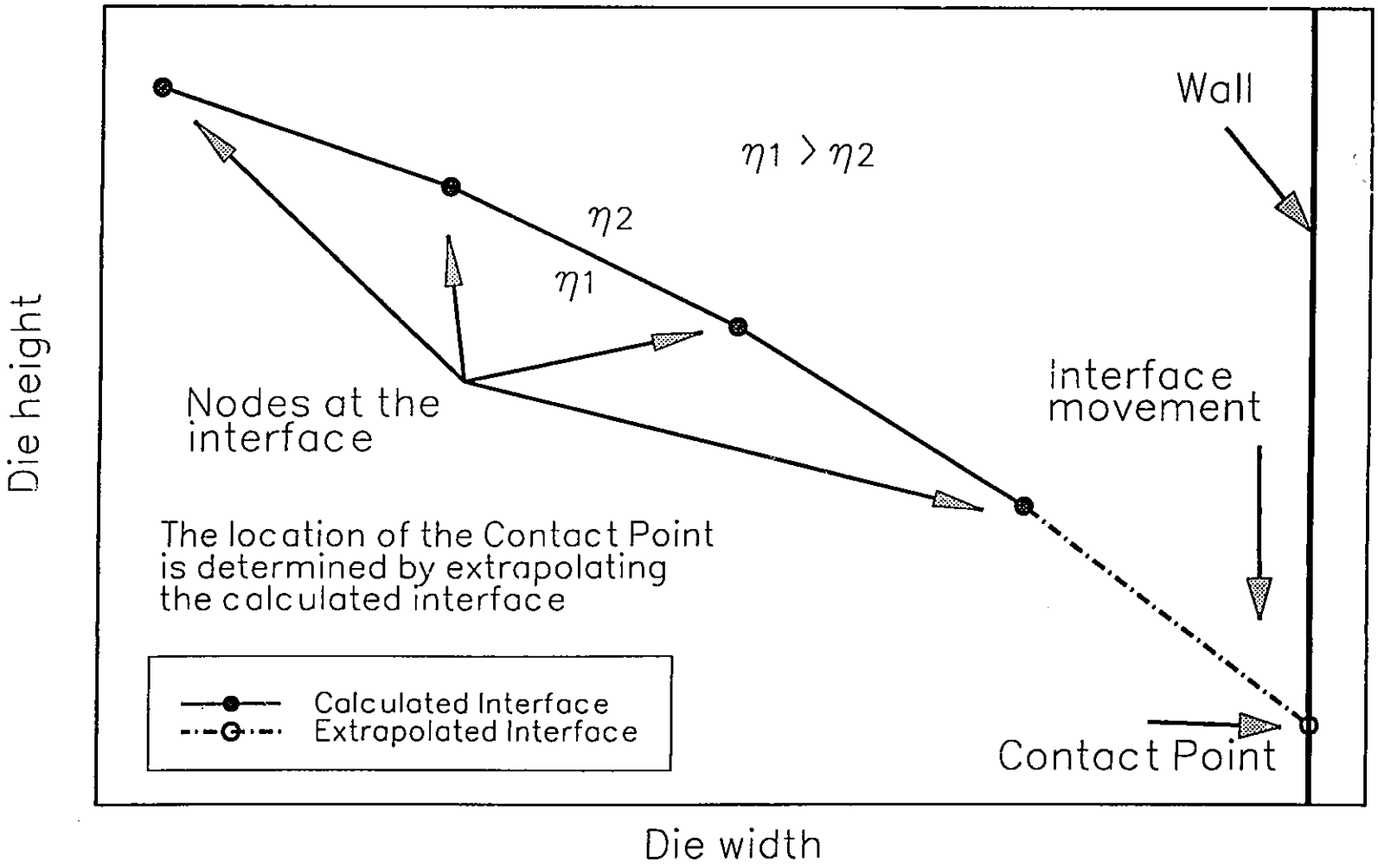

Figure 4.1. Extrapolation method.

In the present case, it is assumed that the contact line will be moving in the direction of the encapsulation (less viscous fluid surrounds more viscous fluid), i.e., a one-dimensional movement (Figure 4.1). Using this assumption, equation (4-1) reduces to:

$$u_{sl} = -\beta \tau_w \tag{4-2}$$

where u_{sl} is the slip velocity and τ_w is the wall shear stress (τ_{xz}). $\beta \rightarrow \infty$ indicates perfect slip, and $\beta \rightarrow 0$ indicates a recovery of the no-slip boundary condition. Typical numbers of β for polyethylene (Ramamurthy, 1986) are approximately 10^{-8} m/Pas. with dimensionless values $0.001 < B < 10$ ($B=\beta\mu/L$, μ being a reference viscosity and L a reference distance). Table 4.1 lists some typical values for the slip coefficient, β, in dies for polymer melts and solutions. It is important to emphasize that the contact line condition employed is introduced to overcome a mathematical singularity that appears regardless of the shear level of the system. For this reason, no critical stress is introduced in the model and, therefore, the contact line boundary condition is applied only at the nodes in the contact line. The contact line region is very small, and in the macroscopic approach followed here, it is asummed to lie within the elements containing the contact line. A similar approach was followed by Mavridis (1988) and Coyle, Blake and Macosko (1988) in the 2-D simulation of injection mold filling flows.

Previous research works on single fluid systems in dies have used slip models to account for discrepancies between observations and predictions using the no-slip boundary

condition. For the contact line problem, the slip model is used to relieve a mathematical singularity. All the models for the contact line behavior in this thesis are macroscopic approximations (to the continuum level) to a problem which involves the molecular interactions between an interface and a solid wall.

Table 4.1. Some values for the slip coefficient in one-fluid systems.

Material	Model	β (m/s/MPa)	m	B*	Reference
LLDPE	Linear	0.0061 to 0.0264	1	0.0000384 to 0.0001662	Ramamurthy (1986)
LDPE	Power-law	5.5 to 15.7	4	0.0116 to 0.0330	Hatzikiriakos and Dealy (1993)
LLDPE	Power-law	7.0	4	0.041	Hatzikiriakos (1993)

(*) L=1m for melts were used to obtain B. When a reference viscosity was not available, typical values were used instead (Vlcek and Vlachopoulos, 1995).

4.4 The power-law model.

Some authors (Chauffoureaux et al., 1979; Lau and Schowalter, 1986) have fit power-law models to the slip condition for flows of single fluids of polymeric solution and melts. The power-law model for bulk fluid is used here as a model for the contact line displacement. The power-law model is expressed as:

$$u_{sl} = A(\tau_w)^b \tag{4-3}$$

The power-law model for single fluid systems is confirmed by the experimental work of Chauffoureaux et al.(1979), Ramamurthy (1986) and, more recently, by

Hatzikiriakos and Dealy (1991) for molten polymers flowing in a tube, and by Cohen and Metzner (1985) and Lau and Schowalter (1986) for polymeric solutions. Hill et al.(1990) and Denn (1992) used the theory of adhesive failure to suggest a mechanism for the onset of slippage. Dussan and Davis (1974) suggest that the dependence of slip velocity on shear stress for moving contact lines can be of power-law form. In this work, a modified power-law model is used for the contact line problem in polymer coextrusion flow. The boundary condition implemented is of the form:

$$u_{sl} = \beta \left[\tau_w^{\frac{2}{m}} \right]^{1/2} \tag{4-4}$$

4.5 Hyperbolic model.

Blake (1988) suggested a non-linear slip model for capillary displacement of a polymeric liquid based on both molecular and hydrodynamic considerations. In its simplest form, the proposed contact line condition is:

$$u_{sl} = \beta \sinh(\alpha \tau_w) \tag{4-5}$$

where, once again, β is the slip coefficient and α is a complex function of viscosity, contact angle, temperature and interfacial tension. This leads to a possible mechanism for the behavior of the contact line based on physical grounds. Hatzikiriakos and Dealy (1992a,b,c) and Hatzikiriakos (1993) extended the theory of adhesive failure to take into

account pressure and thermal dependence, as well as molecular parameters, to obtain similar models.

4.6 Stick model and fixed contact angle.

Under certain conditions, it may be possible to have a static contact line. Hocking (1976, 1977) demonstrated, from a theoretical point of view, that the introduction of a slip boundary condition could be seen as a way to introduce wall surface irregularities into the model. The *apparent* movement of the contact line would be caused by those irregularities. At a microscopic level, a very thin film could be seen departing from the initial position of contact line. Hasson et al. (1970a,b) demonstrated experimentally that wall surface irregularities and surface wetting play an important role in the final interface shape and encapsulation level. Dussan and Davis (1974) demonstrated that the no-slip boundary condition and a moving contact line are compatible from a kinematic point of view if one fluid is considered to *roll* over the other. Thus, a static contact line boundary condition is also tested here. The contact line is assumed to remain at the location of the separation plate. This condition is introduced by removing the calculation of the interfacial position at the contact line and leaving it as a fixed (Dirichlet) boundary condition.

Another method that has been proposed to circumvent the numerical breakdown of the solution is to use a contact angle condition (Dheur and Crochet, 1987). The value of the contact angle is selected on the basis of experimental or empirical relationships. A contact angle boundary condition has been used primarily in problems with significant

interfacial tension. As mentioned before, in polymer coextrusion flows viscous forces dominate over interfacial forces (high Capillary number), and the use of a contact angle boundary condition in these types of flow is questionable.

Under the assumption of linear slip, a fixed contact angle can be introduced as a natural boundary condition:

$$\tau_w = \left[\frac{1}{(\beta \cos\theta_c)}\right] u_{sl} \tag{4-6}$$

where θ_c is the apparent contact angle. However, an extrapolation method must be used to determine the contact line position if the no-slip condition is assumed at the contact line.

Note that the "stick" and "slip" models are based on two completely different flow mechanisms. The stick model assumes that the interface remains fixed to the die wall (no displacement of the contact line is possible) while in the slip model the contact line has a vertical movement dictated by the various forms of the model. Both models of the contact line behavior are proposed from a macroscopic point of view to relieve a mathematical singularity. The appropriateness of any of these models depends on polymer / polymer / wall interactions and the form of slip or adhesion will require a more detailed analysis that is beyond the scope of the macroscopic continuum analysis presented here.

4.7 Numerical Results.

In this section, the proposed models for the behavior of the contact line are studied and compared against extrapolation methods. The initial height of the separation plate is calculated using the solver for the inlet boundary condition (Section 2.2) to satisfy the requirements of given flowrate ratios.

4.7.1 Stick model.

A comparison between the stick method and the linear extrapolation method for Newtonian fluids is presented in Figure 4.2a and 4.2b for a square die geometry. Interfaces calculated using the extrapolation method and the stick model are shown. The flowrate ratio of two layers is $Q_1/Q_2 = 13.2$ and the viscosity ratio is $\eta_{01}/\eta_{02} = 2.5$. Figure 4.2a shows the final interface at 10.5 dimensionless lengths downstream from the separation plate. Figure 4.2b shows an enlargement near the contact line. A very thin film of the more viscous liquid (called "primary" film by Dussan, 1976) can be seen near the die walls for the stick model. Note that for the stick model the contact line is at the height of the separation plate. Since the encapsulation by the less viscous fluid is energetically preferred, an interface 'bending effect' is seen. The thickness of this film is in qualitative agreement with the estimates of Durbin (1988) for the slip length of air / water / wall systems. The predicted interface deformation is the same for the extrapolation method and the stick model. The solution was unaffected by grid refinement near the wall (9 nodes and 11 nodes in y-direction were used). However, having the same 11 nodes in the y-direction in positions that are closer to the die wall results in divergence of the

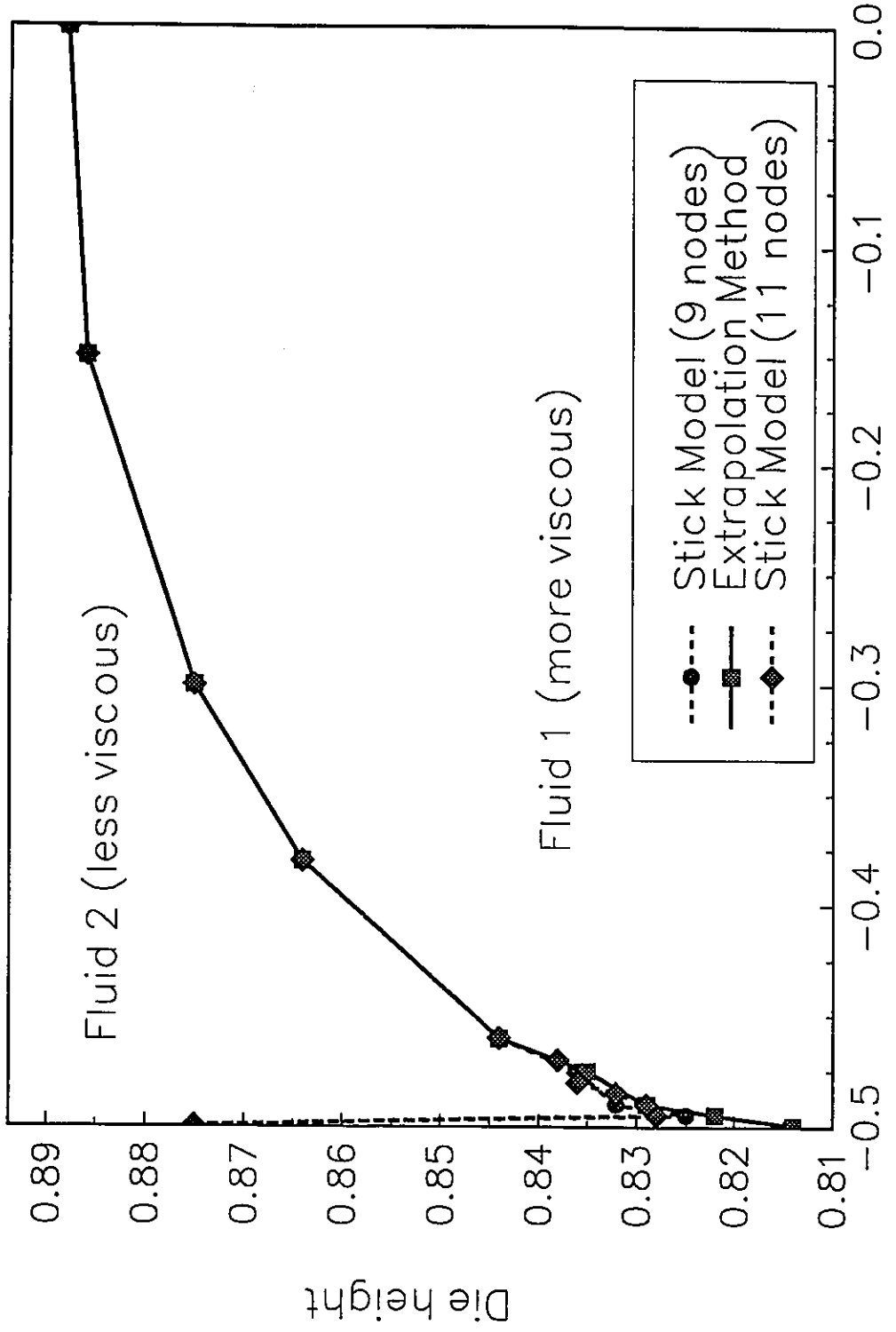

Figure 4.2. Comparison between stick model and extrapolation method (Viscosity ratio: 2.5; Flowrate ratio: 13.2)
(a) Half die.

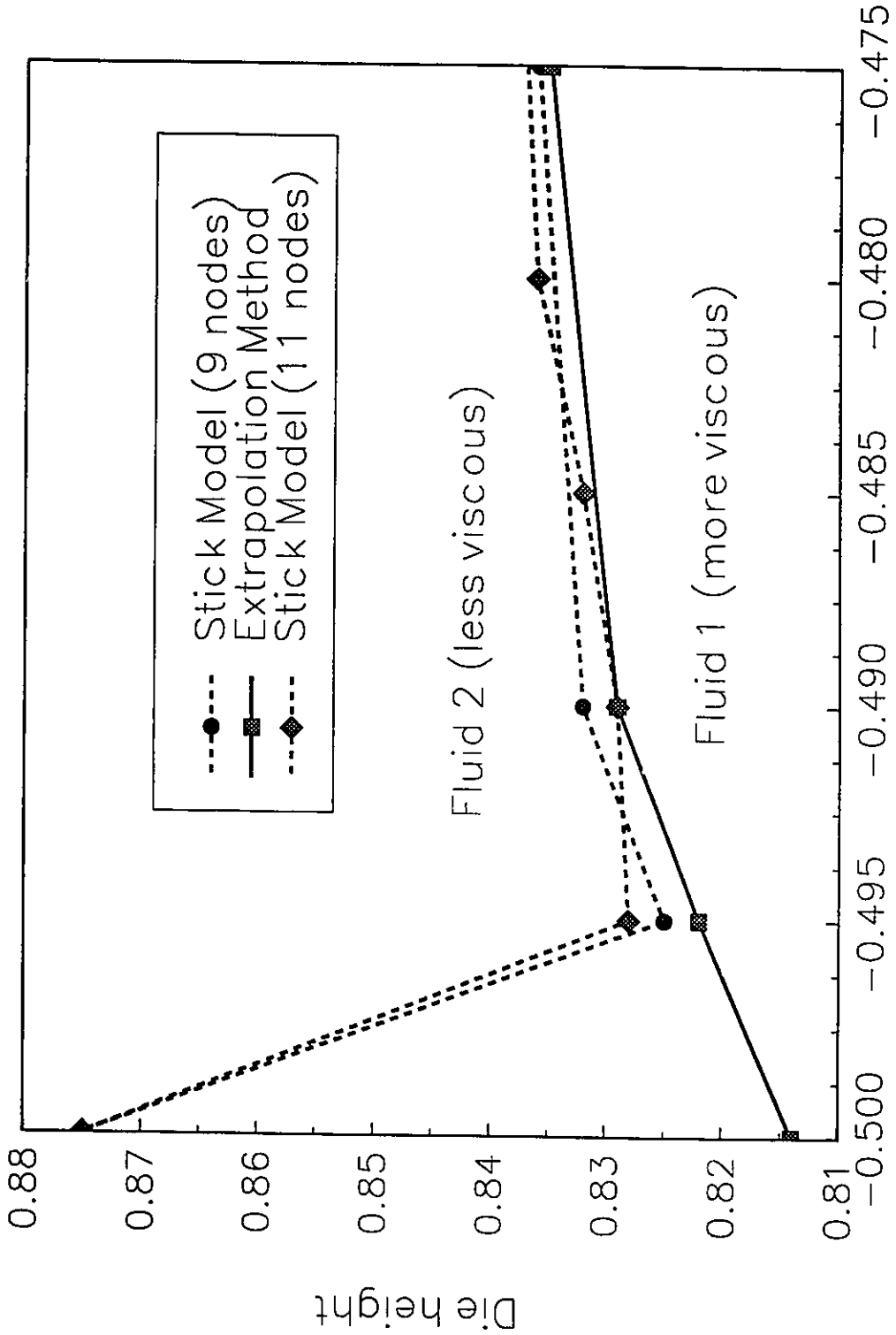

Figure 4.2. Comparison between stick model and extrapolation method (Viscosity ratio: 2.5; Flowrate ratio: 13.2)
(b) Enlargement near the die wall.

solution after few iterations (Table 4.2). The reason for failure is the breakdown of the isoparametric transformation from global to parent elements because of the loss of appropriate aspect ratio. With elements so close to the die walls, the interfacial deformation creates elements with aspect ratios that are higher than the norms proposed for accurate isoparametric transformations (Reddy, 1987). The limit for the possible encapsulation is imposed by the distortion of the 27-node elements that lie at the die walls. In order to avoid the large distortions observed with the 27-node element, a simpler 8-node linear element was used. Even though this is a simple element, it could capture more deformed shapes without a breakdown of the isoparametric transformation. A comparison of the two-dimensional counterparts for the 27-node (9-node) and the 8-node (4-node) elements were done by Huyakorn et al. (1978). In the 8-node brick element the pressure is assumed to be constant within the element and, therefore, many elements will be needed at the region where the two fluids meet due to the pressure discontinuities occurring across the interface (mesh density in three-dimensional modeling becomes a compromise between accuracy and computer speed and disk capacity). Also, due to the lower order of approximation, there is a loss of accuracy that can only be overcome with refined meshes. However, even with very refined meshes, no convergence could be found in all cases tested

Table 4.2. Node locations (dimensionless) in y-direction for the different grids used.

9-node mesh	11-node mesh	11-node mesh, relocated
0.50	0.50	0.50
0.495	0.495	0.499
0.49	0.49	0.498
0.475	0.485	0.494
0.46	0.48	0.49
0.38	0.47	0.475
0.30	0.46	0.46
0.15	0.38	0.38
0.00	0.30	0.30
	0.15	0.15
	0.00	0.00
Convergence	Convergence	No convergence

Note: Wall is located at 0.5, symmetry plane at 0.0

The stick model can be considered only as a limiting case in the bicomponent coextrusion of polymer melts. Adherence to the die walls is governed by wall wettability, surface roughness and other physical parameters (Hocking, 1976).

4.7.2 Slip models.

For the slip model, values of the shear stress at the wall are used in the calculations. The slip boundary conditions are introduced in the surface integral added to the z-momentum equations only for the nodes at the contact line:

$$Rz_s = \int_{-1}^{+1}\int_{-1}^{+1} \left[\frac{w}{B}\right] N^i |J^*| d\eta d\zeta \qquad (\xi=-1) \qquad (4\text{-}7)$$

which alleviates the singularity introduced by the no-slip condition. In all the simulations performed, the element numbering was arranged so that the wall containing a contact line was made to coincide with the face ξ=-1 of the finite elements.

The effect of the B coefficient is examined in Figure 4.3 for a system of Newtonian fluids with η_{01}/η_{02} = 1.5 and Q_1/Q_2 = 1. As B changes from zero (no-slip) to infinity (perfect slip) a limiting encapsulation is observed. At 0.1 dimensionless lengths away from the die walls, interface shapes predicted by slip models, stick models, and extrapolation methods behave similarly. This is expected, since all the contact line boundary conditions are local, and their effect is limited to the immediate vicinity of the contact line region. In all cases studied, the effect of the contact line boundary condition is limited to the element adjacent to the die wall. The interface deformation wholly within the bulk fluid responds to material properties and local velocities.

A comparison between stick and slip models is performed, using a very low slip coefficient (B=0.0001), thus recovering, in part, the no-slip feature. Results for a test

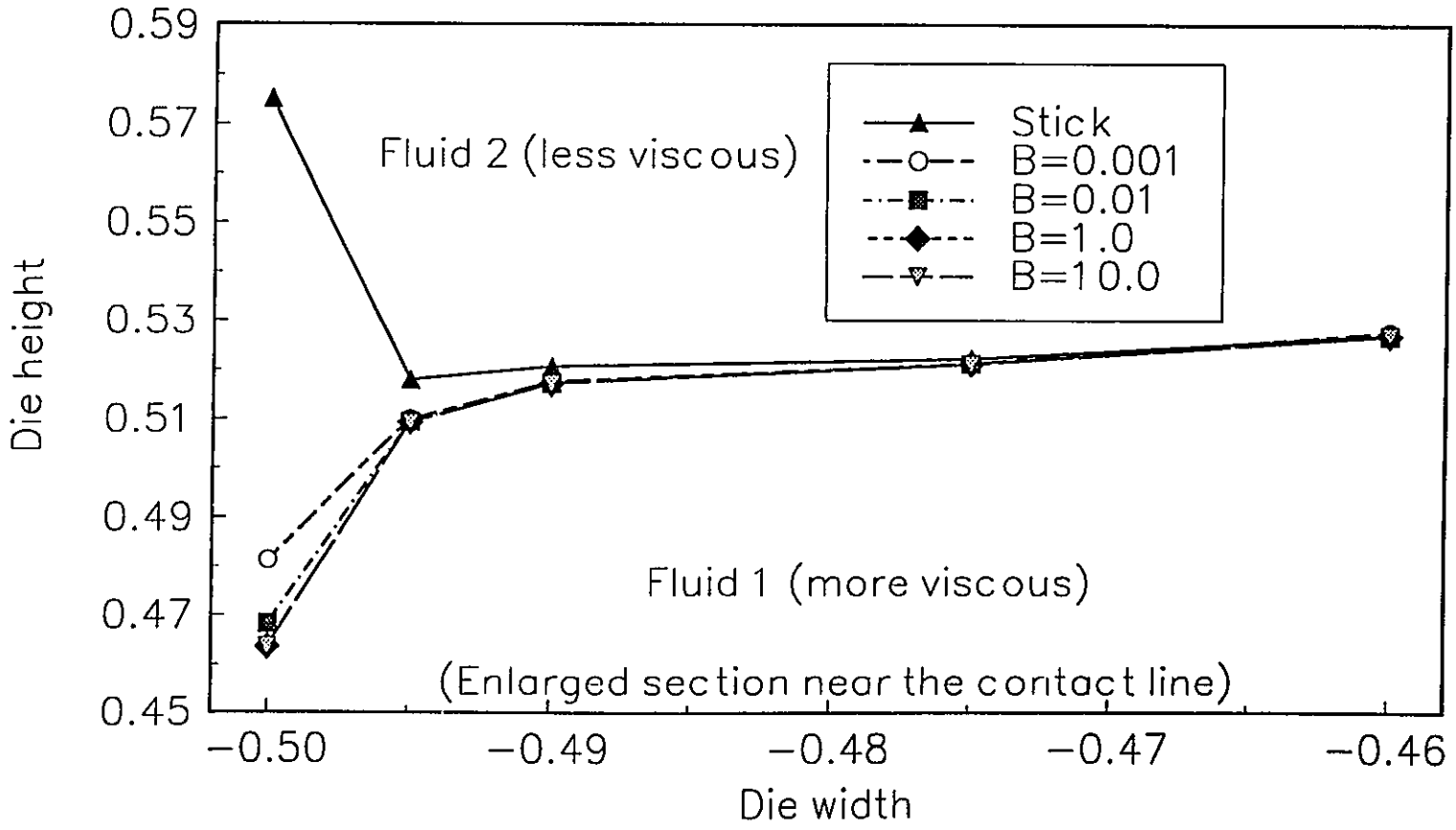

Figure 4.3. Effect of the B coefficient (Viscosity ratio: 1.5; Flowrate ratio: 1.0).

problem with the die geometry of Figure 2.4 (Newtonian fluids, η_{01}/η_{02}=2.5, Q_1/Q_2=13.2) are shown in Figure 4.4. Note that the predicted interface position at the die exit is the same for every model after 0.025 dimensionless units away from the die wall. The interface shape for the slip model shows the characteristic bending of the stick model at small values of the slip coefficient. This suggests that a larger slip coefficient is needed to eliminate the bending near the contact line. This bending of the interface near the contact line can not be captured using the extrapolation method.

The effect of the viscosity ratio on solutions using the extrapolation method and the slip model is shown in Figure 4.5. The slip model shows more encapsulation than the extrapolation method, for the same flow conditions, in all cases studied. Note that for the case of equal viscosities (η_{01}/η_{02}=1) a small encapsulation is observed due to differences in flowrate ratios. For the case of a viscosity ratio of one and flowrate ratio of one, the interface remains stable for all the models proposed. It is interesting to note that the use of an extrapolation method can hide abrupt changes in the interface near the die wall, as Figure 4.5 suggests.

A computational test was performed to check the implementation of the linear slip model. The flowrate ratio is fixed at Q_1 / Q_2 = 13.2, and B=0.01. In Figure 4.6a, the viscosity ratio is η_{01}/η_{02}=2.5. In Figure 4.6b, the viscosity ratio is η_{01}/η_{02}=1 /2.5=0.4. In both cases, the less viscous fluid encapsulates the more viscous fluid for a consistent encapsulation direction regardless of the relative fluid locations.

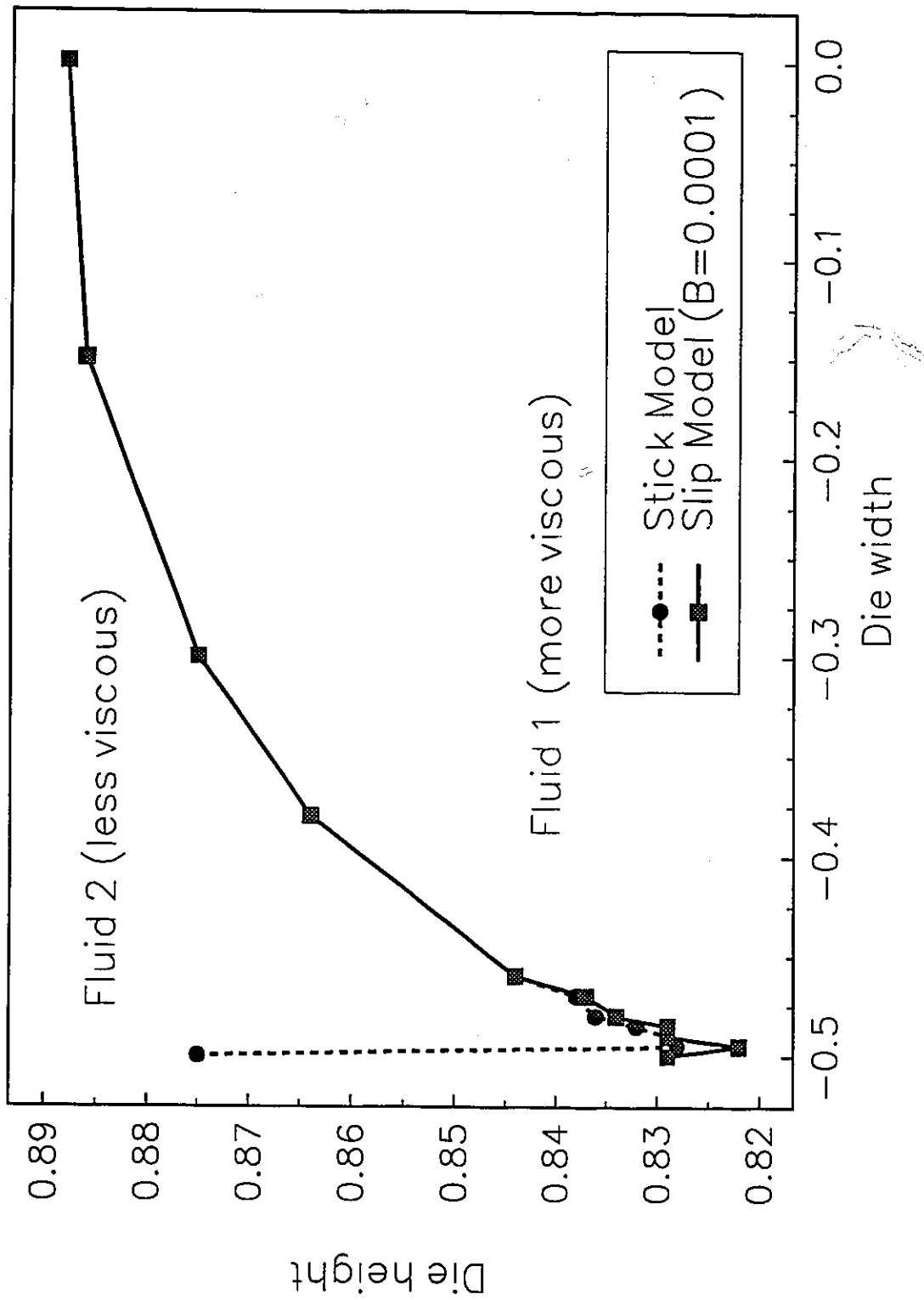

Figure 4.4. Comparison between stick and slip model (Viscosity ratio: 2.5; Flowrate ratio: 13.2).

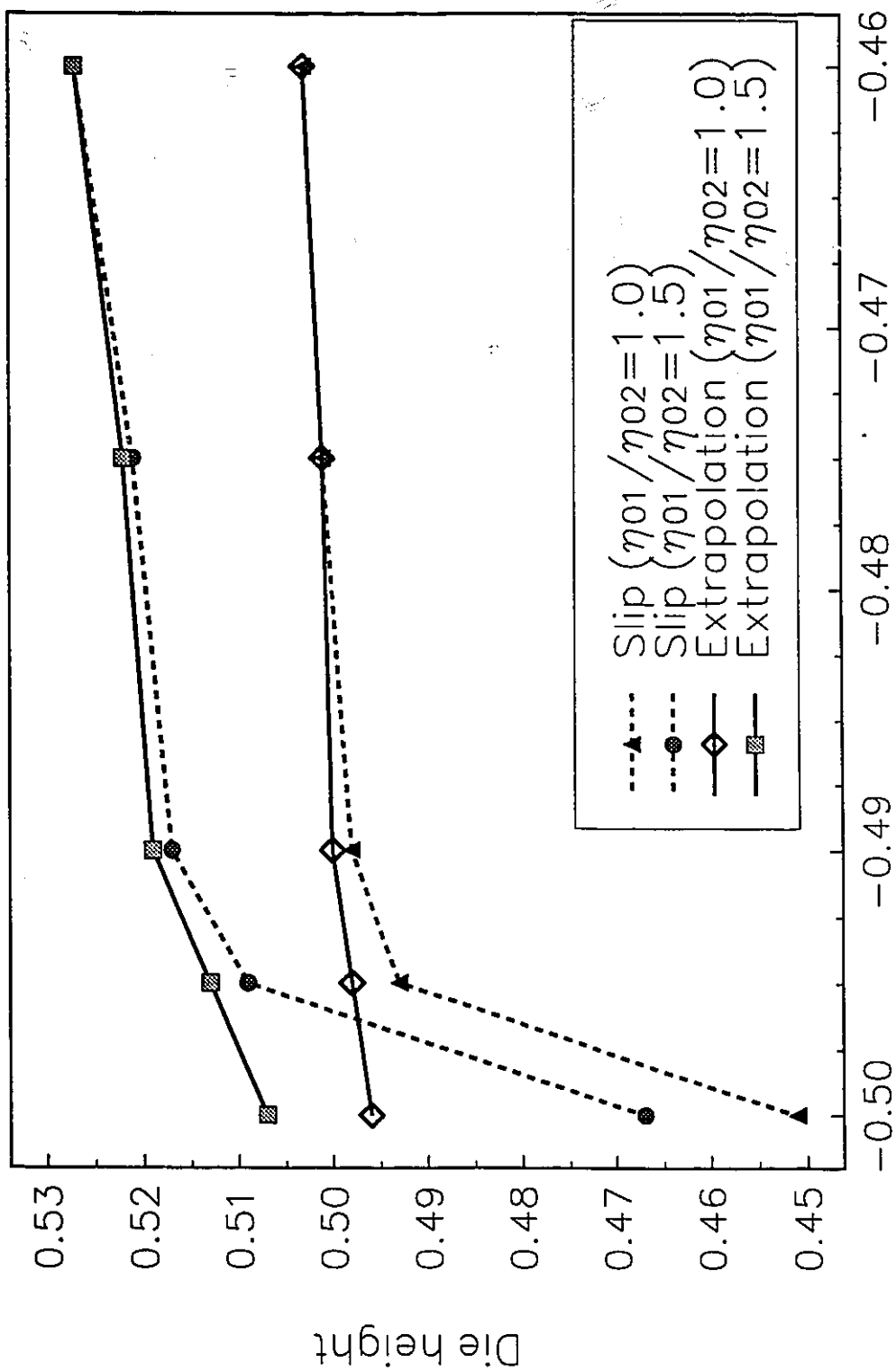

Figure 4.5. Effect of the viscosity ratio on the movement of the contact line (linear slip model, B=0.01)

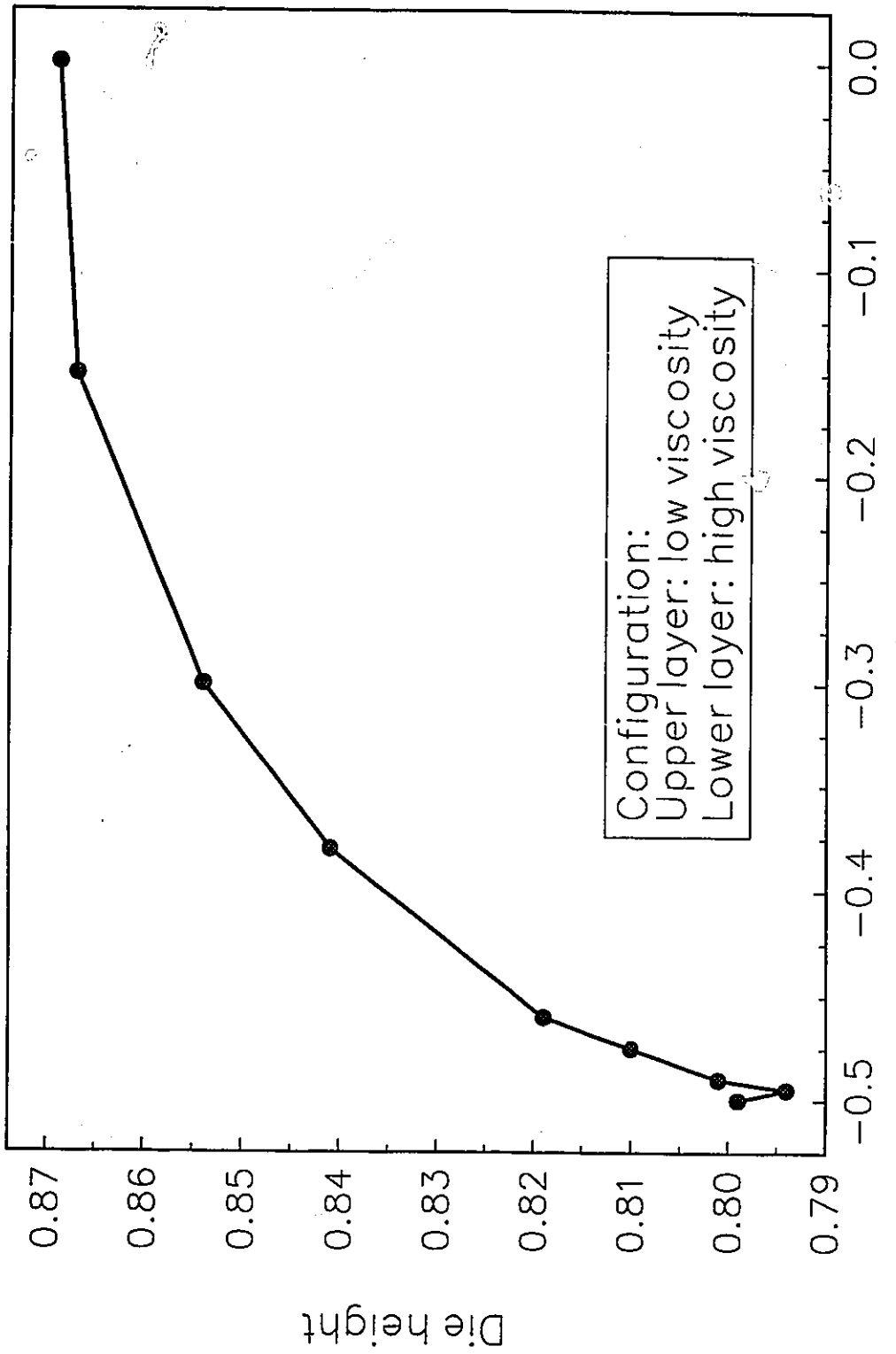

Figure 4.6. Interface displacement for different layer configurations. (a) Upper layer: low viscosity fluid. Lower layer: high viscosity fluid (Viscosity ratio: 2.5; Flowrate ratio: 13.2)

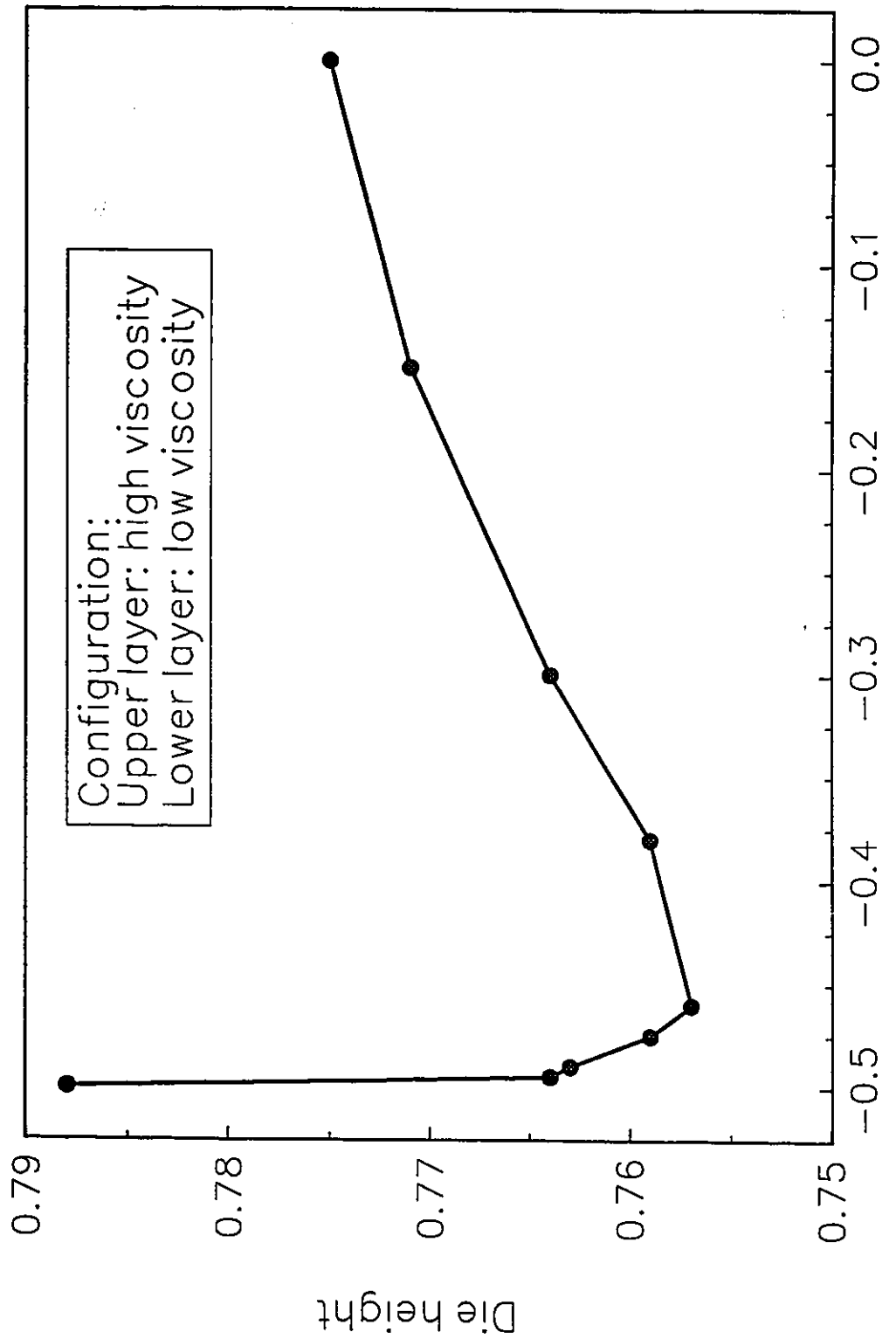

Figure 4.6. Interface displacement for different layer configurations. (b) Upper layer: high viscosity fluid. Lower layer: low viscosity fluid.

4.7.3 Simulation of Southern and Ballman's experimental data.

The experimental data of Southern and Ballman (1973) are modeled with the introduction of a linear slip model. These authors coextruded two polymers (which are defined as PS A and PS B) with viscosity crossover (Figure 4.7) at different flowrates. The Carreau model was fit to their rheological data giving the values shown in Table 4.3

Table 4.3. Carreau parameters for Southern and Ballman (1973) data.

Material	Location	η_0 (Pa.s)	λ(sec)	n
Polystyrene A	upper layer	3251.0	0.4708	0.6185
Polystyrene B	lower layer	4579.0	0.5865	0.5207

The shear rate level for the experiments was defined as:

$$\dot{\gamma}^E = \frac{Q_1 + Q_2}{L^3} \tag{4-8}$$

where Q_i indicates the layer i flowrate and L is a characteristic dimension (die height). The flowrate ratio Q_1 / Q_2 is 1 and B=0.01.

At a low shear rate ($\dot{\gamma}^E$=0.75 s^{-1}) PS B is more viscous and is encapsulated by PS A . This phenomenon is reversed at a high shear rate ($\dot{\gamma}^E$=29.8 s^{-1}) at which PS B is less viscous than PS A. At the viscosity crossover point ($\dot{\gamma}^E$=14.9 s^{-1}), an almost flat interface is obtained (Figure 4.8a, b). All of these results are in qualitative agreement with the

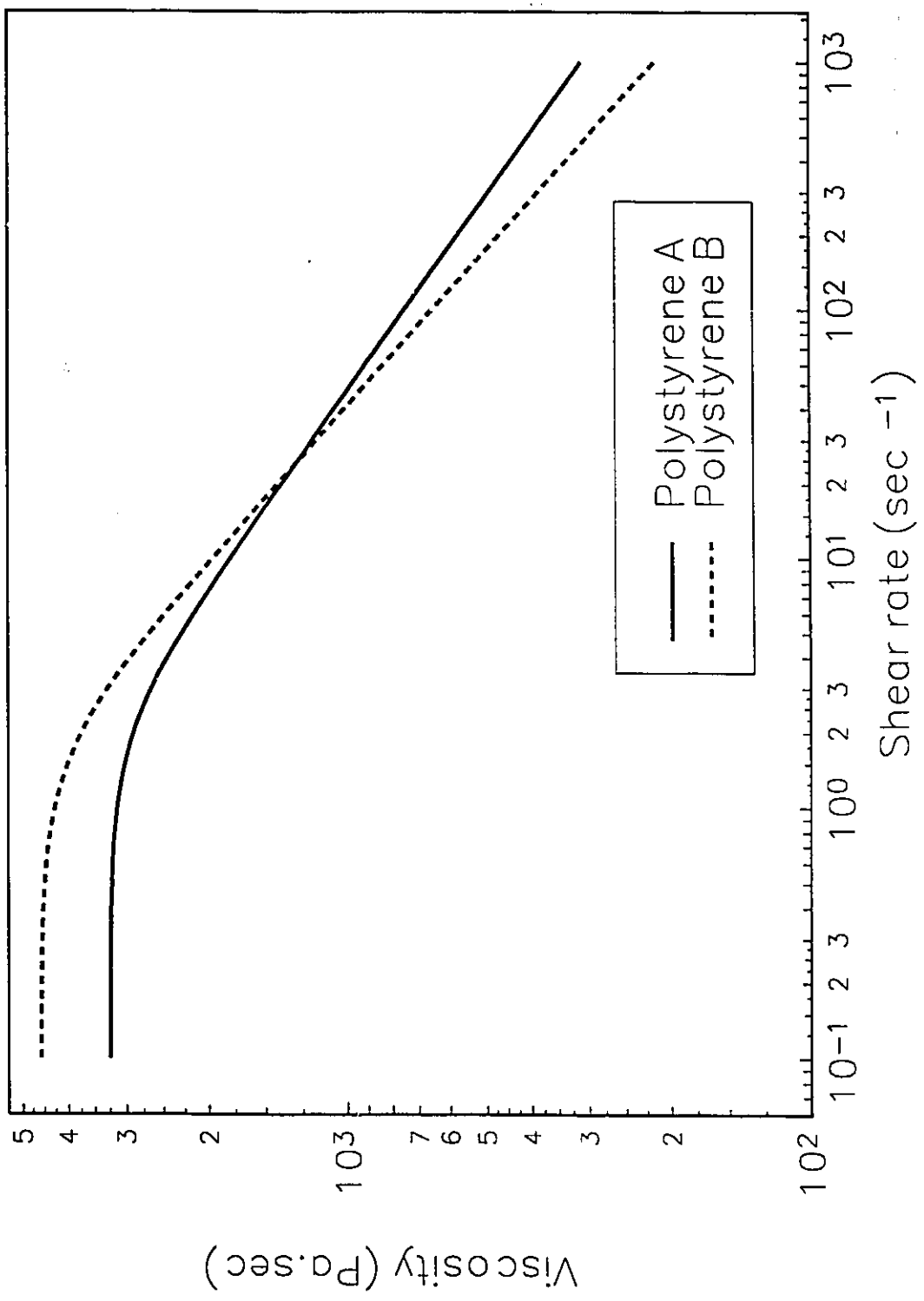

Figure 4.7. Viscosity curves for polystyrenes exhibiting viscosity crossover.

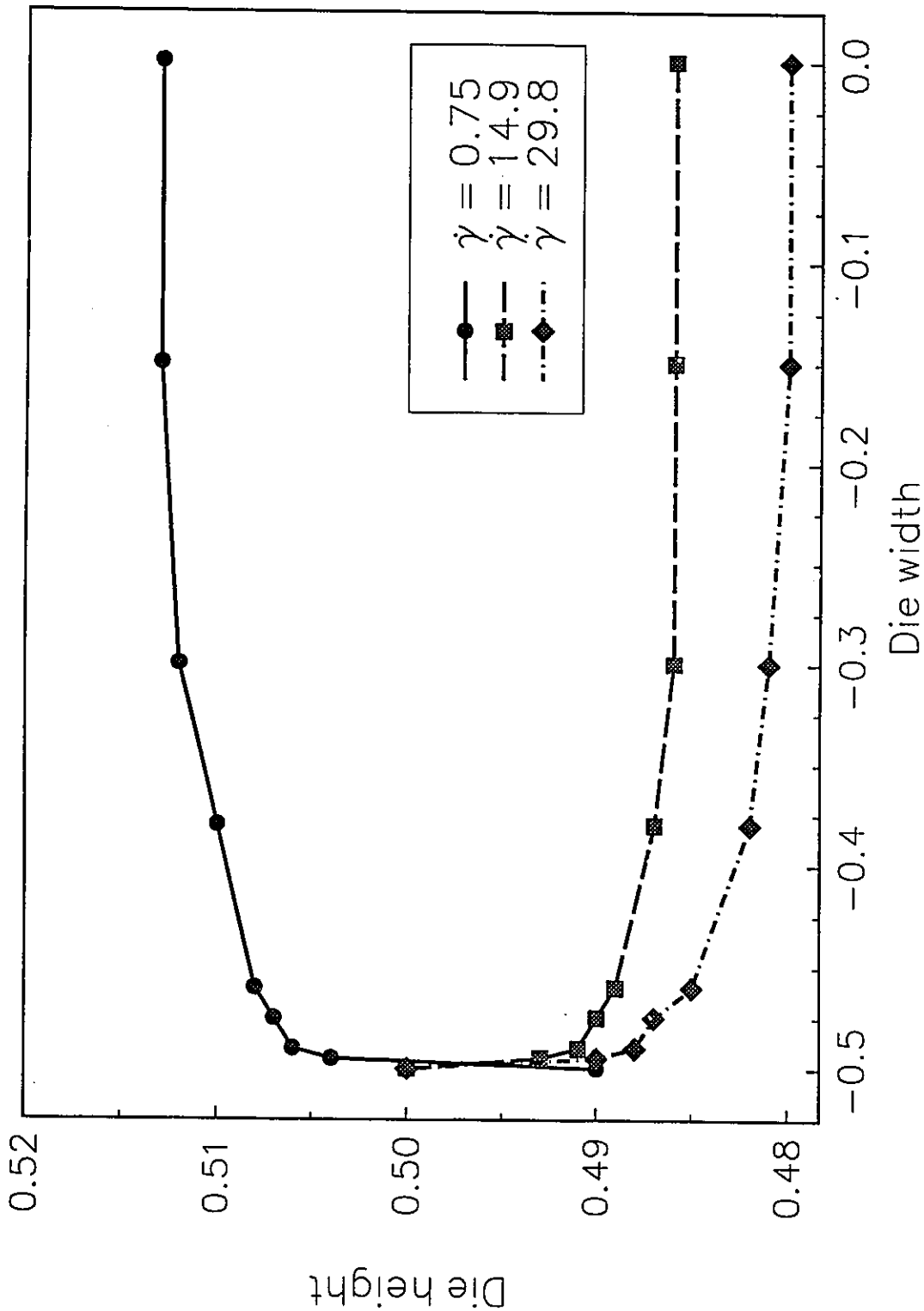

Figure 4.8(a) Predicted interface shape for the Southern and Ballman (1973) data.

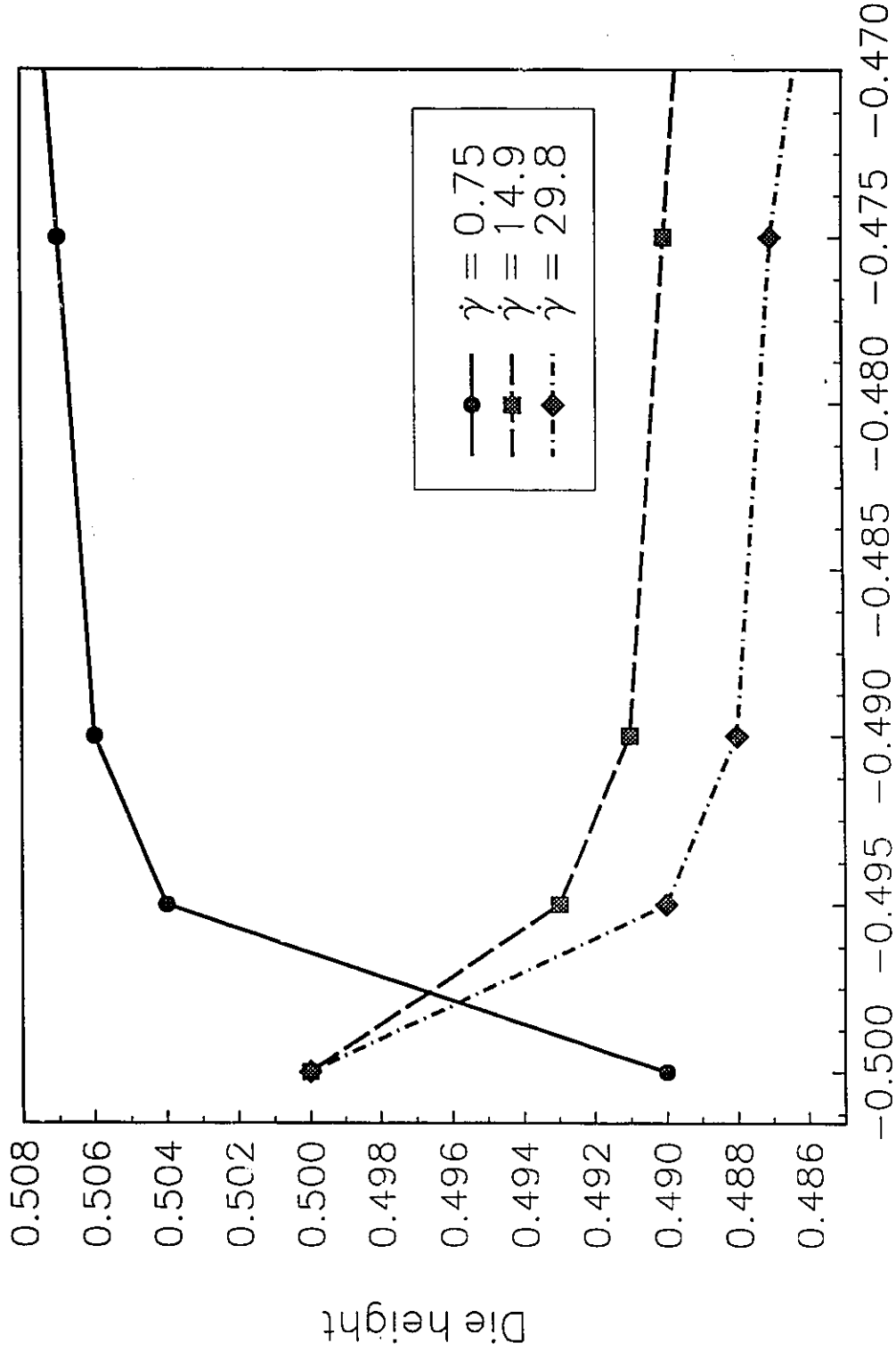

Figure 4.8(b) Enlargement near the die wall.

experimental observations of Southern and Ballman and in agreement with the numerical calculations performed for the same problem by Karagiannis (1989a) using the extrapolation method The shear rate near the wall is larger than in the bulk fluid, thus causing the large contact line displacement. Nominal values for the slip coefficient are chosen since no measurements of wall slip coefficient are available.

The movement of the contact line for the PS system modeled as above, as well for all other simulations performed, is limited to the region near the separation plate. After a sudden flow rearrangement due to pressure differences, the simulation shows that the interface reaches a stable configuration, i.e., there is no further interface displacement (L/D ≈ 3.0, Figure 4.9). However, experiments performed with PS material by Southern and Ballman and other researchers show a more pronounced interface deformation. An explanation for this discrepancy is offered in Chapter 5.

The outflow boundary condition will have an effect on the observed encapsulation simulation. Several meshes with different die lengths (20, 32, 54 L/D) were used. The longer the mesh, the more appropriate the no cross flow boundary condition is for non-elastic fluids (v=w=0, see Figure 2.4). The final interface was the same for all the cases of L/D. Although several authors have proposed refinements to the primitive no cross flow boundary condition used at the die exit (Malamataris and Papanastasiou, 1991), the correct outflow boundary condition remains an open question.

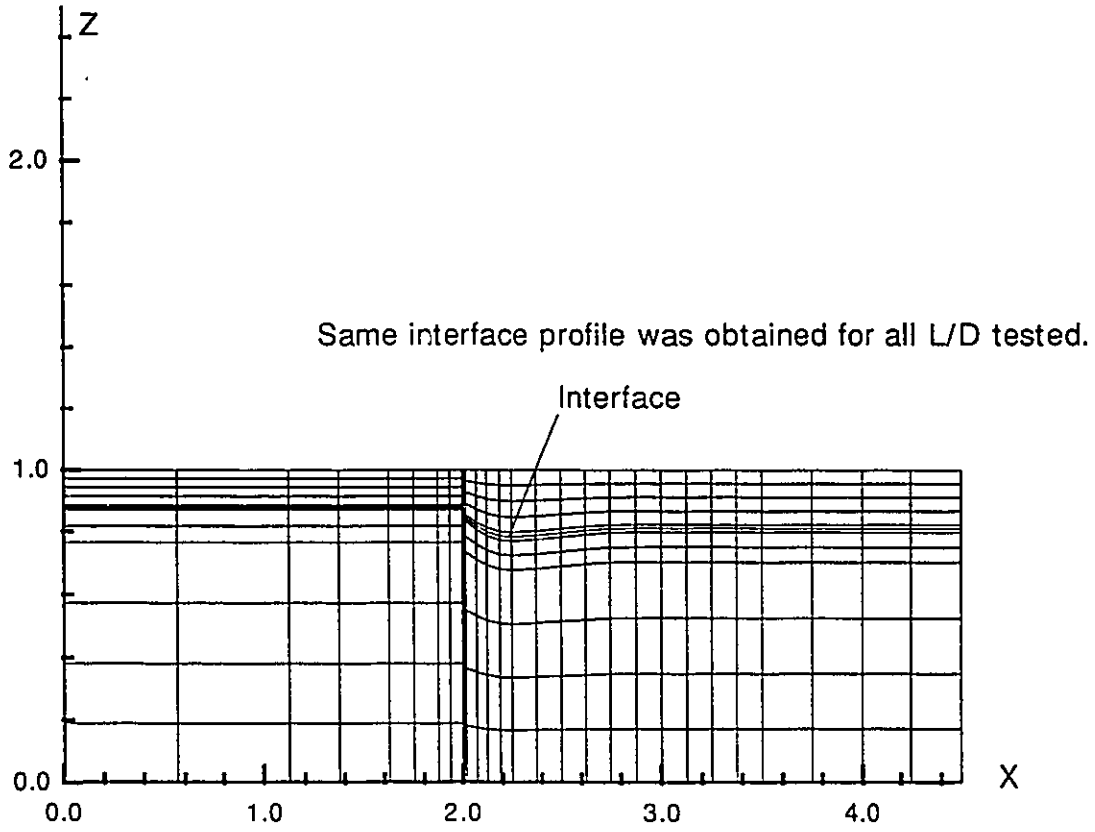

Figure 4.9. Interface development along the die wall.

4.7.4 Other slip models.

Sections 4.4 and 4.5 dealt with modifications to the simple linear slip model, in the form of power-law and hyperbolic models, respectively. As in the linear case, the modified versions are introduced as a surface integral in the z-momentum equation only for nodes at the contact line. The form of the surface integral for the power-law and hyperbolic models are:

$$Rz_s = \int_{-1}^{+1}\int_{-1}^{+1} \left[\frac{1}{B}\right] (w^{2})^{n/2} N^i \, |J^*| d\eta d\zeta \qquad (\xi=-1) \qquad (4\text{-}9)$$

$$Rz_s = \int_{-1}^{+1}\int_{-1}^{+1} \frac{1}{\alpha} \ln\left(\frac{w}{B} + \sqrt{\left(\frac{w}{B}\right)^2 + 1}\right) N^i |J^*| d\eta d\zeta \qquad (\xi=-1) \qquad (4\text{-}10)$$

respectively. A comparison of linear, power-law and hyperbolic slip models behavior is presented in Figure 4.10, for a square die with η_{01}/η_{02}=1.5, Q_1/Q_2=3.0. The similar behavior of the three slip models can be observed by examining a plot of the wall shear stress against the slip velocity (Figure 4.11). Encapsulation may require a long development length, depending on the viscosity and flow rate ratios (Southern and Ballman, 1973; Everage, 1973, 1975). The contact line velocity will be small relative to the mean flow velocity, as observed in the simulations. At very low slip velocities, the

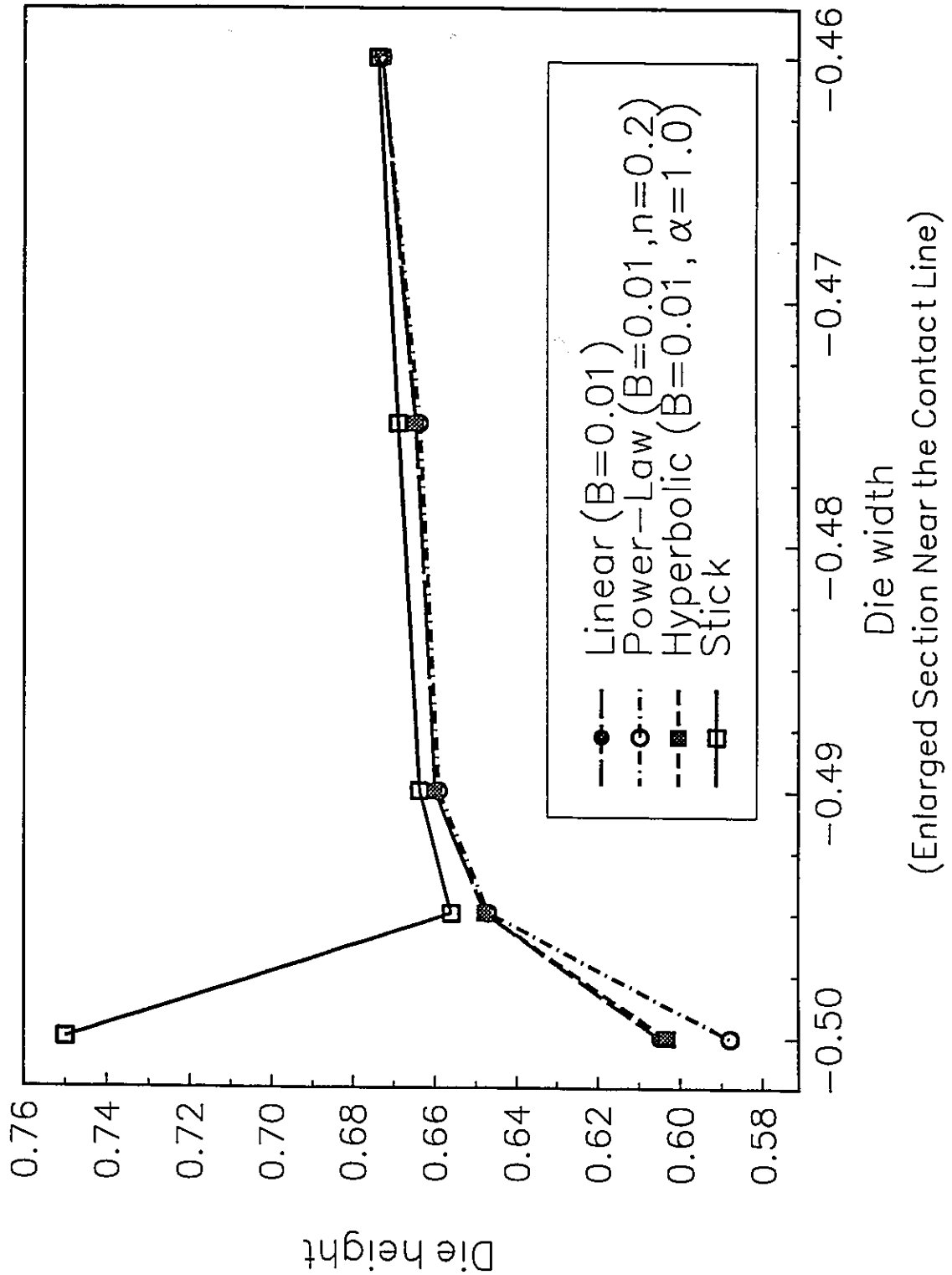

Figure 4.10. Comparison of models for the contact line (Viscosity ratio=1.5; Flowrate ratio=3.0).

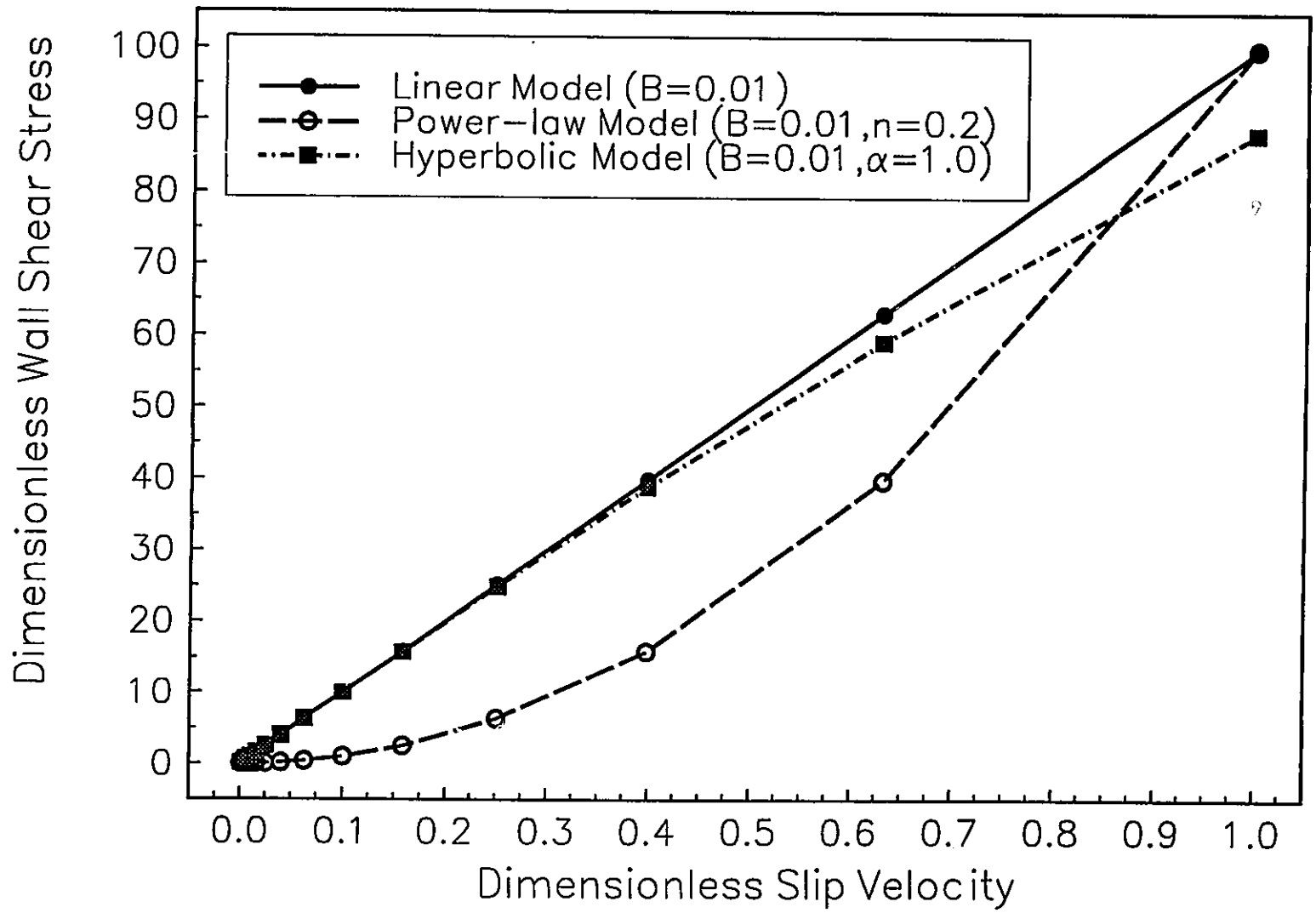

Figure 4.11. Wall shear stress versus slip velocity.

three contact line slip relationships are similar.

From the computational point of view, use of the slip models (or stick models) leads to a numerical scheme that converges quadratically. In Figure 4.12 a plot of the norm of the errors against the iterations is done for a typical problem (η_{01}/η_{02}=2.5 , Q_1/Q_2=13.2) solved by both types of methods. Note that the number of iterations required to reach a norm of the error of 10^{-3} for the Newton method is approximately a third of those required for the extrapolation method in this particular problem and the error is two orders of magnitude lower at a given iteration. Moreover, under certain conditions, introduction of the slip condition allows convergence in cases where the extrapolation method fails.

4.7.5 Simulation of PC/PC coextrusion systems.

Experimental work was carried out to confirm the validity of the proposed boundary condition model for the contact line as well as to gain some understanding on the behavior of contact lines for highly viscous flows. A detailed explanation of the experimental set-up can be found in Dooley and Hilton (1992). The experimental work was carried out at the Dow Plastics facility in Midland, Michigan. The coextrusion line was designed to produce a two-layer structure consisting of a 20% cap layer and 80% substrate layer. Among other shapes, a square die was attached at the exit of the feedblock. The characteristic length of the die (L/D) used in the work reported here was

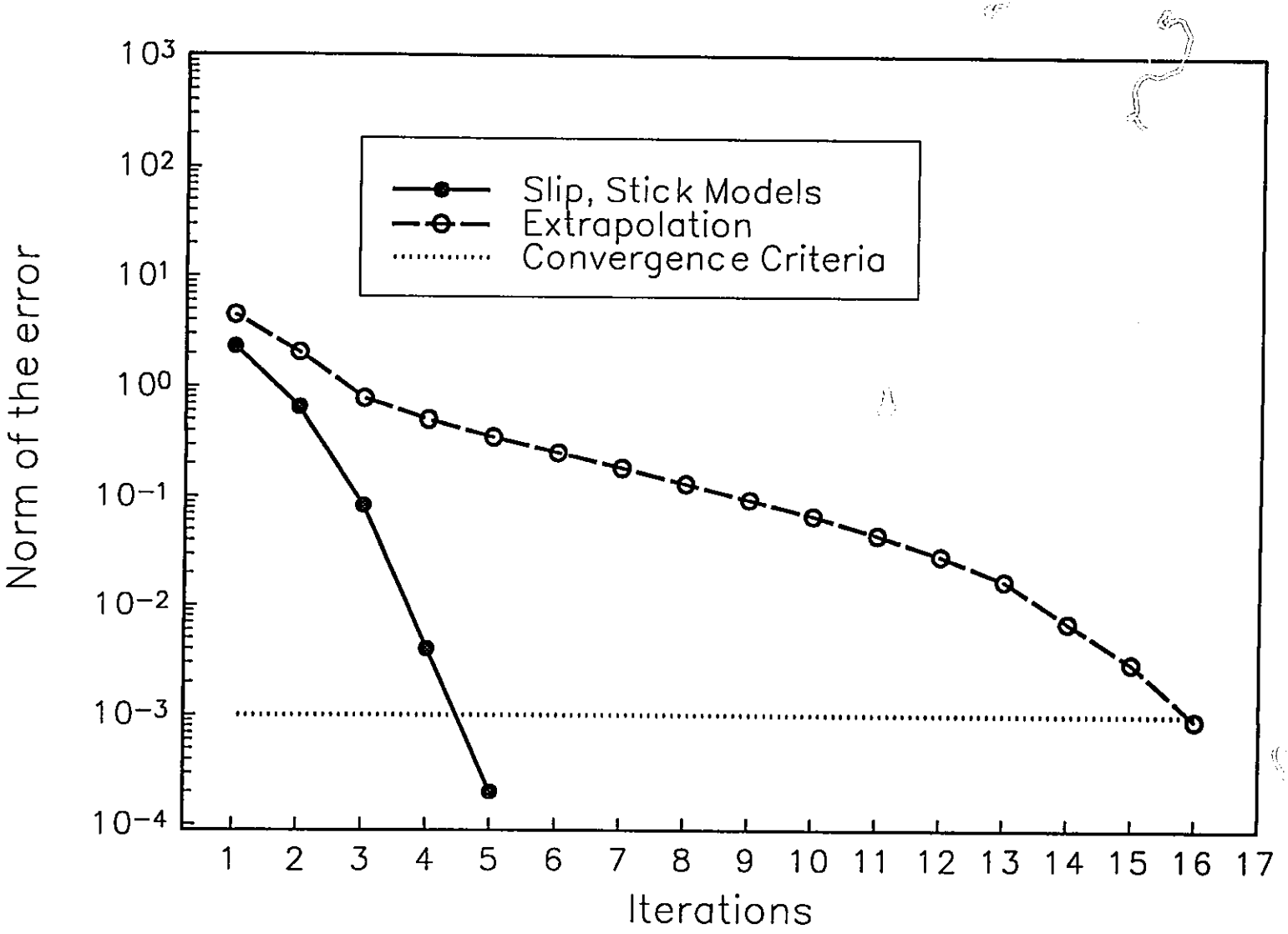

Figure 4.12. Convergence rate for different models. The norm of the error is the 2-norm of the residual vector.

approximately 32:1. A polycarbonate resin (CALIBRE 300-22)[1] was extruded in each extruder. Rheological properties for the resin are shown in Table 4.4. The coextrusion was performed using the same material in each layer to minimize viscosity differences between layers. One of the layers was pigmented black so the interface could be seen. All the experimental runs were performed at the approximately same wall shear rate of 30-40 sec^{-1} (Dooley and Hilton, 1992). Since the two materials are the same, there is no interface in the proper sense. However, since the diffusion normal to the main flow direction is very small, very well defined layers of materials can be seen and little or no mixing occurs. Then, the layer separating the two fluids can be studied as a real interface.

Table 4.4. Physical properties of the CALIBRE 300-22 used in experiments.

Zero-shear viscosity (Pa.s)	7500.0
Relaxation time (secs)	0.3
Power-law index (Carreau model)	0.92
Density (Kg/m^3)	1085
Thermal conductivity (W/m/K)	0.19
Specific heat (J/Kg/K)	1325
Thermal sensitivity coefficient, b (1/K)	0.041

When the polycarbonate/polycarbonate resin was extruded, very little rearrangement was observed. A photograph of the cross-sectional plane of the frozen die

[1] CALIBRE 300-22 is a trademark of The Dow Chemical Company.

heel for L/D=16 is shown in Figure 4.13. The interface shape at two cross-sectional planes downstream from the feedblock are shown in Figure 4.15. Little rearrangement of the interface was observed, and the contact line position attained a stable position. An analysis of the contact line at each cross-section indicates that no primary film appeared. The same experiment was performed with the pigmentation reversed (substrate layer was black) and, again, no indication of the presence of a primary film was observed.

Numerical simulations were performed to model this flow problem. A Newtonian model for viscosity was used because of the power-law index for the polycarbonate resin was nearly unity (0.92). A linear slip condition at the contact line was introduced. Flow conditions are $\eta_{01}/\eta_{02} = 0.787$ and $Q_1 / Q_2 = 3.668$. Viscosity differences are caused by differences in melt temperature for each layer (a full analysis including the energy equation and thermal dependence on viscosity is given in Chapter 5). The cross-sectional view of the mesh used is shown in Figure 4.14. It consists of 5 elements in the die width direction and six elements in the die height direction, with 10 elements in the x-direction. Results presented here are for the case of perfect slip. The interface for L/D=10.67 and L/D=16 were measured and compared to the experimental measurements (Figure 4.15). Differences between experimental observations and numerical results can be attributed to modeling errors, interface measurement errors, and thermal rearrangement of the sample when frozen inside the die, which are difficult to estimate. The latter was checked by comparing extrudate samples with the frozen material inside the die, with the observed differences in this case minimal. Thermal rearrangement can be estimated by measuring the thermal expansion coefficient of the polymers involved and the temperature gradient

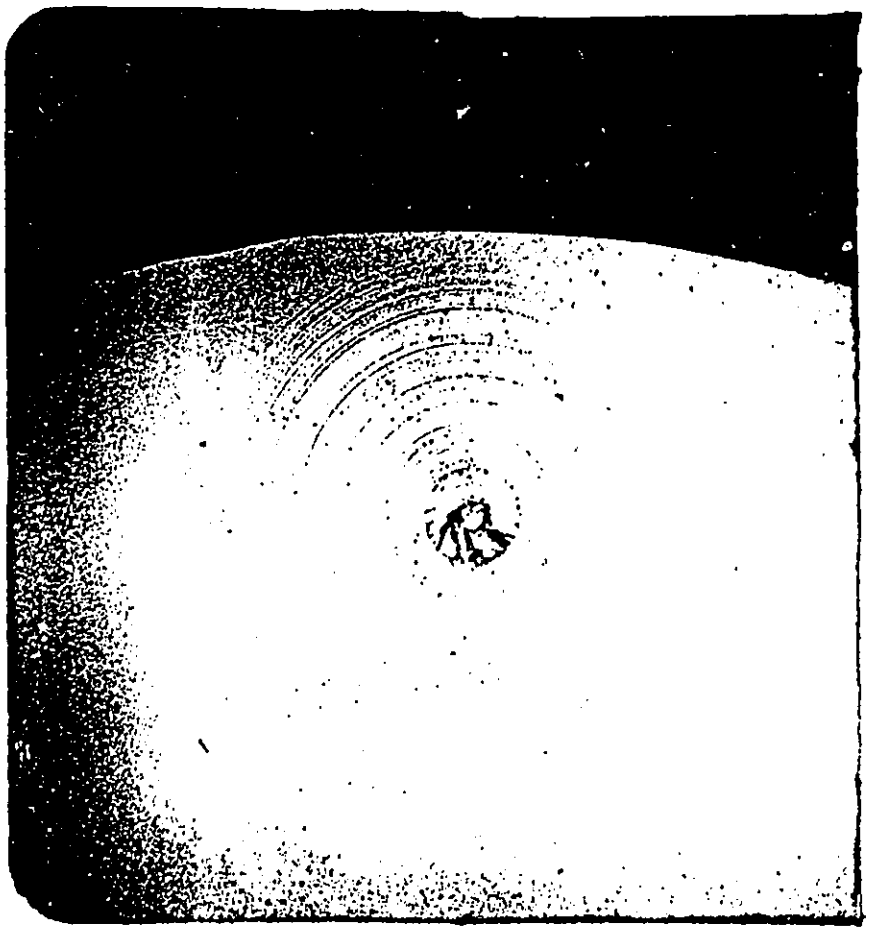

Figure 4.13. Cross-sectional plane interface shape for the PC/PC coextrusion (L/D=16).

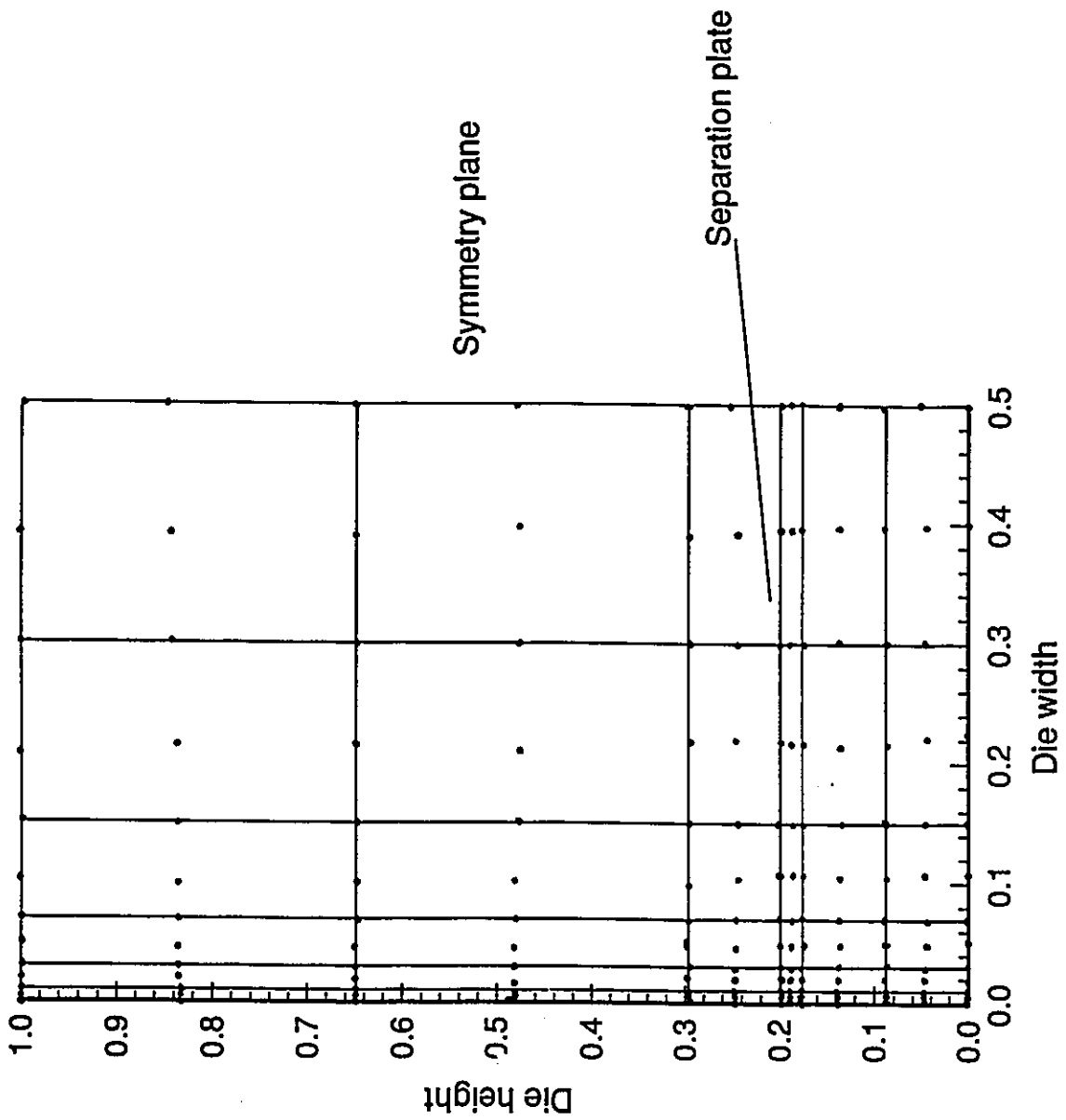

Figure 4.14. Mesh used in PC/PC coextrusion simulation.

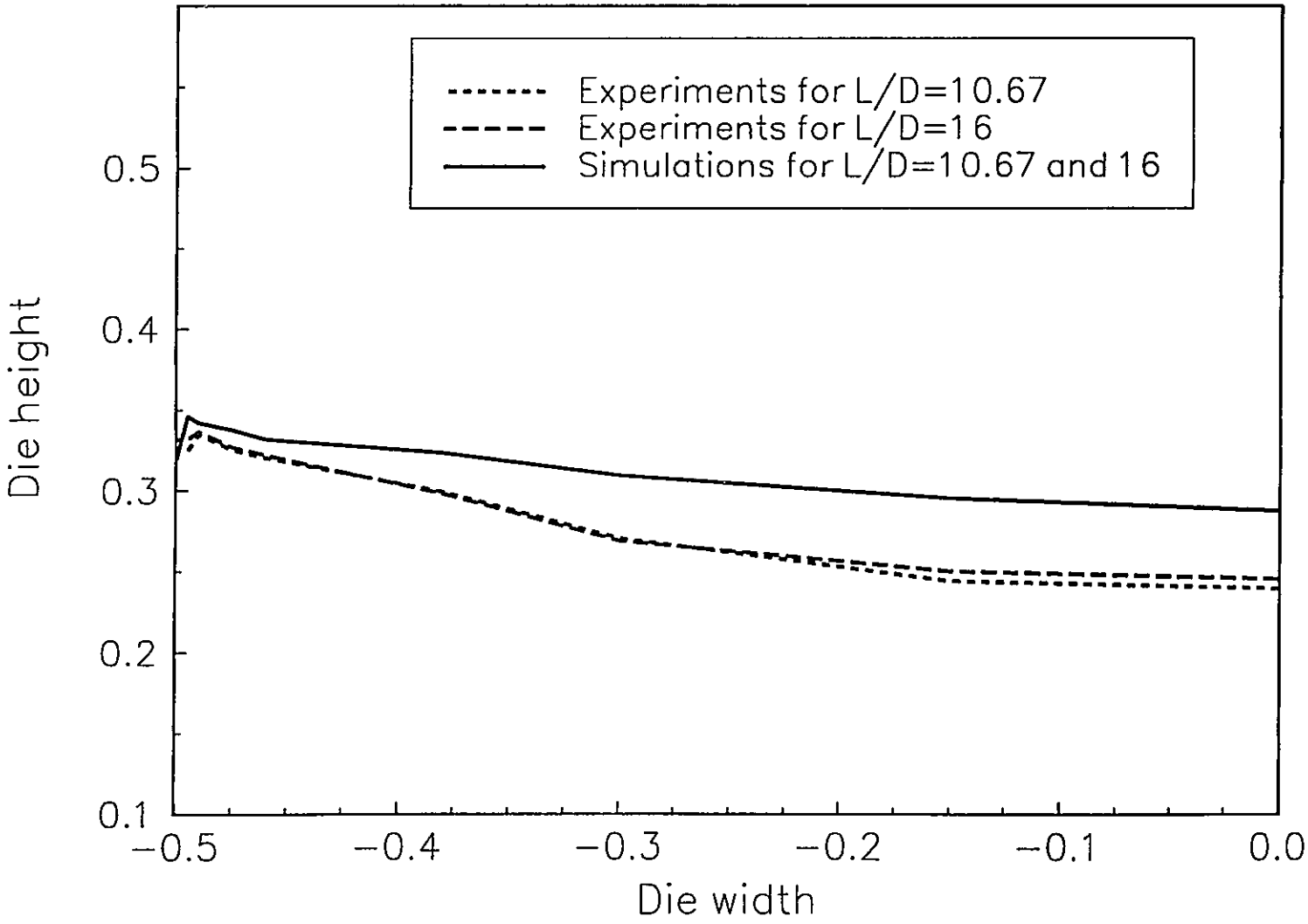

Figure 4.15. Interface position across the die cross-sectional plane at various L/D for polycarbonate /polycarbonate extrusion (Viscosity ratio=0.787 ; Flowrate ratio=3.668).

from the operating temperature to solidification temperature and assesing the amount of distortion each layer will have. Better estimates for the individual melt flowrates and pressure drops are needed since they greatly influence the final interface shape. Despite the experimental uncertainty, the agreement between numerical calculations and experimental results is very good. The computed interface position does not change after $L/D > 2$ and the contact line position does not change after $L/D > 1$; however, the experimental contact line position as well as the interface shape become stable at approximately $L/D = 10$.

The main conclusion from these results is the fact that layer rearrangements occur in layers having the same fluid where the differences in viscosity are due to thermal effects only. Interfacial distortion could be observed in coextrusion cases where the polymer viscosities are relatively well matched.

4.8 Summary.

A fully three dimensional finite element isothermal formulation has been used to model the coextrusion process for two polymer layers. The formulation has the ability to model the contact line boundary condition using several local slip and stick models, features not presently available in most commercial packages. The slip and stick boundary conditions are used to relieve the mathematical singularity caused by the imposition of no-slip at the contact line. The contact line boundary condition has been critically examined using the extrapolation method, slip conditions (linear, power-law and hyperbolic), and stick conditions. The results show that the different assumptions of the

contact line boundary condition show very different interface profiles near the die wall. There is a major difference in the calculated interface profile between the stick and slip contact line assumptions. If the polymer layers are considered to stick to the die wall, as is the common assumption in most fluid models, then a thin entrained layer of the more viscous fluid will be trapped between the less viscous layer and the die wall. Similar interpretations of the effect of the contact line boundary condition were obtained when the fluids were modeled as Newtonian or power-law fluids.

Experiments with a polycarbonate/polycarbonate system showed no entrained layer of the more viscous material at the die wall and a stable interface after an L/D of approximately 10. Computer simulation using a slip boundary condition was consistent with the interface position from experiments, especially near the die wall. Calculations also showed that the interface does not change appreciably after an L/D of approximately 2.

Chapter 5 will discuss the importance of thermal effects on the interface deformation. As well, polymer systems containing PS, HDPE or PP show complex interface deformation near the die wall. The slip boundary condition discussed in this chapter is an important boundary condition needed to explain the observed profiles, in conjunction with possible thermal and non-Newtonian effects.

CHAPTER 5

THERMAL EFFECTS IN COEXTRUSION

5.1 Introduction.

In the previous chapter, several boundary conditions for contact lines in coextrusion flows were introduced and their effect on the final interface shape studied using a three-dimensional finite element code. It was found that a local linear slip (Equation 4-2) or stick boundary condition for the contact line was enough to relieve the mathematical singularity caused by the classical no-slip boundary condition and to capture wall effects, confirmed by experiments with polycarbonate extrusion flows. In this chapter, the code is used to study the effects of temperature on the final interface shape. Also, the mesh generator was modified to take into consideration the entrance angle of the different melts.

The computer code was used to simulate a number of bicomponent flow situations. Unless otherwise stated, a mesh of 5 elements and 11 nodes in the die width (y-direction) and 6 elements and 13 nodes in the die height (z-direction, 3 elements for each fluid) is used in this chapter (Mesh 1, Figure 5.1a). Entrance angle is set to 0; B is set to 0.1 for both fluids; n_j=1 (equation 2-11) and the effects of interfacial tension are neglected. Viscosity and flowrate ratios are given as a ratio of fluid 1 to fluid 2 (lower / upper). After several mesh designs, it was found that the mesh used was an appropriate

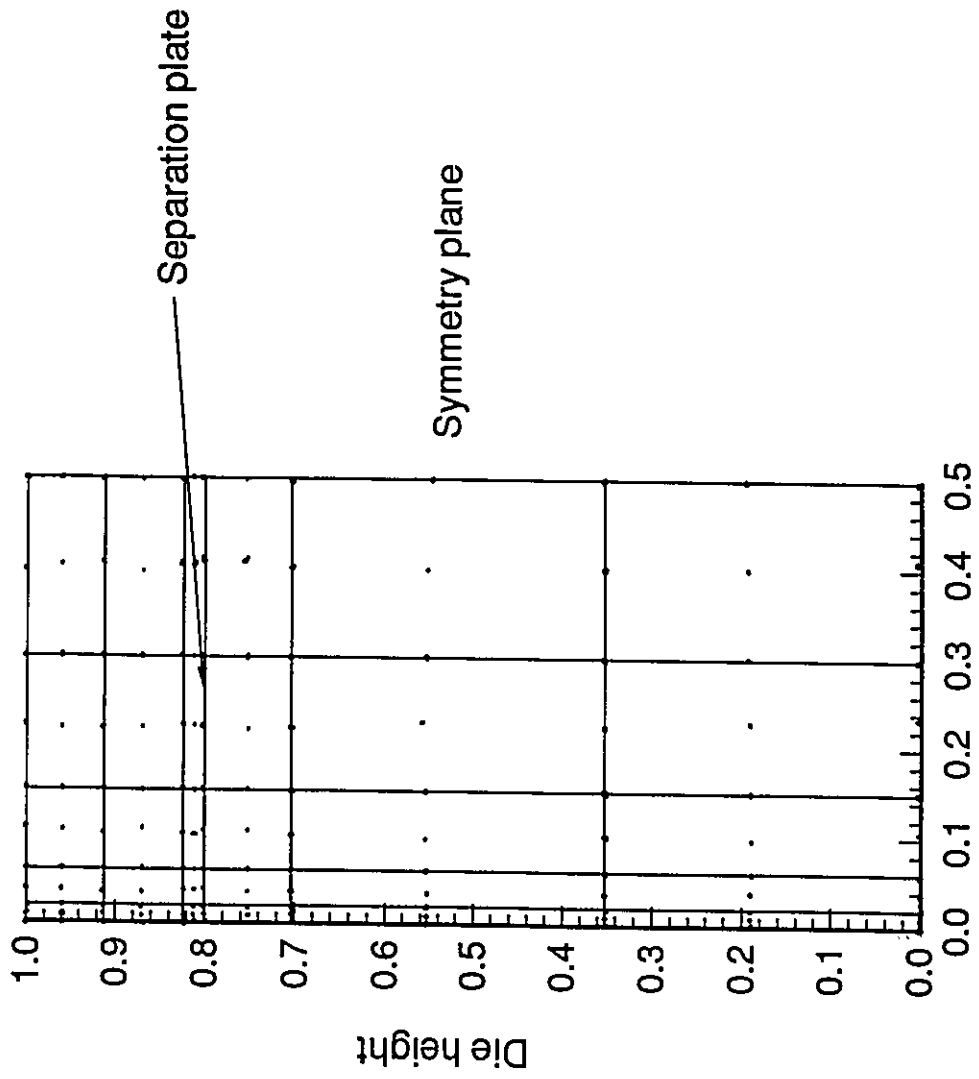

Figure 5.1(a) y-z cross-section of the mesh used in simulations (5x6 in the cross section).

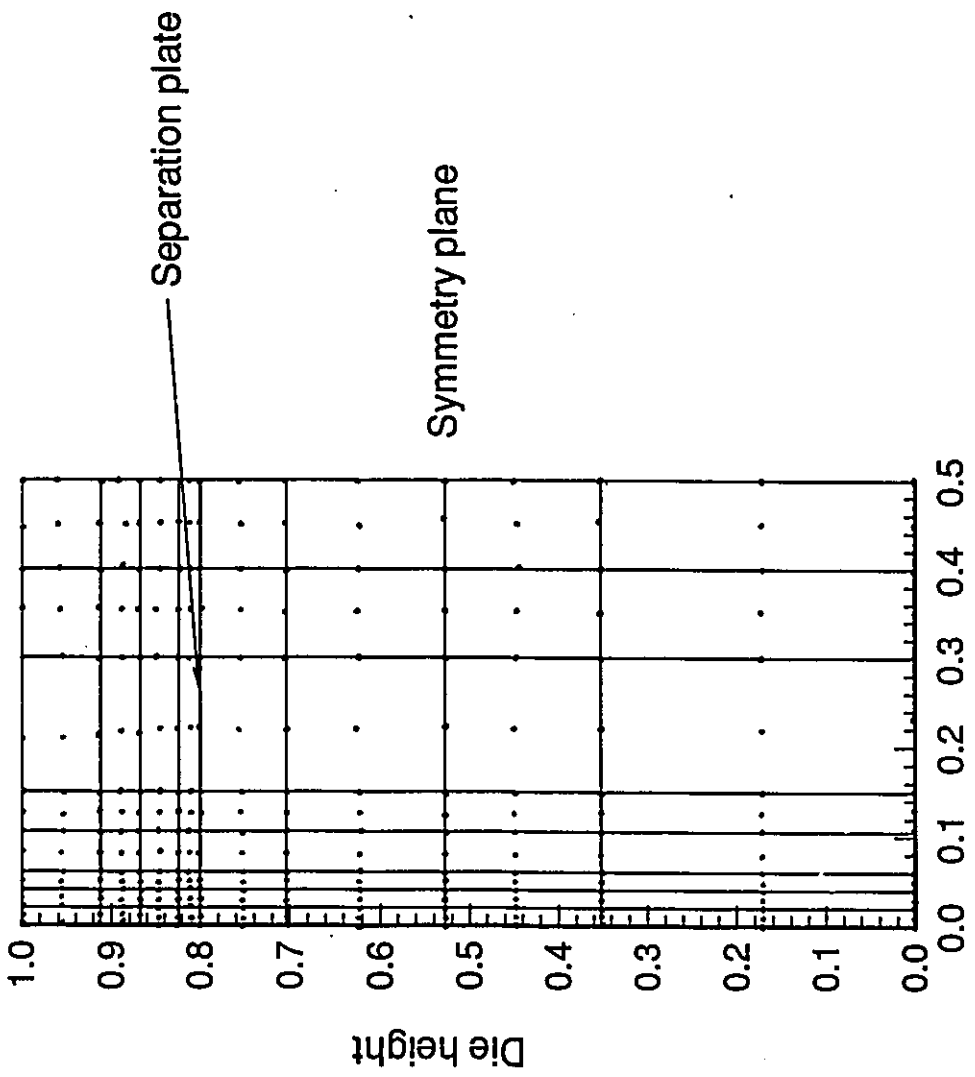

Figure 5.1(b) y-z cross-section of the mesh used in simulations (8x8 in the cross section).

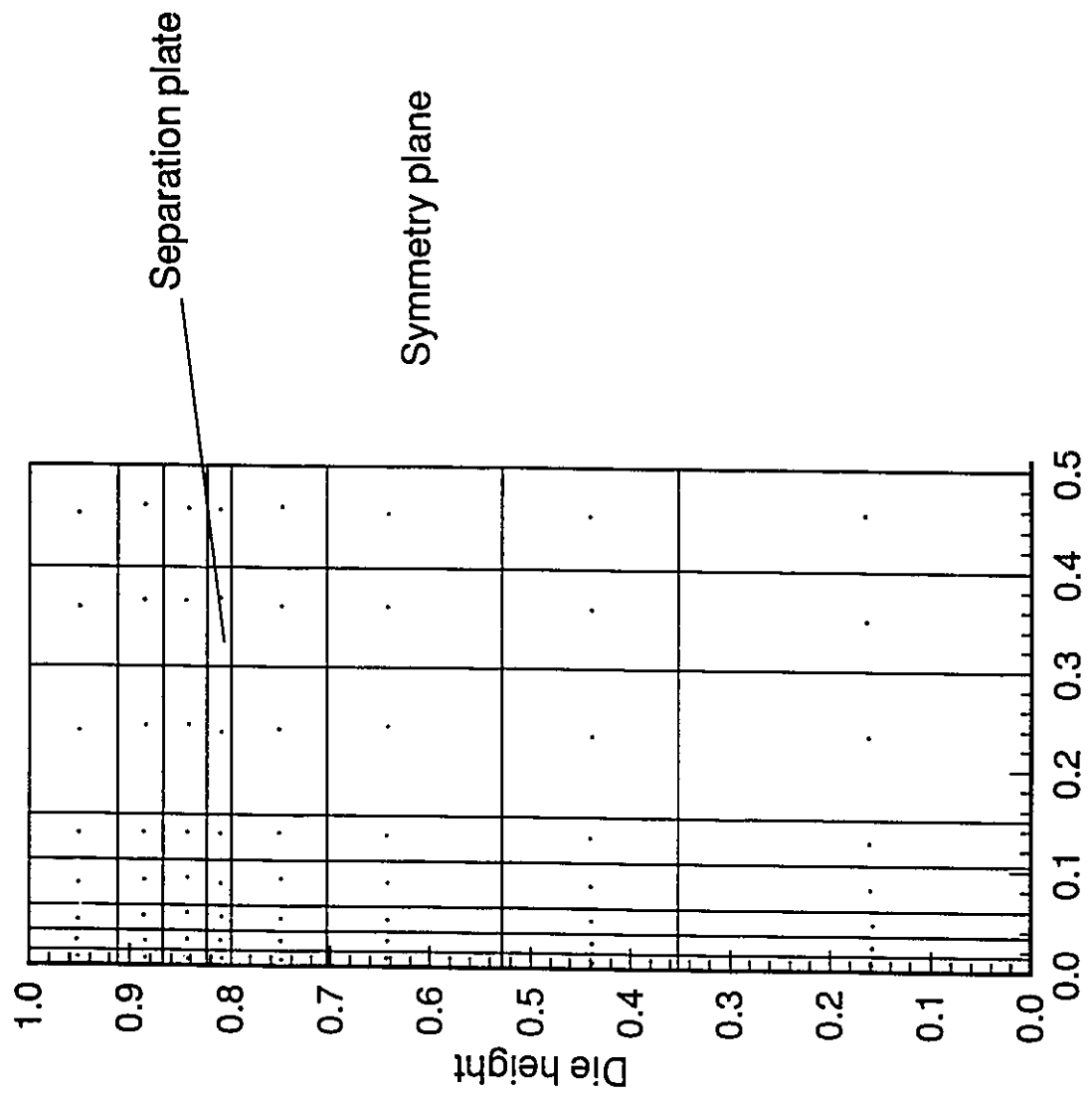

Figure 5.1(c) y-z cross-section of the mesh used in simulations (8x8 in the cross section).

compromise between accuracy and computational effort. Figure 5.1b shows a more refined mesh (Mesh 2) with a cross sectional density of 8 elements and 17 nodes in the y-direction and 8 elements and 17 nodes in the z-direction (4 elements for each fluid). Figure 5.1c shows a mesh with the same number of elements as in Mesh 2, but the mesh density is increased near the die wall (first two columns of elements, Mesh3). In Mesh 1, Mesh 2, and Mesh 3, 11 elements (23 nodes) in the flow direction (x-direction) are used for a total of 330, 704 and 704 elements, respectively. Figure 5.2 shows the final interface shape for a typical coextrusion case in which $\eta_{01} / \eta_{02} = 2.0$ and $Q_1 / Q_2 = 10.0$ with Pe=500, Br=0.06, b=2.0 using the meshes shown in Fig. 5.1a, 5.1b,and 5.1c . The maximum difference between predicted interface locations on the two meshes is less than 0.6%. Table 5.1 summarizes the differences in predicted outlet flowrates, the difference with respect to imposed inlet flowrates and predicted average velocities at the outlet. Figures 5.3 and 5.4 show the interface development using the mesh in Figure 5.1b coupled with the u-velocity component and temperature, respectively. Figures 5.5 and 5.6 are enlargements near the die walls of Figures 5.3 and 5.4, respectively that indicate the complex interactions that occur near the contact line. Note that the fully developed flow situation is reached at L/D=1 after the separation plate. In all cases studied, the effect of the local boundary condition for the contact line is localized within the elements adjacent to the contact line. Figure 5.7 shows the convergence rate for both meshes. The mesh shown in Fig. 5.1b requires about 300 Mb of hard drive space for the frontal solver alone (frontwidth is 1293), and memory requirements are near the maximum allowable for the machines used.

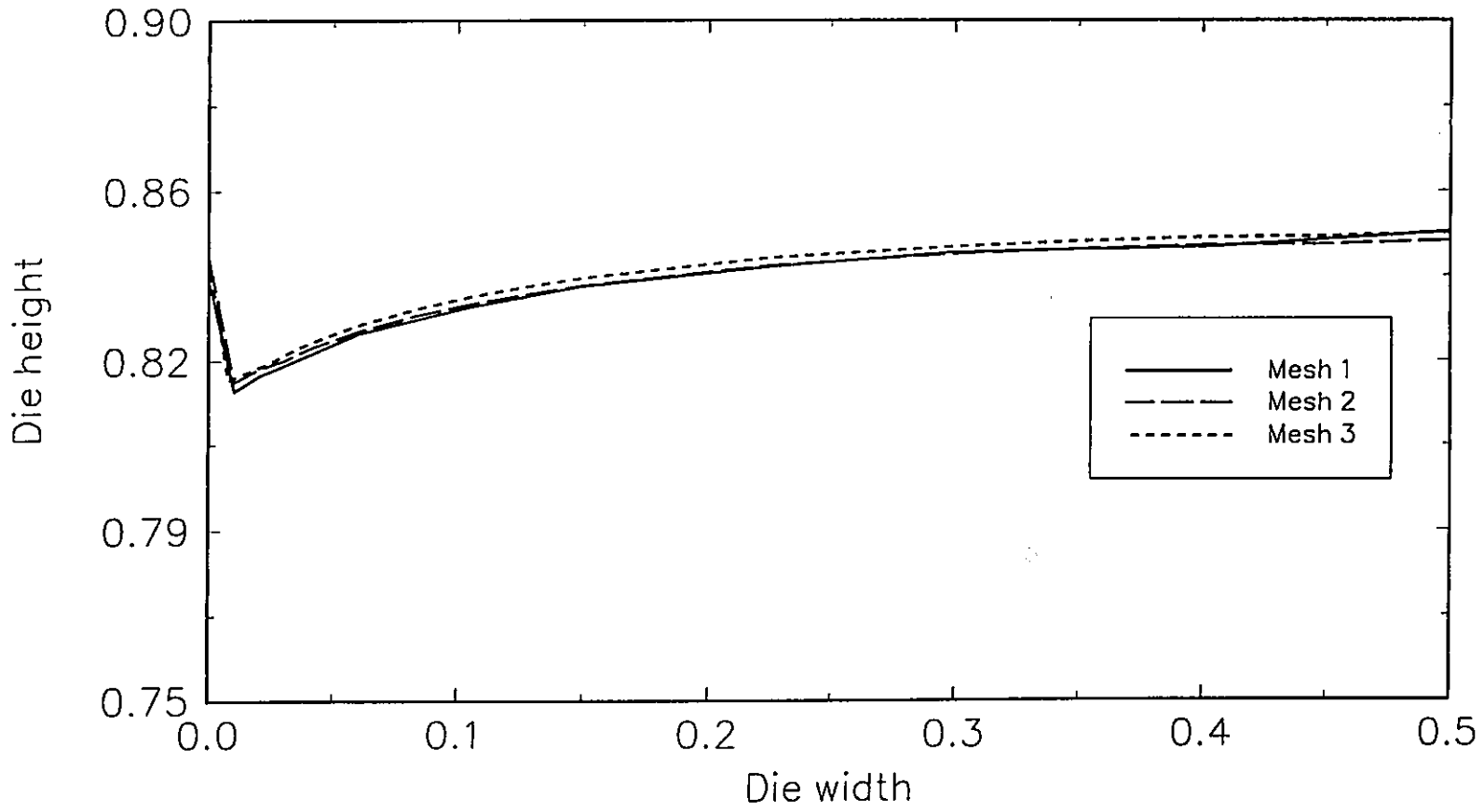

Figure 5.2. Final interface shape for the meshes of Fig 5.1a, Fig. 5.1b. and Fig. 5.1c.

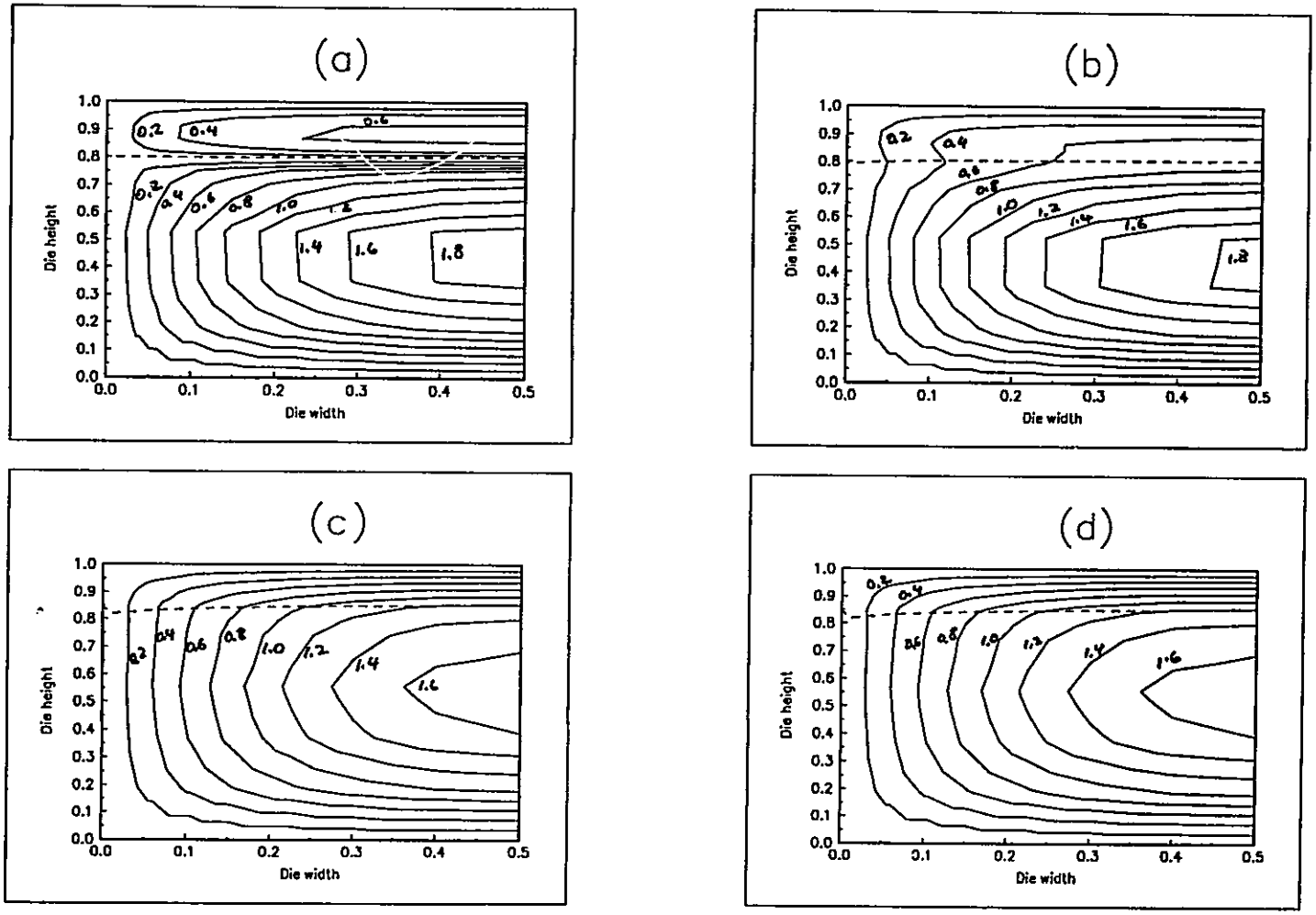

Figure 5.3. *u*-velocity contours in *y*-*z* planes along the *x*-axes. (a) L/D=0; (b) L/D=0.0725; (c) L/D=1.0; (d) L/D=2.0. Dotted lines indicate the interface. Contours are from 0.0 to 1.8 in 0.2 increments (dimensionless)

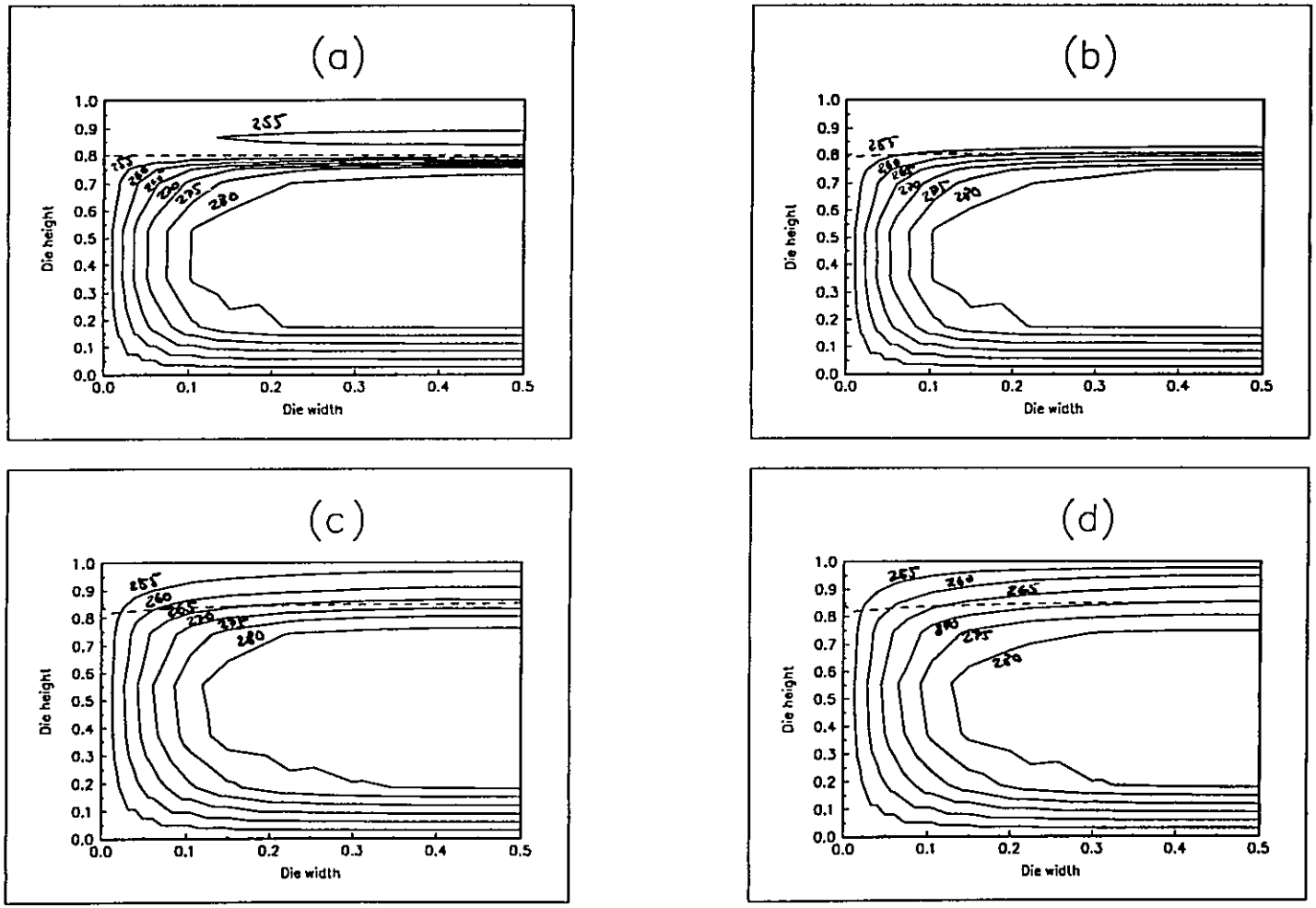

Figure 5.4. Temperature contours in y-z planes along the x-axes. (a) L/D=0; (b) L/D=0.0725; (c) L/D=1.0; (d) L/D=2.0. Dotted lines indicate the interface. Contours are from 250°C to 285°C in 5°C increments.

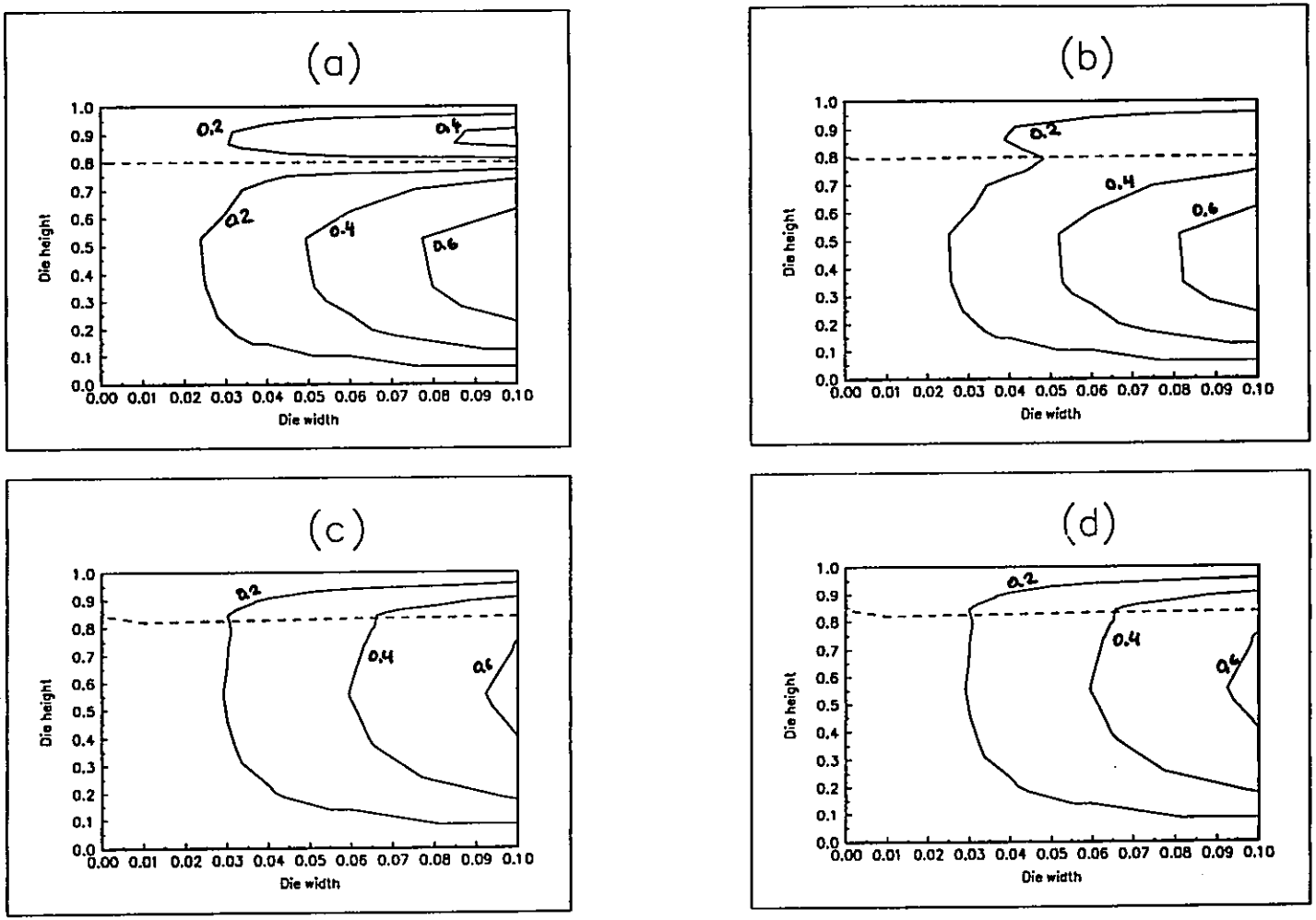

Figure 5.5 *u*-velocity contours in *y*-*z* planes along the *x*-axes. (a) L/D=0; (b) L/D=0.0725; (c) L/D=1.0; (d) L/D=2.0. Dotted lines indicate the interface. Enlargement near the die walls.

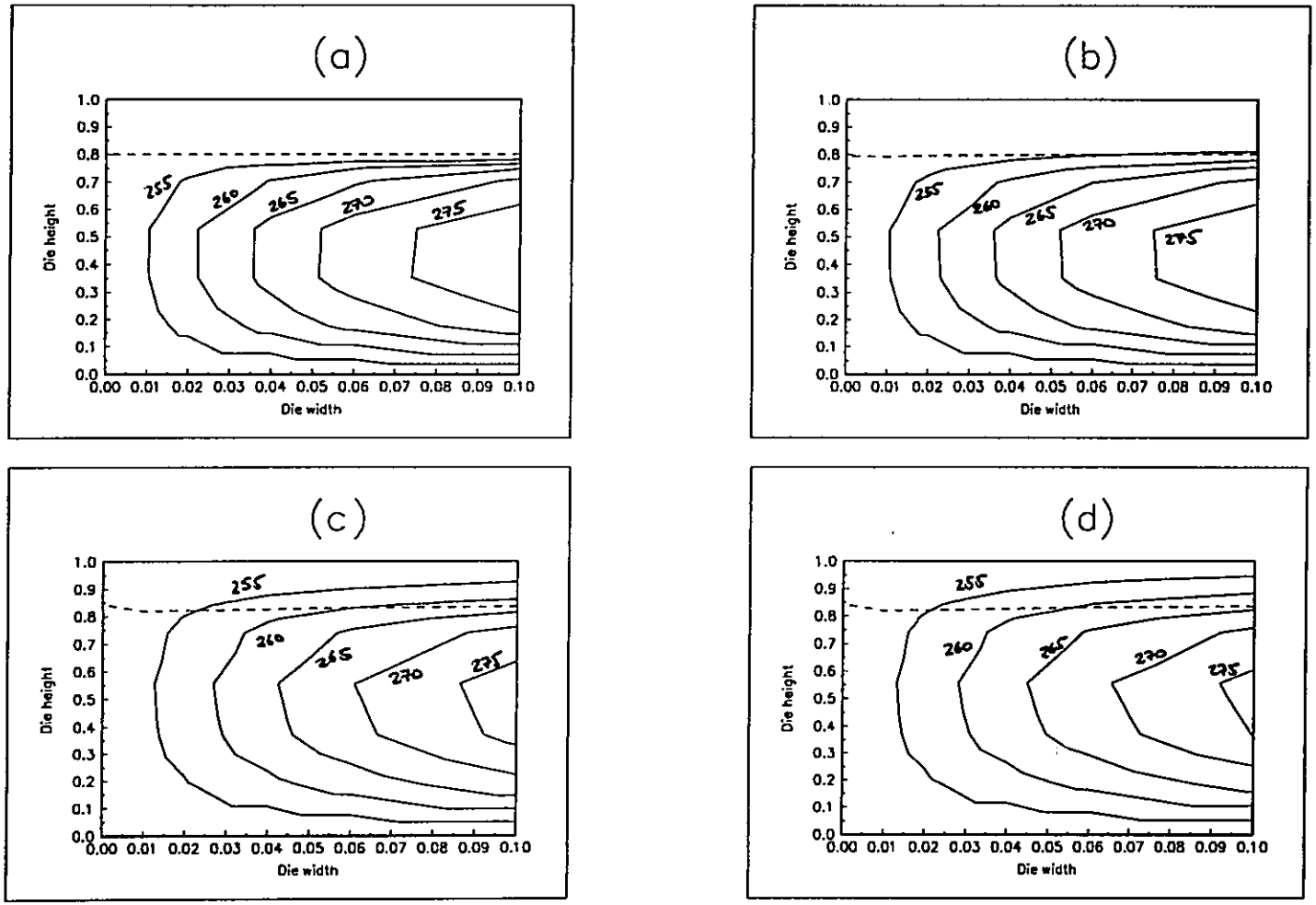

Figure 5.6. Temperature contours in *y*-*z* planes along the *x*-axes. (a) L/D=0; (b) L/D=0.0725; (c) L/D=1.0; (d) L/D=2.0. Dotted lines indicate the interface. Enlargement near the die walls.

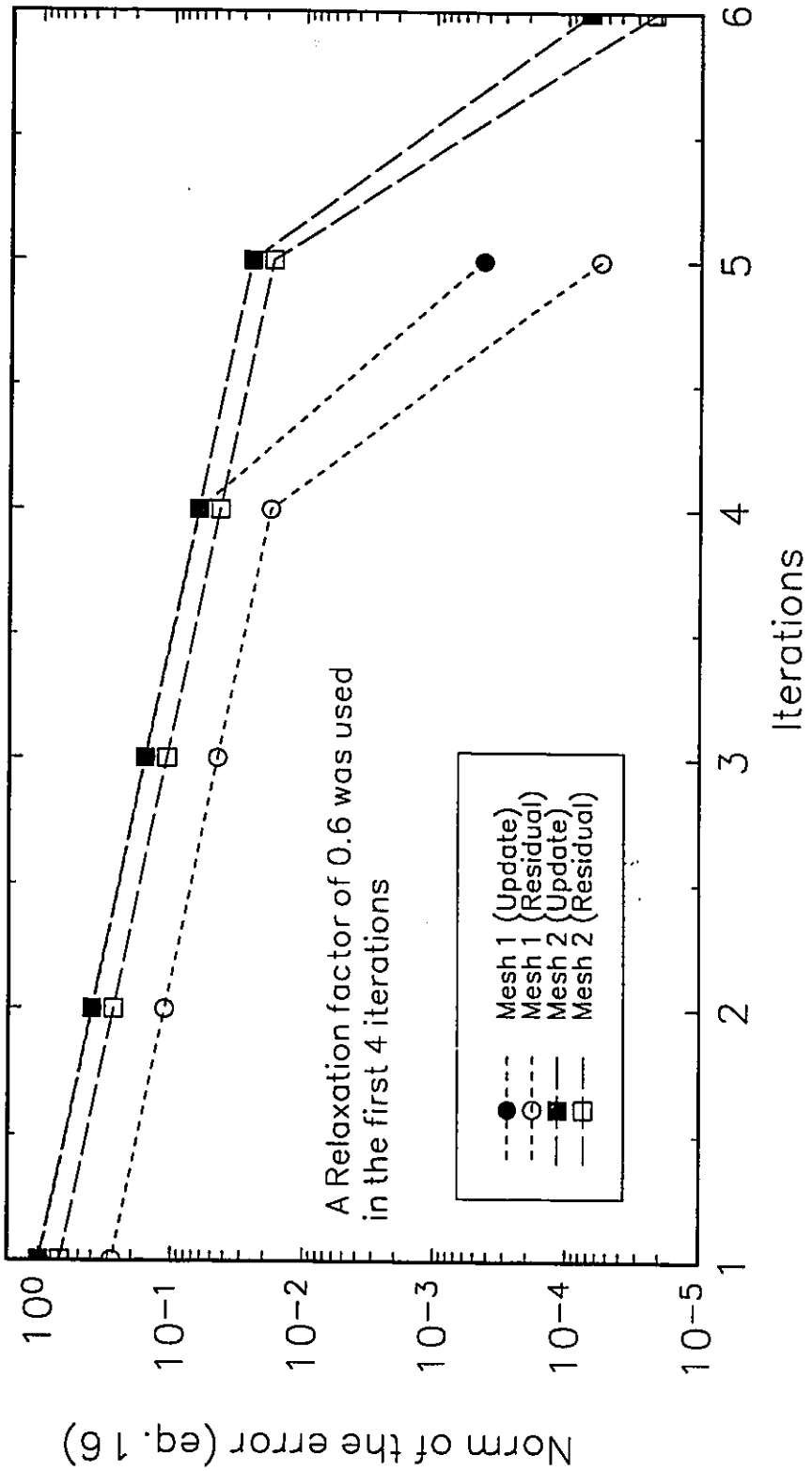

Figure 5.7. Convergence rate for the meshes of Fig. 5.1a and Fig. 5.1b.

TABLE 5.1. Mesh comparison.

	Mesh 1 (Fig. 5.1a)	Mesh 2,3 (Fig. 5.1b,c)
Number of elements	330	704
Number of equations	10800	23030
Q_2, outlet	0.0392	0.0390
Q_2, inlet (difference, %)*	0.0389 (0.78%)	0.0387 (0.77%)
Q_1, outlet	0.3843	0.3844
Q_1, inlet (difference, %)*	0.3843 (0%)	0.3844 (0%)

* difference = 100 * (outlet-inlet) / inlet, only four significant figures used.

5.2 Effect of entrance angle.

For this case, a Newtonian system with a viscosity ratio $\eta_{01} / \eta_{02} = 2$ and a flowrate ratio $Q_1 / Q_2 = 10$ is modeled. The temperature of the system is kept constant at 250°C, and perfect slip is approximated by using a large number for the slip coefficient (B=10). Final interface shapes are shown in Figure 5.8. Note the presence of a primary film displacement near the die wall. When the entrance angle is varied from 0 to 30 degrees, the intrusion of the upper, less viscous fluid is also displaced downwards. A study of the velocity field for entrance angles of 0 and 30 degrees shows that the major influence of the entrance angle is a displacement of the lower fluid by the upper fluid. No significant cross-flow appeared at the meeting point of the two fluids in any of the cases tested.

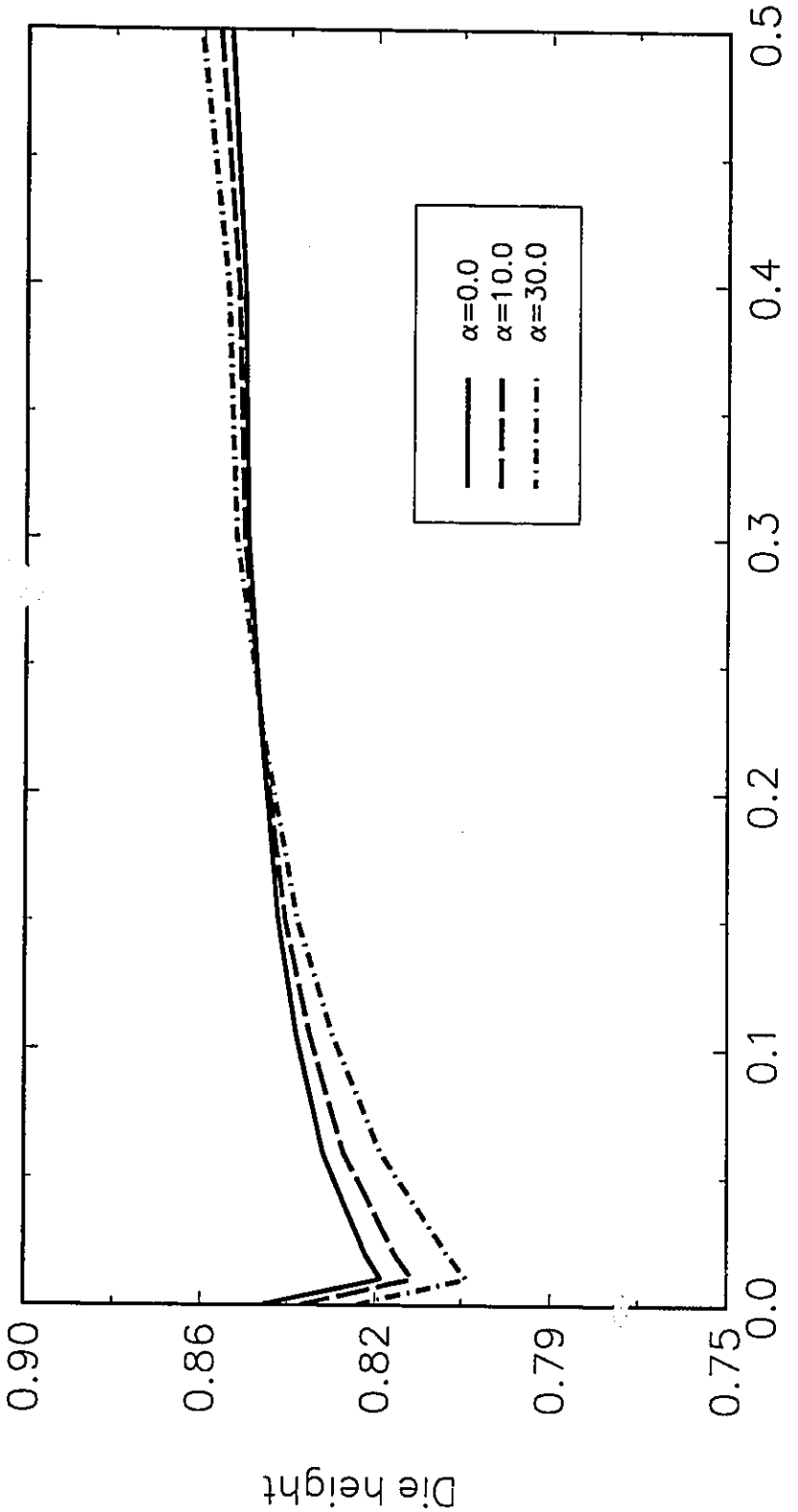

Figure 5.8 Final interface shape for various entrance angles, α. η_{01} / η_{02} =2;Q_1 /Q_2 =10; B=0.1 (dimensionless).

One of the benefits of three-dimensional simulations is the possibility of studying the full three-dimensional displacement of the interface shape. In the case of one-dimensional and two-dimensional multilayer flow modeling, only the location of the interface at the centre of the die is approximated (far right in Figure 5.8). One might be misled to believe that the entrance angle effect is relatively unimportant by only studying the centre-line location of the interface. Note that this is not the case near the die walls, and for precise product applications the displacement near the die walls must be taken into consideration especially over long runners and die manifolds.

5.3 Effect of flowrate ratios.

Figure 5.9 shows the effect of variations of flowrate ratios on the final interface shape. The system has a $\eta_{01} / \eta_{02} = 1.5$ and Q_1/Q_2 is varied from 1 to an increase of 10% in flowrate in each channel in turn. The overall shape of the final interface is not affected by a variation of the flowrate in either channel, but it is displaced accordingly, as expected. For this case, a variation of 10% in the inlet flowrate produces a displacement of the interface of 3% (average taken along the die width) of the die height. Similar responses were observed in other flow situations tested, up to a Q_1/Q_2 of 10.

5.4 Effect of inlet and wall temperature.

The effects of variations in inlet and wall temperatures are also studied for the cases of negligible Pe number (Pe=0) and Pe=2000, which is common in extrusion flows. The case of Pe=0 is intended as a limiting case to establish the influence of the viscous

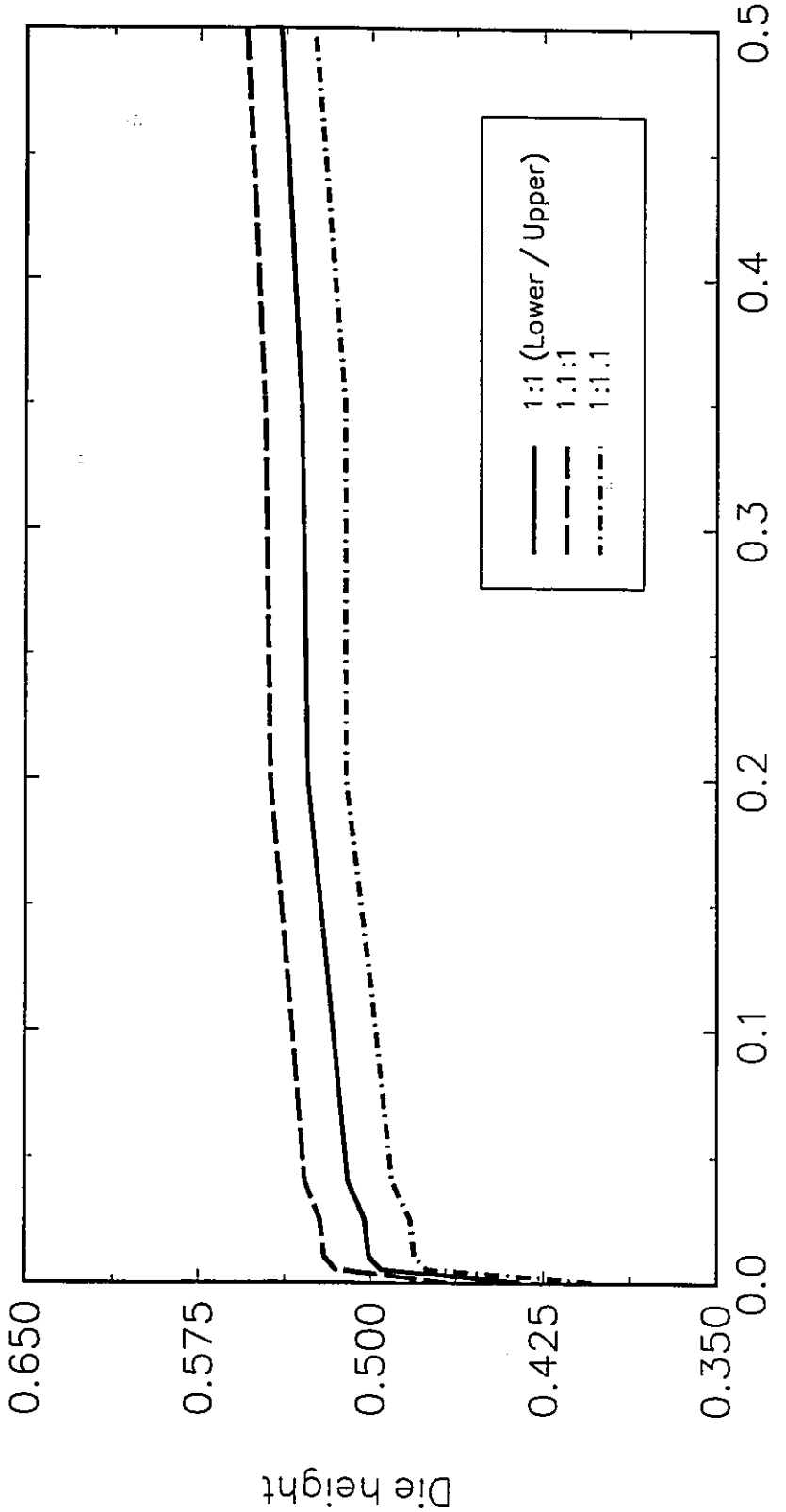

Figure 5.9. Final interface shape for different flowrate ratios. η_{01} / η_{02} =1.5; Perfect slip.

dissipation term on the final interface shape. The dimensionless coefficient for the viscosity dependence in temperature is b=5 and the reference temperature is T_0=250°C. (dimensional b'=0.02 1/°K; T_∞=0°C). The dimensionless slip coefficient is B=0.1. Variations of 30°C on the two inlet temperatures and wall temperatures were introduced and each variation studied in turn.

Figure 5.10 shows the final interface shape for the case of Br=0.11 and Pe=0. The interface shape for the "isothermal" case (Br=0.0, b_1=b_2=0, T_1=T_2=T_w=250°C) is also plotted as a reference. Figure 5.10 shows an interface displacement upwards with the presence of a primary-film displacement. In the base case, the viscosity ratio is 2 everywhere in the flow domain, whereas in the cases in which the temperature affects the viscosity, there is a local viscosity ratio that depends on temperature (through the temperature dependence of the viscosity). The final interface shape is the same regardless of which inlet temperature is varied, as expected for Pe=0. In the limiting case of Pe=0, the dominating thermal force is the viscous dissipation, and the wall temperature plays a secondary role. The flow structure at the die exit is not as simple as in the isothermal case. Figure 5.11 shows the temperature contours at the exit cross-section (Figure 5.11a) and along the die centre (Figure 5.11c) for the case of T_w=280°C, T_1=T_2=250°C, and Pe=0. Due to the temperature profile inside the die, there is also a viscosity profile. So the term viscosity ratio loses its meaning as an *overall* flow parameter, since it varies locally. Figure 5.12 shows the final interface shape for the case of Br=0.11 and Pe=2000. In all these cases, a flat temperature profile is assumed at the inlet and fixed temperature at the die walls.

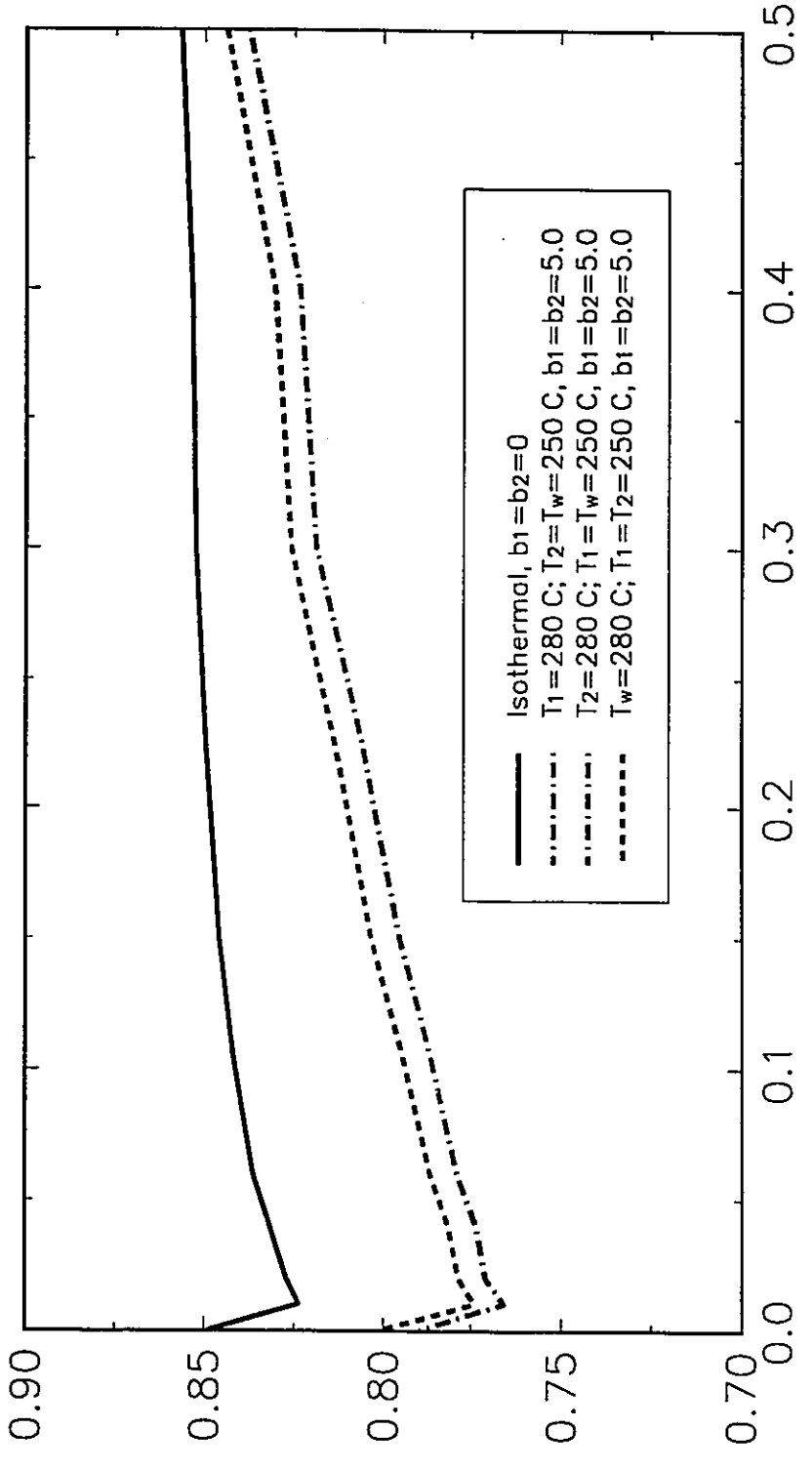

Figure 5.10. Effect of variations of inlet and wall temperatures on the final interface shape. η_{01} / η_{02} =2; Q_1/Q_2=10; B=0.1 (dimensionless), Pe=0.

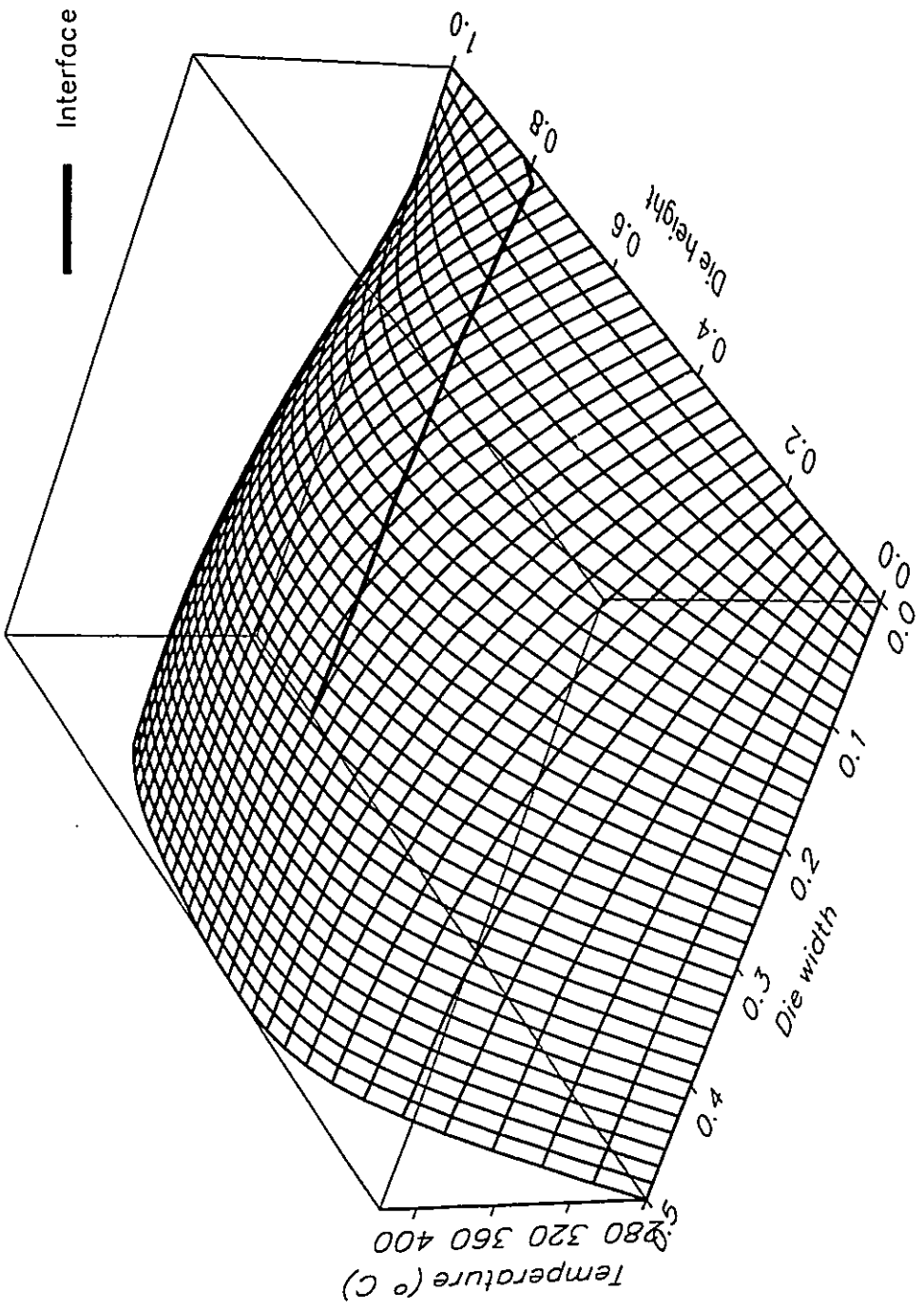

Figure 5.11 (a) Temperature profile at the die exit (°C). Conditions as in Figure 5.10.

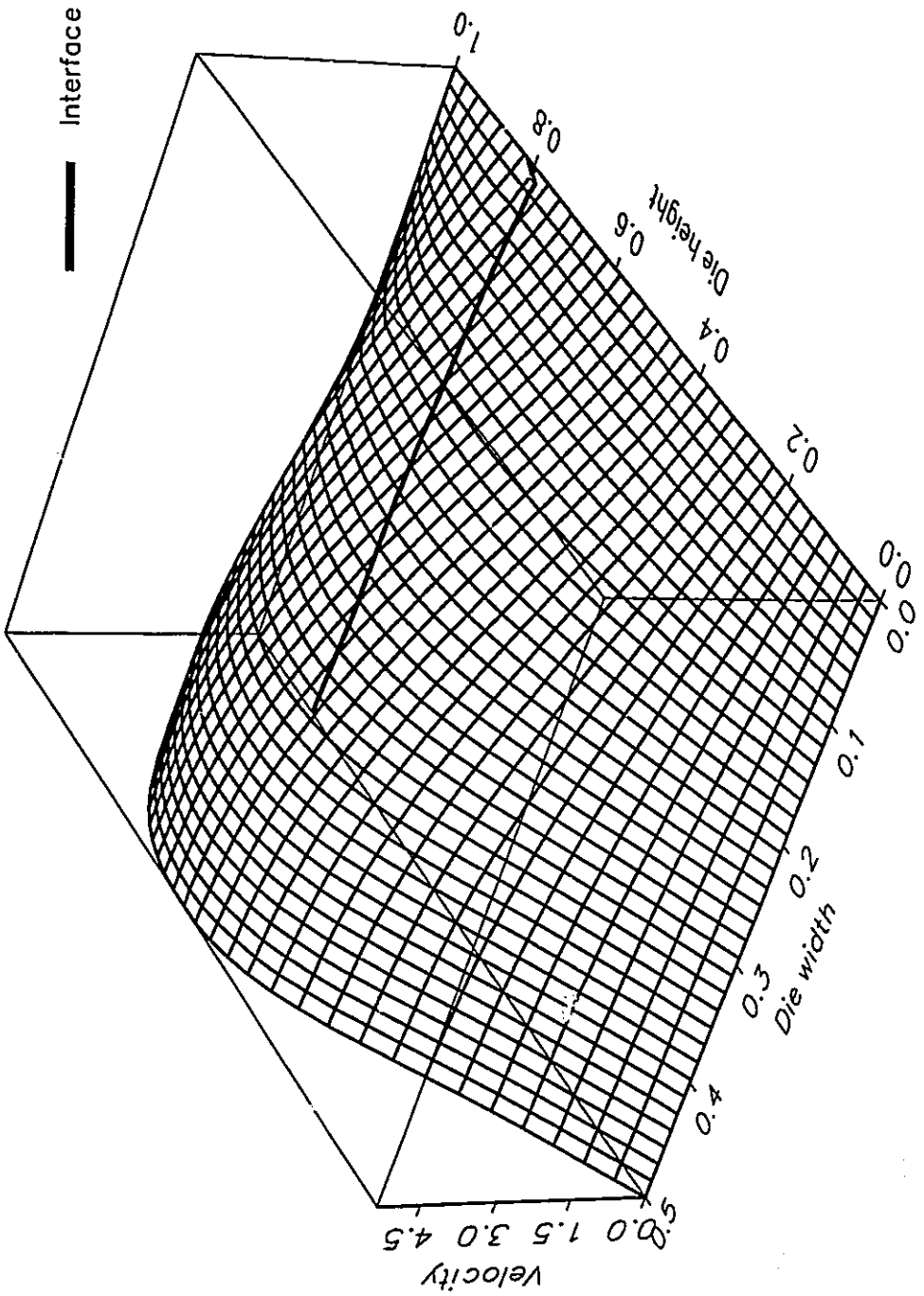

Figure 5.11 (b) u-velocity distribution. Conditions as in Figure 5.10.

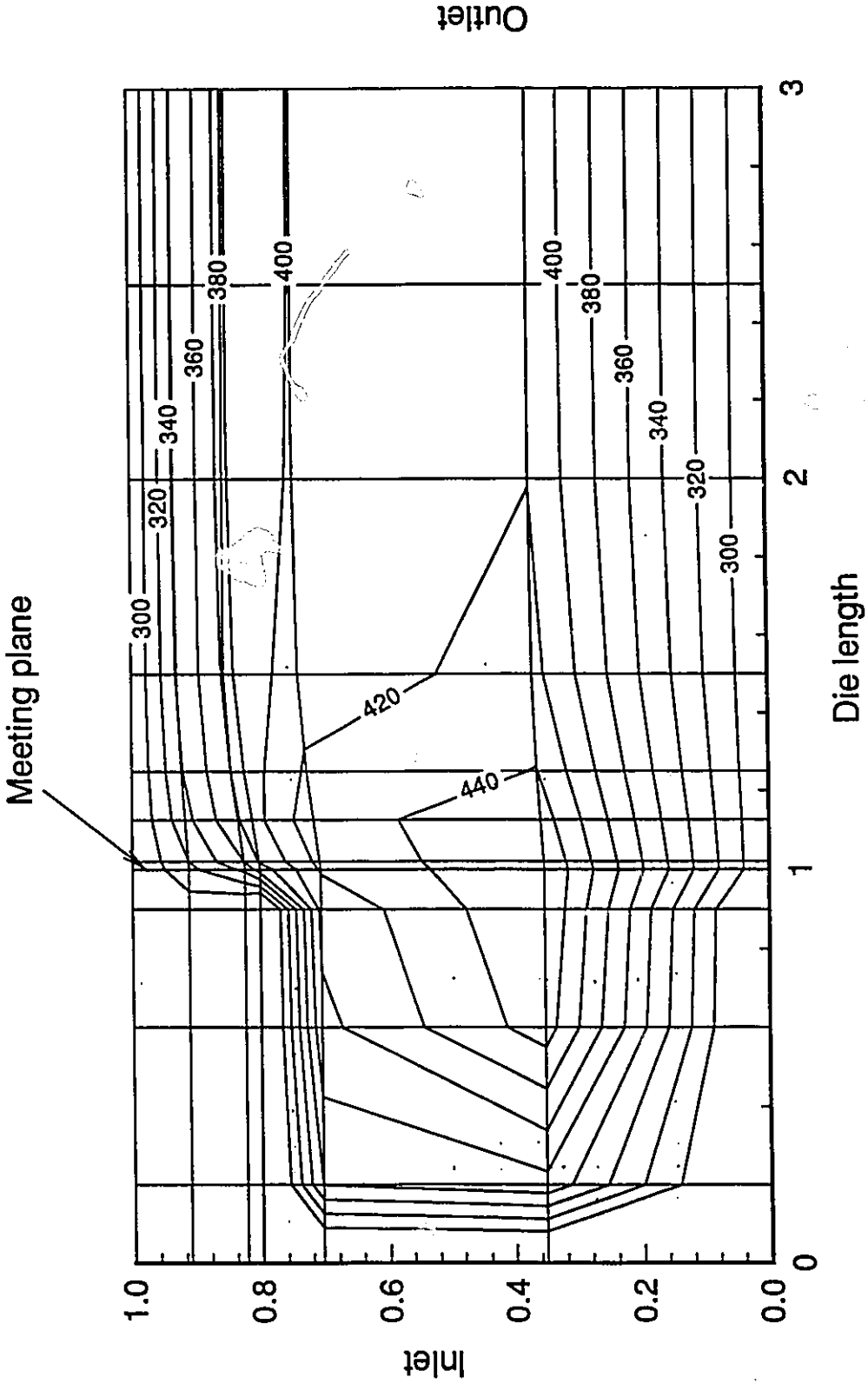

Figure 5.11 (c) Temperature profile along the die centre (°C). Conditions as in Figure 5.10.

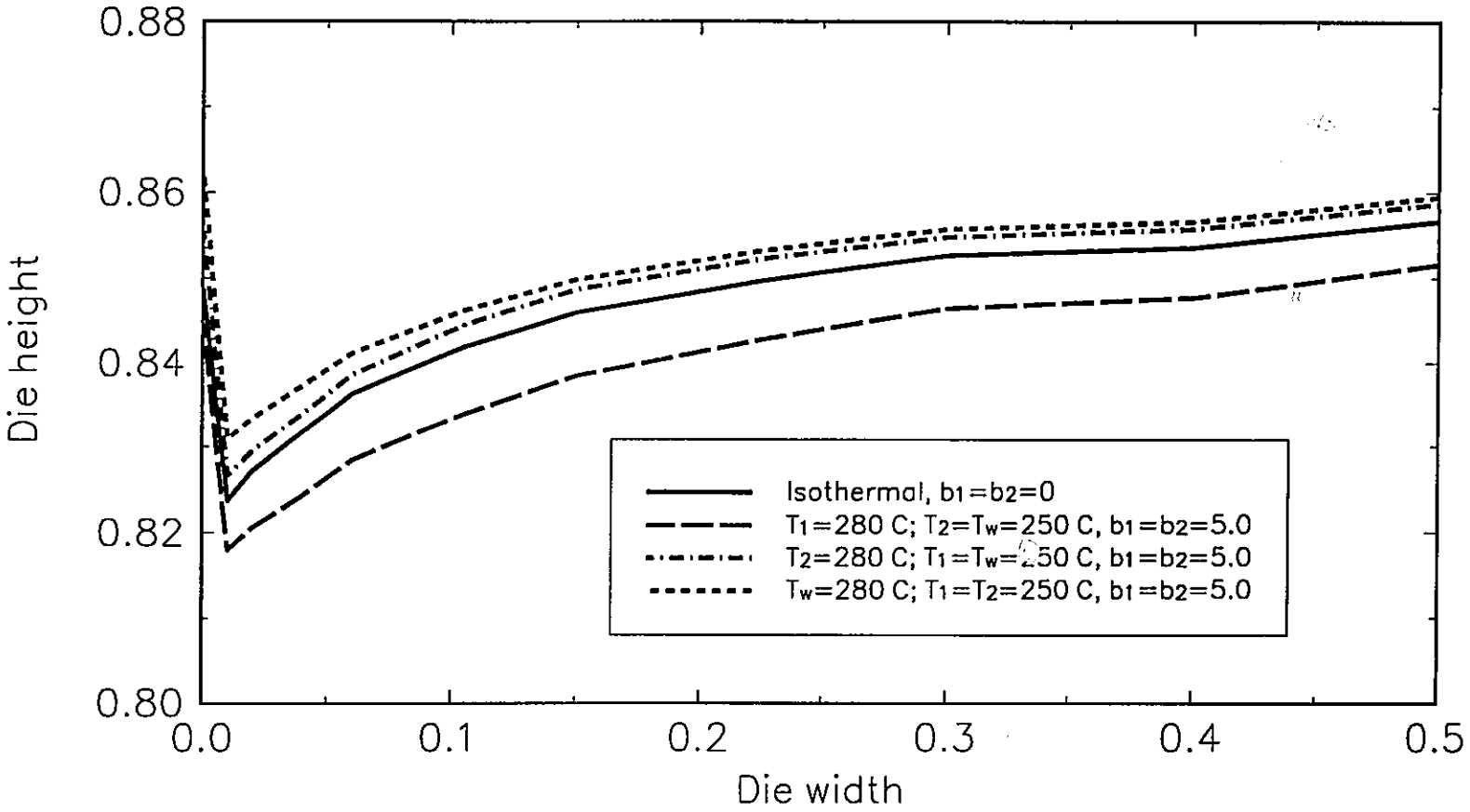

Figure 5.12. Effect of variations of inlet and wall temperatures on the final interface shape. η_{01} / η_{02} =2; Q_1/Q_2=10; B=0.1 (dimensionless), Pe=2000.

Inlet and wall temperatures can be used to adjust the final interface shape. Wall temperatures are easier to control than inlet temperatures. Inlet melt flows typically have a temperature profile across the die inlet, sometimes with substantial temperature differences across the die cross-section, which are difficult to predict.

5.5 Effect of the sensitivity of viscosity to temperature.

Figure 5.13 shows the final interface shape for the same flow conditions as in the previous section. The inlet temperature of fluid 2 (280°C) is greater than the inlet temperature of fluid 1 and the die wall temperature, which are both 250°C. The dimensionless b (viscosity thermal coefficient) for both fluids is varied from 0.0 to 10.0. A coefficient value of b=0.0 decoupled the dependence between the energy and momentum equations. Assuming a reference temperature of T_0=250°C and T_∞=0°C, a b coefficient of 10 will have a dimensional value of 0.04 K^{-1}. Typical polymer values for b lie between 0.01 and 0.04 K^{-1} (Vlcek and Vlachopoulos, 1993).

The results are shown in Figure 5.14 for the case in which only b_1 is varied, while b_2 is kept constant at a fixed value of 10. The inlet temperature for fluid 1 is 280°C, a temperature of 250°C for the inlet of fluid 2 and for the die wall. The primary film displacement disappears when b_1 is zero. Figure 5.14 shows that the effect of the thermal sensitivity of viscosity is more pronounced in the bulk flow than in the vicinity of the contact line, the location is primarily determined by the local slip boundary condition. Note that in Figure 5.14 the slip boundary coefficient is the same for all three cases. For b_1=0.0 and b_1=5.0 (b_2=10.0 for both) the contact point position is the same but the

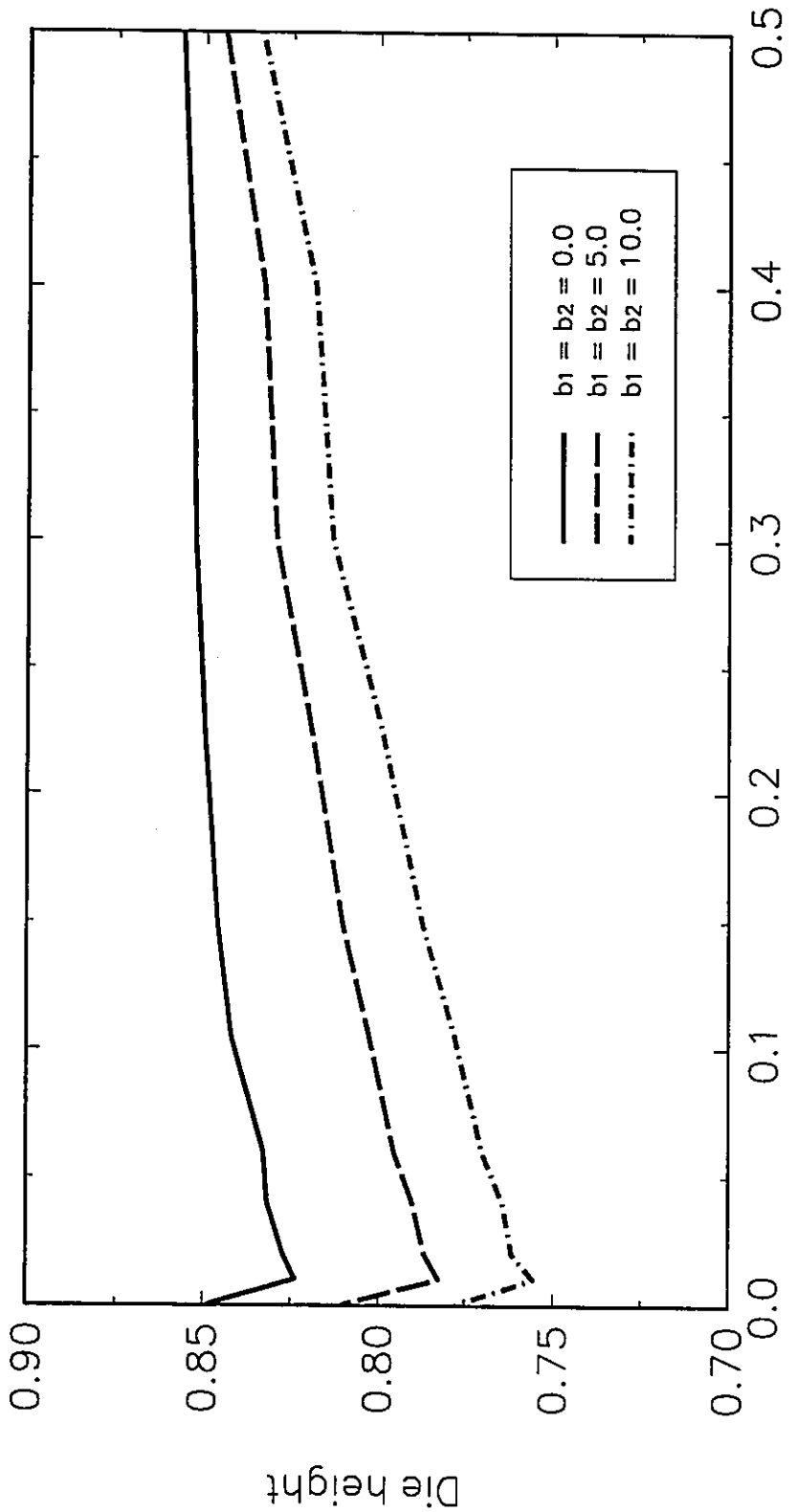

Figure 5.13. Effect of b, variation in both fluids; $\eta_{01} / \eta_{02} = 2$; $Q_1 / Q_2 = 10$.

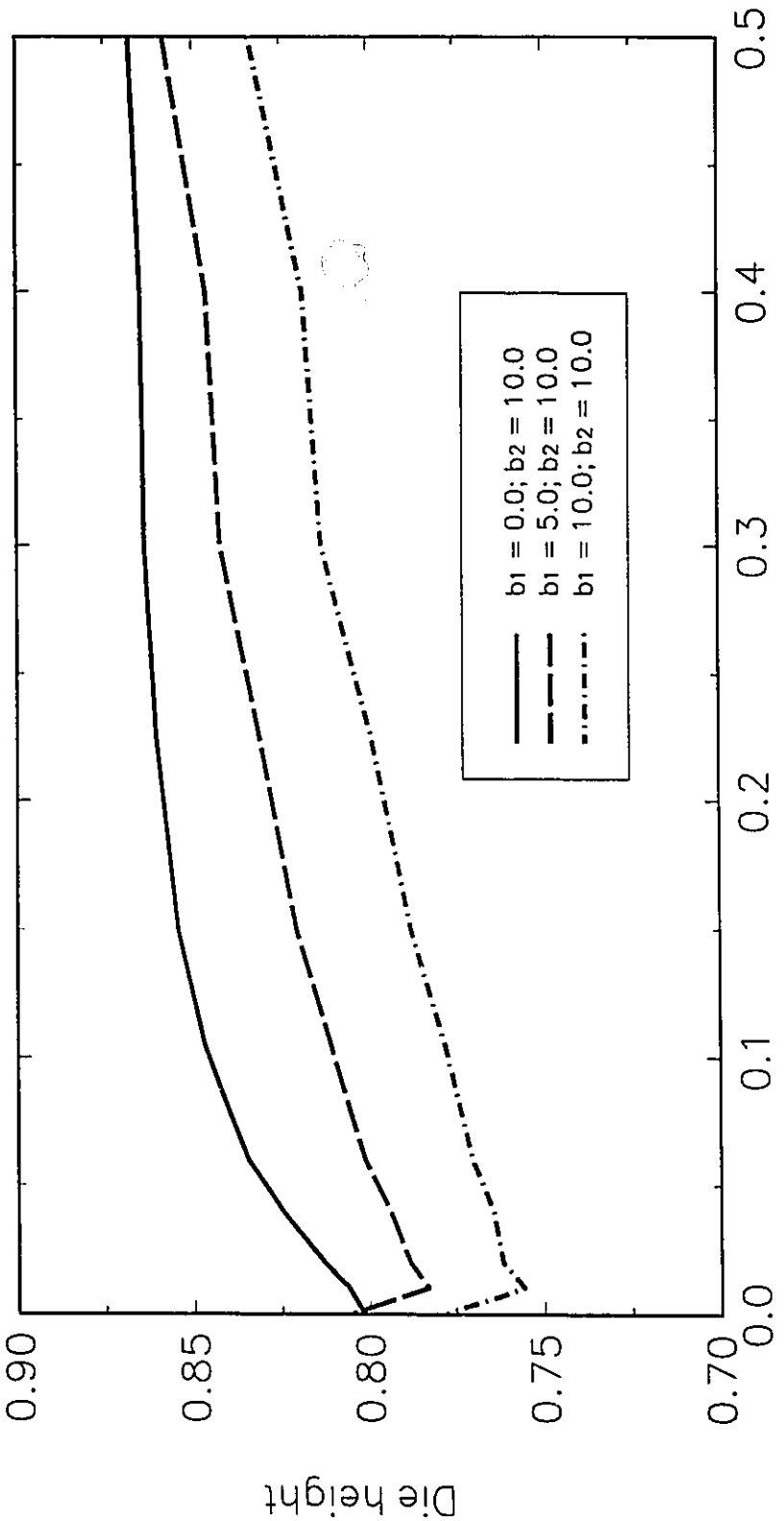

Figure 5.14. Effect of b, variation in fluid 1; $\eta_{01} / \eta_{02} = 2$; $Q_1 / Q_2 = 10$; $b_2 = 10.0$ (dimensionless).

interface curvature reverses due to bulk flow effects. With b_1=10.0, the thermal sensitivity of the viscosity is sufficient to significantly affect the interface position both at the contact line and into the bulk fluid.

The inlet temperature profiles are assumed uniform in these simulations. In practice, a uniform inlet temperature profile could be achieved by using in-line mixers. There is little difference in the final interface shape between uniform and fully developed inlet thermal conditions in the computations. At the outlet, the overall flow picture is complicated due to thermal effects (Figures 5.11a,b,c). These results shows that the temperature sensitivity of the polymer system being extruded, as well as the melt and die temperatures, affect the interface shape.

5.6 Effect of the Carreau model parameters.

Table 5.2 contains rheological data for a typical HDPE (Tadmor and Gogos, 1979) and PS (Vlcek and Vlachopoulos, 1993). These parameters are used to investigate the effect of varying the power-law index and the "relaxation time" in the Carreau model on the final interface shape, using a flow system for which the zero-shear viscosity ratio is 1.5 and Q_1/Q_2=1.0 at a reference temperature of 250°C. A uniform temperature profile of 250°C is imposed at the two inlets and the die walls. Figure 5.15 shows the final interface shape for a Newtonian fluid (λ=0.0 and n=1.0) and for two systems using PS (λ=0.00793 and n=0.236) and HDPE (λ=0.05 and n=0.58) rheological values, respectively. In both cases, b_j = 0 (to decouple thermal effects and examine shear thinning effects only) and B= 0.1 values are used. The main effect of shear thinning is a reduction in local

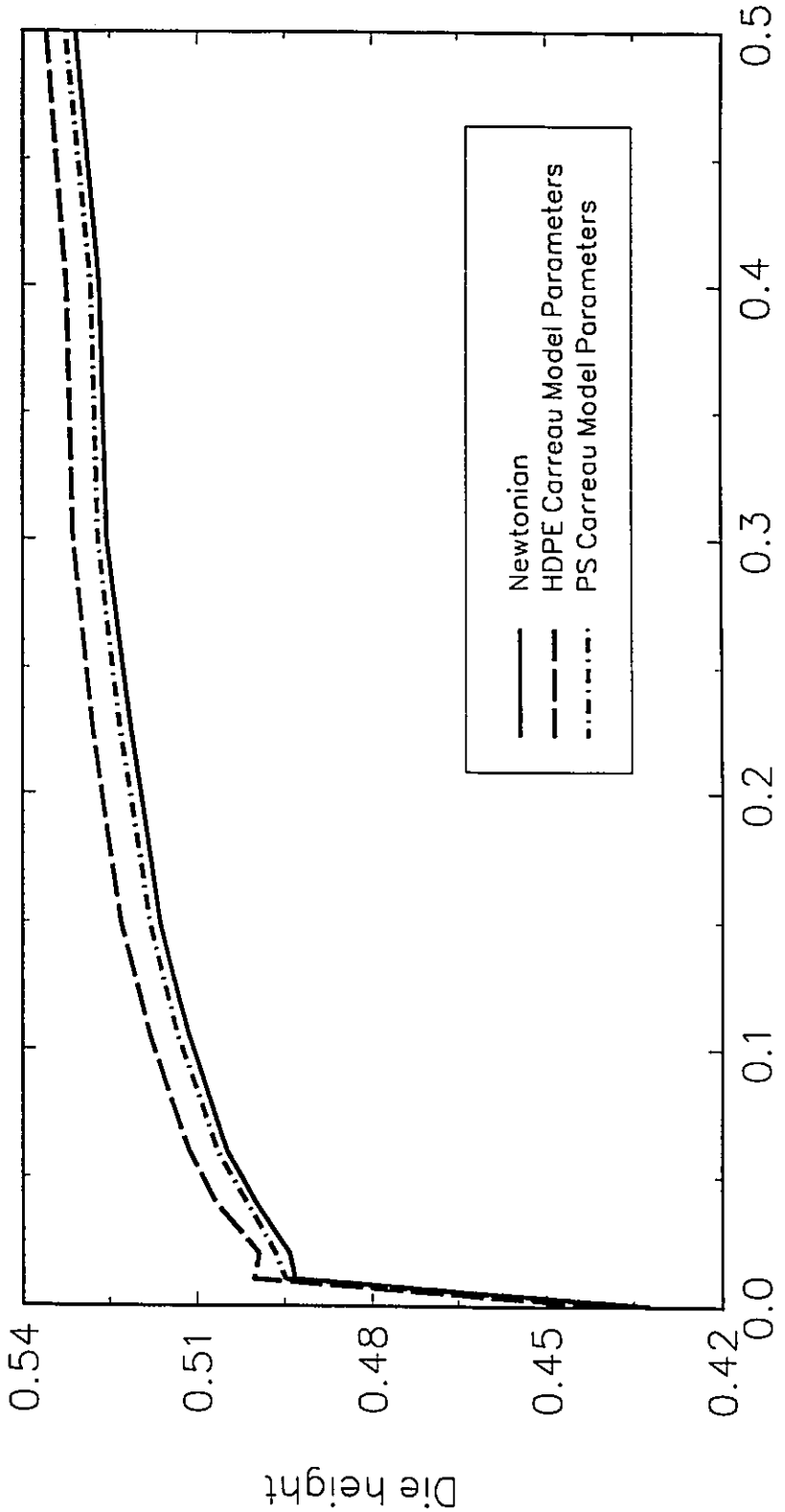

Figure 5.15. Effect of Carreau parameters on the final interface shape. η_{01} / η_{02} =1.5; Q_1 /Q_2 =1.0; B=0.1 (dimensionless).

viscosities and a displacement of the location of the interface. Note that for HDPE there is a more pronounced interface distortion near the die walls.

TABLE 5.2. Carreau parameters for HDPE and PS

Material	η_0 (Pa.sec), upper layer	λ (sec)	n	Ref. Temp.(T_0 ,°K)
HDPE (Tadmor and Gogos, 1987)	1170	0.05	0.58	493
PS (Vlcek and Vlachopoulos, 1993)	10000	0.00793	0.236	493

The general observation is that variations in Carreau parameters show less effect on interface displacement as compared to the effects caused by the inclusion of thermal effects. However, experimental observations by Dooley and Hilton (1993) with LDPE and PS show a complicated interface deformation pattern. Their results cannot be obtained with the Generalized Newtonian Fluid model employed in this work, suggesting that viscoelastic effects are also driving the interface displacement, and must be added to the model.

Interfacial tension effects were also studied. Values for interfacial tension coefficients have been reported in the literature using various methods: breaking thread method (Elemans et al., 1986), spinning drop method (Elmendrop and de Vos, 1990), and the pendant drop method (Wu, 1974). In all reports, values for surface and interfacial tension are on the order of magnitude of a few dyn/cm, not exceeding 25 dyn/cm (Wu, 1974). A relatively large interfacial tension coefficient of 50 dyn/cm was introduced

(Ca=0.0001) to test the effects of the Capillary number in the interface development. There is no significant change in the interfacial displacement caused by the introduction of interfacial tension forces.

5.7 Polycarbonate coextrusion problem revisited.

In Chapter 4, an isothermal version of the code with a zero entrance angle was used to simulate the experimental work reported by Dooley and Hilton (1993). In this chapter, the energy equation is included and an entrance angle of the feeding channel is set to 30° according to the die configuration that can be found in Dooley and Hilton (1993). The polycarbonate / polycarbonate coextrusion process shows very little layer rearrangement. The interface deformation is negligible at a distance of a few L/D and there is no appearance of a primary film along the die wall (Dooley and Hilton, 1993).

A Newtonian model for viscosity was employed because the power-law index of the polycarbonate resin was nearly unity (n=0.92). The mesh, as shown in Figure 5.16, consists of 6 elements in the y-direction (die width), 6 elements in z (3 elements for each flow channel), and 10 elements in the flow direction. The dimensionless thermal parameters that govern this problem are Pe=2879, Br=0.11 and b=9.635 (b'= 0.041 1/K, assuming T_0-T_∞= 235°C). The results presented here are for the case of perfect slip. The computed interface at L/D=3 is compared to the experimental result. After L/D=2, the calculated interface attained a stable position and is not deformed significantly. The experimental interface position also deforms within a L/D=3 and becomes completely stable at approximately L/D=10.

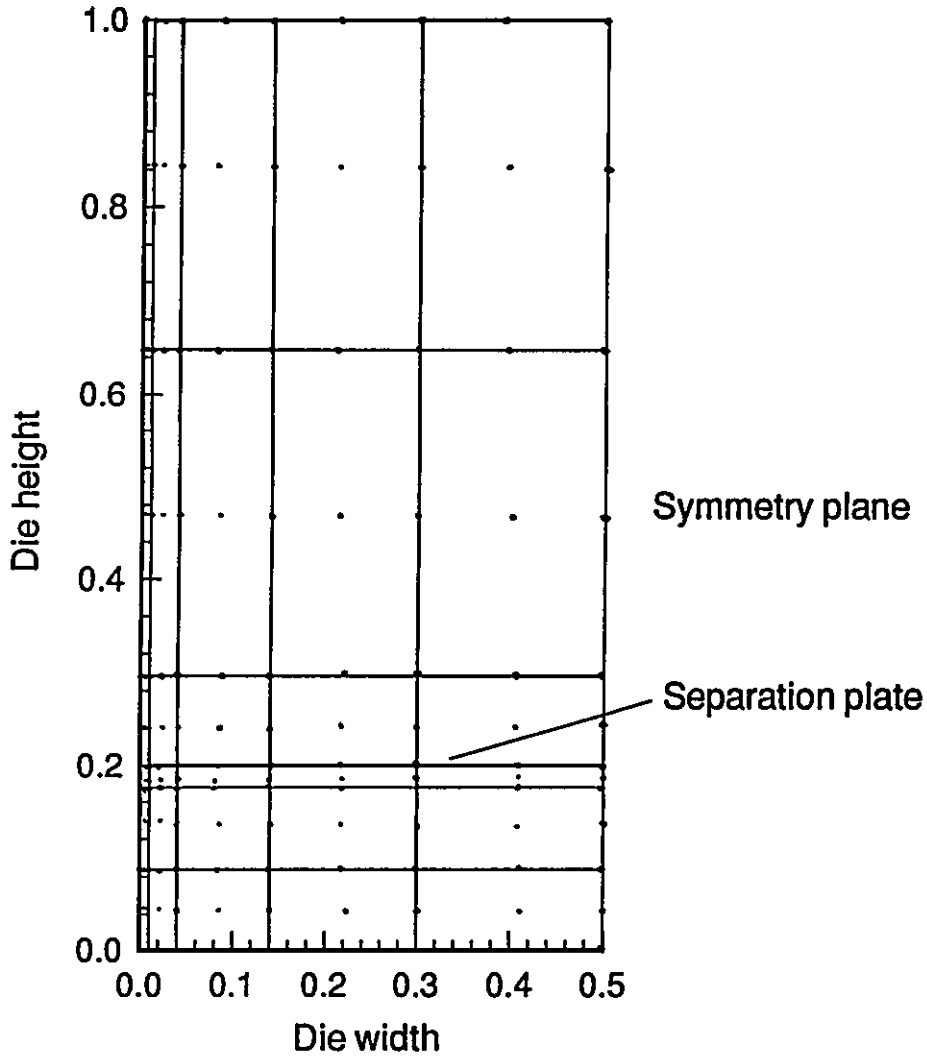

Figure 5.16. y-z cross-section of the mesh used in simulations of the CALIBRE 300-22 coextrusion system.

Figure 5.17 shows the results of calculated interface positions and experimental measurements. Maximum differences between the computed and experimental final interface are approximately 4% of the die height, which can be considered very good, given the experimental error. At the contact line region differences between the experimental and calculated interface shapes are larger.

The effect of Pe is important. The differences in the final interface shape between numerical and experimental observations are less than 3% of the die height and the temperature rise is significantly decreased inside the die due to thermal transport. In the case of Pe=0, the maximum temperature inside the die is approximately 50°C higher than the die walls whereas for the case of Pe=2879, the maximum temperature increase is approximately 15°C. Figures 5.18 and 5.19 show the temperature and velocity contours at the die exit for the Pe=0.0 and Pe=2879 cases, respectively. The classical numerical difficulties associated with high Pe number calculations (spurious oscillations in temperature and velocity fields, lack of convergence) were not found in these simulations. A possible explanation is that the flow is mainly unidirectional (the u component of velocity is much larger as compared to v,w) with the possible exception of the meeting point of the two flow channels. However, at this location, the grid is very refined and the local Pe number is small. The very good agreement between numerical and experimental results and the fact that all the residuals were below 10^{-3} when convergence is achieved also indicates that no significant numerical problems were encountered.

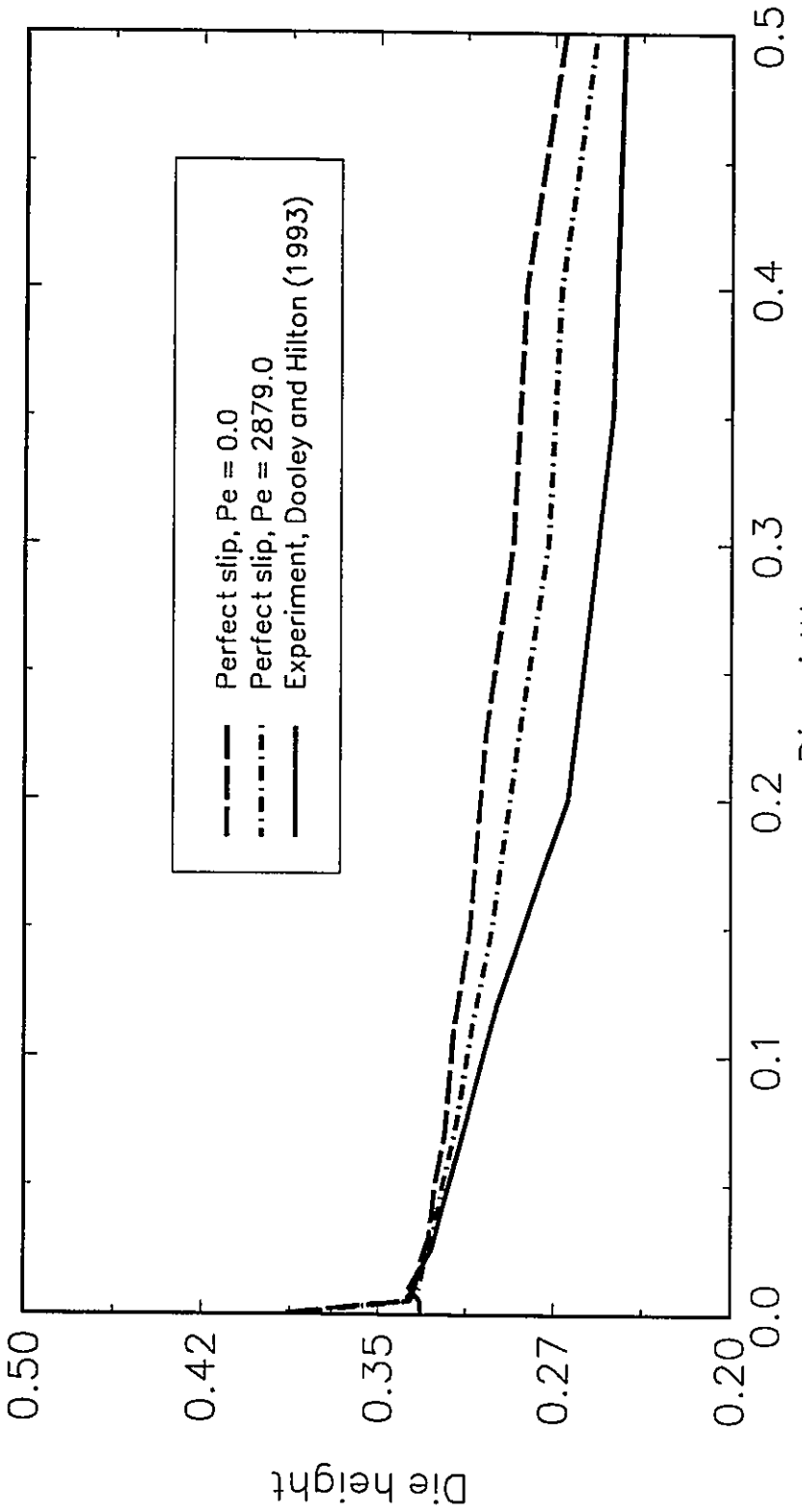

Figure 5.17. Final interface shape for the CALIBRE 300-22 coextrusion system.

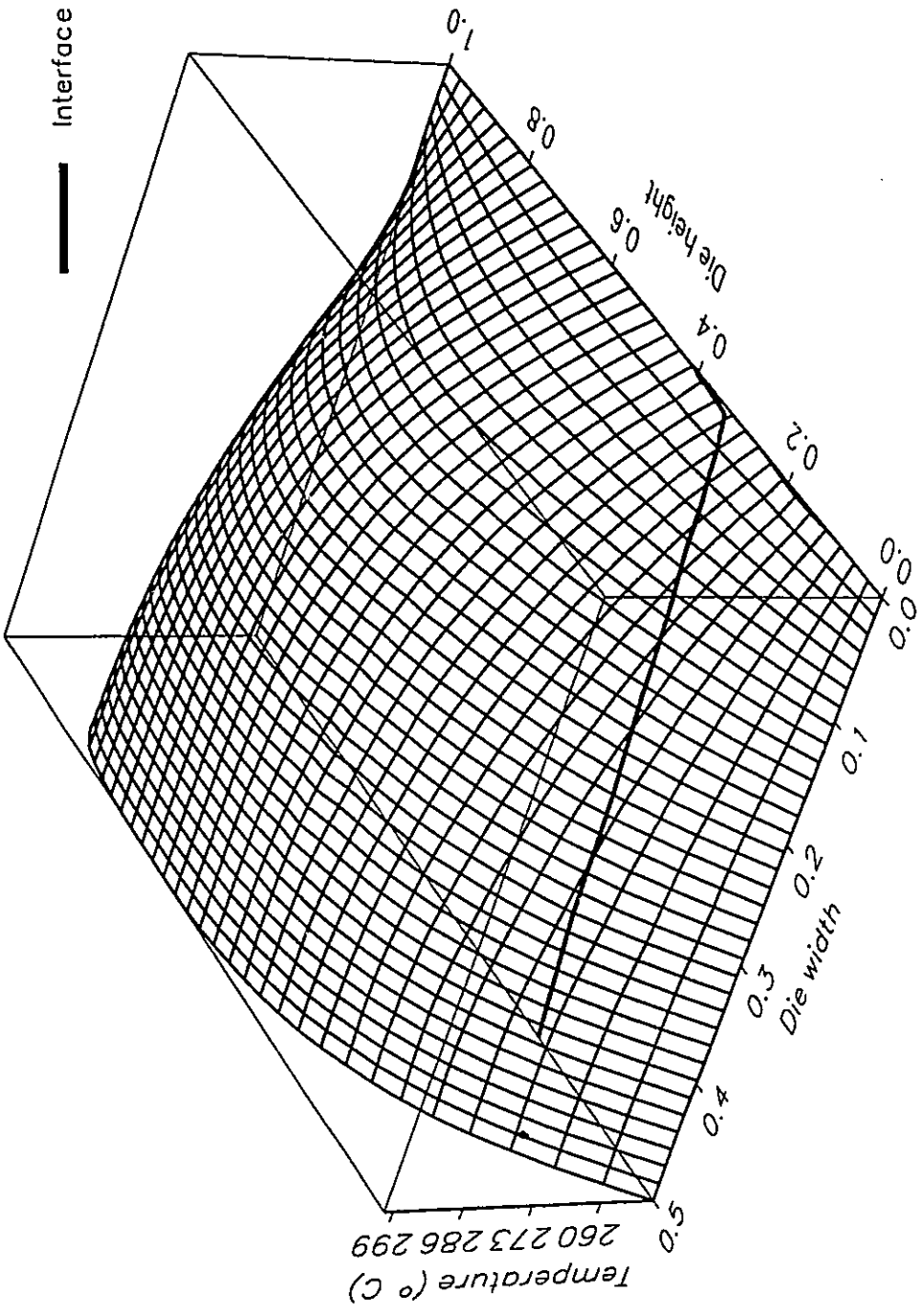

Figure 5.18(a) Temperature contours (°C) at the die exit for the CALIBRE 300-22 coextrusion system (Pe=0).

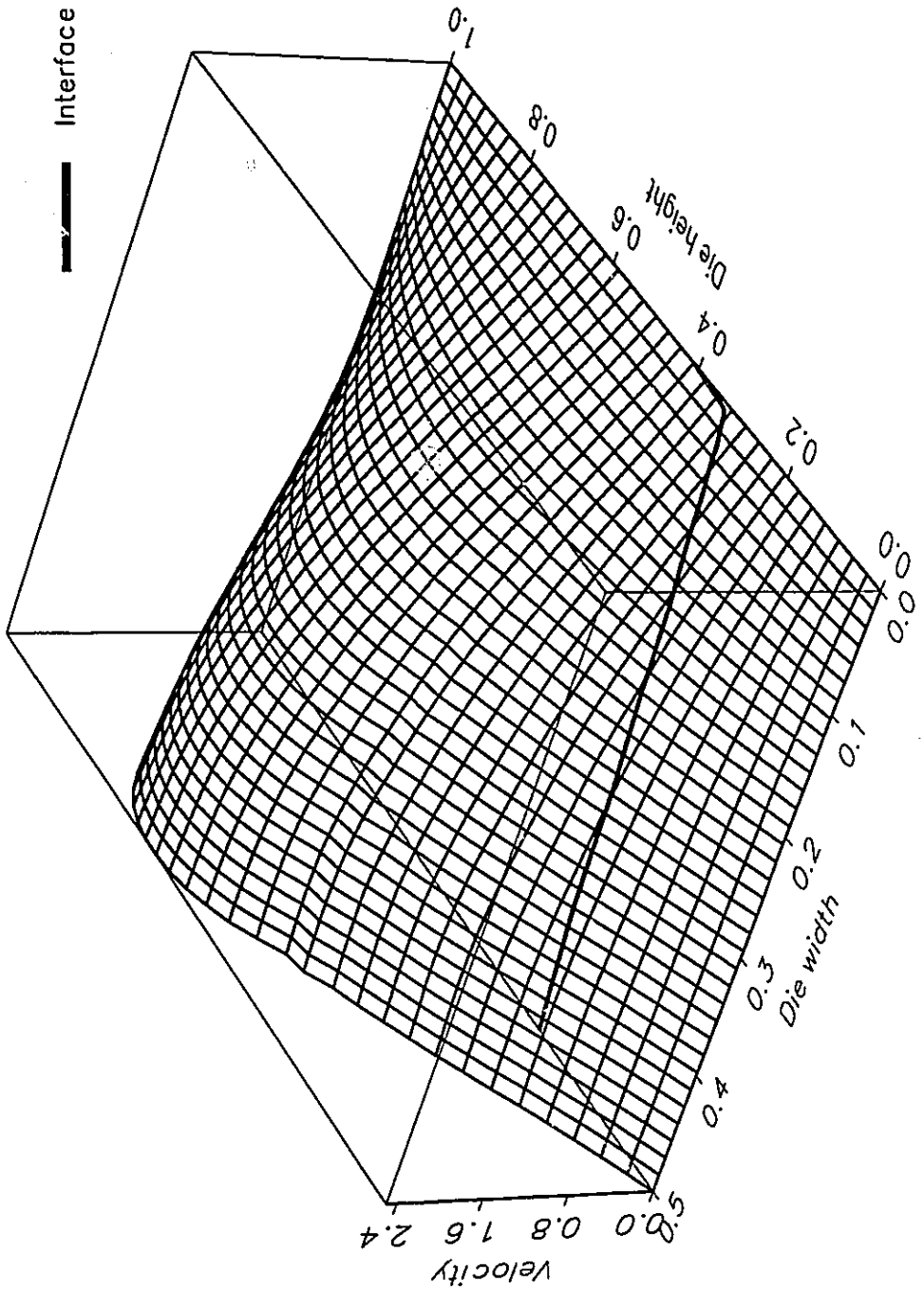

Figure 5.18(b) u-velocity distribution at the die exit.

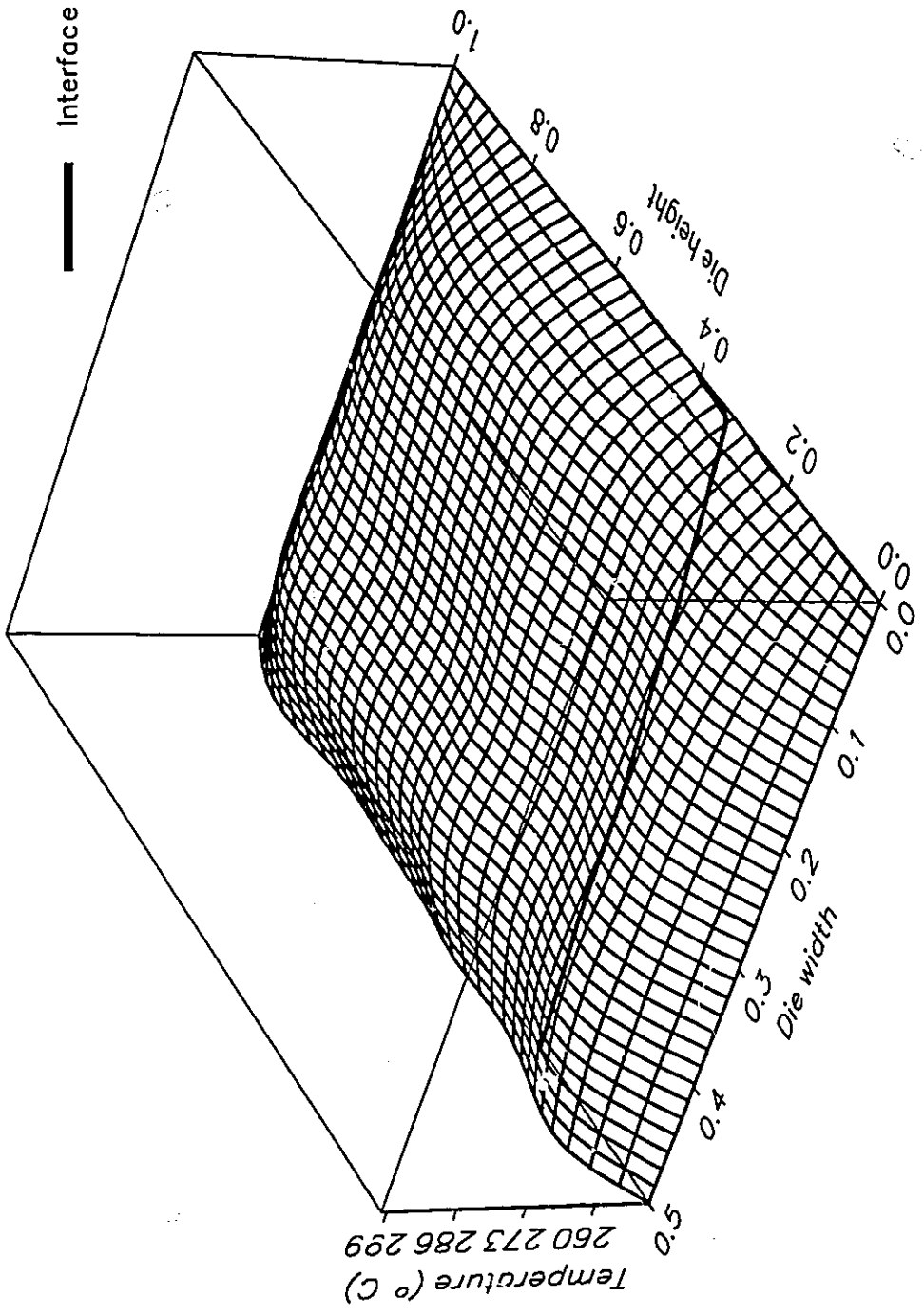

Figure 5.19(a) Temperature contours (°C) at the die exit for the CALIBRE 300-22 coextrusion system (Pe=2879).

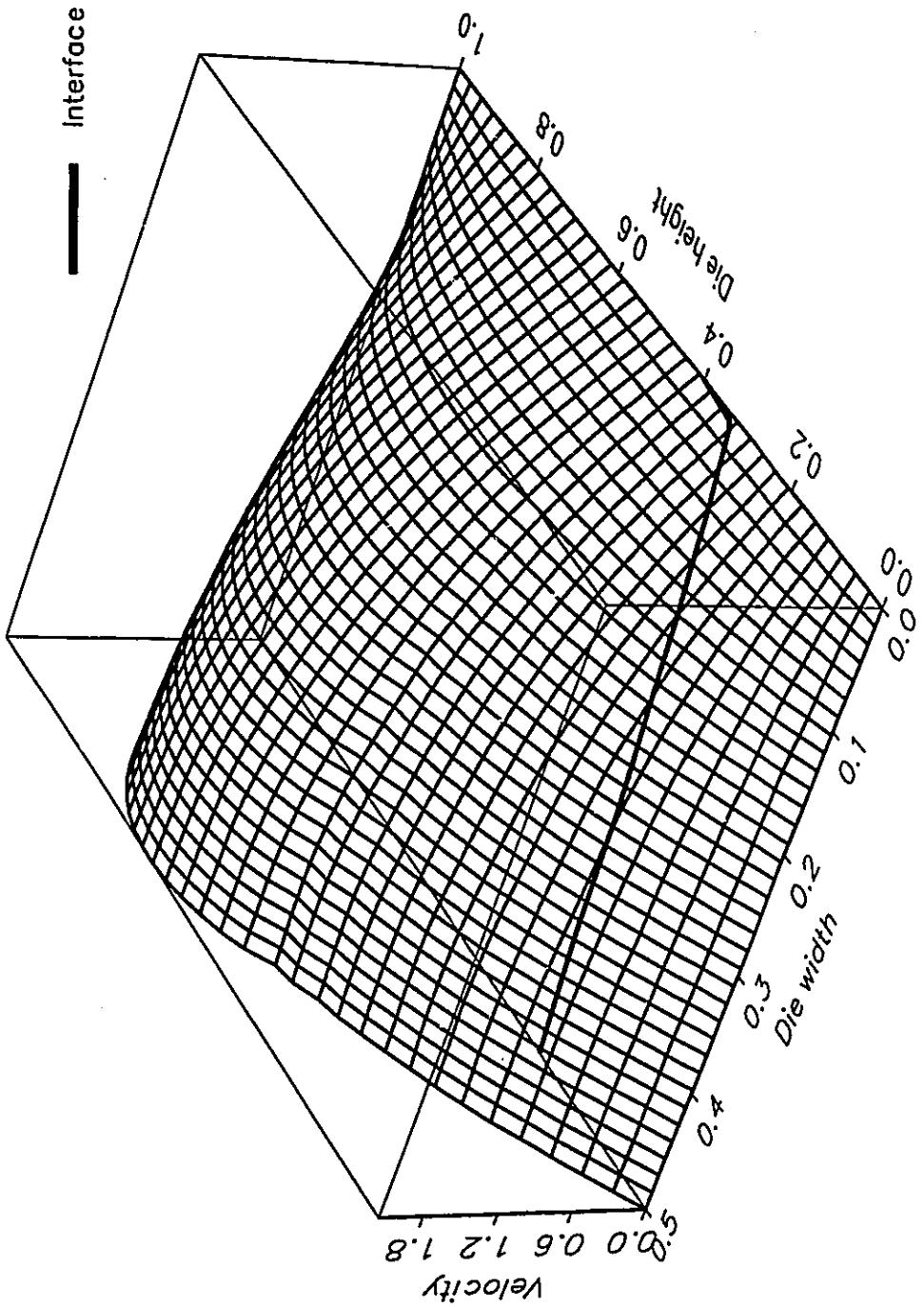

Figure 5.19(b) *u*-velocity distribution at the die exit.

5.8 Interface Displacement near the die wall.

The simulation results and available experimental evidence show that there are at least two distinct types of interface deformation near the die wall. Consider Figure 5.20a which shows a simplified sketch of an initial interface position separating the less viscous (upper) fluid from the more viscous (lower) fluid in a typical polymer melt coextrusion situation like the one discussed in the previous section. The first type of interface deformation (Type I) at the exit plane has the less viscous fluid wetting the die walls below the initial interface position. This type of interface deformation suggests a displacement of the more viscous fluid, by the less viscous fluid, from the die wall. Type I deformations have been observed in numerical simulations where the contact line is modelled with perfect slip and observed experimentally in PC systems. The second type of interface deformation near the die wall (Type II) is shown in Figure 5.20b. The less viscous fluid wets the die wall may be at or below its initial interface position but there is a further intrusion of the less viscous fluid into the more viscous fluid just a short distance into the bulk fluid. Type II interface deformation shows a primary film effect. The Type II interface deformation has been observed in numerical simulations where the contact line behavior range from perfect "stick" to perfect slip depending on flow conditions (Torres et al., 1993) and experimentally observed in LDPE systems (Dooley and Ramanathan, 1994) and HDPE/HDPE and PP/PP systems (Takács et al., 1994). Takács et al. (1994) performed experiments with the same dies and operating conditions using PP/PP and HDPE/HDPE systems (Figure 5.21, Table 5.3).

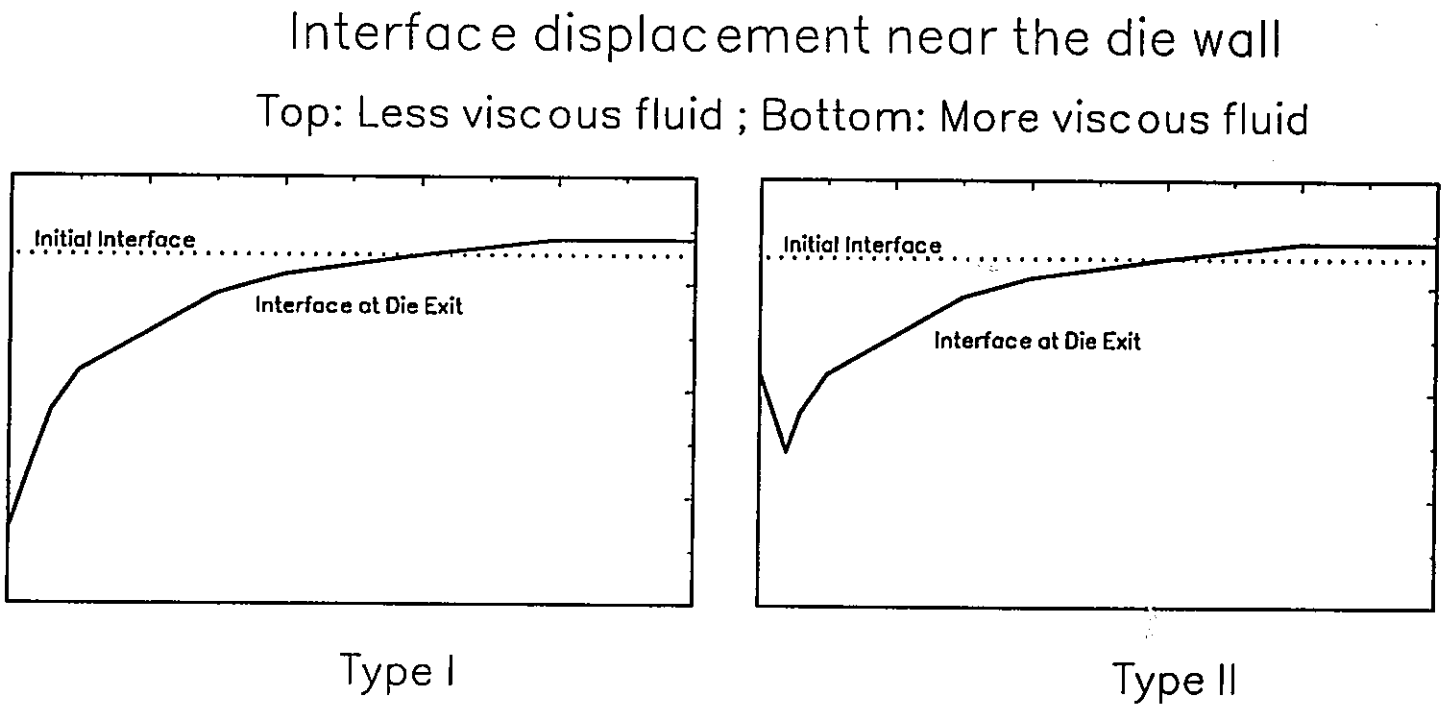

Figure 5.20 Interface displacement near the die wall: (a) Type I. (b) Type II.

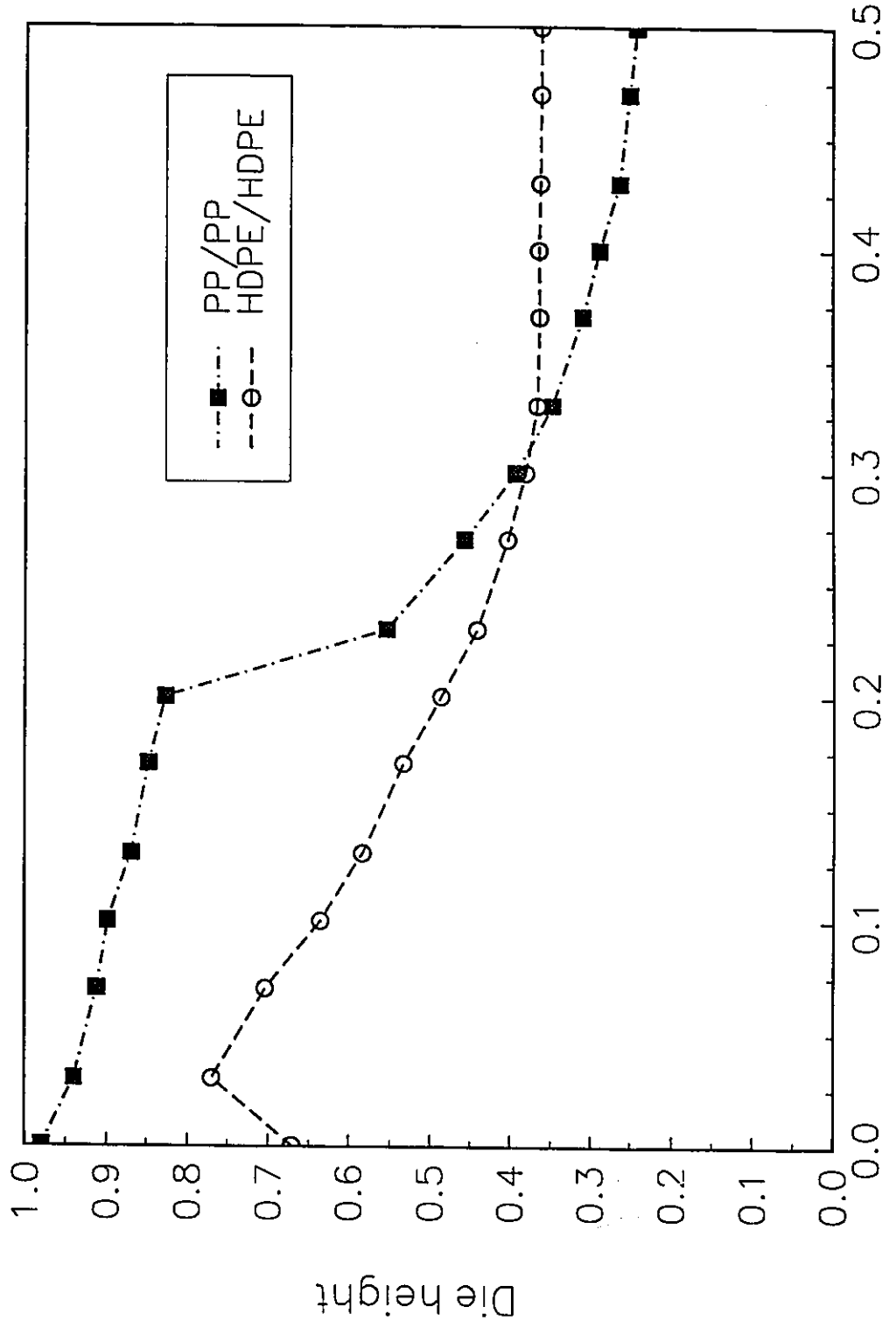

Figure 5.21 Interface shape for the PP/PP and HDPE/HDPE systems. η_{01} / η_{02} =1.0; Q_1 /Q_2 =1.0.

Table 5.3. Power-law parameters and operating conditions for HDPE and PP experiments (Takács et al., 1994).

Material	PP	HDPE
η_0, Pa.sec	13692	10291
b, 1/K	0.009	0.007
n	0.358	0.481
Ref Temp., T_0, °C	190	210
T_1, °C	250	250
T_2, °C	212	212
T_w, °C	190	190
Q_1/Q_2	1.0	1.0

Note that the PP/PP interface shows the characteristic Type I interface shape while the HDPE/HDPE shows the Type II interface shape. Incidentally, the HDPE/HDPE extrudate was more difficult to remove from the die walls than the PP/PP extrudate. Figure 5.21 shows that the contact line for HDPE/HDPE and PP/PP extrusion moves significantly. An assumption that the contact line does not move is incompatible with the experimental evidence. Superimposed on the local wall effects are the bulk interface changes due to thermal effects and non-Newtonian behavior.

Dooley and Ramanathan (1994) have also observed more complicated interface deformation patterns for long dies. The presence of a primary film effect described here is not to be confused with the classical fingering phenomena reported elsewhere (Saffman

and Taylor, 1958; McLean and Saffman, 1981; Saffman, 1958, 1986 in 2-D and Zimmerman and Homsy, 1992 in 3-D). Transient, unstable phenomena are seen when the interface of two superimposed fluids is displaced in a Hele-Shaw cell with a velocity perpendicular to the interface. In the present case, the predominant flow direction is tangent to the interface (side-by-side coextrusion), and an encapsulation will occur as the fluids travel inside the die. This encapsulation attains a steady-state configuration (Dooley and Hilton,1993; Takács et al., 1994; Dooley and Hughes, 1995). The contact line phenomena reported in this paper results from the interaction of the polymer interface and the die walls. The flow mechanisms responsible for interface deformation in Hele-Shaw cells and side-by-side coextrusion are different.

Type I and II deformation can be captured using the 3-D thermal model formulation described in this work but the shape depends on the interplay between the material and die parameters. The value of the slip coefficient at the contact line is important and may be a fundamental characteristic of the particular polymer melt / polymer melt / die material system. It is important to remember that the contact line boundary condition is an approximation at the macroscopic (continuum) level to a more complicated phenomenon at the molecular level. In all simulations performed, the effect of the local boundary condition is localized within the elements that contain the contact line. Away from the wall, the interface location is determined by the complex interaction of thermal and flow mechanisms. A more detailed analysis of the wall / polymer / polymer interaction near the contact line will require an analysis that goes beyond the scope of the macroscopic finite element analysis presented here.

The thermal dependence of the viscosity for both fluids is also important in defining the nature of the near-wall deformation. Note that a 2-D model in the gap/length plane would not capture the deformation near the die walls. 3-D models show similar interface deformations along the die centre-line for both Type I and Type II systems, all other parameters equal.

5.9 Summary.

A fully three-dimensional finite element formulation for the calculation of velocity components, temperature and pressure fields, as well as interface locations, was used to model the flow of two molten polymers in coextrusion dies.

The centreline interface position is not affected significantly when the entrance angle is varied, but significant changes in the interface occur near the die walls that may affect the uniformity of the final product. The interface deformation near the contact line region may show the appearance of a primary film or intrusion of the less viscous fluid into the more viscous fluid. The degree of this deformation is dependent on the contact line conditions as well as the thermal and shear rate dependence of viscosity. The intrusion of the less viscous material is distinct from the displacement of the more viscous material, by the less viscous material, from the die wall. The interface deformation near the die wall can become significant over long runner/die lengths and cause large deformations into the die interior.

The effects of inlet and wall temperatures were also studied. A change in wall or inlet temperatures can change the interface position depending on the thermal dependence

of the fluid viscosity. The effect of variations in inlet and wall temperature on the final interface shape is similar, even though the importance of inlet temperatures is more pronounced as the Pe number increases, as expected. Based on the simulations performed in this study, the most important parameter is the viscosity sensitivity coefficient b, which can drastically affect the final interface shape. The effect of this coefficient is more pronounced near the die wall, where the highest viscous heat generation occurs.

The value of the power-law coefficient influenced interface movement, but the changes were much less as compared to those caused by thermal effects. The significant influence of non-Newtonian effects occur near the die walls, where the shear rate is larger than in the bulk. In the case of fluids having shear-rate or thermal dependence of viscosity, the term viscosity ratio should not be used as an overall flow parameter, since this ratio varies locally according to the local temperature and shear rate.

Finally, the model was tested against an experiment in which a polycarbonate / polycarbonate resin was coextruded, assuming perfect slip at the contact line. Computer simulations for these types of problems (with Generalized Newtonian constitutive relationship) show that the interface does not change appreciably after an L/D of approximately 2 for all cases tested. It was found that for purely viscous flow situations, the agreement between computed and experimentally measured interface profiles is very good.

CHAPTER 6

VISCOELASTIC EFFECTS IN DIE FLOW

6.1 Introduction.

In the previous two chapters, a full three-dimensional finite element model was developed to study the non-isothermal flow of two molten polymers in a die, with a particular emphasis on the interface development. Computer simulations, confirmed experimentally, show that the displacement of the more viscous fluid by the less viscous fluid near the die walls stops (i.e., not complete encapsulation) after a few L/D for polymers that exhibit low elasticity levels (Karagiannis, 1989a; Torres et al., 1993, 1995, Dooley and Hilton, 1993, 1994; Takács et al, 1994; Dooley and Hughes, 1995). Fluids with high elasticity levels show interface shapes that are much more complex and complete encapsulation may or may not occur. The predictions of the numerical code developed thus far are in good agreement with the experimental observations for polycarbonate / polycarbonate systems (Figure 5.17). The model was unable to reproduce the complex interface shapes for more elastic materials (PP and HDPE systems, Figure 5.21) under similar operating conditions.

A three-dimensional space marching algorithm for the simulation of viscoelastic flow in ducts is developed to shed some light on the mechanisms that may trigger the complex interface shapes observed for the above mentioned systems.

Viscoelastic secondary flows have been the subject of many investigations since the late 1950s. In Generalized Newtonian Flow, the fully developed flow condition in a duct is a rectilinear flow with no secondary flow (i.e., no velocity components normal to the axial direction). In a viscoelastic fluid, the fully developed flow condition in a square duct channel shows the presence of secondary flows that are two to four orders of magnitude smaller than the main (axial) flow (Bird et al., 1987; Larson, 1988; Gervang and Larsen, 1991). Dodson et al. (1974) showed that the second normal stress difference (N_2) being a constant multiple of η (shear viscosity) is a sufficient, but not necessary, condition to ensure rectilinear flow.

One of the reasons for a lack of many three-dimensional analyses is the complexity of the problem. To the already difficult and computationally expensive problem of three-dimensional flow modeling, the addition of implicit viscoelastic constitutive equations makes the problem even more expensive.

In this chapter, an alternative solution algorithm for the three-dimensional viscoelastic flow simulations is offered. It is based on the Parabolized Navier-Stokes Equations formulation (PNSE), (Patankar and Spalding, 1972; Comini and Del Giudice, 1988) which reduces the 3-D problem to a sequence of 2-D problems marched along a preferred direction (the dominant flow direction in the duct).

6.2 Numerical modeling of three-dimensional viscoelastic flow in ducts.

In this section, a review of the past literature on segregated and space marching techniques is presented. A review of the research on normal stress coefficients is also

presented. Segregated algorithms for finite element methods as presented by Haroutunian et al. (1993) are extended to the limit of Re→0 (creeping flows), and the PNSE algorithm is extended to creeping, viscoelastic flows. The numerical results obtained with a Criminale-Ericksen-Filbey (CEF) model and a Modified Phan-Thien-Tanner (MPTT) model are compared against previous numerical and experimental data.

6.2.1 Literature review.

Segregated algorithms in FEM.

In the early stages of Computational Fluid Dynamics (CFD), finite difference methods (FDM) were employed to discretize and solve the momentum and heat transfer equations for fluid flow. Limited computer capacity forced early researchers to use iterative methods of solution and segregated approaches. A segregated approach is a strategy to solve the coupled set of conservation equations (momentum, mass and/or energy) in a sequential manner, as opposed to fully coupled methods, in which all conservation equations are solved simultaneously. Traditionally, finite element methods (FEM) have been used with fully coupled solution algorithms with direct Gauss (or related) solvers when applied to fluid flow problems, as presented in previous chapters. A fully coupled approach is a storage intensive method of solution that is highly effective for simple 2-D problems, but its advantages diminish as the level of complexity increases (non-linearities and 3-D). To overcome these limitations, researchers have followed two paths: to make use of segregated solvers and/or to make use of iterative linear equation solvers. Both approaches have been extensively used in the finite difference community.

Segregated solvers used in the modeling of three-dimensional fluid flows were performed by Montgomery and Wibulswas (1967) by neglecting the cross-flow velocity components in the thermal and hydrodynamical development of duct flow. The most successful segregated solvers in FDM are known as SIMPLE (Patankar, 1980) and its variants (SIMPLER, SIMPLEC, PISO, etc) now currently available in most commercial finite volume based codes. The first sketches of the SIMPLE methodology appeared in a paper by Patankar and Spalding (1972). Segregated and fully coupled solvers may or may not use iterative solvers to solve the resulting set of linear (or linearized) equations. The use of iterative linear equation solvers becomes imperative when the number of equations increases beyond a few thousand, and currently iterative solvers are widely used. A concise review of the current state-of-the-art on iterative methods can be found in Axelsson (1994) and Barrett et al., (1994).

In a fully coupled solver, the global system of equations that results after the application of the Galerkin method and imposition of boundary conditions is solved for all the nodal unknowns simultaneously. In a segregated solver, the global system is never assembled and solved at one time. SIMPLE-like methods are based on a variable by variable strategy; i.e., each conservation equation is solved sequentially, using the most recent updates for each variable. Appendix A shows the algorithmic steps of a segregated algorithm.

The biggest disadvantage of segregated methods is the lack of an explicit equation for pressure. A pressure update equation can be obtained by manipulating the discretized momentum and continuity equations, sometimes called the Poisson equation for

pressure). However, the pressure update equation contains the inverses of the matrices from the discretized momentum equations, making it intractable for computational purposes. Simplified pressure equations can be obtained by making approximations of those inverse matrices, replacing them by simpler matrices (simplified momentum matrices, SMM) that are easier to invert. In principle, any matrix, even the identity matrix, could be used (Haroutunian et al., 1993). However, for finite *Re* number problems, the closer the simplified matrix is to the discretized momentum matrix, the faster the algorithm converges.

Marching algorithms.

A set of differential equations, as found in transport phenomena problems becomes parabolic with the introduction of time-dependence. It is also often encountered when the convective transport terms become significant or when hyperbolic constitutive equations are used. However, classical elliptic situations can be transformed into parabolic analogues in one spatial direction if the following conditions hold (Patankar and Spalding, 1972):

(a) There is a dominant flow direction (no recirculation).

(b) The diffusion of momentum, mass or heat (or any other transported quantity) in that direction is negligible. Condition (a) usually implies a negligible momentum diffusion in the predominant flow direction (Caretto et al., 1972).

(c) The downstream pressure field has little or no influence on the upstream flow conditions.

A classical example of this flow situation is in boundary layer theory, and the first space-marching algorithms were developed for this context (for a review, see Roach, 1976; Anderson et al., 1984; Baker, 1985). Montgomery and Wibulswas (1967) used PNSE methodology to study the thermal entrance length in ducts neglecting secondary flows. Patankar and Spalding (1972) studied the coupled mass, momentum and heat transfer flow in ducts considering secondary flows. SIMPLE-like methods are particularly well suited for marching solvers. Del Giudice (1979) extended SIMPLE / PNSE methods to the finite element method.

The general parabolic equation governing the behavior of some variable ϕ can be written, in two-dimensional form, as (Comini and Del Giudice, 1988):

$$a\phi_t = c(\phi_{yy} + \phi_{zz}) - b(v\phi_y + w\phi_z) + S \qquad (6\text{-}1)$$

in which a,b,c are material properties and S is a source term, and the coordinates x, y, z are defined as in Figure 2-4, with x being the axial, predominant direction of flow, and y-z defining the cross-sectional plane perpendicular to the dominant flow direction. Secondary flows are defined as the velocity components in the y and z direction. The two most common problems in which equation (6-1) applies are transient heat conduction and energy transport in the presence of a flow field. Table 6.1 shows some of the different problem classes that can be solved with (6-1) (Comini and Del Giudice, 1988).

Table 6.1. Some problem classes that can be solved using parabolic equations.

Equation	ϕ	a	b	c	S
Heat conduction	T	ρC_p	0	k	q'
Energy	T	ρC_p	ρC_p	k	q'
3-D energy [1]	T	$u\rho C_p$	ρC_p	k	q'
Diffusion	c	ρ	0	D	S_c
Navier-Stokes	v,w	ρ	ρ	η_0	Pressure, diffusion and body forces
3-D Parabolic Navier-Stokes[1]	u,v,w	ρu	ρu	η_0	Pressure and body forces

[1] x replaces t in equation (6-1).

Under the above mentioned circumstances, the time variable can be replaced by a third, predominant direction of flow. The most common case is the three-dimensional heat transport equation in the presence of a flow field:

$$uT_x = \frac{1}{Pe}(T_{yy} + T_{zz}) - (vT_y + wT_z) + q' \qquad (6\text{-}2)$$

where q' is the internal heat generation.

The objective of this chapter is to use PNSE algorithms for simulating viscoelastic flow in ducts. Of all the above mentioned requirements to transform elliptic problems into parabolic analogues, the most controversial one is the neglect of axial diffusion. If the flow is considered to be unidirectional in the predominant flow direction (no axial recirculation), the diffusive transport of information from a downstream section upstream will be limited to pressure contributions and the second order derivative terms with

respect to x (the axial, predominant direction) will be, in fact, negligible. This has been a classical assumption in previous analyses (Patankar and Spalding, 1979, Comini and Del Giudice, 1988). Changes in axial velocity with respect to y- and z- directions are much bigger than in the axial direction. The only information being transmitted upstream will be the pressure terms, and algorithmic procedures have been devised to circumvent this problem. Comparison of numerical results with experimental data for GNF fluids shows that neglecting axial diffusion does not introduce significant errors in velocity and temperature predictions (Section 6.2.3).

Modeling of 3-D viscoelastic flows.

Published simulations of viscoelastic flows in three dimensions are very scarce. As mentioned before, the added complexity of an implicit, hyperbolic constitutive equation, renders the problem computationally expensive. In a bicomponent 3-D simulation, there could be up to 12 nodal variables (three velocities, six stress components, two pressures and the interface location).

In addition to the size of the problem, the imposition of inlet and outlet boundary conditions still remains an open question. As mentioned in Chapter 2, since viscoelastic constitutive equations are implicit in the extra-stress tensor, specification of the stress boundary conditions is necessary. The inlet stress profile is dependent on the previous deformation history of the fluid and, therefore, it is not easily determined. At the outlet, the outflow condition may again depend on the deformation history of the fluid inside the die. In most cases, secondary flows are present and the classical condition of zero cross

flow is not true even for long domains. Most simulations assume fully developed flow at the inlet (in both velocities and stresses) and the fully developed condition ($u=u(y,z)$, $v=w=0$) at the outlet (Keunings, 1989). These simplifying boundary conditions would not allow the calculation of secondary flows as observed in experiments.

For constitutive equations devoid of a Newtonian component, two major problems appear: change of type and loss of evolution. Change of type is the transition from elliptic to hyperbolic behavior and it is related to a viscoelastic Mach number (Keunings, 1989). Loss of evolution is the ill-posedness of the initial value problem governing the evolution of perturbations of arbitrary motions (Keunings, 1989). Loss of evolution and change of type cannot occur in models with a Newtonian component since they have second-order derivatives of the velocity field, but the governing equations show some degree of hyperbolicity through the constitutive equations. The presence of hyperbolicity in viscoelastic flow models introduces a series of complications that are not present in classical GNF flows (Chapter 2).

A literature review showed only a few papers in which 3-D simulations of viscoelastic flows were performed. Tran-Cong and Phan-Thien (1988c) modeled the extrudate swell of a Phan-Thien-Tanner (PTT) fluid using the Boundary Element Method (BEM). Shiojima and Shimazaki (1990) also studied the extrudate swell of an Upper Convected Maxwell (UCM) fluid with a penalty formulation using FEM. UCM and PTT models (as expressed by Tran-Cong and Phan-Thien) do not allow N_2 in shear flows, and no secondary flows can be predicted. Gervang and Larsen (1991) studied the secondary flows of a CEF fluid in straight ducts using finite differences and periodic boundary

conditions. Matsunaga et al. (1995) used an approximate method to estimate the stress field in three-dimensional polymer melt flow. Based on a Generalized Newtonian flow field, the viscoelastic stresses are calculated with streamwise integration. No iteration cycle on the coupled velocity / stress fields is performed. The range of applicability of this method is limited to flow for which the flow field of a Generalized Newtonian Fluid and a viscoelastic fluid are similar.

Previous research in 2-D viscoelastic secondary flows.

Most of the predictions for square duct flow have been made using perturbations to viscous fully developed flows with second-order or higher-order constitutive equations (CEF, for example). Langlois and Rivlin (1956) showed that for first-, second- and third-order models with constant coefficients, the fully developed condition for flow in ducts of non-circular cross sections is a rectilinear flow with no transverse flow. However, for a fourth-order model, the same fully developed conditions show a superimposed transverse flow to the rectilinear flow. The form of the secondary flow is dependent upon the geometry of the channel. Wheeler and Whisler (1966) used a finite difference method with a Reiner-Rivlin constitutive equation to predict eight vortices in a square duct. Thangham and Speziale (1987) used finite differences with a Maxwell model in laminar pressure driven flow in ducts of rectangular and square cross section. Wheeler and Whisler (1966) and Thangham and Speziale (1987) used a simplified 2-D analysis of the duct cross-section by assuming that the velocity components do not depend on the axial flow direction (fully developed flow assumption). The same assumption of fully

developed flow was used by Dodson et al. (1974) who used a perturbation of the fully developed flow in square and rectangular ducts to analyze the secondary flow pattern of a CEF equation in which the second normal stress coefficient (ψ_2) is the perturbation parameter, assumed to be small and constant. Townsend et al. (1976) extended Dodson's work and considered ψ_2 to be dependent on shear rate. From previous work, the main conclusion is that the determining factor on the shape and strength of the secondary flow pattern is the second normal stress difference, N_2. Dodson et al. (1974) showed that a change in the sign of N_2 reverses the direction of the streamlines in secondary flow. Gervang and Larsen (1991) used three-dimensional finite differences with a CEF equation to model flow in straight ducts. To minimize the size of the problem, periodic boundary conditions on a short mesh were used. Initially, the fully developed Newtonian flow is assumed at the inlet. After one iteration cycle, the outflow condition at a given L/D was used as the inlet boundary condition for the next iteration cycle. Iterations were stopped when changes in inlet and outlet velocity conditions were below a specified tolerance. The predicted secondary flow consisted of eight vortices symmetrically arranged, which were two to four orders of magnitude smaller than the average axial velocity, in agreement with previous simulations and analysis. All these papers used a square duct geometry.

Normal stress differences.

A measure of the viscoelastic behavior of a liquid is the presence of normal stresses in simple flows. In order to eliminate the static pressure contribution to normal forces, two normal stress differences are introduced: the first normal stress difference N_1,

which for shear flow in ducts is $\tau_{xx} - \tau_{yy}$ or the difference of the stress component acting in the direction of flow minus the stress component acting in the direction of flow variation; and the second normal stress difference, N_2, which is $\tau_{yy} - \tau_{zz}$ or the difference between the stress component acting in the direction of flow variation minus the stress component in the neutral direction. The sign and magnitude of N_1 and N_2 is a measure of the elasticity of a given material. For steady simple shear flow, N_1 and N_2 are directly related to the first and second normal coefficients, ψ_1 and ψ_2, respectively. While standard laboratory procedures can provide accurate estimates of ψ_1 (Bird et al., 1987; Larson, 1988), experimental techniques for the determination of ψ_2 are scarce and not very accurate. Indirect estimates of ψ_2 are obtained through the normal stress ratio, N_2/N_1. However, most results are available for polymer solutions and liquid crystal polymers at relatively high shear rates (Meissner et al., 1989; Magda et al., 1991a,b; Magda et al., 1993; Baek et al., 1993a,b). Magda et al., (1991a,b; 1993) showed that for PS solutions and liquid crystal polymers N_2 increases and changes sign from negative to positive as the shear rate increases. For polymer melts, it is now believed that N_2 is negative (Tanner, 1985; Larson, 1988; Table 6.2). Larson (1988) summarized relationships for N_2 using various constitutive equations that are summarized in Table 6.2.

Table 6.2. Model predictions for N_2 or N_2/N_1, (Larson, 1988).

Model	Predictions
Lower-Convected Maxwell	$N_2/N_1 = -1$
Upper-Convected Maxwell	$N_2=0$
Doi-Edwards	$N_2/N_1 = -0.14$
Johnson-Seagalman	N_2/N_1 from -0.05 to -0.3, depending on ζ, material parameter
Larson	$N_2=0$
White-Metzner	$N_2=0$
Leonov / Giesekus	at large $\dot{\gamma}$, $\psi_2=\psi_2(\dot{\gamma}^2)$; at low $\dot{\gamma}$, $N_2/N_1 = -0.25$
Phan-Thien-Tanner	$N_2=0$ for $\zeta=0$; $N_2\neq0$ for $\zeta\neq0$
Bird-Carreau	$N_2/N_1=\varepsilon/2$, ε material parameter.
FENE dumbbell	$N_2/N_1=-0.027$
CEF	$N_2=N_2(\dot{\gamma}^2)$
Experiments	$N_2/N_1=-0.05$ to -0.14 at high $\dot{\gamma}$ for very polydisperse polymer melts (PS)
Experiments	$N_2/N_1=-0.02$ and may change sign once or twice as $\dot{\gamma}$ increases for liquid crystal polymers solutions (Magda et al.,1991a,b; 1993)

Note that there are many different predictions for N_2 and the ratio N_2/N_1 depending on the constitutive model chosen. More research is needed to elucidate the values and behavior of N_2 with shear rate. As Larson (1988) wrote:

> *It is unfortunate that there are so few measurements of N_2/N_1, especially for melts or concentrated solutions of narrow polydispersity, for the prediction of this quantity is a sensitive test of constitutive equations.*

6.2.2 Segregated algorithms.

Haroutunian et al. (1993) proposed three different algorithms to solve the finite element weak form of the Navier-Stokes equations in a segregated manner, as opposed to the fully coupled algorithm described in previous chapters. The first algorithm is the *pressure correction* (PC) algorithm, a finite element counterpart to the SIMPLE method of Patankar (1980). The second algorithm is known as the *pressure projection* (PP) method, a finite element counterpart to the SIMPLER method (Patankar, 1980) and the third algorithm is known as the *pressure update* (PU) algorithm, with no known counterpart in the finite difference community.

In this work, the PC, PP, and PU algorithms have been implemented for the Re=0 case in three-dimensional situations. Description of the algorithmic details as well as theoretical details are explained in Haroutunian et al. (1993). Appendix A shows the algorithmic steps for the PC algorithm as presented by Haroutunian et al. (1993) for three-dimensional problems. The simplified momentum matrices [R'] were either the identity matrix or the lumped diagonal matrix $R'_{ii}=\sum R_{ij}$. Full matrix storage and operations were used and no advantage of the banded structure of the matrix is taken since only small problems were modeled. In larger problems, matrix storage and operations becomes a critical issue, and efficient storage strategies and matrix operation algorithms must be used.

The PP and PU algorithms failed to converge for Re=0 problems, for the range of relaxation factors used, and therefore, they are not discussed here. The PC method has also been proposed by Shaw (1991), Rice and Schnipke (1986) and Benim and Zinser

(1986). The first two papers proposed an equal-order interpolation for velocities and pressure while the third used a biquadratic-bilinear element. All the authors limited their research to two-dimensional cases with Re > 1. Relaxation factors of the form:

$$\phi^i = \phi^{i-1} + \alpha \phi' \qquad (6\text{-}3)$$

have to be used to avoid divergence, where ϕ is either the velocities or the pressure, superscript ^{i} indicates the iteration counter and (') indicates the corrected values. Convergence is achieved when the maximum change in a variable at any node is below a specified tolerance.

The PC algorithm was tested for the simple case of fully developed flow of a Newtonian fluid in a square channel with Re=0 (Tables 6.3 and 6.4). For this case, a number of analytical and numerical solutions are available in the literature (Shah and London, 1978). As expected, any [R'] matrix, even the identity matrix, provided convergence for the method. When an identity matrix was used instead of the lumped matrix mentioned above, the number of iterations were lower, but the errors in pressure (the most critical variable for convergence) were higher (Table 6.3). As cited by many researchers, the relaxation factor for pressure was around 0.1 to obtain convergence. Convergence was almost independent of the relaxation factors used for velocities. Table 6.4 shows the comparison of the PC method against classical fully coupled method of solution (Chapter 3).

Table 6.3. Effect of relaxation factors for PC method for the problem of fully developed flow in ducts.

α (pressure)	α (velocities)	Num. of. iterations	[R']
1.0	1.0	13	[I]
1.1	1.0	12	[I]
1.2	1.0	23	[I]
0.9	1.5	15	[I]
0.1	1.5	>30	[I]
0.1	1.5	30	$[R']=R'_{ii}=\Sigma_j\|R_{ij}\|$
0.1	3.0	30	$[R']=R'_{ii}=\Sigma_j\|R_{ij}\|$
0.1	30.0	diverges	$[R']=R'_{ii}=\Sigma_j\|R_{ij}\|$

Table 6.4. Comparison of PC method versus fully coupled method (Chapter 3) for the problem of fully developed flow in ducts.

α_P	α_V	[R']	Iter.	P_{max}	Error (%)	P_{min}	Error (%)	tol.
1.0	1.0	[I]	13	8.0039	0.0399	3.9976	0.0590	10^{-2}
0.6	1.0	[I]	11	8.0217	0.2714	3.9908	0.2312	10^{-3}
0.6	1.0	[I]	19	8.0051	0.0634	3.9991	0.0230	10^{-4}
0.1	1.0	$[R']=\Sigma_j\|R_{ij}\|$	30	8.0009	0.0114	3.9945	0.1375	10^{-3}
0.1	1.0	$[R']=\Sigma_j\|R_{ij}\|$	21	8.0036	0.0445	3.9985	0.0385	10^{-4}

Note: P_{max} and P_{min} indicate maximum and minimum calculated pressure, respectively; tol.: tolerance, α_P and α_V are the relaxation factor for pressure and velocity, respectively. Error is defined as $100*|(P_c - P_a) / P_a|$, where P_c is the pressure calculated with the segregated algorithm and P_a is the pressure calculated with analytical solutions (Hagen-Poiseuille).

In summary, it is clear from Tables 6.3 and 6.4 that no significant errors are introduced by choosing a segregated solver over the standard fully coupled solver. PC method is suitable for simulation of Re=0 flow situations, while PP and PU methods failed to provide convergence in the limit of creeping flow. The segregated algorithm will be used to solve the parabolic Navier-Stokes equations for Newtonian and viscoelastic flows in ducts.

6.2.3 Parabolized Navier-Stokes Equations (PNSE).

A space-marching variation of equation (6-1) is applied to 3-D laminar flow ducts (Comini and Del Giudice, 1988). The method is presented for Newtonian flows and in section 6.2.4 it will be extended for viscoelastic flows. The three-dimensional momentum and continuity equations are: (where x is considered to be the predominant flow direction):

$$uu_x + vu_y + wu_z = -P_x + \frac{1}{Re}\left[2u_{xx} + (u_y + v_x)_y + (u_z + w_x)_z\right] = 0 \qquad (6\text{-}4)$$

$$uv_x + vv_y + wv_z = -P_y + \frac{1}{Re}\left[2v_{yy} + (u_y + v_x)_x + (w_y + v_z)_z\right] = 0 \qquad (6\text{-}5)$$

$$uw_x + vw_y + ww_z = -P_z + \frac{1}{Re}\left[2w_{zz} + (w_x + u_z)_x + (v_z + w_y)_y\right] = 0 \qquad (6\text{-}6)$$

$$u_x + v_y + w_z = 0 \tag{6-7}$$

where $Re=\rho UL/\eta_0$ is the Reynolds number, ρ being the fluid density. By introducing (6-7) into (6-4)-(6-6), the momentum equations reduce to:

$$uu_x + vu_y + wu_z = -P_x + \frac{1}{Re}\left[u_{xx} + u_{yy} + u_{zz}\right] = 0 \tag{6-8}$$

$$uv_x + vv_y + wv_z = -P_y + \frac{1}{Re}\left[v_{xx} + v_{yy} + v_{zz}\right] = 0 \tag{6-9}$$

$$uw_x + vw_y + ww_z = -P_z + \frac{1}{Re}\left[w_{xx} + w_{yy} + w_{zz}\right] = 0 \tag{6-10}$$

In the PNSE approach axial diffusion of momentum is considered negligible, and the terms $\partial/\partial x^2$ are discarded (x is the main flow direction). This assumption is reasonable when no recirculation is present (Patankar and Spalding, 1979; Patankar, 1980; Comini et al., 1980; Pougare and Lakshminarayana, 1986; Comini and Del Giudice, 1988). The other factor that prevents a straightforward application of a space marching technique is the axial pressure gradient. To decouple pressure effects, the pressure drop is decomposed into one component in the axial direction, P^a, which is considered constant at every

cross-sectional *y-z* plane, and another component in the cross sectional plane *P*(y,z) which can be considered as a correction term to account for pressure variations within each cross-section. With these additional considerations, equations (6-8)-(6-10) can be rewritten as:

$$uu_x = \frac{1}{Re}\left[u_{yy}+u_{zz}\right] - vu_y - wu_z - P_x^a = 0 \qquad (6\text{-}11)$$

$$uv_x = \frac{1}{Re}\left[v_{yy}+v_{zz}\right] - vv_y - wv_z - P_y = 0 \qquad (6\text{-}12)$$

$$uw_x = \frac{1}{Re}\left[w_{yy}+w_{zz}\right] - vw_y - ww_z - P_z = 0 \qquad (6\text{-}13)$$

The pressure variable in this formulation is made dimensionless as:

$$P = \frac{P'}{\rho U^2} \qquad (6\text{-}14)$$

Appendix B shows the algorithmic steps in detail together with the finite element matrix formulation. The algorithm was originally developed by Comini and del Giudice (1988), but the overall mass flow correction used in this work is the one proposed by Briley (1974). This method is simpler to implement and is physically more sound than

the other methods available (Patankar and Spalding, 1972; Comini and del Giudice, 1988).

Initially, an extension of the segregated PC formulation of Haroutunian et al. (1993) was attempted (Re=0), but the method failed to converge, probably due to a lack of convective terms. By neglecting the convective transport term, the naturally "marching" component is neglected and the method fails. Mathematical or physical analysis of the possible breakdown causes are beyond the scope of this work. The space-marching algorithm of Comini and del Giudice, (1988) is employed through the simulations.

Note (Appendix B) that the marching algorithm uses a segregated strategy to solve for the primary variables. Computationally, there are two major differences between SIMPLE-like method and PNSE methods: one is the requirement of an additional iteration loop in the latter. Under PNSE, the u-velocity is corrected through the constant $\partial P^a/\partial x$ term to satisfy overall mass continuity. For every cross-section, the v and w velocity components are then corrected in SIMPLE-like fashion through the $P(y,z)$ term to satisfy local continuity. This process is repeated until the desired axial integration length is reached. The other major difference is that pressure is approximated with the same interpolating functions as velocities. Since the solution method is segregated by variable, traditional problems with same-order interpolation functions for velocity and pressure are not present here (Haroutunian et al., 1993; Comini and Del Giudice, 1988).

To test the code, the classical problem of developing flow of Newtonian fluids in ducts is used. This is a very well documented problem in the literature. An excellent review of numerical and experimental work in the area can be found in Shah and London (1978). Pougare and Lakshminarayana (1988) used a space-marching finite-difference

algorithm to model this problem. Figures 6.1 and 6.2 show the centreline u-velocity and axial pressure drop, respectively, for several mesh configurations. Figures 6.3 and 6.4 show the same variables for several Re number problems (Re=0.01,1 and 100) solved and plotted in dimensionless fashion, respectively. Note that all the curves are coincident, showing the applicability of the method for a wide range of Re numbers, in particular for low Re problems, which are characteristic of polymer melt flows. The final pressure drop matches well with the correspondent values calculated from the Hagen-Poiseuille equation. The code is also capable of solving the energy equation (2-8) as well as Generalized Newtonian Fluids. Figure 6.5 shows the results of the present code for the thermal and hydrodynamic development in a square duct compared to the results of Neti and Eichhorn (1983), who used finite differences. Pr indicates the Prandtl number, $Pr=C_p\eta_0/k$. The extension of the PNSE algorithm for modeling viscoelastic flow in ducts is presented in the next section.

6.2.4 Extension of PNSE to viscoelastic modeling.

The success of PNSE methods to model the thermal and hydrodynamical length entry problem for a variety of Re numbers, and the fact that the addition of viscoelastic constitutive equations renders the problem non-elliptic, makes the use of PNSE methods for the simulation of three-dimensional viscoelastic flow in ducts an attractive and economical alternative. The models of Criminale-Ericksen-Filbey (CEF) and Modified Phan-Thien-Tanner (MPTT) are used to capture secondary flow phenomena in ducts with the help of PNSE. By introducing a dimensionless stress tensor as:

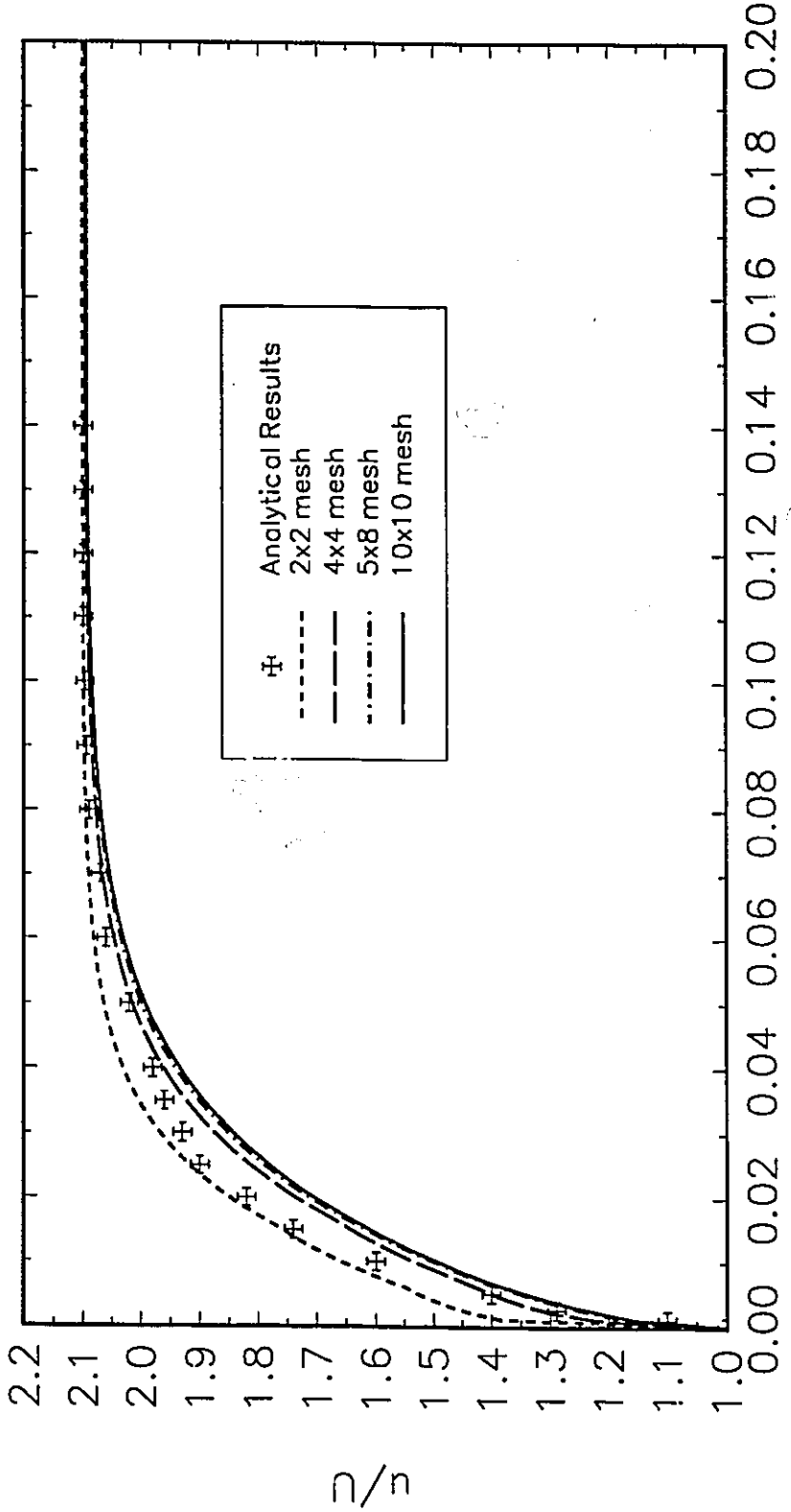

Figure 6.1. Maximum axial velocity for several mesh configurations.

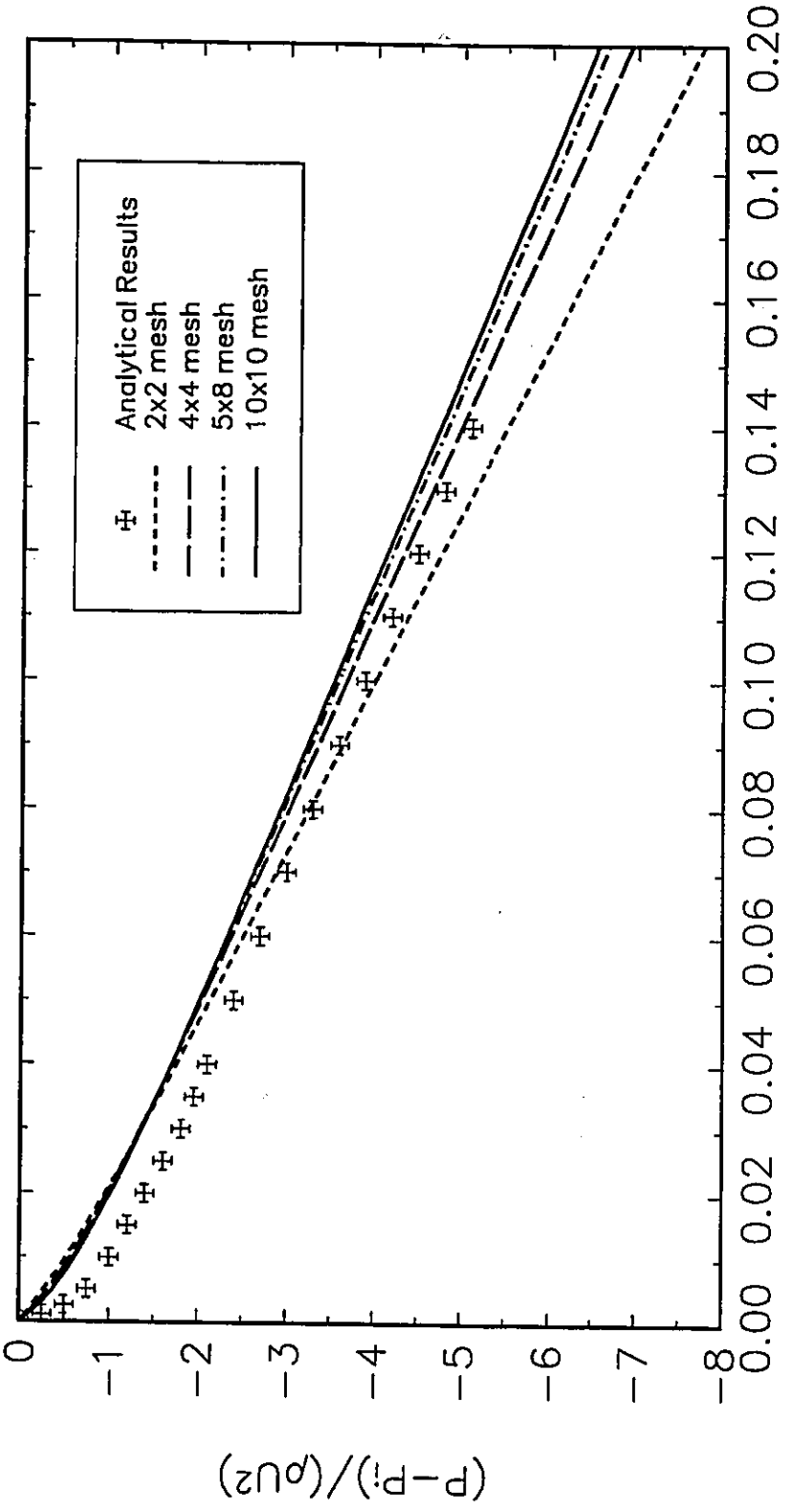

Figure 6.2. Axial pressure drop for several mesh configurations.

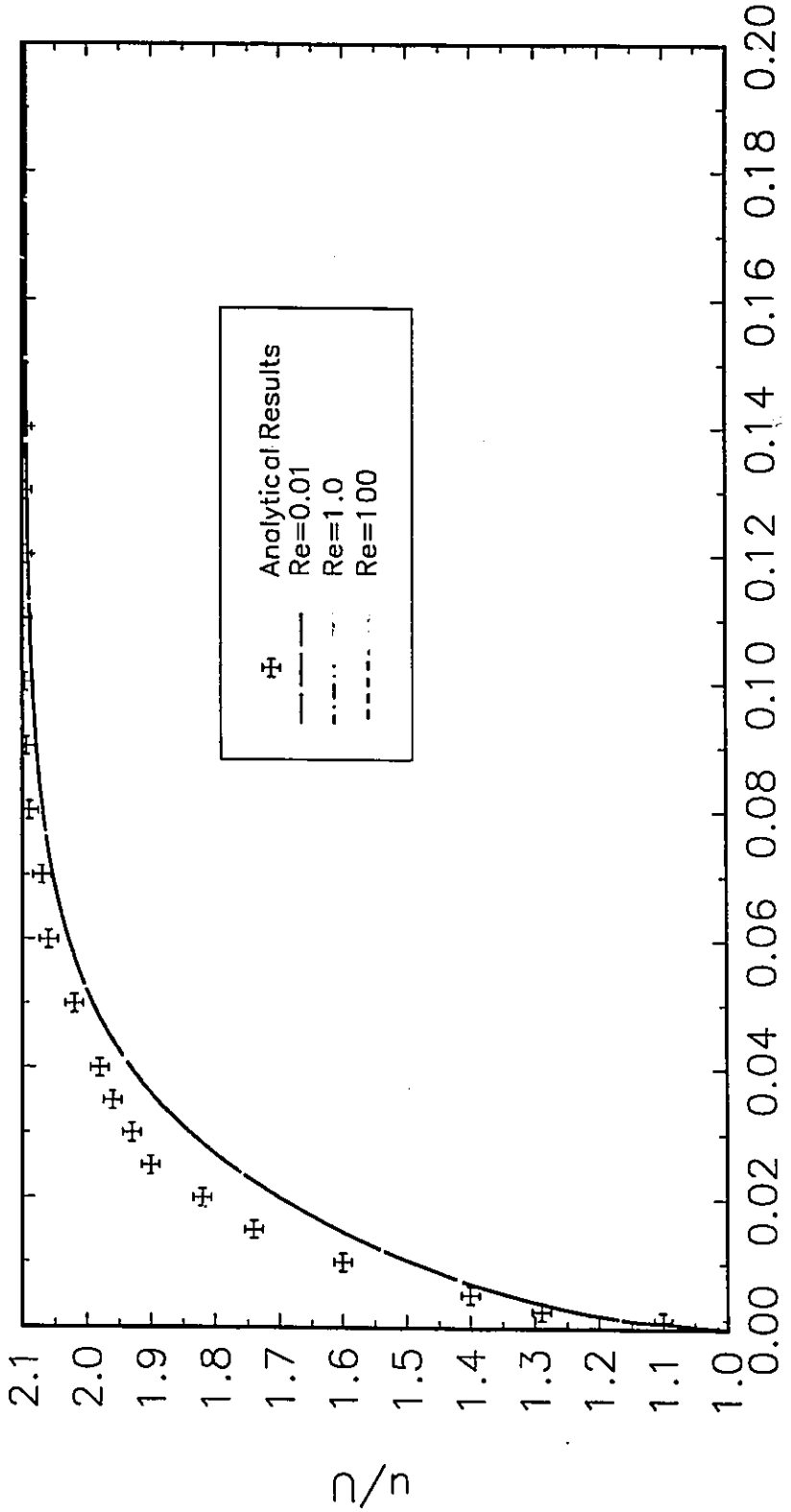

Figure 6.3. Maximum axial velocity for several Re number.

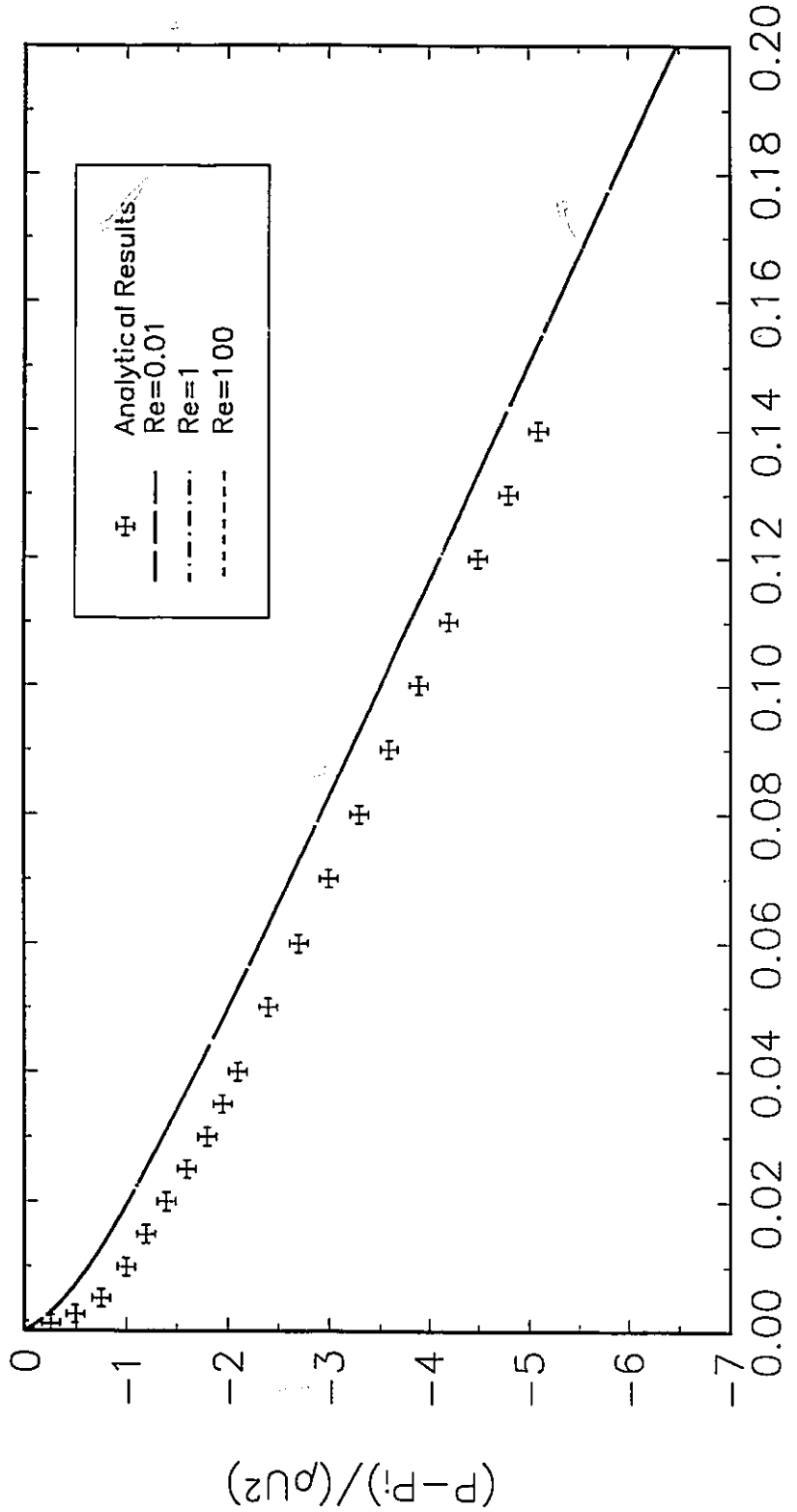

Figure 6.4. Axial pressure drop for several Re number.

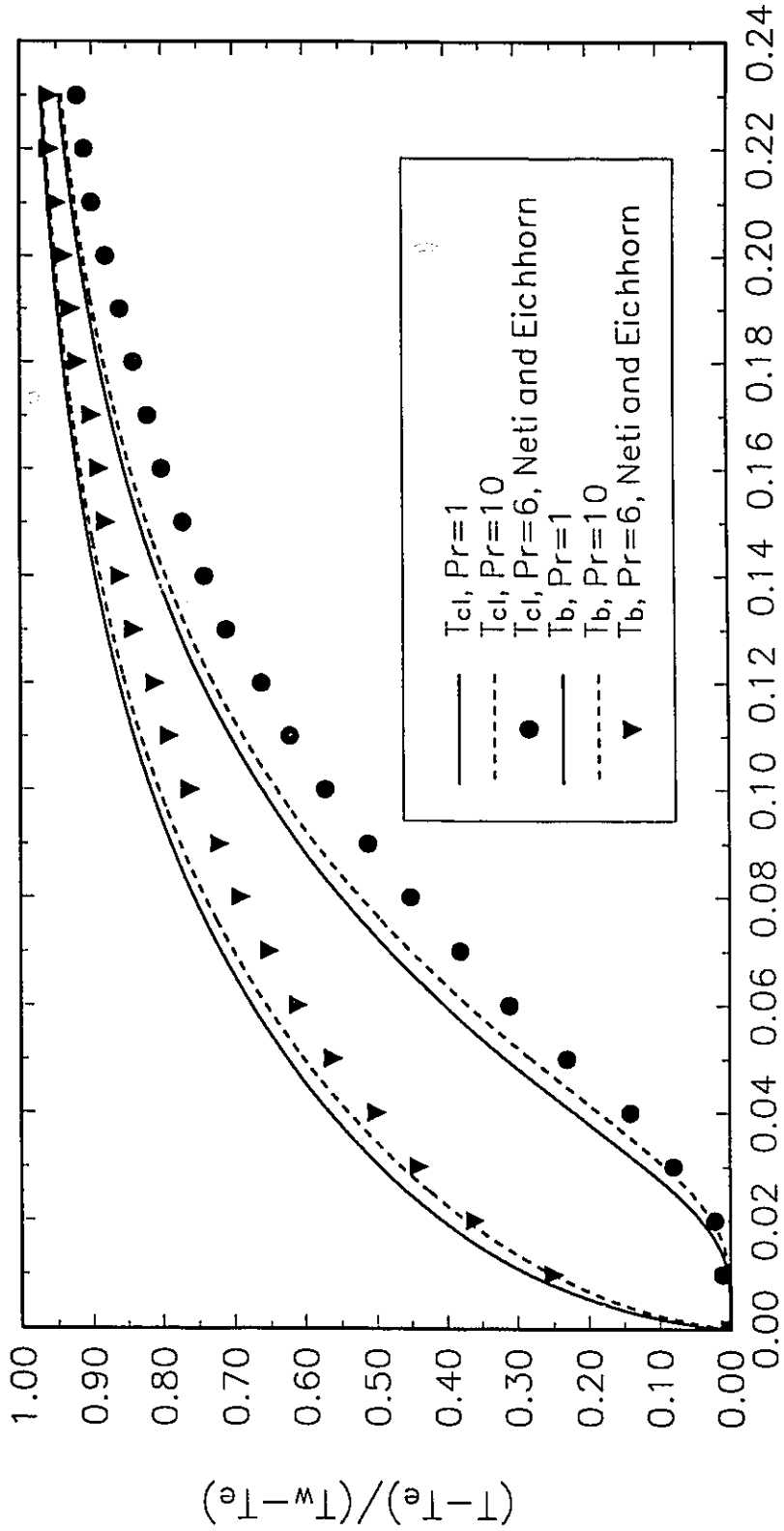

Figure 6.5. Thermal and hydrodynamic development in a square duct. T_{cl} indicates centre-line temperature.

$$\tau = \frac{\tau'}{\rho U^2} \tag{6-15}$$

and splitting the extra-stress tensor into viscous and elastic components, equations (6-11), (6-12) and (6-13) become, respectively:

$$uu_x = \frac{1}{Re}\left[u_{yy} + u_{zz}\right] - vu_y - wu_z - P_x^x - \left(\tau_{xx,x} + \tau_{xy,y} + \tau_{xz,z}\right) = 0 \tag{6-16}$$

$$uv_x = \frac{1}{Re}\left[v_{yy} + v_{zz}\right] - vv_y - wv_z - P_y - \left(\tau_{yx,x} + \tau_{yy,y} + \tau_{yz,z}\right) = 0 \tag{6-17}$$

$$uw_x = \frac{1}{Re}\left[w_{yy} + w_{zz}\right] - vw_y - ww_z - P_z - \left(\tau_{zx,x} + \tau_{zy,y} + \tau_{zz,z}\right) = 0 \tag{6-18}$$

Note that in equations (6-16) to (6-18) and subsequent ones, τ indicates the viscoelastic part of the extra-stress tensor. The difference between equations (6-11) to (6-13) and the viscoelastic counterparts, equations (6-16) to (6-18) is the addition of the spatial derivatives of the extra-stress tensor, that are an additional load vector (Appendix B). The assumptions made for parabolizing the Navier-Stokes equations are still valid. Moreover, the presence of hyperbolic constitutive equations (which do not need to be modified), accentuates the parabolic behavior of the system (Keunings, 1989). The MPTT model,

after some algebraic manipulations, can be written as:

$$(A - Wi_c B_{ij})\tau_{ij} + Wi_c(u\tau_{ijx} + v\tau_{ijy} + w\tau_{ijz}) - Wi_c D_{ij} = 0 \qquad (6\text{-}19)$$

(i=x,y,z; j=x,y,z), which is suitable for the marching procedure described above. A is defined in Equation (2-5).

The CEF model can also be written in a similar manner:

$$\tau_{ij} = \frac{1}{2}(u\dot{\gamma}_{ijx} + v\dot{\gamma}_{ijy} + w\dot{\gamma}_{ijz}) - \frac{1}{2}\psi_1 T_{1ij} + \left(\frac{1}{2}\psi_1 + \psi_2\right) T_{2ij} \qquad (6\text{-}20)$$

which, again, is amenable to marching procedures. The terms B_{ij} ,D_{ij}, T_{1ij}, T_{2ij}, as well as the finite element matrix formulation for the MPTT and CEF case, are described in Appendix B. The total extra-stress tensor description for both models includes an elastic part, described by (6-19) or (6-20) and a viscous part, of the form $\tau=\eta_v\dot{\gamma}$, with η_v constant for the MPTT case. In the CEF model, ψ_1 and η_v are dependent on the second invariant of the shear rate tensor (I_2) as (Dodson et al., 1974):

$$\eta_v = \eta_0\left[\frac{1+\sigma_2 I_2^2}{1+\sigma_1 I_2^2}\right]$$
$$\psi_1 = \eta_0\left[\frac{(\lambda_1-\lambda_2)+(\lambda_1\sigma_2-\lambda_2\sigma_1)I_2^2}{1+\sigma_1 I_2^2}\right] \qquad (6\text{-}21)$$

ψ_2 is considered to be constant in the whole shear rate range.

6.3 Numerical Results.

Initially, a full three-dimensional coupled simulation of channel flow of viscoelastic fluids was attempted, but the size of the system, its complexity and lack of convergence using standard procedures, coupled with the enormous requirements of CPU time and disk space, forced the use of simpler approaches. A three-dimensional formulation also has the problem of the outlet boundary condition. Selection of the proper outlet boundary condition for complex viscoelastic flows that show secondary flow patterns is not clear. Dooley and Hughes (1995) showed that for flow of LDPE and PS in ducts of non-circular geometry, there are secondary flows up to 64 L/D. The PNSE algorithm is well suited for viscoelastic flows, since they are convection-dominated and the constitutive equations of the differential type are known to show hyperbolic behavior (Larson, 1988; Keunings, 1989). The space-marching procedure of the PNSE does not require the imposition of any outflow boundary condition, except for the flow domain length. A complete and detailed study of viscoelastic flow in channels would require extensive analysis and testing. In this research, focus was made on the flow in a square duct, for which numerical and experimental evidence is available (Townsend et al., 1976; Dodson et al., 1974, Dietsche and Dooley, 1995; Dooley and Hughes, 1995). A better understanding of the secondary flow phenomena in dies may provide an explanation for the distorted interfaces observed in coextrusion of highly elastic polymers (Figure 5.21). Such distortions can not be captured using purely viscous flow simulators (Chapter 4 and 5). In purely viscous flow, a fully developed, rectilinear flow, is achieved a few L/D after the imposition of a disturbance, like a channel entrance or the contact of two fluids with

different viscosities. Viscoelastic flow, on the other hand, shows secondary flows that are related to the presence of a second normal stress difference (Tanner, 1985). CEF and MPTT models predict a second normal stress difference (N_2), which is related to ψ_2 and ζ, respectively (Larson, 1988; Macosko, 1994).

In the present case, a square duct was modeled using both the MPTT and CEF models. Careful studies of mesh dependence and axial step size were performed to test the code. A quarter symmetry was imposed due to the fact that numerous theoretical and experimental analyses show that this assumption is valid (for example, Green and Rivlin, 1956; Wheeler and Whisler, 1966; Dodson et al., 1974; Townsend et al., 1976; Dooley and Hughes, 1995). It was found that a regular mesh composed of 5x5 biquadratic, nine-node elements in the cross-sectional plane and a step size in the axial direction of 0.1 L/D were enough to provide accurate results. A 10x10 element mesh was used to confirm findings on the coarse mesh. As initial conditions, a fully developed flow in both viscoelastic stresses and axial velocity is imposed. However, several other choices were used for the inlet conditions, all of them providing similar results. Those were:

* a flat velocity profile and zero viscoelastic stress (this cause divergence at Wi_c > 0.1, or high flowrates)

* a fully developed flow and zero extra-stress.

The elasticity level is measured by the Weissenberg number (MPTT) or the Stress Ratio number (CEF). The Weissenberg number can defined in two different ways:

$$Wi_c = \lambda\, U/L \quad ; \quad Wi_w = \lambda\, \dot{\gamma}_w \tag{6-22}$$

where U and L are characteristic velocities and length, whereas $\dot{\gamma}_w$ indicates wall shear stress. By using characteristic dimensions, the range of Weissenberg number studied in this work varies between 0.01 and 0.05. By using the wall shear stress, Wi varies between 0.3 and 1.5. The Stress Ratio, S_R, is defined as:

$$S_R = \frac{N_1}{2\tau_w} \tag{6-23}$$

The CEF model, being a second-order model, is valid only as a slight departure from Newtonian fluids. The inlet conditions for the problems were obtained using a Poisson solver (Chapter 3). In order to compare both models, simulations are performed at low shear rates (up to 40 sec^{-1}). Experimental work was also carried at similar shear rates.

6.3.1 Criminale-Ericksen-Filbey (CEF) model.

The simple shear behavior of CEF model is shown in Figure 6.6. The CEF fluid shows a small deviation from the Newtonian behavior in viscosity and a corresponding first and second normal stress difference that can be considered constant over the shear rate range studied. The material values studied are those of a polymer solution with η_0=1, λ_1=0.01, λ_2=0.005, σ_1=0.000125, σ_2=0.0000625, and ψ_2=-0.01 and they were chosen after Dodson et al., (1974) in order to compare results. For the range of shear rates studied, η_v and ψ_1, are constant.

Figure 6.7a shows the cross-sectional velocity plot for a negative ψ_2. Even though

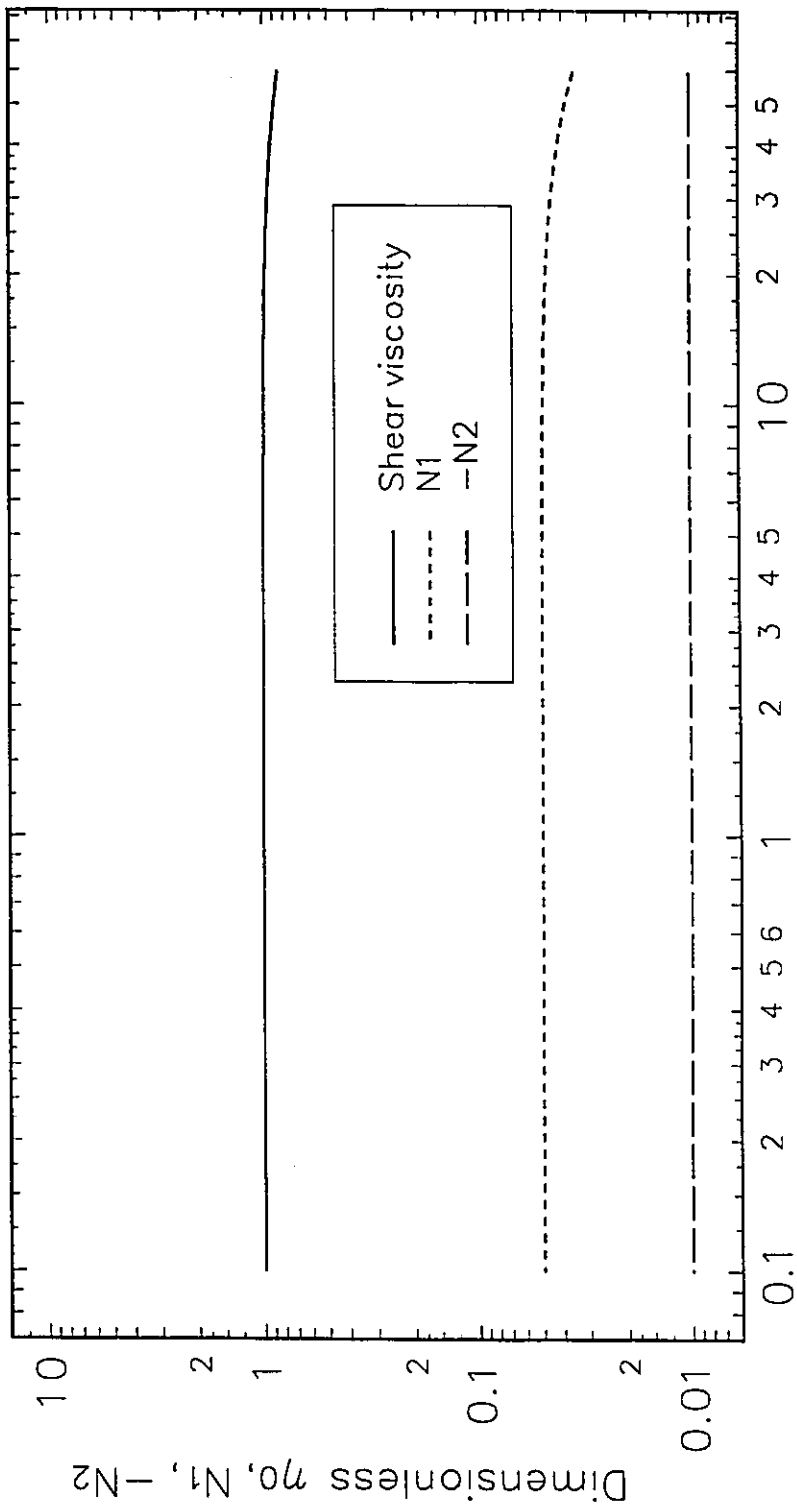

Figure 6.6. Simple shear behavior for CEF fluid. σ_1=0.000125 ; σ_2=0.0000625; λ_1=0.01; λ_2=0.005, Ψ_2=-0.01.

there are two different, symmetrical flow patterns that move from the die wall towards the centre of the die, the characteristic eight-vortex pattern predicted by many researchers (Dodson et al., 1974; Townsend et al., 1976; Thangam and Speziale, 1987) using analytical methods and two-dimensional simulations is not observed. The direction of flow is reversed when the sign of ψ_2 is changed (Figure 6.7b), in accordance with the numerical observations of Dodson et al. (1974). This type of flow is compatible with experimental predictions of polymer solution flow in ducts (Figure 6.8; Townsend et al., 1976). By having constant N_2 and a constant viscosity, no vortex can be predicted according to the theoretical analysis of Langlois and Rivlin (1963),a fact that was confirmed with the marching algorithm. There are several differences between the numerical scheme presented here and previous two-dimensional analysis. The most important are:

a) The marching algorithm takes into consideration the three-dimensional deformation pattern of the fluid particles, which is neglected in 2-D analysis.

b) 2-D analysis used a perturbation of a Newtonian flow to calculate secondary flows through a streamfunction formulation (Dodson et al., 1974). The perturbation factor is N_2. In the marching algorithm, the full set of governing equation is solved.

c) In the 2-D analysis, the pressure field is assumed to be constant within the cross-section, and the axial pressure drop is also assumed to be constant. The marching algorithm assumes that the axial pressure drop is constant at each cross-section, but the pressure may vary within a given cross section.

d) The shear rate is calculated using only the contributions from the main axial

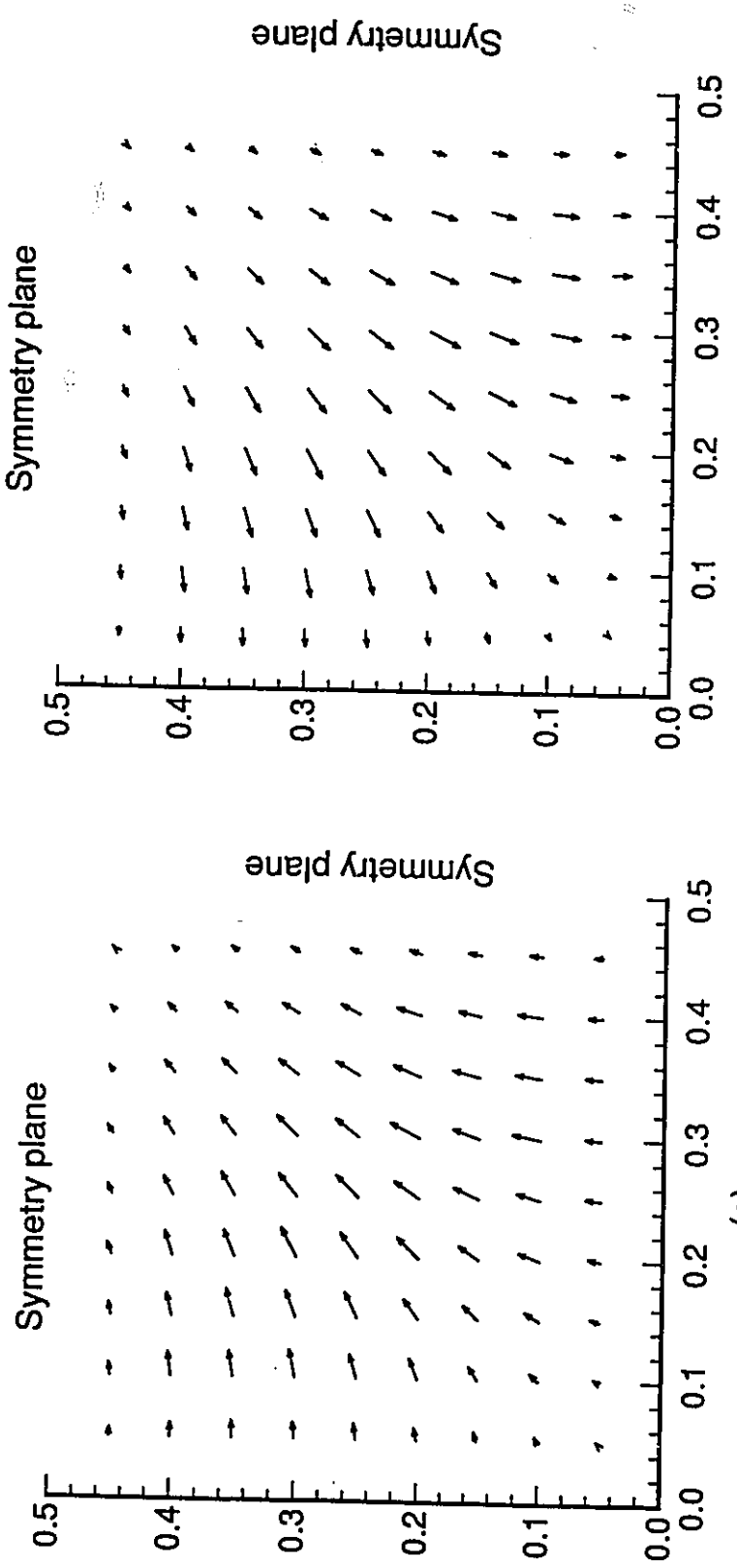

Figure 6.7. Cross-sectional velocities for CEF fluid. σ_1=0.000125 ; σ_2=0.0000625; λ_1=0.01; λ_2=0.005. (a) Ψ_2=-0.01; (b) Ψ_2=0.01

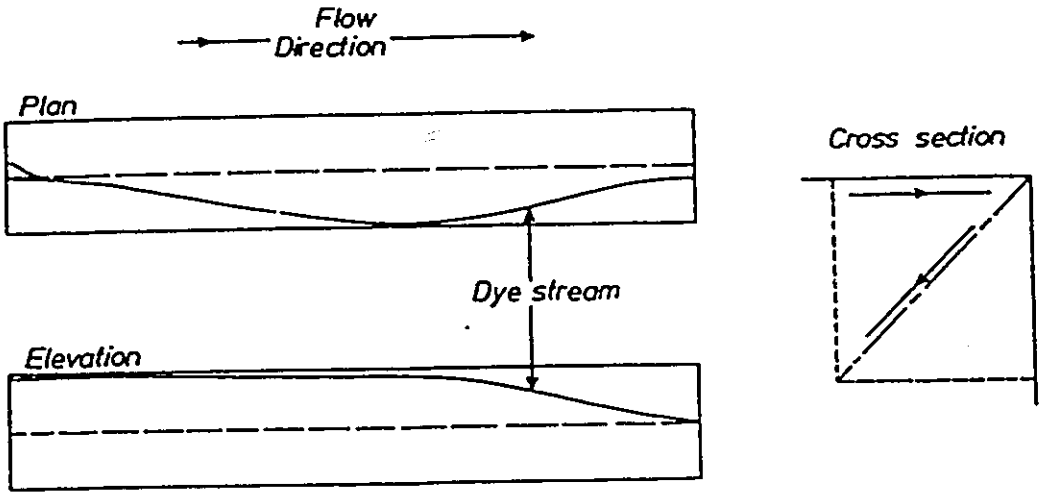

Figure 6.8. Experimental observations of Townsend et al. (1976).

velocity components (u-velocity component), while the cross-sectional velocity contributions are neglected in the 2-D formulation (Dodson et al., 1974). The 3-D marching algorithm uses contributions from all velocity components.

The effect of mesh density and axial step size were analyzed. Figure 6.9 shows the results for 10 elements in each cross-sectional direction compared to a 5x5 mesh. Table 6.5 shows the maximum velocity components and its y- and z-coordinate locations for various mesh sizes and axial step sizes. However, having a very small (dx<0.01) or very large step size (dx>1) results in divergence for solution of the problem. No cross-flow velocities are shown for ψ_2=0, confirming theoretical analysis and previous numerical simulations (Langlois and Rivlin, 1963 and Townsend et al., 1976).

Table 6.5. Comparison of meshes and axial steps for CEF model.

Mesh	dx	Max. u	Location (y,z)	Max. v	Location (y,z)	Max w	Location (y,z)
5x5	0.1	1.4733	(0.5,0.5)	0.01176	(0.2,0.3)	0.01177	(0.3,0.2)
10x10	0.1	1.4734	(0.5,0.5)	0.01169	(0.15,0.3)	0.01170	(0.3,0.15)
5x5	0.2	1.4746	(0.5,0.5)	0.01177	(0.2,0.3)	0.01176	(0.3,0.2)
5x5	0.025	1.4747	(0.5,0.5)	0.01110	(0.2,0.3)	0.01110	(0.3,0.2)

The present code is also compared against the work of Gervang and Larsen (1991) who used 3-D finite differences and a CEF model to study secondary flows in ducts using periodic boundary conditions. The CEF parameters dependence on shear rate is as follows:

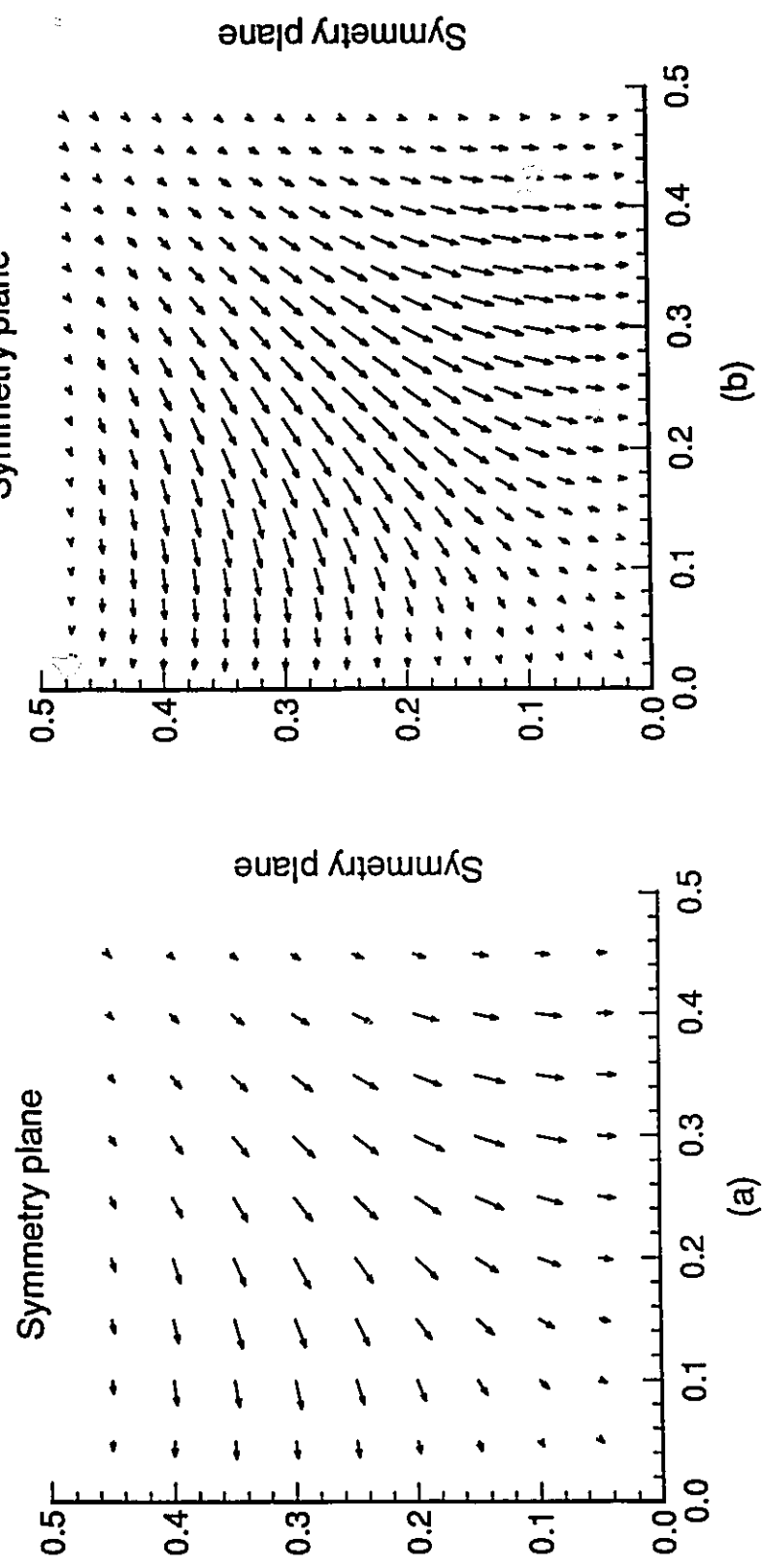

Figure 6.9. Comparison of meshes for CEF model. Parameters as in Figure 6.7. (a) 5x5. (b) 10x10.

$$\eta_v = k\,\dot{\gamma}^{n-1}$$

$$\psi_1 = k_1\,\dot{\gamma}^{n_1} \qquad (6\text{-}24)$$

$$\psi_2 = -0.15\,\psi_1$$

where, for the case studied, k=8.5 Pa.s; k_1=5.96; n=0.37; n_1=-1.35. Gervang and Larsen (1991) observed eight symmetric vortices for the fully developed flow condition (Figure 6.10a). Figure 6.10b shows the cross-flow velocities at L/D=1.9 obtained with the marching algorithm presented here for the same problem. The major difference is that the marching algorithm predicts only four recirculation zones near the die corners. To obtain eight vortices with the present 3-D marching code it is necessary to define ψ_2 such that there is a change in sign with increasing shear rate (Section 6.3.3). Table 6.6 shows the comparisons of vortex strength and other relevant parameters of the two numerical simulations. Experiments performed by the Gervang and Larson (1991) showed the measured magnitude of the cross-flow velocities as twice as predicted by their code. The main difference between the code of Gervang and Larsen (1991) and the marching algorithm presented here is the treatment of boundary conditions. While a marching algorithm does not require the imposition of outflow boundary conditions, Gervang and Larsen (1991) imposed homogeneous Neumann conditions as the outflow boundary condition.

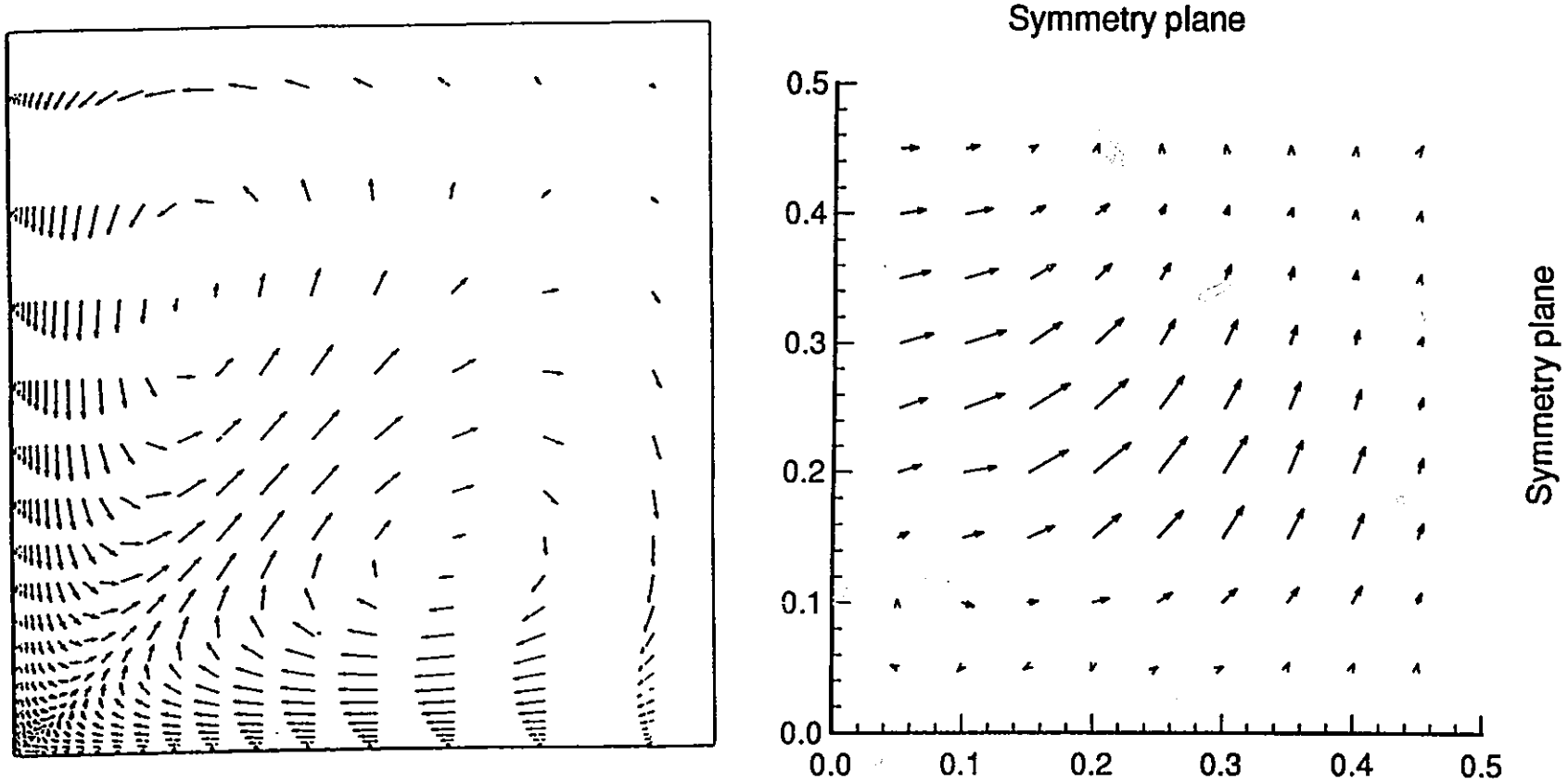

Figure 6.10. Secondary flow patterns for the data of Gervang and Larsen (1991). (a) Gervang and Larsen (1991); (b) Marching algorithm.

Table 6.6. Comparison of the marching algorithm and Gervang and Larson (1991).

Variable	Present code	Gervang and Larson
Max. *u*-velocity (m/s)	0.843	0.815
Max. *v*-velocity (m/s)	0.0288	0.00502
Max. *w*-velocity (m/s)	0.0266	0.00486
Min. streamfunction (m^2/s)	-1.12×10^{-5}	-2.14×10^{-6}
Max. streamfunction (m^2/s)	2.60×10^{-5}	2.11×10^{-6}

6.3.2 Modified Phan-Thien Tanner (MPTT) model.

The simple shear behavior of the MPTT model is shown in Figure 6.11. The behavior of MPTT fluids is more realistic than the CEF model. It is capable of predicting shear thinning, and a dependence of N_1 on shear rate for simple shear flows. In Figure 6.11, shear viscosity shows shear-thinning behavior with zero-shear and infinite-shear plateaus, but N_1 (the first normal stress difference) grows unbounded with the shear rate, N_2 is constant and negative. Larson (1988) showed analytically that N_2 is proportional to ζ and independent of shear rate (Figure 6.11) for MPTT fluids.

A case study for which η_e=4000; η_v=6000; λ=0.01; ζ=0.2 (Equation 6-19) is used. The ratio of elastic to viscous components of viscosity was chosen to avoid numerical instabilities characteristic of the method used to solve for the elastic components of the extra-stress tensor (Rajagopalan et al., 1990). Values for λ and ζ can be found in most simulations that used MPTT models and have been used to fit experimental data (Bush et al., 1985; Tran-Cong and Phan-Thien, 1988c).

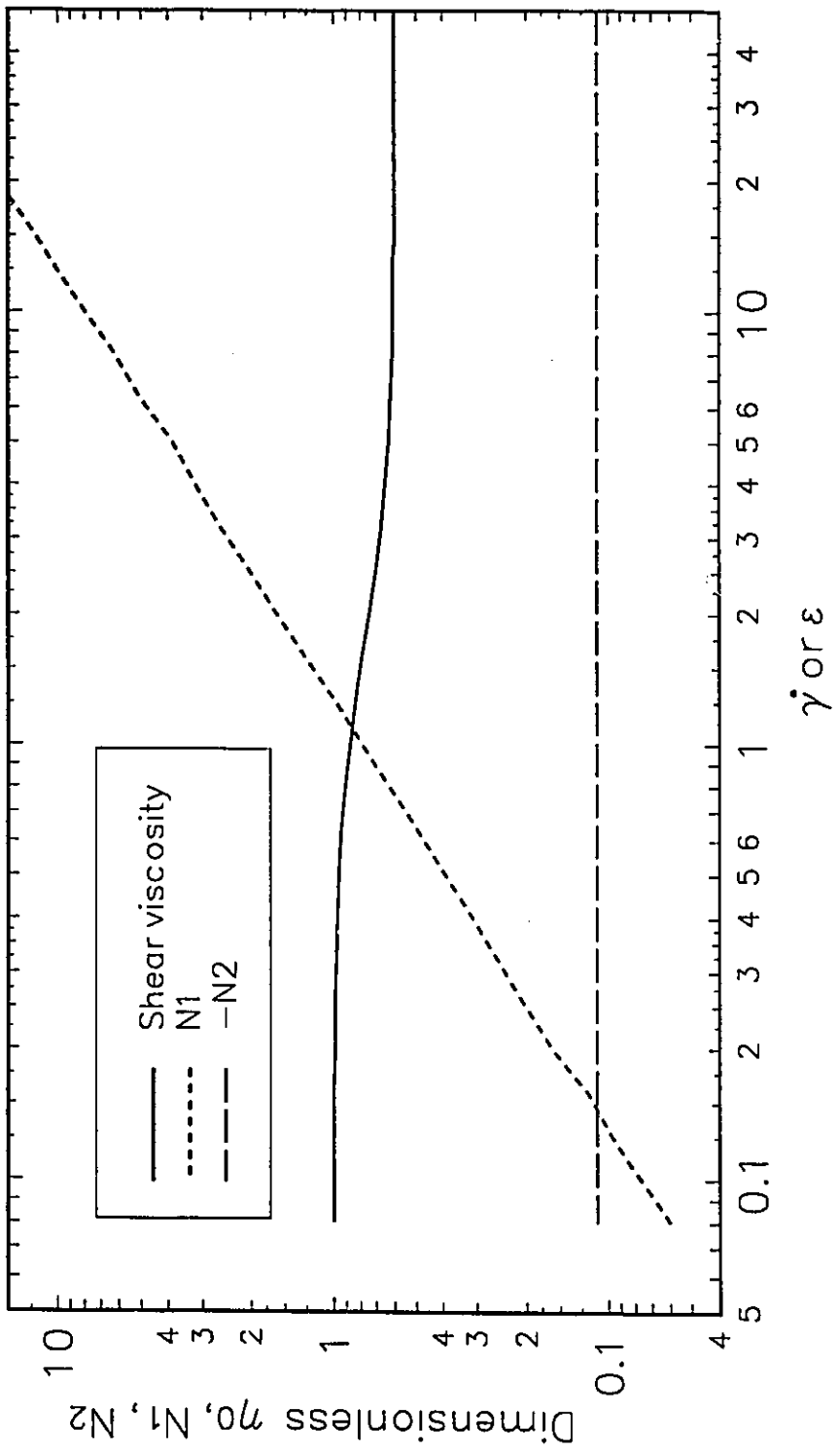

Figure 6.11. Simple shear behavior of the MPTT model. η_e=0.4; η_v=0.6; λ=1; ξ=0.2.

As in the CEF case, a 10x10 mesh is used to confirm the results obtained (Figure 6.12b) with the coarse mesh of 5x5 elements (Figure 6.12a). Table 6.7 shows the maximum velocity components and its y- and z-coordinate locations for various mesh sizes and axial step sizes. As in the CEF case, having a very small step size (dx<0.01) or too large (dx>1) results in divergence. A very small step size possibly results in errors in the numerical differentiation of the stress terms (Appendix B).

Table 6.7. Comparison of meshes and axial steps for MPTT model.

Mesh	dx	Max. u	Location (y,z)	Max. v	Location (y,z)	Max w	Location (y,z)
5x5	0.1	2.268	(0.5,0.5)	0.01820	(0.2,0.3)	0.01820	(0.3,0.2)
10x10	0.1	2.266	(0.5,0.5)	0.01778	(0.15,0.3)	0.01777	(0.3,0.15)
5x5	0.2	2.268	(0.5,0.5)	0.01822	(0.2,0.3)	0.01826	(0.3,0.2)
5x5	0.025	2.268	(0.5,0.5)	0.01821	(0.2,0.3)	0.01821	(0.3,0.2)

The predictions obtained using two different viscoelastic models are in qualitative agreement. The reversal of the secondary flow when the sign of N_2 is reversed and the absence of secondary flows for $N_2=0$ are fully in agreement with theoretical predictions.

6.3.3 New model for ψ_2 and ζ at low shear rates.

A model is proposed in which ψ_2 for the CEF model or ζ for the MPTT model (the variables directly related to N_2) change sign depending on the shear rate as follows:

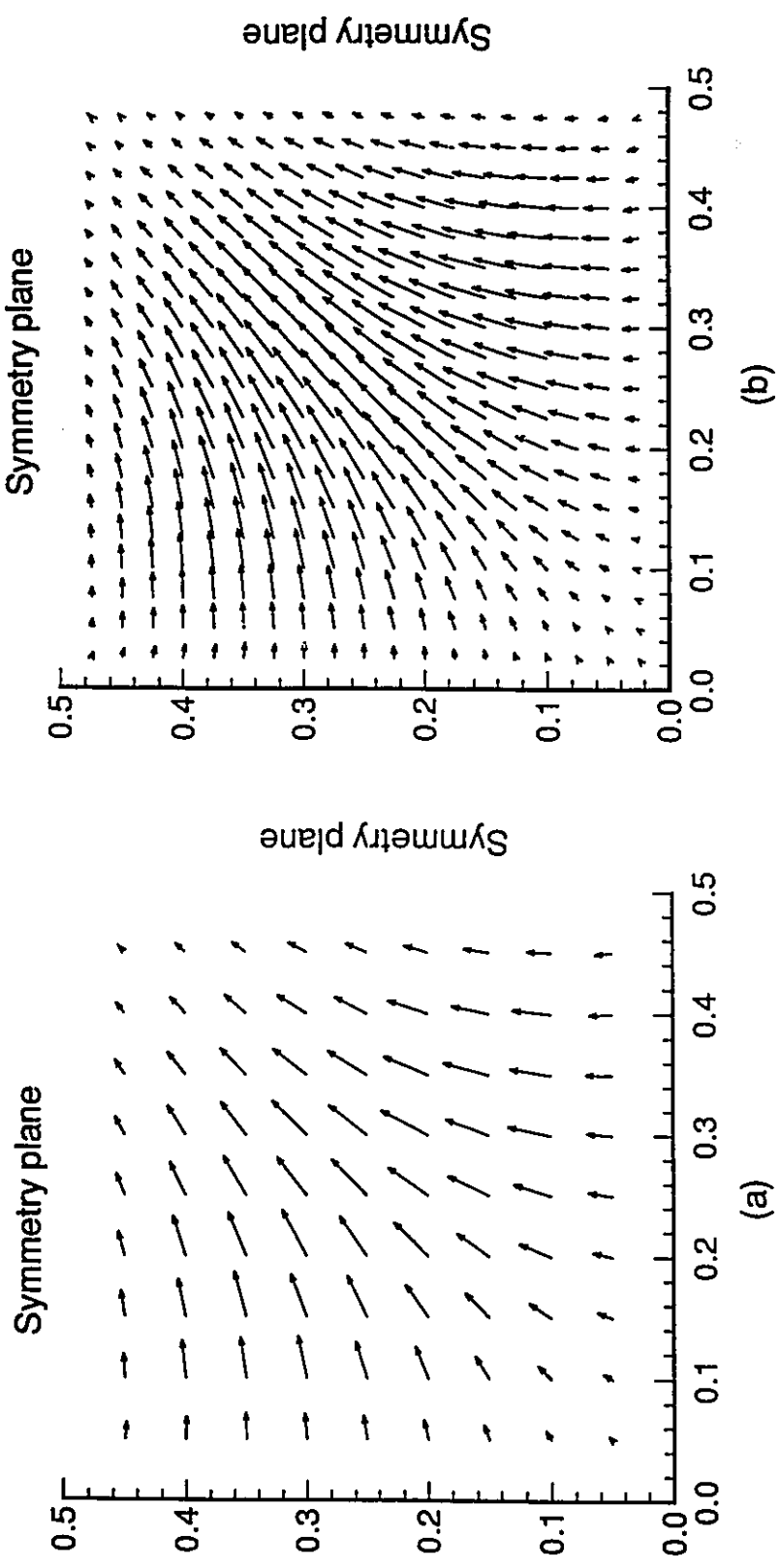

Figure 6.12. Cross-sectional velocities MPTT fluid for different mesh densities η_e=4000; η_v=6000; λ=0.01; ξ=0.2.
(a) 5x5. (b) 10x10.

$$\psi_2 = -\psi_1(1-\theta I_2)$$
$$\zeta = \zeta_0(1-\theta I_2) \qquad (6\text{-}25)$$

for the CEF and MPTT models, respectively, where I_2 is the second invariant of the shear rate tensor, ζ_0 is the fixed ζ value of the original MPTT equation (usually 0.2), θ is a characteristic constant that defines the critical shear rate for sign change (Figure 6.13). Equation (6-25) predicts a change of sign for ψ_2 (CEF) and ζ (MPTT) at a shear rate equal to $1/\theta$. Change in sign for N_2 have been observed for polymer solutions, liquid crystal polymers and Boger fluids (Magda et al., 1991a,b; Magda et al, 1993). Information for polymer melts is limited to high shear rates ($\dot{\gamma} > 10$ sec^{-1}; Magda et al., 1993; Larson, 1988). Equation (6-25) allowed the prediction of eight vortices in both the MPTT and CEF models (Figures 6.14a and 6.14b, respectively). The shape and location of the vortices depends on θ. Through this work, θ is set to 0.04 for the CEF model and to 0.015 for the MPTT, in order to have a sign change in the range of shear rate in which this sign change has been experimentally observed ($\dot{\gamma}_w < 40$ sec^{-1}, Magda et. al, 1991a,b; Magda et al., 1993). For all the problems studied, if $\theta < 0.005$ or $\theta > 0.1$ no vortex is observed, since the crossover point for ψ_2 or ζ lie beyond the range of shear rates studied. It is important to note that ψ_2 and ζ in (6-25) grow without bound with shear rate, and its range of applicability is limited to the low shear rate flows. Improved versions of (6-25) may be devised to avoid the unrealistic growth with shear rate (Carreau-like equations), but further research on the physical nature of N_2 is necessary.

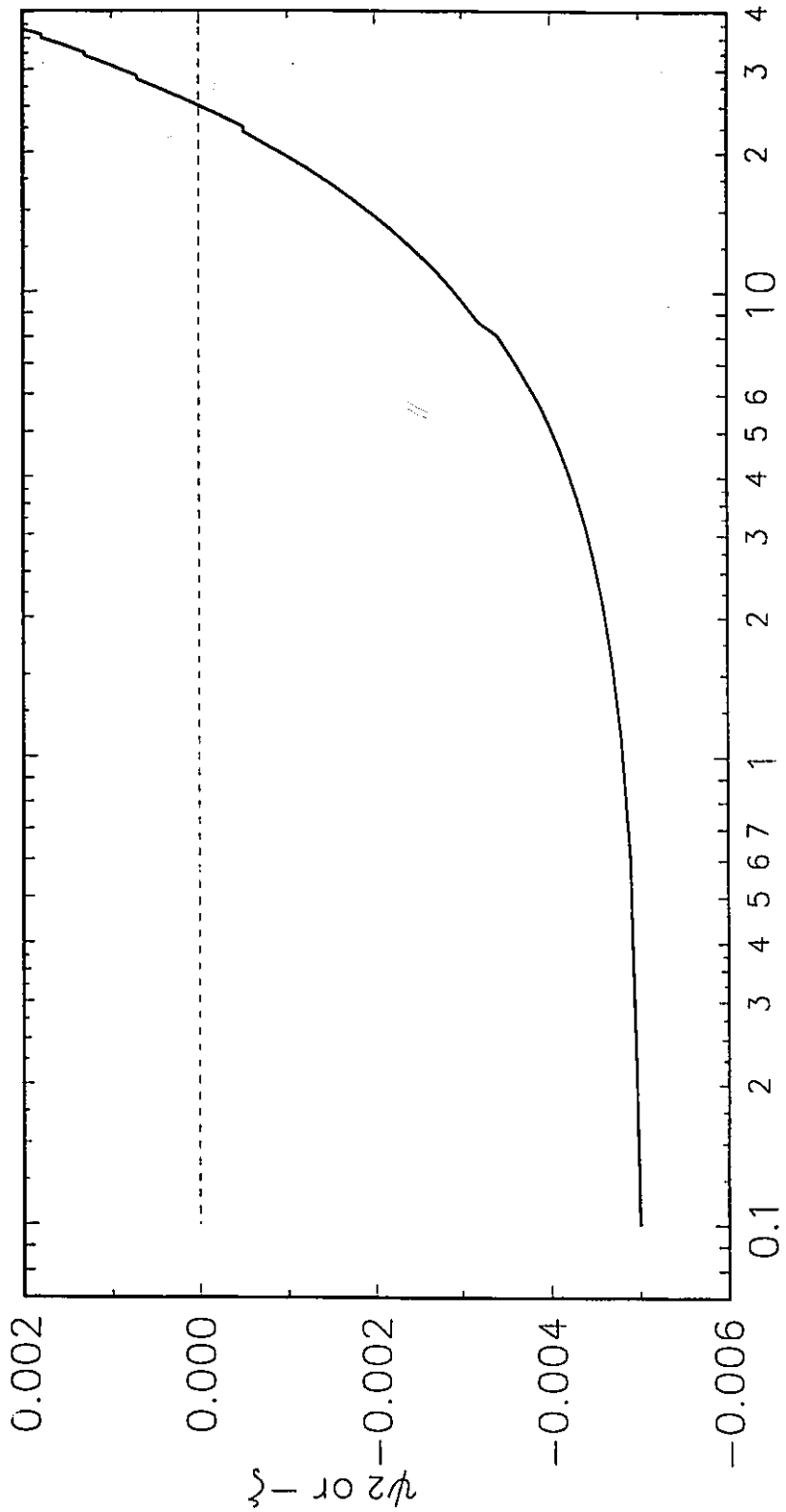

Figure 6.13. Proposed new behavior for ζ or ψ_2.

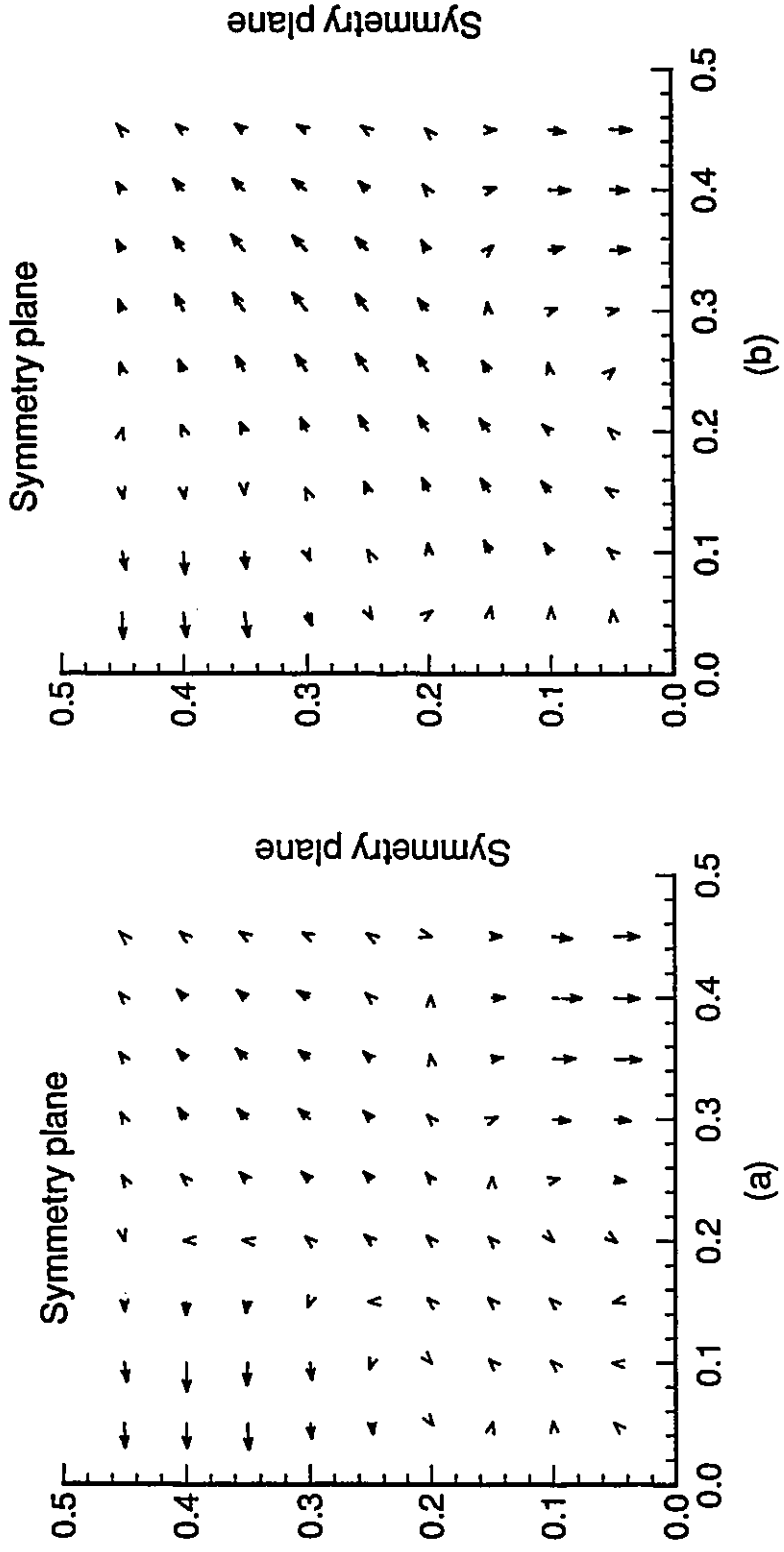

Figure 6.14(a) Secondary flow of a MPTT fluid using the new model for ζ. Parameters as in Fig. 6.12. (b) Secondary flow of a CEF fluid using the new model for ψ_2. Parameters as in Fig. 6.7.

Figure 6.15 shows a comparison of the present code using the MPTT model with the parameters in Figure 6.12a (right) compared to experiments using STYRON 484[1] (Dooley and Hughes, 1995) and simulations performed using POLYFLOW[2], a commercial finite element code (Dietsche and Dooley, 1995). No information could be found in the open literature about the solution algorithm and other computational details used in the POLYFLOW calculation. The present code shows the intrusion of fluid from the corner to the centre of the die, and two vortices symmetrically located at each side of the diagonal. These results are consistent with experimental data available (Dooley and Hughes, 1995). Results were qualitatively similar using either CEF or MPTT models.

In all the simulations performed with MPTT fluids, the cross-flow profile at long enough L/D (L/D > 20) oscillates between two different secondary flow configurations, while the simulations performed with the CEF model attains a stable secondary flow configuration as shown in Figure 6.14b. For the CEF model, a true steady-state solution is reached in which a definite secondary flow pattern is obtained. For the MPTT flows, an approximate fixed oscillation between two possible secondary flow arrangements are observed as far as 20 L/D and there is no evidence that the oscillations will either diminish or grow. In one arrangement, one vortex outgrows the other (Figure 6.16a), while at the other extreme the situation is reversed (Figure 6.16b). Whether these solutions are of a numerical or physical nature is not clear. Experiments (Dooley and Hughes, 1995) do not provide conclusive support (Figure 6.17).

---

[1] Styron 484 is a trademark of the Dow Chemical Company.

[2] POLYFLOW is a trademark of POLYFLOW s.a.

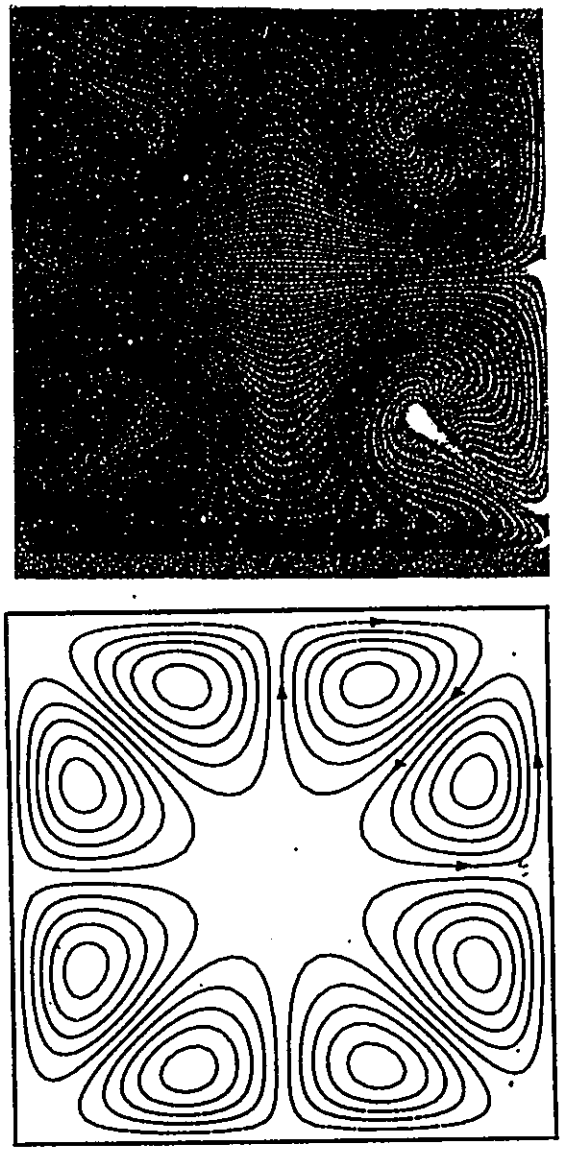

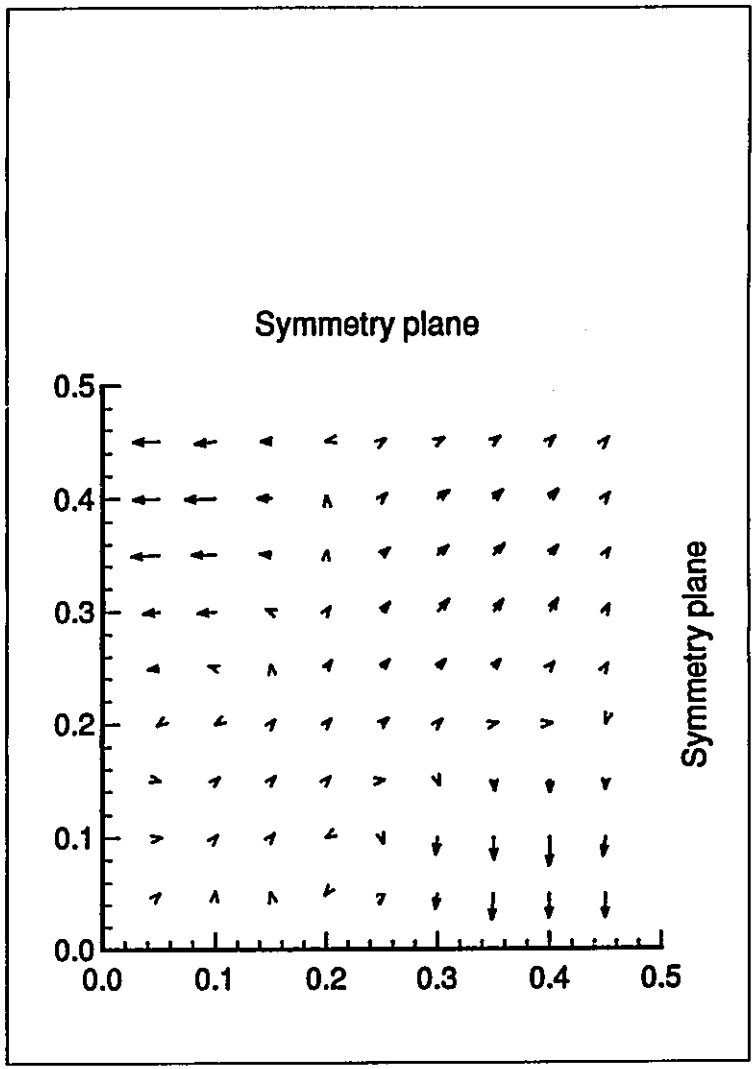

Figure 6.15.Comparison of the present code (right; MPTT model, parameters as in 6.12) against experiments (top left; Dooley and Hughes, 1995) and simulations (bottom left; Ditsche and Dooley, 1995).

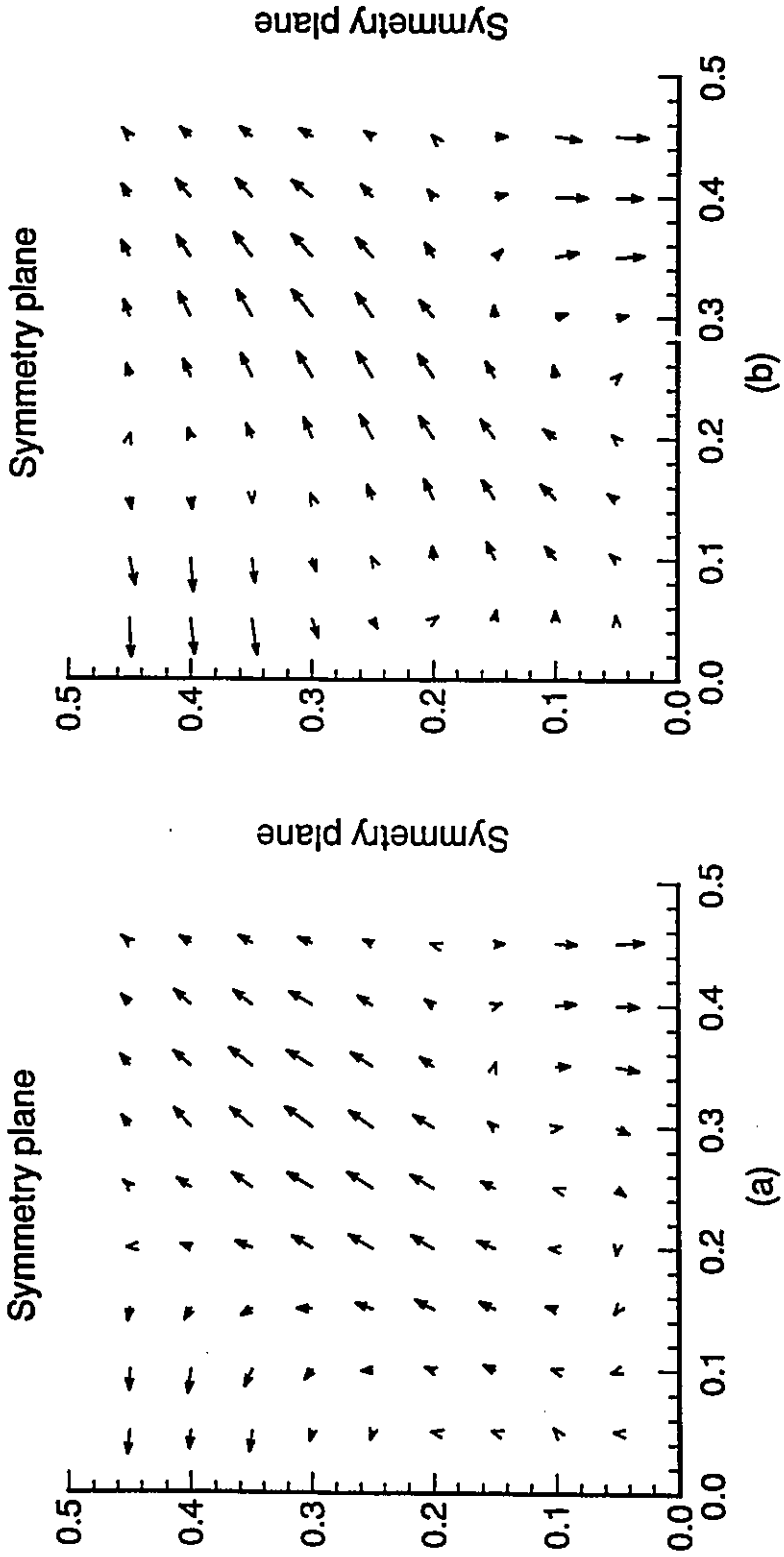

Figure 6.16. Extremes of the two oscillations for MPTT flows at long L/D ($L/D > 8$). Parameters as in Fig. 6.12.

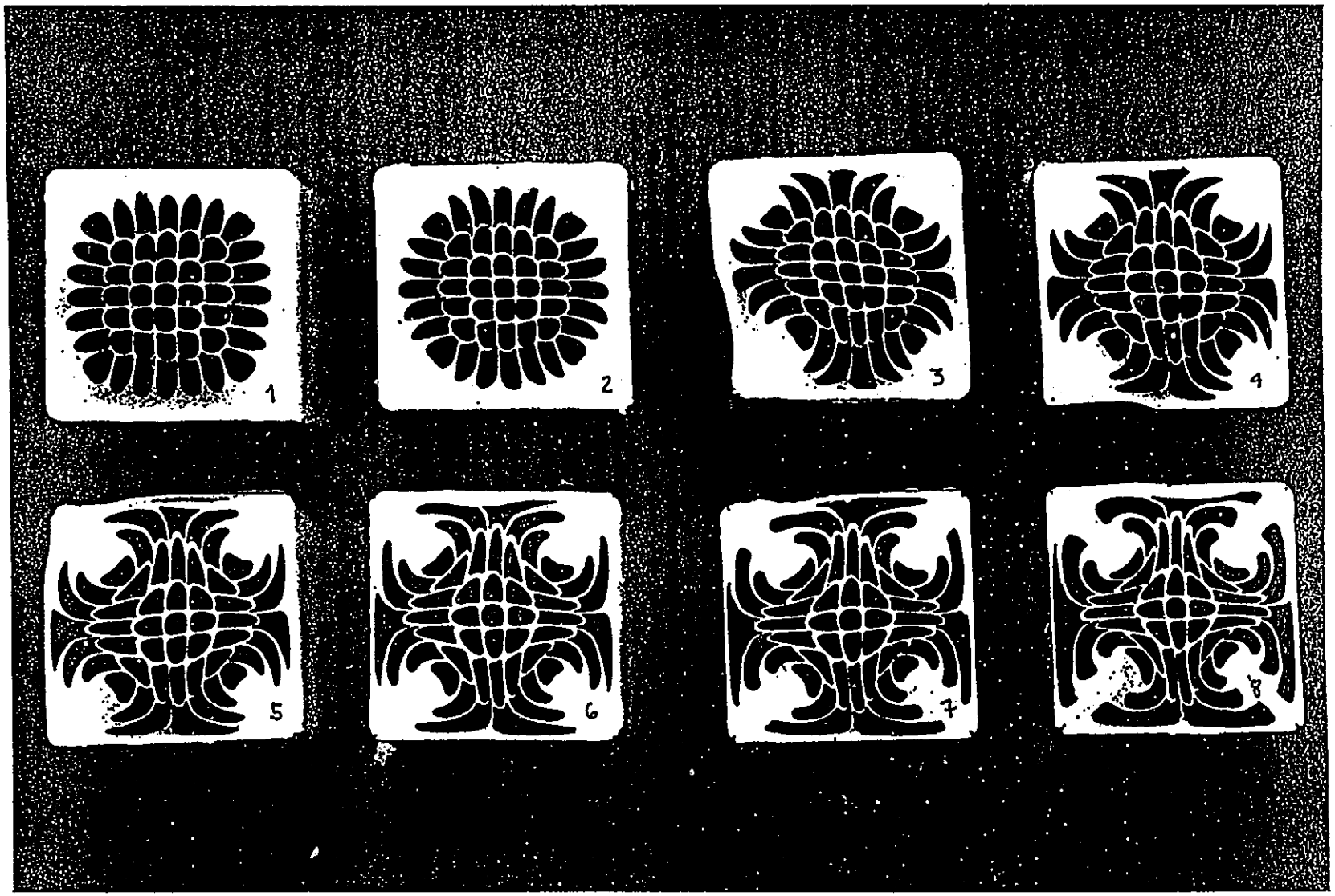

Figure 6.17. Sequences of secondary flows patterns in extrusion of PS from the die inlet (1) to die exit (8). (Dooley and Hughes, 1995).

Dooley and Hughes (1995) traced the deformation pattern of PS by producing a unique coextruded structure consisting of an array of 49 individual strands (7 rows by 7 columns). The frozen polymer "heel" from inside the die was then examined. Figure 6.17 shows cuts at 8 planes from the die inlet (1) to the die exit (8). The velocity field obtained with the marching algorithm using a MPTT model was used to obtain particle traces along the die, in order to compare it with the experimental deformation patterns obtained by Dooley and Hughes (1995). Figure 6.18 shows how massless particles dropped at the die inlet would deform according to the predicted velocity field. In Figure 6.18a, a view from the die inlet to the die outlet is shown to better visualize the deformation pattern in the cross-section of the die. Figure 6.18b shows the deformation of a square strand as it travels along the die. The three-dimensional marching algorithm agrees qualitatively with the experiments. Particles along the diagonal travel to the center of the die, being the center of the die a rectilinear flow point. As one moves from the die corner to the die centre, near the die walls, there is a change of direction in the particle movement. Near the die bottom wall, particles will move towards the centre of the die. As one moves from the die bottom wall to the centre, particles change direction and move towards the die wall. Note that the symmetry along the diagonal is observed in both simulation and experiment. Table 6.8 compares the maximum cross-flow velocities calculated with the proposed marching algorithm versus numerical simulations using POLYFLOW (Dietsche and Dooley, 1995) and experimental data (Dooley and Hughes, 1995). Note that POLYFLOW predictions are sensitive to the shear rate range over which rheological data were fitted.

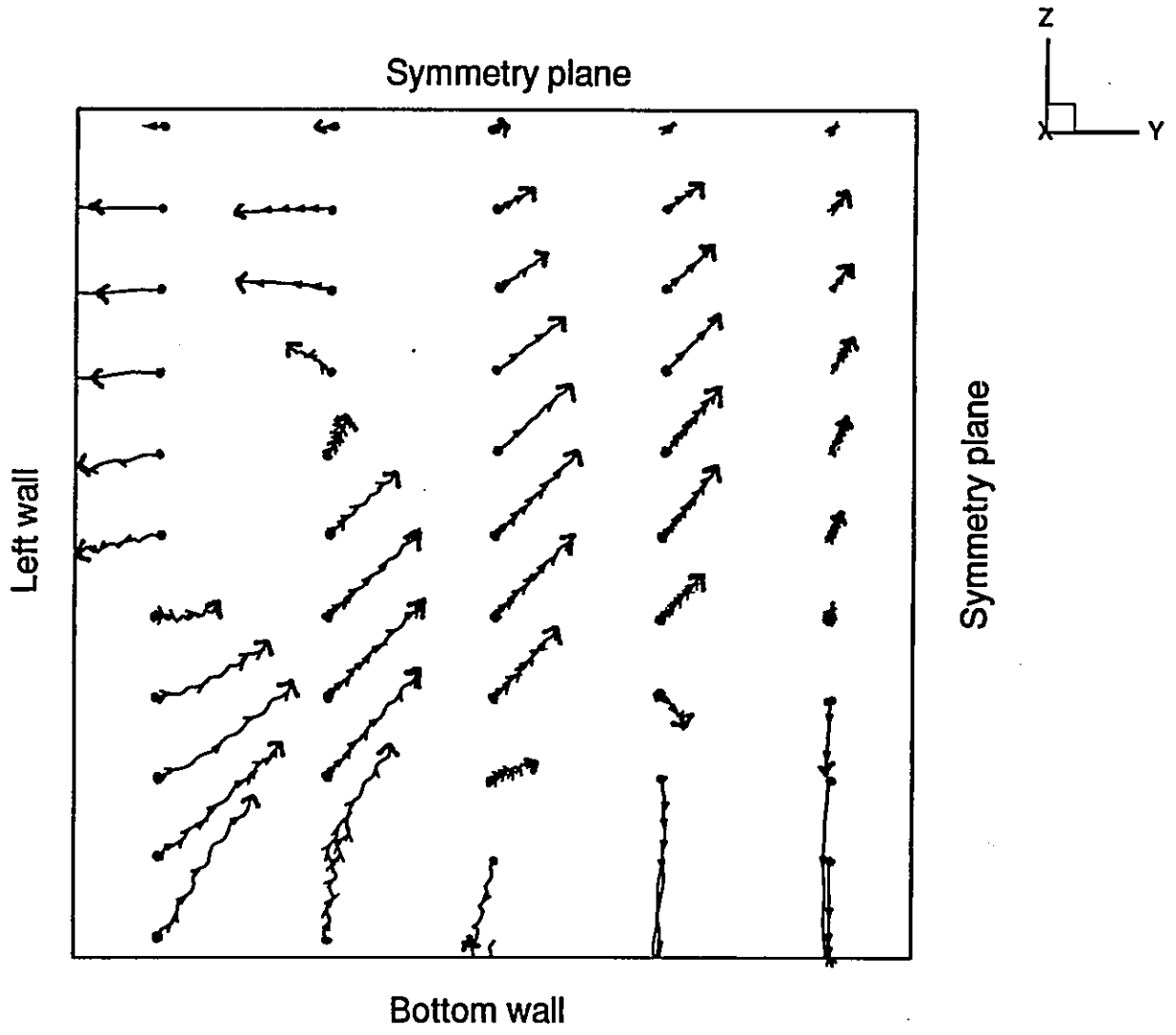

Figure 6.18(a) Massless particle trajectories using the MPTT model (parameters as in Figure 6.12).

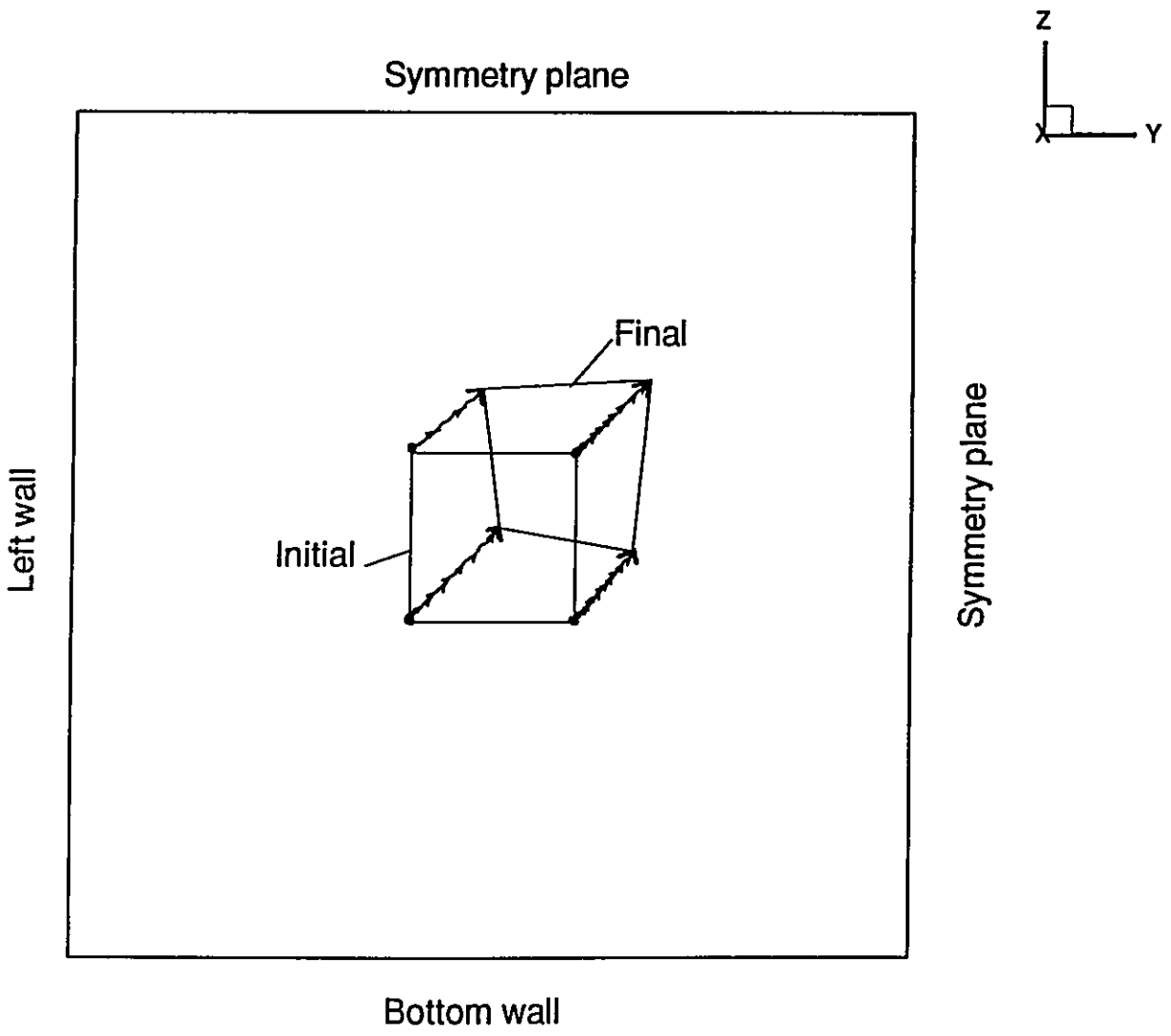

Figure 6.18(b) Trajectories of a square strand as it travels along the die.

Table 6.8. Comparison of maximum cross-flow velocities in experimental data (Dooley and Hughes, 1995), POLYFLOW predictions (Dietsche and Dooley, 1995) and marching algorithm.

	Max. cross-flow velocity (cm/s)
Experiments (Dooley and Hughes, 1995)	0.0055
Marching algorithm	0.0013
POLYFLOW (*), (Dietsche and Dooley, 1995)	order of 10^{-3}
POLYFLOW (**), (Dietsche and Dooley, 1995)	order of 10^{-4}

(*) PTT model fitted rheological data over 1-10 1/sec shear rate range.
(**) PTT model fitted rheological data over 10-100 1/sec shear rate range.

6.4 Summary.

A three-dimensional space marching technique (PNSE) for viscoelastic flows is implemented to model the secondary flow development phenomena in ducts using a second-order model (CEF) and a differential model (MPTT). Qualitative results of secondary flows are the same for both models and in agreement with known facts in literature (reversal of direction with sign change of N_2; zero secondary flow for constant N_2) except for the presence of the eight-vortex pattern in square ducts. A model for N_2 that predicts a sign change at a given shear rate was used to obtain the eight-vortex pattern. Again, the qualitative shape of those patterns were similar for CEF and MPTT models. Comparison with experimental evidence (Dooley and Hughes, 1995) and numerical simulations with a commercial package (Dietsche and Dooley, 1995) are in qualitative agreement. Particle trajectories calculated with the three-dimensional code compare well against experimental measurements of those trajectories in a strand profile

progression in a square channel (Dooley and Hughes, 1995).

The main conclusion from the present study is the fact that secondary flows are a definite pattern in viscoelastic flow in ducts. Cross-flow velocities will interact with the interface in co-extrusion flows, distorting it significantly as compared to Generalized Newtonian Flows, for which there are no secondary flows. Coextrusion experiments performed at McMaster (Takács et al., 1994) and Dow Chemical (Dooley and Stout, 1991; Dooley and Hughes, 1995) indicate that the interface in co-extrusion flows tends to deform with the secondary flow patterns. Simulations using purely viscous models agree well with polymers exhibiting relatively low elasticity levels. The interface shape for different materials through the same die and operating conditions are completely different depending on polymer elasticity levels (Takács et al., 1994; Dooley and Stout, 1991; Dooley and Hughes, 1995). A new approach has been proposed to perform simulations of complex viscoelastic fluids (such as those characterized by a MPTT model) in a three-dimensional fashion. Even though the results presented in this chapter should be considered preliminary and more research is needed, the marching algorithm seems to be an appropriate approach to the computationally expensive problem of modeling three-dimensional viscoelastic flows in ducts.

More extensive and detailed research is needed to experimentally assess the nature and shape of these secondary flows and, in particular, its possible relation to interface deformation. Numerical algorithms must be improved and optimized to extend the models to full three-dimensional simulations to allow a definite critique of the proposed algorithm. The qualitative agreement between numerical simulations and experimental

research (Dooley and Hughes, 1995), suggests that more experiments have to be performed to quantitatively determine the shape and three-dimensional evolution of those secondary flows at various shear rates by measuring particle trajectories.

CHAPTER 7

CONCLUSIONS AND RECOMMENDATIONS

7.1 Conclusions.

A three-dimensional finite element program has been developed for the simulation of bicomponent flow in dies of Generalized Newtonian Flows (GNF). It allows a simultaneous calculation of velocity, pressure, temperature fields, and interface locations. The code agrees well with experiments for low elasticity fluids.

Polymer/polymer/wall interactions are important in the interface deformation across the die for coextrusion flows. A study, with the inclusion of energy equation and geometrical effects, has been completed for GNF fluids in bicomponent coextrusion flows. Three-dimensional analysis of interface deformation in polymer coextrusion flows is required in order to fully understand this process. Simulations show that even though interface deformation criteria might be met at the die centre, the same criteria might be violated near the die wall. This code could be used to provide an estimation of the necessary trimming at the edges of a coextruded product due to layer nonuniformity.

Several models of contact line behavior are proposed. Mathematical singularity is relieved by applying either a "stick" or slip local boundary condition at the contact line nodes while retaining the no-slip boundary condition elsewhere in the die walls. The "stick" model shows an entraining layer of the less viscous fluid into the more viscous

one, called "primary film". Detailed analysis of wall effects are now possible. New interface shapes showed that extrapolation methods can not capture certain shapes at the die walls, particularly the "primary film" phenomena. (Torres et al., 1993).

Based on experimental evidence, two distinct interface movement mechanisms have been proposed: Type I involves a displacement of the more viscous fluid by the less viscous one, due to slippage of the contact line. Type II shows an entraining layer of the less viscous fluid into the more viscous one, and it is related to a limited slip at the die walls. The two types have been experimentally observed and they depend strongly on polymer/polymer/wall interactions. (Torres et al., 1995).

An extensive analysis of the thermal effects in coextrusion flows was performed. The effect of entrance angle on the final interface shape is most critical near the die walls, whereas near the die centre is not very important, a fact that can not be captured using two-dimensional simulations. The most critical factor in the layer uniformity problem, with Generalized Newtonian Fluids, is the thermal dependence of viscosity. The code provides the possibility of developing operating windows for the various parameters involved that might be useful to the designer. It can also be used to assess the particular effects of operating conditions and design parameters, even though all these effects are coupled and are not suited for isolated study (Torres et al., 1995).

A space-marching three dimensional finite element code for single fluids has been developed for the simulation of viscoelastic flow in ducts, capturing the secondary flow effect. The space-marching algorithm can use the Criminale-Ericksen-Filbey (CEF) and Modified Phan-Thien-Tanner (MPTT) constitutive equations. The algorithm is based on

an extension of the Parabolized Navier-Stokes Equations (PNSE). Complex 3-D flow simulations are performed as a succession of 2-D simulations at a fraction of the time required for full 3-D simulations. It allows the study of the secondary flow development along the die. PNSE models do not require the imposition of an outflow boundary condition, which may be difficult to estimate for viscoelastic flows. Previous 2-D simulations studied the problem as a perturbation of a Newtonian flow field. For square duct flow, the secondary flow consisted of eight flow patterns symmetrically arranged. The direction of the secondary velocity components change sign under certain conditions. The secondary flow patterns agree well with previous simulations and some experimental data. Unusually distorted interface shapes observed in coextrusion of highly viscous flow suggest that the predicted secondary flows might cause such great distortion.

7.2 Recommendations for future work.

The physics of contact line behavior in a highly viscous flow system is not clear yet. Detailed molecular analysis as well as experimentation is required to understand the mechanisms of adhesion of an interface between two polymer melts and a die wall, as well as to estimate the extent of the slip region. The slip and stick models proposed in this work are macroscopic approximations to a much more complex molecular interaction.

Although several models for the contact line boundary condition have been proposed, there remains other boundary conditions that need further study. Probably the most important one is the outflow boundary condition. The assumption of zero cross-flow velocities would be valid only for long dies in the absence of viscoelasticity. Other

boundary conditions that must be studied in detail are the inlet thermal condition and the interfacial boundary condition in the presence of elastic effects.

Computer times for the solution of three-dimensional simulations of the type performed here becomes an issue for the average computer power available today. Two trends of research should be followed in order to obtain accurate results in a reasonable time: 1) To develop efficient matrix storage that takes advantage of the banded structure of the finite element global matrix; implementation of iterative solvers that reduce the CPU time required; and 2) To develop alternative algorithms like those proposed in Chapter 6 (Segregated Solvers and PNSE methods) that become a reasonable compromise between accuracy and computer time.

Mesh generation for three-dimensional finite element models could become a lengthy process. Creating meshes manually leads to errors in most cases, and, therefore, some automatic mesh generation schemes must be used. Even though the present code can automatically generate the meshes (including coordinates and boundary conditions) for simple geometries, extension to more complex geometries will be difficult. In future work, the code should be coupled with a commercial mesh generator. This code can create output files that can be read by Tecplot[1], but it should be modified in order to produce standardized metafiles that can be used by other visualization packages.

This work and recent experimental research have confirmed the importance that secondary flows may have in determining the final interface shape for polymer

---

[1] Tecplot is a trademark of Amtec Engineering, Inc.

coextrusion flows. The proposed algorithm in Chapter 6 should be extended to solve the interface deformation problem of two viscoelastic fluids in a die. Experiments should be carried out to precisely determine the influence of secondary flows in the final interface shape. The proposed algorithm in Chapter 6 showed that N_2 (the second normal stress difference) influences the direction and shape of the secondary flow. However, there is virtually no experimental evidence how N_2 / N_1 depends on shear rate. Careful experimental work must be carried out to understand better the behavior of N_2 in polymer melts, particularly at low shear rates.

When an MPTT constitutive equation was used to model the secondary flow phenomena in ducts, the secondary flow pattern oscillates between two different flow configurations. This suggests that the steady-state assumption for viscoelastic flow in ducts must be reviewed. Marching algorithms are well suited for transient analysis, and they could be used to validate the steady-state assumption for viscoelastic flow in ducts.

REFERENCES

Allan, W. "Newtonian Die Swell Evaluation for Axisymmetric Tube Exit Using a Finite Element Method". Int J Num Meth Eng, 11, 1621, (1977).

Anderson, D.A., Tannehill, J.C., Pletcher, R.H. Computational Fluid Mechanics and Heat Transfer, Hemisphere, (1984).

Anturkar, N.R., Papanastasiou, T.C., Wilkes, J.O. "Stability of Multilayer Extrusion of Viscoelastic Liquids". AIChE J, 36, 710, (1990a).

Anturkar, N.R., Papanastasiou, T.C., Wilkes, J.O. "Linear Stability Analysis of Multilayer Plane Poiseuille Flow". Phys. Fluids A 2, 530, (1990b).

Anturkar, N.R., Papanastasiou, T.C., Wilkes, J.O. "Lubrication Theory for *n*-Layer Thin-Film Flow with Application to Multilayer Extrusion and Coating". Chem. Eng. Sci., 45, 3271, (1990c).

Axelsson, O. Iterative Solution Methods. Cambridge University Press, (1994).

Baek, S.G., Magda, J.J., Cementwala, S. "Normal stress differences in liquid crystalline hydroxypropylcellulose solutions", J. Rheol, 37, 395, (1993a)

Baek, S.G., Magda, J.J, Larson, R.G. "Rheological differences among liquid-crystalline polymers. I. The first and second normal stress differences of PGB solutions", J Rheol, 37, 1201, (1993b).

Baker, A.J. Finite Element Computational Fluid Mechanics, Hemisphere, McGraw-Hill, (1985).

Basu, S. "A Theoretical Analysis of Non-Isothermal Flow in Wire-Coating Co-Extrusion Dies". Polym Eng Sci, 21, 17, 1128 (1981).

Barrett, R., Berry, M., Chan, T., Demmel, J., Donato, J., Dongarra, J., Eijkhout, V., Pozo, R., Romine, C., van der Vorst, H. Templates for the Solution of Linear Systems: Building Blocks for Iterative Methods. SIAM, Philadelphia, (1994).

Benim, A.C., Zinser, W. "A Segregated Formulation of Navier-Stokes Equations with Finite Elements", Comp. Meth. Appl. Mech. Eng., 57, 223 (1986).

Benney, D.J., Timson, W.J. "The Rolling Motion of A Viscous Fluid On and Off a Rigid

Surface". St App Math., 63, 98, (1980).

Bentwich, M. "Two-Phase Viscous Axial Flow in a Pipe". J Basic Eng. 669 (1964).

Bernstein, B., Keorsley, E.A., Zapas, L. "A Study of Stress Relaxation with Finite Strain." Trans. Soc. Rheo., 7, 391, (1985).

Bird, R.B. Armstrong, R.C., Hassager, O. Dynamics of Polymeric Liquids, vol. 1,Wiley (1987).

Blake, T.D. "Wetting Kinetics: How Do Wetting Lines Move?." AIChE International Symposium on the Mechanics of Thin-Film Coating, (1988).

Binding, D.M., Walters, K., Dheur, J., Crochet, M.J. "Interfacial Effects in the Flow of Viscous and Elastoviscous Liquids". Phil. Trans. R. Soc. London A 323, 449 (1987).

Briley, W.R. "Numerical Method for Predicting Three-Dimensional Steady Viscous Flow in Ducts". J. Comp. Phys., 14, 8, (1974).

Bruns, F.W. "A Moving Solid/Fluid/Solid Contact Line: The Removal of the Force and Pressure Singularity by a Slip and Filtration Flow." J. Coll & Int. Sci., 74, (2), 341, (1980).

Bush, M.B., Tanner, R.I., Phan-Thien, N. "A Boundary Element Investigation of Extrudate Swell". J Non-Newt Fluid Mech, 18, 143, (1985).

Bush, M.B., Phan-Thien, N. "Three Dimensional Viscous Flows with a Free Surface: Flow Out of a Long Square Die". J Non-Newt Fluid Mech, 18, 211 (1985).

Burnett, D. Finite Element Analysis. Addisson Wesley, (1987).

Caretto, L.S., Curr, R.M., Spalding, D.B. "Two Numerical Methods for Three-Dimensional Boundary Layers". Comp Meth. Appl. Mech. Eng., 1, 39, (1972).

Chaffoureaux, J.C., Dehennau, C., Van Rijckevorsel, J. "Flow and Thermal Stability of Rigid PVC". J Rheo, 23 (1), 1 (1979).

Chin, H.B., Kim, Y.J., Han, C.D. "A Study on Non-Isothermal Flat-Film Coextrusion". Polym Eng Rev, 4, 4, 281 (1984).

Cohen, Y., Metzner, A.B. "Apparent Slip Flow of Polymer Solutions". J Rheo, 29(1), 67 (1985).

Coleman, C.J. "A Finite Element Routine for Analysing Non-Newtonian Flows. Part I: Basic Method and Preliminary Results". J. Non-Newt Fluid Mech, 7, 289 (1980).

Comini, G., Del Giudice, S., Strada, M. "Finite Element Analysis of Laminar Flow in the

Entrance Region of Ducts", Int. J. Num. Meth. Eng., 15, 507, (1980).

Comini, G., Del Giudice, S. "Parabolic Systems: Finite Element Method", in Numerical Heat Transfer Handbook, chapter 4, ed. by Minkowycz, W.J., Wiley (1988).

Coyle, D.J., Blake, J.W., Macosko, C.W. "The kinematics of Fountain Flow in Mold-Filling", AIChE J, 33, 1168, (1987).

Crochet, M.C., Davies, A., Walters, K. Numerical Simulation of Non-Newtonian Flow. Elsevier, (1984).

Crochet, M.J. "Numerical Simulation of Viscoelastic Flow: A Review". Rubber Chem Tech., 62, 426 (1989)

Davis, S.H. "Contact-Line Problems in Fluid Mechanics". J. Appl Mech, 50, 977 (1983).

Debbaut, B., Marchal, J.M., Crochet, M.J. "Numerical Simulation of Highly Viscoelastic Flows Through on Abrupt Contraction". J Non Newt Fluid Mech, 29, 199, (1988).

Del Giudice, S. "Step-by-Step Analysis of Flow Development in Ducts". Num. Heat Transfer, 2, 291, (1979).

Denn, M.M. "Surface-Induced Effects in Polymer Melt Flow". Proc XIth, Int. Cong. on Rheology, Brussels, 45, (1992).

Dhatt, G., Touzot, G. The Finite Element Method Displayed. John Wiley and Sons (1984).

Dheur, J., Crochet, M.J. "Newtonian Stratified Flow Through an Abrupt Expansion". Rheol Acta 26, 401 (1987).

Dietsche, L., Dooley J. "Numerical Simulation of Viscoelastic Polymer Flow - Effect of Secondary Flows on Multilayer Coextrusion". SPE ANTEC, Boston, (1995).

Dodson, A.G., Townsend, P., Walters, K. "Non-Newtonian Flow in Pipes of Non-Circular Cross Section". Comp & Fluids, 2, p. 317, (1974).

Doi, M., Edwards, S.F. "Dynamics of Concentrated Polymer Systems, Part I". J Chem Soc Faraday Trans II, 74, 1789, (1978a).

Doi, M., Edwards, S.F. "Dynamics of Concentrated Polymer Systems, Part II". J Chem Soc Faraday Trans II, 74, 1802, (1978b).

Doi, M., Edwards, S.F. "Dynamics of Concentrated Polymer Systems, Part III". J Chem Soc Faraday Trans II, 74, 1818, (1978c).

Doi, M., Edwards, S.F. "Dynamics of Concentrated Polymer Systems, Part IV". J Chem Soc Faraday Trans II, 75, 38 (1978d).

Dooley, J., Hilton, B.T. "Coextrusion Layer Rearrangement in Different Geometric Channels". SPE ANTEC, New Orleans, (1993).

Dooley, J., Hughes, K. "Coextrusion Layer Thickness Variation - Effect of Polymer Viscoelasticity on Layer Uniformity". SPE ANTEC, Boston, (1995).

Dooley, J., Ramanathan, R. "Coextrusion Layer Thickness Variation - Effects of Geometry on Layer Rearrangement". SPE ANTEC, San Francisco, (1994).

Dooley, J., Stout, B. "An Experimental Study of the Factors Affecting the Layer Thickness Uniformity of Coextruded Structures". SPE ANTEC, (1991).

Dupont, S., Crochet, M.J. "The Vortex Growth of a KBKZ Fluid in an Abrupt Contraction." J Non-Newt. Fluid Mech. 29, 81 (1988).

Dupont, S., Marchal, J.M., Crochet, M.J. "Finite Element Simulation of Viscoelastic Fluids of the Integral Type". J Non Newt Fluid Mech. 17, 157, (1985).

Durbin, P. "Considerations on the Moving Contact-Line Singularity, with Applications to Frictional Drag on a Slender Drop". J Fluid Mech. 197, 157 (1988).

Dussan, E.B. "On the Spreading of Liquids on Solids Surfaces: Static and Dynamic Contact Angles". Am Rev Fluid Mech. 11, 371 (1979).

Dussan, E.B. "On the Difference Between a Bounding Surface and a Material Surface". J Fluid Mech. 75, 609 (1976a)

Dussan, E.B. "The Moving Contact Line: The Slip Boundary Condition". J Fluid Mech. 77, 665 (1976b).

Dussan, E.B., Davis, S.H. "On the Motion of a Fluid-Fluid Interface Along a Solid Surface". J Fluid Mech. 65, 71 (1974).

Elemans, P.H.M. Jansen, J.M.H., Meijer, H.E.H. "The measurements of interfacial tension in polymer/polymer systems: the breaking threat method", Polym. Eng. Sci., 26, p. 415, (1986).

Elmendrop, J.J., de Vos, G. "Measurements of Interfacial Tension of Molten Polymer Systems by Means of the Spinning Drop Method", J. Rheol. 34, p. 1311, (1990).

Everage, A.E. "Theory of Stratified Bicomponent Flow of Polymer Melts. I. Equilibrium Newtonian Tube Flow". Trans Soc Rheo. 17:4, 629 (1973).

Everage, A.E. "Theory of Stratified Bicomponent Flow of Polymer Melts. II. Interface Motion in Transient Flow". Trans Soc Rheo. 19:4, 509 (1975).

Finch, C.R. Coextrusion Seminar: A Coextrusion Overview Regarding Real World Problems in Coextrusion, SPE Ed., (1991).

Galt, J., Maxwell, B. "Velocity Profiles for Polyethylene Melts". Plastic Eng., 115, (Dec. 1964).

de Gennes, P.G. "Écoulements viscométriques de polymères enchevêtrés". C.R. Acad. Sc. Paris, 288, 219 (1979).

Gervang, B., Larsen, P.S. "Secondary flows in straight ducts of rectangular cross section". J Non-Newt Fluid Mech., 39, 217, (1991).

Giesekus, H. "A Simple Constitutive Equation for Polymer Fluids Based on the Concept of Deformation Dependent Tensorial Mobility". J Non Newt Fluid Mech, 11, 69, (1982).

Green, A.E., Rivlin, R.S. "Steady Flows of Non-Newtonian Fluids Trough Pipes". Quart. Appl. Math, 14, 299 (1956).

Han, C.D., Shetty, R. "Studies on Multilayer Film Coextrusion. I. The Rheology of Flat Film Coextrusion". Polym Eng Sci, 16, 697 (1976).

Haroutunian, V., Engelman, M.S., Hasbani, I. "Segregated Finite Element Algorithms for the Numerical Solution of Large-Scale Incompressible Flow Problems". Int J Num Meth Fluids, 17, p. 323, (1993).

Hasson, D., Mann, U., Nir, A. "Annular Flow of Two Immiscible Liquids. I. Mechanisms". Can J Chem Eng, 48, 514, (1970a).

Hasson, D., Nir, A. "Annular Flow of Two Immiscible Liquids. II. Analyisis of Core-Liquid Ascent". Can J Chem Eng, 48, 521, (1970b).

Hatzikiriakos, S.G., Dealy, J.M. "Wall Slip of Molten High Density Polyethylenes I. Sliding Plate Rheometer Studies". J. Rheol.,35,497 (1991)

Hatzikiriakos, S.G., Dealy, J.M. "Wall Slip of Molten High Density Polyethylenes II. Capillary Rheometer Studies". J. Rheol.,36,703, (1992a)

Hatzikiriakos, S.G., Dealy, J.M. "Start-Up Pressure Transients in a Capillary Rheometer", SPE ANTEC, (1992b)

Hatzikiriakos, S.G., Dealy, J.M. "Role of Slip and Fracture in the Oscillating Flow of HDPE in a Capillary". J. Rheol.,36, 845(1992c).

Hatzikiriakos, S.G. "A Slip Model for Linear Polymers Based on Adhesive Failure". Int. Polym. Proc., VIII, 135, (1993)

Hatzikiriakos, S.G., Stewart, C.W., Dealy, J.M. "Effect of Surface Coatings on Wall Slip of LLDPE". Int. Polym. Proc., VIII,1, (1993).

Hill, D.A., Hasegawa, T., Denn, M.M. "On the Apparent Relation Between Adhesive Failure and Melt Fracture". J Rheol, 34, 891, (1990).

Hocking, L.M. "A Moving Fluid Interface on a Rough Surface". J Fluid Mech., 76, 801 (1976).

Hocking, L.M. "A Moving Fluid Interface. Part 2. The Removal of the Force Singularity by a Slip Flow". J Fluid Mech., 79, 209 (1977).

Hughes, T.J.R., Brooks, A. "A Theoretical Framework for Petro-Galerkin Methods with Discontinous Weighting Functions Applied to Streamline-Upwind Procedure". Finite Elements in Fluids, 4, 47 (1982).

Huh, C., Mason, S.G. "The Steady Movement of a Liquid Meniscus in a Capillary Tube". J Fluid Mech, 81, 401 (1977).

Huh, C., Scriven, L.E. "Hydrodynamic Model of Steady Movement of a Solid/Liquid/Fluid Contact Line". J Coll Interf Sci, 35, 85 (1971).

Huyakorn, P.S., Taylor, C., Lee, R.L., Gresho, P.M. "A Comparison of Various Mixed-Interpolation Finite Elements in the Velocity-Pressure Formulation of the Navier-Stokes Equations". Comp. Fluids. 6, 25 (1978).

Joanny, J.F., Andelmann, D. "Steady-State Motion of a Liquid/Liquid/Solid Contact Line". J Coll & Int Sci, 119, 451 (1987).

Joseph, D.D., Renardy, M., Renardy, Y. "Instability of the Flow of Two Immiscible Liquids With Differents Viscosities in a Pipe". J. Fluid Mech, 141, 309 (1984).

Karagiannis, A. Modelling of Single Component and Bicomponent Extrusion Flows. Ph.D. Thesis. McMaster University, (1989a)

Karagiannis, A., Hrymak, A.N., Vlachopoulos, J. "Three-Dimensional Non-Isothermal Extrusion Flows". Rheol Acta, 28, 121 (1989b).

Karagiannis, A., Hrymak, A.N., Vlachopoulos, J. "Three-Dimensional Studies on Bicomponent Extrusion". Rheol Acta, 29, 71 (1990).

Kaye, A. College of Aeronautics, Note No. 134, (1962).

Keunings, R. "Simulation of Viscoelastic Fluid Flow" in Computational Modelling for Polymer Processing, Charles Tucker III, ed., Hanser, (1989).

Khan, A.A., Han, C.D. "On the Interface Deformation in the Stratified Two-Phase Flow of Viscoelastic Fluids". Trans Soc Rheo 20:4, 595 (1976).

Khan, A.A., Han, C.D. "A Study on the Interfacial Instability in the Stratified Flow of Two Viscoelastic Fluids Through a Rectangular Duct". Trans Soc Rheo 21:1, 101 (1977).

Khomami, B. "Interfacial Stability and Deformation of Two Stratified Power Law Fluids in Plane Poiseuille Flow. Part I. Stability Analysis". J Non-Newt Fluid Mech, 36, 289 (1990a).

Khomami, B. "Interfacial Stability and Deformation of Two Stratified Power Law Fluids in Plane Poiseuille Flow. Part II. Interface Deformation". J Non-Newt Fluid Mech, 37, 19 (1990b).

Kistler, S.F., Scriven, L.E. "Coating Flow Theory by Finite Element and Asymptotic Analysis of the Navier-Stokes System". I J Num Met Fluids, 4, 207, (1984).

Kozicki, W., Hasari, S.N., Rao, A.R.K., Tiu, C. "Anomalous Effects in Laminar Capillary Flow of Polymers Solutions". Chem. Eng. Sci., 25, 41, (1970).

Langlois, W.E., Rivlin, R.S. "Slow steady-state flow of visco-elastic fluids through non-circular tubes". Rend. Mat. Roma, 22, 169, (1963).

Larson, R.G. Constitutive Equations for Polymer Melts and Solutions. Butterworths, (1988).

Lau, H.C., Schowalter, W.R. "A Model for Adhesive Failure of Viscoelastic Fluids During Flow". J Rheo, 30(1), 193, (1986).

Lee, B.L., White, J.L. "An Experimental Study of Rheological Properties of Polymer Melts in Laminar Shear Flow and of Interface Deformation and Its Mechanisms in Two-Phase Stratified Flow". Trans Soc Rheo, 18:3, 467 (1974).

Li, D., Lin, F.Y.H., Neumann, A.W. "Effect of the Corrugations of the Three-Phase Line on Drop Size Dependence of Contact Angles". J Coll & Int Sci, 142, 224 (1991).

Lodge, A.S. Elastic Liquids. Academic Press (1964).

Lowndes, J. "The Numerical Simulation of the Steady Movement of a Fluid Meniscus in a Capillary Tube". J Fluid Mech, 101, 631 (1980).

Luo, X.L., Mitsoulis, E. "Memory Phenomena in Extrudate Swell Simulations for Annular Dies". J Rheo, 33(8), 1307 (1989).

Luo, X.L., Mitsoulis, E. "A Finite Element Study of Viscoelastic Effects in Double-Layer Coextrusion of Polymer Melts". Adv Polym Tech, 10, 47 (1990).

Macosko, C.W. Rheology Principles, Measurements amd Applications, VCH Publishers (1994).

MacLean, D. "A Theoretical Analysis of Bicomponent Flow and the Problem of Interface Shape". Trans Soc Rheo, 17:3, 385 (1973).

MacLean, D., Saffman, P.G. "The effect of Surface Tension in the Shape of Fingers in Hele-Shaw Cells" J Fluid Mech, 102, 455, (1981).

Magda, J.J., Baek, S.G., DeVries, K.L., Larson, R.G. "Shear Flows of Liquid Crystal Polymers: Measurements of the Second Normal Stress Difference and the Doi Molecular Theory", Macromolecules, 24, 4460, (1991a).

Magda, J.J., Lou, J., Baek, S.G. DeVries, K.L. "Second Normal Stress Difference of a Boger Fluid", Polymer, 32, 2000, (1991b)

Magda, J.J., Lee, C-S, Muller, S., Larson, R.G. "Rheology, Flow Instabilities, and Shear-Induced Diffusion in Polystyrene Solutions", Macromolecules 26, 1696, (1993)

Malamataris, N.T., Papanastasiou, T.C. "Unsteady Free Surface Flows in Truncated Domains". Ind Eng Chem Res, 30, 2211, (1991).

Marchal, J.M., Crochet, M.J. "A New Finite Element for Calculating Viscoelastic Flow". J Non Newt Fluid Mech, 26, 77 (1987).

Matsunaga, K., Sakaki, K., Kajiwara, T., Funatsu, K. "Approximate Simulation Method on the Three-Dimensional Polymer Melts Flow in a Die". Inter. Polymer Processing, X, 1, (1995).

Mavridis, H. Finite Element Studies in Injection Mold Filling Ph. D. Thesis. McMaster University, (1988).

Mavridis, H., Hrymak, A.N., Vlachopoulos, J. "Finite-Element Simulation of Stratified Multiphase Flows". AIChE J, 33, 410 (1987).

Meissner, J., Garbella, R.W., Hostettler, J. "Measuring Normal Stress Differences in Polymer Melt Shear Flow", J. Rheol., 33, 843, (1989).

Mitsoulis, E. Finite Element Analysis of Two-Dimensional Polymer Melt Flows. Ph.D. Thesis. McMaster University, (1984).

Mitsoulis, E. "Extrudate Swell in Double-Layer Flows". J Rheo, 30(S), S23-S44 (1986).

Mitsoulis, E. "Multilayer Sheet Coextrusion: Analysis and Design". Adv. Polym Tech. 8, 225 (1988).

Moffat, H.K. "Viscous and Resistive Eddies near a Sharp Corner". J Fluid Mech, 18, 1, (1964).

Montgomery, S.R., Wibulswas, P. "Laminar Flow Heat Transfer for Simulatneously Developing Velocity and Temperature Profiles in Ducts of Rectangular Cross Section". Appl. Sci. Res., 18, 247, (1967).

Neti, S., Eichhorn, R. "Combined Hydrodynamic and Thermal Development in a Square Duct". Num. Heat Transfer, 6, 497, (1983).

Ngan, C.G., Dussan, E.B. "The Moving Contact Line with a 180 degrees Advancing Contact Angle". Phys. Fluids, 27, 2785, (1984).

Nickell, R.E., Tanner, R.I., Caswell, B. "The Solution of Viscous Incompressible Jet and Free Surface Flows using Finite Element Methods". J Fluid Mech, 65, 189, (1974).

Oldroyd, J.G. "On the Formulation of Rheological Equations of State". Proc Roy Soc A, 200, 523 (1950).

Papanastasiou, T.C., Macosko, C.W., Scriven, L.E. "Streamlined Finite Elements and Transient Times". Finite Elements in Fluids, 6, 263. (1985).

Patankar, S.V. Numerical Heat Transfer and Fluid Flow. Hemisphere, (1980)

Patankar, S.V., Spalding, D.B.. "A Calculation Procedure for Heat, Mass and Momentum Transfer in Three-Dimensional Parabolic Flows". I J Heat Mass Transfer, 15, p. 1787, (1972).

Phan-Thien, N., Tanner, R.I. "A New Constitutive Equation Derived From Network Theory". J Non-Newt Fluid Mech, 2, 353, (1977).

Pismen, L.M., Nir, A. "Motion of a Contact Line". Phys Fluids, 25, 3 (1982).

Pomeau, Y., Pumir, A. "Remarks on the Problem of the Moving Contact Line". C.R. Acad. Sc. Paris II, 299, 909, (1984).

Pouagare, M., Lakshminarayana, B. "A Space-Marching Method for Viscous Incompressible Internal Flows", J Comp. Phys., 64, 389, (1986).

Rajagopalan, D., Armstrong, R.C., Brown, R.A. "Finite Element Methods for Calculation of Steady, Viscoelastic Flow using Constitutive Equations with a Newtonian Viscosity". J Non-Newt. Fluid Mech., 36, 159, (1990).

Ramamurthy, A.V. "Wall Slip in Viscous Fluids and Influence of Materials of Construction". J Rheo, 30, 337 (1986).

Reddy, J.N. Introduction to the Finite Element Method. McGraw-Hill, (1984).

Rice, J.G., Schnipke, R.J. "An Equal-Order Velocity-Pressure Formulation that does not Exhibit Spurious Pressure Modes". Comp. Meth. Appl. Mech. Eng., 58, 135, (1986).

Roach, P.J. Computational Fluid Dynamics. Hermosa Publishers, Albuquerque, (1976).

Ruschak, K. "A Method for Incorporating Free Boundaries With Surface Tension in Finite Element Fluid-Flow Simulators". I J Num Met Eng., 15, 639 (1980).

Russell, T.W.F., Charles, M.E. "The Effect of the Less Viscous Liquid in the Laminar Flow of Two Immiscible Liquids". Can J Chem Eng, 18 (1959).

Saffman, P.G. "Exact Solutions for the Growth of Fingers from a Flat Interface Between Two Fluids in a Porous Medium or a Hele-Shaw Cell". Q J Mech App Math, 12, p. 146, (1958).

Saffman, P.G.. "Viscous Fingering in Hele-Shaw Cells". J Fluid Mech, 173, p. 73, (1986).

Saffman, P.G., Taylor, G. "The Penetration of a Fluid in a Porous Medium or a Hele-Shaw Cell Containing a More Viscous Liquid". Proc. R. Soc London A245, 312 (1958).

Schwartz, L.W., Garoff, S. "Contact Angle Hysteresis and the Surface of the Three-Phase Line". J Coll & Int Sci, 106, 423, (1985).

Shah, R.K., London, A.L. Laminar Flow Forced Convection in Ducts. Advances in Heat Transfer, Supplement 1, Academic Press, (1978).

Shaw, C.T. "Using a Segregated Finite Element Scheme to Solve the Incompressible Navier-Stokes Equations", Int J Num. Meth. Fluids, 12, 81, (1991).

Shiojima, T., Shimazaki, Y. "Three-Dimensional Finite Element Method for Extrudate Swells of a Maxwell Fluid". J Non-Newt Fluid Mech, 34, 269, (1990)

Silliman, W.J., Scriven, L.E. "Separating Flow Near a Static Contact Line: Slip at the Wall and Shape of a Free Surface". J Comp Phys. 34, 287 (1980).

Sornberger, G., Vergnes, B., Agassant, J.F. "Two Directional Coextrusion Flow of Two Molten Polymers in Flat Dies". Polym Eng Sci, 26, 455 (1986a).

Sornberger, G., Vergnes, B., Agassant, J.F. "Coextrusion Flow of Two Molten Polymers Between Parallel Plates: Non Isothermal Computation and Experimental Study". Polym Eng Sci, 26, 682

(1986b).

Southern, J.H., Ballman, L.R. "Stratified Bicomponent Flow of Polymer Melts in a Tube". App. Polym Sci, 20, 175 (1973).

Stokes, G.G. "On the Alleged Slipping at the Boundary of a Liquid in Motion". Trans. Cambr. Phil. Soc., 9, 8, (1851).

Su, Y.Y., Khomami, B. "Purely Elastic Interfacial Instabilities in Superposed Flow of Polymeric Liquids", Rheol Acta, 31, 413, (1992a).

Su, Y.Y., Khomami, B. "Stability of Multilayer Power-law and second-order fluids in plane Poiseuille flow", Chem. Eng. Comm, 309, 209, (1992b).

Tadmor, Z., Gogos, C.G. Principles of Polymer Processing. Wiley-Interscience, (1979).

Takács, E., Torres, A., Vlachopoulos, J., Hrymak, A.N. "Interface Distortion of Two-Layer Coextrusion Flows". Xth Polymer Processing Society Meeting (1994).

Tanner, R.I. Engineering Rheology, Clarendon Press, Oxford, (1985).

Taylor, C., Hood, P. "A Numerical Solution of the Navier-Stokes Equations using the Finite Element Technique". Comp. Fluids, 1, 73, (1973).

Taylor, C., Hughes, T.G. Finite Element Programming of the Navier-Stokes Equations. Pineridge Press, Ltd., (1981).

Thangham, S., Speziale, C.G. "Non-Newtonian Secondary Flows in Ducts of Rectangular Cross-Section". Acta Mechanica,68, 121 (1987)

Tilton, J.N. "The Steady Movement of an Interface Between Two Viscous Liquids in a Capillary Tube". Chem Eng Sci, 43, 1371, (1988).

Torres, A., Hrymak, A.N., Vlachopoulos, J., Dooley, J., Hilton, B.T. "Boundary Conditions for Contact Lines in Coextrusion Flows". Rheol. Acta, 32, 513 (1993). Errata Note, Rheol. Acta,33, p.241, (1994).

Torres, A., Hrymak, A.N., Vlachopoulos, J. "Thermal Effects in Polymer Coextrusion Flows". In preparation (1995).

Townsend, P., Walters, K., Waterhouse, W.M. "Secondary Flows in Pipes of Square Cross-Section and the Measurement of the Second Normal Stress Difference". J Non-Newt Fluid Mech, 1, 107, (1986).

Tran-Cong, T., Phan-Thien, N. "Die Design by a Boundary Element Method". J Non-Newt Fluid Mech, 30, 37 (1988a).

Tran-Cong, T., Phan-Thien, N. "Three-Dimensional Study of Extrusion Processes by Boundary Element Method. I. An Implementation of High Order Elements and Some Newtonian Results". Rheol Acta, 27, 21 (1988b).

Tran-Cong, T., Phan-Thien, N. "Three-Dimensional Study of Extrusion Processes by Boundary Element Method. II. Extrusion of a Viscoelastic Liquid". Rheol Acta, 27, 639 (1988c).

Tu, Y. "Contact Line Slippage of Fluid Flow in a Rotating Disk". J Coll. & Inter. Sci., 116, 237, (1987).

Uhland, E. "Stratified Two-Phase Flow of Molten Polymers in Circular Dies". Polym Eng Sci. 17, 671 (1977).

Vlachopoulos, J. Lecture Notes from ChE-772. McMaster University, (1990).

Vlcek, J., Vlachopoulos, J. VISCOFIT: User manual. Polydynamics, Hamilton, On, Canada (1993).

Vleck, J., Vlachopoulos, J. Polybank v1.2. Polydynamics, Hamilton, On, Canada (1995).

Wang, H.P., Lee, H.S. "Numerical Techniques for Free and Moving Boundary Problems" in Charles Tucker III, Computer Modeling for Polymer Processing, Hanser P. (1989).

Wesson, R.D., Papanastasiou, T.C. "Flow Singularity and Slip Velocity in Plane Extrudate Swell Computations". J Non-Newt Fluid Mech, 26, 277 (1988).

West, G.D. "On Resistance to the Motion of a Thread of Mercury in a Glass Tube". Proc. Roy. Soc., Ser. A.,86, 20 (1911).

Wheeler, J.A., Wissler, E.H. "Steady Flow of Non-Newtonian Fluids in a Square Duct". Trans. Soc. Rheol,10:1, 353, (1966).

Whetman, W.C.D. "On the Effect of Internal Friction of Fluids on the Motion of Pendulus", Phil. Trans. Roy. Soc. Ser. A,181, 559, (1890).

Williams, M.C. "Migration of Two-Liquids Phases in Capillary Extrusion: An Energy Interpretation". AIChEJ, 21, 1204 (1975).

Wu, S. Interfacial and Surface Tension of Polymers. *J. Macromol. Sci.*, **C10**,(1), p. 1, (1974).

Yarnold, G.D. "The Motion of a Mercury Index in a Capillary Tube". Proc Roy. Soc.,50, 540,

(1938).

Yu, H.S., Sparrow, E.M. "Stratified Laminar Flow in Ducts of Arbitrary Shape". AIChE J, 10 (1967).

Yih, C.S. "Instability Due to Viscosity Stratification". J Fluid Mech, 27, 337 (1967).

Zienkiewicz, O.C. The Finite Element Method, Mc-Graw Hill, (1987).

Zimmerman, W.B., Homsy, G.M. "Three-dimensional viscous fingering: A numerical study". Phys. Fluids A, 4, p. 1901, (1992)

APPENDIX A

PRESSURE CORRECTION (PC) ALGORITHM

Haroutunian et al. (1993) proposed three different algorithms to solve the Navier-Stokes equations in a segregated form discussed in Chapter 6. It was found that the Pressure Correction (PC) algorithm is suitable for creeping flow (Re=0).

To illustrate the segregated algorithmic approach, the implementation of the PC algorithm for two-dimensional situations is explained. Extension to three-dimensional flows is straightforward. The explanation below is taken from Haroutunian et al. (1993) and starts from the global system of equations that results from the application of the classical Galerkin finite element method to the momentum and mass conservation equations:

$$\begin{bmatrix} R_u & R_{uv} & -C_x \\ R_{vu} & R_v & -C_y \\ C_x^T & C_y^T & 0 \end{bmatrix} \begin{bmatrix} u \\ v \\ p \end{bmatrix} = \begin{bmatrix} F_u \\ F_v \\ 0 \end{bmatrix} \qquad \text{(A-1)}$$

R and C matrices are the matrices that result from the application of Galerkin method to the conservation equations, and u, v, p are the two velocity components and the pressure, respectively. F denotes any possible load vector (body forces, gravity, etc.). This system can be rewritten:

$$
\begin{aligned}
R_u u - C_x p &= F_u - R_{uv} v = f_u \\
R_v v - C_y p &= F_v - R_{vu} u = f_v \\
-C_x^T u - C_y^T v &= 0
\end{aligned}
\qquad \text{(A-2)}
$$

A segregated algorithm consists of solving the three equations shown in (A-2) in a sequential manner, using the most recent calculated values. The only limiting condition for the application of a segregated algorithm approach is the lack of an explicit equation for pressure. Such an equation can be obtained by first left-multiplying the *x*- and *y*-momentum equations by R_u^{-1} and R_v^{-1}, respectively, and then by left-multiplying again by C_u^T and C_v^T:

$$
\left[C_x^T R_u^{-1} C_x + C_y^T R_v^{-1} C_y\right] p = - C_x^T R_u^{-1} f_u - C_y^T R_v^{-1} f_v + C_x^T u + C_y^T v \qquad \text{(A-3)}
$$

In principle, this a linear system of equations that could be solved without difficulty. However, for systems of practical interest, the computation of the inverses of *R* matrices becomes expensive. Simplified *R* matrices that are less expensive to invert have been used. The obvious choice is to replace *R* by *R'*, a diagonal matrix. Such matrices range from the identity matrix to the absolute values of the rows. Simplified *R'* matrices are used to solve either directly for pressure (*p*, PP, PU algorithms) or indirectly for a pressure increment (Δp, PC algorithm), (Haroutunian et al., 1993). The algorithm

used in the present work, PC, is a finite element counterpart of the well-known SIMPLE algorithm. The SIMPLE algorithm and its derivation process are discussed in detail in Patankar (1980) in finite differences and Haroutunian et al. (1993). A brief description of the algorithmic steps will be presented here.

In the PC algorithm, a corrective version of (A-3) is used. Starting from known values of u,v,p, (denoted by a superscript *), a pressure correction factor is obtained, that is used to modify the velocity field in order to satisfy continuity. The velocity values obtained at this step are known as the corrective values. These intermediate values are obtained and used in the momentum conservation equations to solve for the new values of velocity. This process is repeated until the change in all primary variables is below a specified tolerance.

PC/SIMPLE ALGORITHM

at a given iteration i:

1. Solve Pressure equation as:

$$\left[C_x^T (R_u^{/*})^{-1} C_x + C_y^T (R_v^{/*})^{-1} C_y\right] \Delta p^{i+1/2} = - C_x^T u^i - C_y^T v^i \qquad \text{(A-4)}$$

2. Mass adjust velocity and increment pressure:

$$u^{i+1/2} = u^i + (R_u^{/*})^{-1} C_x \Delta p^{i+1/2}$$

$$v^{i+1/2} = v^i + (R_v^{/*})^{-1} C_y \Delta p^{i+1/2} \qquad \text{(A-5)}$$

$$p^{i+1} = p^i + (1 - \alpha_p) \Delta p^{i+1/2}$$

3. Solve x-momentum equation:

$$\left[\alpha_u R_u^{/} + R_u\right]^* u^{i+1} = f_u^* + C_x p^{i+1} + \alpha_u R_u^{/} u^{i+1/2} \qquad \text{(A-6)}$$

4.Solve y-momentum equation:

$$\left[\alpha_v R_v^{/} + R_v\right]^* v^{i+1} = f_v^* + C_y p^{i+1} + \alpha_v R_v^{/} v^{i+1/2} \qquad \text{(A-7)}$$

5. Solve other conservation equations (z-momentum, energy, species, etc.) similarly to (A-6) and (A-7).

6. If changes in u, v, p, and other primary variables are below specified tolerance, stop. If not repeat steps 1-6.

APPENDIX B

PNSE FORMULATION FOR VISCOELASTIC FLOWS

The set of momentum and mass conservation equations for viscoelastic fluids are defined in (6-16),(6-17),(6-18) and (6-7). They are:

$$u[u_x] = \frac{1}{Re}[u_{yy} + u_{zz}] - v(u_y) - w(u_z) - P_x^a - (\tau_{xx,x} + \tau_{xy,y} + \tau_{xz,z}) = 0 \qquad \text{(B-1)}$$

$$u[v_x] = \frac{1}{Re}[v_{yy} + v_{zz}] - v(v_y) - w(v_z) - P_y - (\tau_{yx,x} + \tau_{yy,y} + \tau_{yz,z}) = 0 \qquad \text{(B-2)}$$

$$u[w_x] = \frac{1}{Re}[w_{yy} + w_{zz}] - v(w_y) - w(w_z) - P_z - (\tau_{zx,x} + \tau_{zy,y} + \tau_{zz,z}) = 0 \qquad \text{(B-3)}$$

$$u_x + v_y + w_z = 0 \qquad \text{(B-4)}$$

The space-marching algorithm of Comini and Del Giudice (1988) is extended for viscoelastic flows. By marching in the dominant flow direction at a fixed step size dx, solutions are obtained at each cross-section. As in the segregated algorithm, marching algorithms are based on separating the velocities and pressure into primary (*) and corrective(') values as:

$$
\begin{aligned}
u &= u^{*} + u' \\
v &= v^{*} + v' \\
w &= w^{*} + w' \\
P &= P^{*} + P'
\end{aligned}
\qquad \text{(B-5)}
$$

The starred (*) values are the best estimates available (usually from the previous section) while the primed (') values correspond to corrections made in order to satisfy local continuity. The momentum equations (B-1) to (B-3) are decomposed in (*) and (') components. For the x-momentum equation, the corrective component is neglected and the equation reduces to:

$$
u^{*}(u_x^{*}) = \frac{1}{Re}\left[u_{yy}^{*} + u_{zz}^{*}\right] - v^{n}(u_y^{*}) - w^{n}(u_z^{*}) - P_x^{a} - \left(\tau_{xx,x}^{n} + \tau_{xy,y}^{n} + \tau_{xz,z}^{n}\right) = 0 \qquad \text{(B-6)}
$$

where n indicates values from the previous cross-section. Since the flow is confined, the overall flowrate at a given section should be a constant, named Q. The new calculated velocity field u^* will not provide Q, but Q*. The term P_x^a is used to correct the overall flow rate Q* until matches Q up to a certain tolerance. A simple bisection method is used (Briley, 1974). It is a physically sound algorithm that is simpler than the more complex algorithms proposed by Patankar and Spalding (1972) and Comini and Del Giudice (1988). For Newtonian flows, convergence is achieved within three iterations, since the relationship is linear. For more complex flows, more iterations are required.

Once the new u^* has been calculated, it is used to update the other two starred velocity components. Introducing into the y- and z- momentum equations the (*) and (')

components:

y-momentum:

$$u^{n}(v_x^{*}) = \frac{1}{Re}\left[v_{yy}^{*} + v_{zz}^{*}\right] - v^{n}(v_y^{*}) - w^{n}(v_z^{*}) - P_y^{*} - \left(\tau_{yx,x}^{n} + \tau_{yy,y}^{n} + \tau_{yz,z}^{n}\right) = 0 \qquad \text{(B-7)}$$

$$u^{n}(v_x^{/}) = P_y \qquad \text{(B-8)}$$

z-momentum:

$$u^{n}(w_x^{*}) = \frac{1}{Re}\left[w_{yy}^{*} + w_{zz}^{*}\right] - v^{n}(w_y^{*}) - w^{n}(w_z^{*}) - P_z^{*} - \left(\tau_{zx,x}^{n} + \tau_{zy,y}^{n} + \tau_{zz,z}^{n}\right) = 0 \qquad \text{(B-9)}$$

$$u^{n}(w_x^{/}) = P_z \qquad \text{(B-10)}$$

In (B-8) and (B-10), the diffusion and convective contributions in the y- and z-directions are neglected (Comini and Del Giudice, 1988). Equations (B-8) and (B-10) are used to derive a simplified pressure equation, which is obtained by taking the derivative with respect to x of the continuity equation, and splitting into (*) and (') components (Comini and Del Giudice, 1988). After some rearrangement and dropping the second derivatives with respect to x, the pressure equation is:

$$\left(\frac{1}{u^*}P_y'\right)_y + \left(\frac{1}{u^*}P_z'\right)_z = \frac{1}{dx}\left(\frac{u^* - u^n}{dx} + v_y^* + w_z^*\right) \qquad \text{(B-11)}$$

To obtain the stress field expressed in equations (B-6), (B-7) and (B-9), a constitutive equation of the form (6-19) or (6-20) is used depending on the model. The derivatives with respect to x of a given variable ϕ (velocities, pressure or extra-stress) are approximated with finite differences as:

$$\phi_x = \frac{\phi^n - \phi^{n-1}}{dx} \qquad \text{(B-12)}$$

where superscript n indicates current cross-section and n-1 indicates previous section. Straightforward application of Galerkin's method to (B-6), (B-7), (B-8), (B-9), (B-10) and (B-11), results in the following matrix system:

$$\left[\frac{M}{dx} + \frac{1}{Re}H + H_v\right]\{u\} = \frac{[M]\{u\}^{n-1}}{dx} - Q_u \qquad \text{(B-13)}$$

$$\left[\frac{M}{dx} + \frac{1}{Re}H + H_v\right]\{v\} = \frac{[M]\{v\}^{n-1}}{dx} - Q_v \qquad \text{(B-14)}$$

$$\left[\frac{M}{dx}+\frac{1}{Re}H+H_v\right]\{w\}=\frac{[M]\{w\}^{n-1}}{dx}-Q_w \tag{B-15}$$

$$[H_p]\{P'\}=\frac{1}{dx}[Q_p] \tag{B-16}$$

$$\left[\frac{M}{dx}\right]\{v'\}=-Q'_v \tag{B-17}$$

$$\left[\frac{M}{dx}\right]\{w'\}=-Q'_w \tag{B-18}$$

respectively, where

$$[M] = \int_{\Omega} u\, {}^{n}N^{i}N^{j} d\Omega \qquad [H] = \int_{\Omega} \left(N_y^i N_y^j + N_z^i N_z^j\right) d\Omega$$

$$[Q_u] = \int_{\Omega} N^i P_x^a \, d\Omega \qquad [H_v] = \int_{\Omega} N^i \left(v\, {}^{n}N_y^j + w\, {}^{n}N_z^j\right) d\Omega$$

$$[Q_v] = \int_{\Omega} N^i P_y \, d\Omega \qquad [Q_w] = \int_{\Omega} N^i P_z \, d\Omega \qquad [Q_p] = \int_{\Omega} \left(\frac{u^* - u^n}{dx} + v_y^* + w_z^* \right) d\Omega \tag{B-19}$$

$$[H_p] = \int_{\Omega} \frac{1}{u^*} \left(N_y^i N_y^j + N_z^i N_z^j\right) d\Omega \qquad [Q'_v] = \int_{\Omega} N^i P'_y \, d\Omega \qquad [Q'_w] = \int_{\Omega} N^i P'_z \, d\Omega$$

The stress profile is obtained by solving each stress tensor component in a segregated manner according to (6-19) or (6-20) if the model is MPTT or CEF, respectively.

MPTT model.

The MPTT model can be written as:

$$\left(A - Wi_c B_{ij}\right)\tau_{ij} + Wi_c \left(u\tau_{ij,x} + v\tau_{ij,y} + w\tau_{ij,z}\right) - Wi_c D_{ij} - \eta_v \dot{\gamma}_{ij} = 0 \tag{B-20}$$

where:

$D_{xx} = \zeta\ (2v_x\tau_{xy} + 2w_x\tau_{xz}) + (\zeta\text{-}1)\ (2u_y\tau_{xy} + 2u_z\tau_{xz})$

$D_{xy} = \zeta\ (v_x\tau_{yy} + w_x\tau_{yz} + u_y\tau_{xx} + w_y\tau_{xz}) + (\zeta\text{-}1)\ (u_y\tau_{yy} + u_z\tau_{yz} + v_x\tau_{xx} + v_z\tau_{xz})$

$D_{xz} = \zeta\ (v_x\tau_{yz} + w_x\tau_{zz} + u_z\tau_{xx} + v_z\tau_{xy}) + (\zeta\text{-}1)\ (u_y\tau_{yz} + u_z\tau_{zz} + w_x\tau_{xx} + w_y\tau_{xy})$

$D_{yy} = \zeta\ (2u_y\tau_{xy} + 2w_y\tau_{yz}) + (\zeta\text{-}1)\ (2v_x\tau_{xy} + 2v_z\tau_{yz})$

$D_{yz} = \zeta\ (u_y\tau_{xz} + w_y\tau_{zz} + u_z\tau_{xy} + v_z\tau_{yy}) + (\zeta\text{-}1)\ (v_x\tau_{xz} + v_z\tau_{zz} + w_x\tau_{xy} + w_y\tau_{yy})$

$D_{zz} = \zeta\ (2u_z\tau_{xz} + 2v_z\tau_{yz}) + (\zeta\text{-}1)\ (2w_x\tau_{xz} + 2w_y\tau_{yz})$

$B_{xx} = (2\zeta\text{-}1)\ (2u_x)$

$B_{xy} = (2\zeta\text{-}1)\ (u_x + v_y)$

$B_{xz} = (2\zeta\text{-}1)\ (u_x + w_z)$

$B_{yy} = (2\zeta\text{-}1)\ (2v_y)$

$B_{yz} = (2\zeta\text{-}1)\ (v_y + w_z)$

$B_{zz} = (2\zeta\text{-}1)\ (2w_z)$

The most recent values for τ_{ij} are used to calculate the entries D_{ij}. After applying Galerkin, equation (B-20) can be written in matrix form as:

$$\left[\frac{M_v}{dx} + H_{eij} + H_v\right]\{\tau_{ij}\} = \frac{[M_v]\{\tau_{ij}^n\}}{dx} - Q_{eij} \tag{B-21}$$

where,

$$[M_v] = Wi_c \int_\Omega u\, {}^nN^i N^j d\Omega \qquad [H_{eij}] = \int_\Omega N^i (A - Wi_c B_{ij}) N^j d\Omega$$
$$[Q_{eij}] = \int_\Omega N^i (Wi_c D_{ij} + \eta_0 \dot{\gamma}_{ij}) d\Omega \qquad [H_v] = Wi_c \int_\Omega N^i \left(v\, {}^nN_y^j + w\, {}^nN_z^j\right) d\Omega \tag{B-22}$$

CEF model.

In Equation (6-20), the CEF model is defined as:

$$\tau_{ij} = \frac{1}{2}\left(u\dot{\gamma}_{ijx} + v\dot{\gamma}_{ijy} + w\dot{\gamma}_{ijz}\right) - \frac{1}{2}\psi_1 T_{1ij} + \left(\frac{1}{2}\psi_1 + \psi_2\right) T_{2ij} \tag{B-23}$$

After applying Galerkin, eq. (B-23) can be rewritten as:

$$\int_{\Omega}[N^i N^j]d\Omega\{\tau_{ij}\}=\int_{\Omega}N^i\left[\frac{1}{2}(u\dot{\gamma}_{ij,x}+v\dot{\gamma}_{ij,y}+w\dot{\gamma}_{ij,z})-\frac{1}{2}\psi_1 T_{1ij}+\left(\frac{1}{2}\psi_1+\psi_2\right)T_{2ij}\right]d\Omega \quad \text{(B-24)}$$

where,

$T_{1xx} = (u_x u_x + v_x v_x + w_x w_x) - (u_x u_x + u_y u_y + u_z u_z)$

$T_{1xy} = (u_x u_y + v_x v_y + w_x w_y) - (u_x v_x + u_y v_y + u_z v_z)$

$T_{1xz} = (u_x u_z + v_x v_z + w_x w_z) - (u_x w_x + u_y w_y + u_z w_z)$

$T_{1yy} = (u_y u_y + v_y v_y + w_y w_y) - (v_x v_x + v_y v_y + v_z v_z)$

$T_{1yz} = (u_y u_z + v_y v_z + w_y w_z) - (v_x w_x + v_y w_y + v_z w_z)$

$T_{1zz} = (u_z u_z + v_z v_z + w_z w_z) - (w_x w_x + w_y w_y + w_z w_z)$

$T_{2xx} = \dot{\gamma}_{xx}\dot{\gamma}_{xx} + \dot{\gamma}_{xy}\dot{\gamma}_{xy} + \dot{\gamma}_{xz}\dot{\gamma}_{xz}$

$T_{2xy} = \dot{\gamma}_{xx}\dot{\gamma}_{xy} + \dot{\gamma}_{xy}\dot{\gamma}_{yy} + \dot{\gamma}_{xz}\dot{\gamma}_{yz}$

$T_{2xz} = \dot{\gamma}_{xx}\dot{\gamma}_{xz} + \dot{\gamma}_{xy}\dot{\gamma}_{yz} + \dot{\gamma}_{xz}\dot{\gamma}_{zz}$

$T_{2yy} = \dot{\gamma}_{xy}\dot{\gamma}_{xy} + \dot{\gamma}_{yy}\dot{\gamma}_{yy} + \dot{\gamma}_{yz}\dot{\gamma}_{yz}$

$T_{2yz} = \dot{\gamma}_{xy}\dot{\gamma}_{xz} + \dot{\gamma}_{yy}\dot{\gamma}_{yz} + \dot{\gamma}_{yz}\dot{\gamma}_{zz}$

$T_{2zz} = \dot{\gamma}_{xz}\dot{\gamma}_{xz} + \dot{\gamma}_{yz}\dot{\gamma}_{yz} + \dot{\gamma}_{zz}\dot{\gamma}_{zz}$

Note that eq. (B-23) could be solved explicitly for τ_{ij}, but the finite element formulation was kept similar to the MPTT model, for simplicity in the code and to keep

the same algorithmic approach for both models. The algorithmic steps for PNSE method used in this work, applied to either MPTT or CEF flows, is shown below.

ALGORITHMIC STEPS FOR PNSE METHODS APPLIED TO VISCOELASTIC FLOWS.

in section 0, Q (flowrate) is known, inlet boundary conditions for primary variables known, P^a known.

at a given section n (n=1,2,...)

$P^a_x = P^a_x$ from previous section n-1; $u^* = u^{n-1}$; $v^* = v^{n-1}$; $w^* = w^{n-1}$; $\tau_{ij}^* = \tau_{ij}^{n-1}$

do
    solve (B-13) to obtain u*
    calculate Q*
    use (Q - Q*) to calculate new P^a_x, using bisection method.
    if |Q - Q*| < tolerance, exit loop
loop

do
    do k=1,6
        solve (B-21) or (B-24) for MPTT or CEF models, respectively.
    end do
    check convergence (changes in τ_{ij} below specified tolerance)
    if convergence is met, exit loop
end do

do
    solve (B-14) to obtain v*
    solve (B-15) to obtain w*
    solve (B-16) to obtain P'
    solve (B-17) to obtain v'
    solve (B-18) to obtain w'
    P = P* + P'
    v = v* + v'
    w = w* + w'
    check convergence (changes in *u, v, w, p* below specified tolerance).
    if convergence is met, exit loop
loop

$x^{n+1} = x^n + dx$
if x^{n+1} > specified L/D STOP; else repeat above procedure.